THE UNIVERSITY
of EDINBURGH

Investigating early cellular and molecular responses to misfolded PrP protein

Declan J P King

Doctor of Philosophy

College of Medicine and Veterinary Medicine

University of Edinburgh

2018

Addenda page

Updated Acknowledgements section.

Dr D King
13/01/23

Declaration

I declare that this thesis has been composed solely by myself and that it has not been submitted, in whole or in part, in any previous application for a degree. The work described in this thesis is my own work and any collaborative contributions have been clearly indicated in the text. Due references have been provided on all supporting literatures and resources.

Declan J P King

August 2018

Abstract

The generation and spread of misfolded protein aggregates is common to all Protein Misfolding Diseases (PMDs) including but not limited to Alzheimer's, Parkinson's and Prion disease. Yet despite this common feature, the early mechanisms underpinning the apparent perturbation in protein handling and processing in such conditions remain poorly understood. Research in our lab has previously shown protein misfolding may be seeded and supported in different ways in the brain. Mice homozygous for the P101L mutation in murine PrP (101LL) are capable of supporting protein misfolding and amyloid plaque formation after challenge with pre-formed PrP fibrils and wild type mice of the same genetic background do not, and appear to be capable of curtailing this accumulation of abnormal protein *in vivo*. Thus, both mouse lines provided ideal tools to investigate early cellular and molecular responses to abnormal PrP fibril challenge. PMDs occur in *vivo* with a regional dependant progression however; such investigations are more amenable to controlled initiation and visualisation *in vitro*. Therefore, primary neuronal hippocampal cell cultures were generated from each line (101LL and WT) and were thoroughly assessed at the cellular level. Comparative molecular analysis of these cultures and *in vivo* hippocampal tissue from both WT and 101LL lines was carried out and transcriptome analysis confirmed a broadly comparable global expression profile at a basal level between *in vivo*, *in vitro* and genotype. Interestingly, this suggests that the genotype specific differential protein misfolding responses are therefore likely to be the result of regulatory cascades initiated after inoculation. To examine this at the cellular level, cultures were then challenged with fluorescently labelled recombinant PrP fibrils.

Fibrils were directly interacting with PrP^{C} on neuronal surfaces but did not cause neurotoxicity. However, post-synaptic marker PSD-95 was significantly reduced in 101LL cultures suggestive that 101LL neurons were more susceptible to fibril insult than WT. Microglial cells were activated post fibril challenge in both genotypes. This generic response was possibly to limit neuronal damage and promote fibril degradation through phagocytosis.

Transcriptome analyses supported these observations and showed an increase in expression of genes associated with phagocytosis was occurring after fibril challenge in both genotypes. Hypertrophic astrocytes and an increase in expression of genes associated with astrocyte differentiation and development was only evident in WT fibril-challenged cultures indicating differential glial responses were occurring between genotypes. Intracellular labelling showed localisation with endosomes and lysosomes in WT cells indicating an endolysosomal pathway was operative however; localisation in 101LL cells was primarily in endosomes indicating an impairment in abnormal protein degradation pathways was occurring in 101LL fibril-challenged cultures. Transcriptomic analysis identified reduced gene expression of lysosomal associated genes *Laptm5* and *Ctsz* in 101LL fibril-challenged cultures, supporting endolysosomal processing was reduced in this genotype. Additional transcriptomic profiles obtained post-fibril challenge showed an increase in gene expression in WT cultures associated with endocytosis, macrophage engulfment, immune and defence response and ER-associated misfolded protein catabolic processes none of which were induced in 101LL fibril-challenged cultures. These analyses suggest a dysfunction of multiple mechanisms may be associated with an inability to clear misfolded protein.

These data provide key information on pathways and cellular mechanisms involved in either clearance of misfolded protein or initiation of amyloid formation. Identifying these pathways will provide a number of possible test targets with the potential of impacting diagnosis and/or intervention in PMD's such as AD, PD and prions.

Lay Summary

Protein misfolding in the brain can lead to its accumulation into structures referred to as amyloid plaques. These plaques are a hallmark of many neurodegenerative diseases including but not limited Alzheimer's, Parkinson's and Prion (BSE/Mad Cow) diseases. However, the formation of amyloid plaques are still poorly understood. To provide more insights into this poorly understood area a number of objectives were carried out as listed below.

1) To model the brain, cells from living brain tissue were obtained and were kept living and functional in dishes. This is known as primary neuronal culturing. These cultures provided easily accessible models for looking at protein misfolding. Such primary cultures were made from two different types of mouse brain, one which is susceptible to protein misfolding (here called 101LL), and another which is not (here called WT). Thus, a comparison would provide ideal models for studying protein misfolding interactions with cells.

2) To initiate protein misfolding in our cell cultures we need to add a "seed" (here called fibrils - a collection of artificially produced misfolded protein) which once added to the cells will encourage other protein from the cell to interact and accumulate around the fibril thereby "growing" a plaque. Thus, fibrils were made and were labelled with a fluorescent marker to allow visualisation of fibrils once added to primary cell cultures.

3) By doing this in both WT and 101LL cultures the following questions can be addressed; how do the fibrils get into the cells, where they go, how do they change and importantly how does the composition (the molecular recipe) of the cell change in response?

The data generated in this thesis enhances our understanding and knowledge of amyloid plaque formation, distribution and the cellular responses, which are important for helping and hindering this process. Such knowledge will be essential for the development of potential therapeutics for treatment of misfolded protein diseases.

Acknowledgements

I would like to express my thanks to my supervisors Dr Rona Barron, Dr Paul Skehel and Dr Tom Wishart for their help and support during my thesis. I would particularly like to acknowledge Dr Tom Wishart whom took over as my primary supervisor due to some unforeseen circumstances for his guidance and encouragement in the final months. Special thanks also goes to Dr Paul Skehel who was instrumental in teaching me the art of hippocampal dissection, which was critical to this project.

I would also like to thank the following people for provision of mouse lines, information or advice: Prof Jean Manson (previously Roslin Institute and R(D)SVS, University of Edinburgh, UK) for provision of 101LL mouse lines used in this project; Dr Andy Gill (Joseph Banks Laboratories, Lincolnshire, UK) for provision of E. coli stocks used in this project and for allowing me the use of the proteomic facility; Prof Neil Mabbott (University of Edinburgh, UK) and Dr Barry McColl (UK Dementia Research Institute, University of Edinburgh) for allowing me to join their joint group meetings and for providing advice; Dr David Donaldson (University of Edinburgh, UK) and Dr Barry Bradford (University of Edinburgh, UK) for all the insightful discussions, advice and for supplying the odd antibody here and there and finally Robert Flemming (University of Edinburgh, UK) for advice and support on fluorescent imaging. I would like to thank the animal house staff for their support during this project. Dave Davies, Rebecca Greenan and Izabela Sabok. Without the care and attentiveness, this project would not have been a success.

Most importantly, I would like to thank my loving family, who have always supported and believed in me, without which I would only be half the person I am now. I dedicate this thesis to all of you with all my love.

Table of Contents

Abbreviations

PMDs	**Protein misfolding diseases**
AD	**Alzheimer's disease**
PD	**Parkinson's disease**
HD	**Huntington's disease**
TSEs	**Transmissible spongiform encephalopathies**
GSS	**Gerstmann-Sträussler-Scheinker**
APP	**Amyloid precursor protein**
ALS	**Amyotrophic Lateral Sclerosis**
Aβ	**Amyloid beta**
CJD	**Creutzfeldt Jacob disease**
FFI	**Fatal Familial Insomnia**
BSE	**Bovine Spongiform Encephalopathy**
PrP^{C}	**Cellular prion protein**
PrP^{Sc}	**Insoluble aggregated isoform of PrP^{C}**
MVBs	**Multivesicular body vesicles**
ER	**Endoplasmic reticulum**
GPI	**Glycosylphosphatidylinositol anchor**
NMR	**Nuclear Magnetic Resonance**
NCAM	**Neural Cell Adhesion Molecule**
SAF	**Scrapie-associated fibrils**
SDS-PAGE	**Sodium Dodecyl Sulphate Polyacrylamide Gel Electrophoresis**
vCJD	**Variant Creutzfeldt-Jakob disease**
101LL	**Transgenic mice with proline to leucine point mutation**
IC	**Intracerebral**
GFAP	**Glial fibrillary acidic protein**
M-CSF	**Macrophage colony stimulating factor**
EM	**Electron microscopy**
ER	**Endoplasmic reticulum**
ERQC	**Endoplasmic reticulum quality control**
ERAD	**Endoplasmic reticulum-associated degradation**

UPS	**Ubiquitin-proteasome system**
Ub	**Ubiquitin**
CMA	**Chaperone mediated autophagy pathway**
ILVs	**Intraluminal vesicles**
UPR	**Unfolded protein response pathway**
PERK	**Protein kinase RNA-like endoplasmic reticulum kinase**
DNA	**Deoxyribonucleic acid**
PCR	**Polymerase chain reaction**
dH_2O	**Distilled water**
dNTP	**Deoxyribonucleotide triphosphate**
BME	**Basal Medium Eagle**
PLL	**Poly-L-Lysine**
PDL	**Poly-D-Lysine**
LDH	**Lactate Dehydrogenase Assay**
DIV	**Days *in vitro***
PS	**Phosphatidylserine**
DPBS	**Dulbecco's Phosphate Buffered Saline**
PMSF	**Phenyl Methyl Sulfonyl Fluoride**
BCA	**Bicinchoninic acid assay**
PVDF	**Polyvinylidene fluoride**
RNA	**Ribonucleic acid**
DAPI	**4', 6-Diamidino-2-Phenylindole, Dihydrochloride**
E.coli	***Escherichia coli***
LB	**Luria-Bertani**
DNase	**Deoxyribonuclease I from bovine pancreas**
IMAC	**Immobilized-Metal Affinity Chromatography**
TEM	**Transmission Electron Microscopy**
DMSO	**Dimethylsulfoxide**
H_2O_2	**Hydrogen peroxide**
RINe	**Integrity number equivalent**
ANOVA	**Analysis of variance**
PANTHER	**Protein Annotation Through Evolutionary Relationship**

GOrilla	**Gene Ontology enrichment analysis visualisation tool**
DAVID	**Database for Annotation, Visualisation and Integrated Discovery**
Ct	**Cycle threshold**
BOSC	**Brain organotypic brain slice cultures**
aCSF	**Artificial cerebrospinal fluid**
MAP2	**Microtubule Associated Protein 2**
CD11b	**Cluster of differentiation molecule 11b**
Iba1	**Ionized calcium-binding adapter molecule 1**
IPTG	**Isopropyl ß-D-1-thiogalactopyranoside**
Ni-NTA	**Nickel-Nitrilotriacetic acid**
RP-HPLC	**Reverse Phase High Performance Liquid Chromatography**
DEGs	**Differentially expressed genes**
PCA	**Principal Component Analysis**
FDR	**False Discovery Rate**
IPA	**Ingenuity Pathway Analysis**

CHAPTER 1

Introduction

1.1 Protein Misfolding Diseases (PMDs)

Proteins are essential constituents of cells and tissues in all living organisms and correct formation and confirmation of these complex macromolecules is essential. Protein folding involves multiple chaperone systems where dysfunction in any of these pathways can provide many opportunities for error (Valastyan and Lindquist 2014). The mechanisms by which failures occur in protein quality systems remain elusive however, factors such as defective or incomplete translation, post-translational misfolding, mutations, environmental or intracellular stressors can all result in the generation of misfolded abnormal protein (Gregersen and Bross 2010). Misfolding of a protein jeopardises its biological function, and failure to degrade such abnormal protein conformations encourages the formation of aggregates resistant to biological clearance resulting in the triggering of a cascade of events leading eventually to disease (Soto 2003).

Protein misfolding diseases (PMDs) such as Alzheimer's disease (AD), Parkinson's disease (PD), Huntington's disease (HD) and transmissible spongiform encephalopathies (TSEs) or prions are a broad group of neurodegenerative disorders associated with the accumulation of abnormally folded proteins in the brain (Knowles, Vendruscolo, and Dobson 2014; Braak et al. 2003; Caughey and Lansbury 2003; Forloni et al. 2002; Bucciantini et al. 2002; Lazarov et al. 2002). These abnormal aggregates are common to all PMDs and once formed, encourage further misfolding of the native host protein, eventually leading to neurotoxicity in the brain. Additionally, these aggregates can accumulate in specific areas of the brain for example, in one form of prion disease (Gerstmann-Sträussler-Scheinker disease) and AD, the hippocampus and cerebral cortex are commonly targeted areas (Knowles, Vendruscolo, and Dobson 2014; Caughey and Lansbury 2003; Bucciantini et al. 2002; Braak, Braak, and Bohl 1993). It has recently been proposed that AD and several other neurodegenerative diseases may spread through a cross seeding mechanism or a "prion-like" mechanism.

The cross seeding mechanism proposes that seeds composed of one protein can accelerate a second misfolding process in an unrelated protein (Morales et al. 2010). The term “prion-like” refers to the introduction of a misfolded protein seed, which acts as a template for the conversion, and misfolding of the normal host protein present resulting in the cell-to-cell spread of protein aggregation in the tissue. Evidence supporting these “prion-like” mechanisms comes from studies using pre-formed amyloid seeds from AD patients as inoculum which were shown to accelerate plaque formation in the brains of amyloid precursor protein (APP) mice (Meyer-Luehmann et al. 2006). Similar results were observed in models of PD (Oueslati, Ximerakis, and Vekrellis 2014) and Amyotrophic Lateral Sclerosis (ALS) (Ayers et al. 2016). Converse to these studies there is no epidemiological data or documentation to suggest neurodegenerative disorders such as AD, PD or ALS diseases are actually infectious and only TSE diseases appear to be transmissible (Irwin et al. 2013; Peters, Ghasemi, and Brown 2015).

The actual role of protein aggregates in neurodegenerative diseases is unclear, and early mechanisms involved in abnormal protein processing are poorly understood (Moreno-Gonzalez and Soto 2011). Due to this lack of understanding it is widely debated whether abnormal protein deposits are toxic to neurons or if they are generated as a protective mechanism to sequester smaller soluble forms of misfolded protein (Wolfe and Cyr 2011; Treusch, Cyr, and Lindquist 2009; Haass and Selkoe 2007). These soluble assemblies of misfolded protein which have a high β-sheet content are referred to as oligomers (Winner, Kohl, and Gage 2011; Simoneau et al. 2007; Quist et al. 2005; Kristiansen et al. 2005; Mucke et al. 2000; Lue et al. 1999; McLean et al. 1999; Kuo et al. 1996), and can cause interference with normal cellular functions (Wolfe and Cyr 2011). For example low molecular weight oligomers have been detected in the brains of AD patients (Gong et al. 2003; Roher et al. 1996) and in the lysates of cultured cells expressing the amyloid β (Aβ) protein precursor (Walsh et al. 2000).

Transgenic mice (overexpressing human mutant APP and a triple human tau mutation) develop deficits in cognitive impairment and cell function well before the significant accumulation of amyloid plaques, suggesting the severity of cognitive impairment in AD correlates with the abundance of small oligomers rather than with amyloid burden (DaRocha-Souto et al. 2011). Our group, however, has shown that oligomeric forms of misfolded protein inoculated into the brains of mice have no neurotoxic effect on the brain (Barron et al. 2016), highlighting the fact that the relationship between misfolded protein and neurotoxicity is still poorly understood. Thus, further investigation of these “prion-like” molecular mechanisms, and interactions in the initiation and possible misfolded protein spread, will be carried out here using well-characterised prion models. This will provide valuable information on pathological mechanisms that may be shared by the most common forms of neurodegeneration, and so facilitate the development of new therapeutics.

1.2 TSEs and PrP protein

1.2.1 TSE Diseases

TSE's are infectious, fatal neurodegenerative diseases, which include Gerstmann-Sträussler-Scheinker (GSS), Creutzfeldt Jacob disease (CJD), Fatal Familial Insomnia (FFI) in humans and scrapie and Bovine Spongiform Encephalopathy (BSE) in animals (Table 1.1). It has been proposed that TSE diseases can be infectious, genetic or sporadic (Wechselberger et al. 2002; Harris 1999; Prusiner 1998; Prusiner 1993) and the disease pathology has been shown to involve the conversion of the normal cellular prion protein (PrP^{C}) to an insoluble aggregated isoform (PrP^{Sc}) (Prusiner 1996). Sporadic CJD represents the most frequent type of human prion disease (85%) with a worldwide incidence of 1-2 cases per million per year and genetic prion diseases caused by mutations in the prion protein represent 10-15% (Gelpi et al. 2015). Additionally, the PRNP polymorphic residue at codon 129 (ATG-methionine to GTG-valine, M129V) has been studied extensively in the prion field where 129 homozygosity is considered a risk factor for human prion disease (Bishop et al. 2009). Interestingly, variations in genotype frequencies in relation to geographical region occur for example MM and MV frequencies are approximately 40-50% in most countries however in Japan frequencies of MM are 92% and MV 8% (Bishop et al. 2009). The prion hypothesis predicts that PrP^{Sc} alone is the infectious agent of TSE, and is able to seed the conversion of the host glycoprotein PrP^{C} to produce additional protease-resistant forms during disease (Prusiner 1982). These abnormal forms of protein aggregates exist in tissue in the form of amyloid deposits (Ross and Poirier 2004).

The mechanisms involved in PrP^{C} to PrP^{Sc} conversion are poorly understood and may involve several intracellular compartments associated with the endolysosomal system and the Trans-Golgi network (TGN) (Beranger et al. 2002; Magalhaes et al. 2002; Borchelt, Taraboulos, and Prusiner 1992; Taraboulos et al. 1992; Caughey et al. 1991), recycling endosomes (Marijanovic et al. 2009) and multivesicular body vesicles (MVBs) (Yim et al. 2015). Additionally, conversion may also occur at the plasma membrane (Goold et al. 2011) or even at lipid raft transmembrane domains (Rouvinski et al. 2014; Taylor and Hooper 2006).

TSE Disease	Affected Species
Gerstmann-Sträussler-Scheinker (GSS)	Human
Creutzfeldt-Jakob Disease (CJD)	Human
Kuru	Human
Bovine Spongiform Encephalopathy (BSE)	Cattle
Scrapie	Sheep and goats
Chronic Wasting Disease (CWD)	Deer, Elk and Moose
Feline Spongiform Encephalopathy (FSE)	Cats

Table 1.1: TSE diseases are found across multiple species.

TSEs are characterised by lengthy asymptomatic incubation periods that can proceed into clinical symptoms, which include behavioural changes, cognitive impairment and insomnia. TSE studies involving mice clinical progression signs include tremor, ataxia, rigidity of tail and loss of condition. Neuropathological profiling including examining vacuolation of the brain, gliosis, synaptic degradation, abnormal deposition of misfolded PrP and neuronal loss are all quantified post-mortem to determine disease progression.

1.2.2 Normal Cellular PrP (PrP^C)

PrP^C is a cellular 38kDa glycoprotein encoded by the *PRNP* gene on the short arm of chromosome 20 in humans and *Prnp* on chromosome 2 in mice (Figure 1.1). Full length PrP^C is expressed most abundantly in the brain with the highest levels in neurons (Westergard, Christensen, and Harris 2007; Bendheim et al. 1992). However, PrP^C is also detectable in spleen, liver, kidney, heart, testes, gastrointestinal tract and blood platelets (MacGregor 2001; Li et al. 2000).

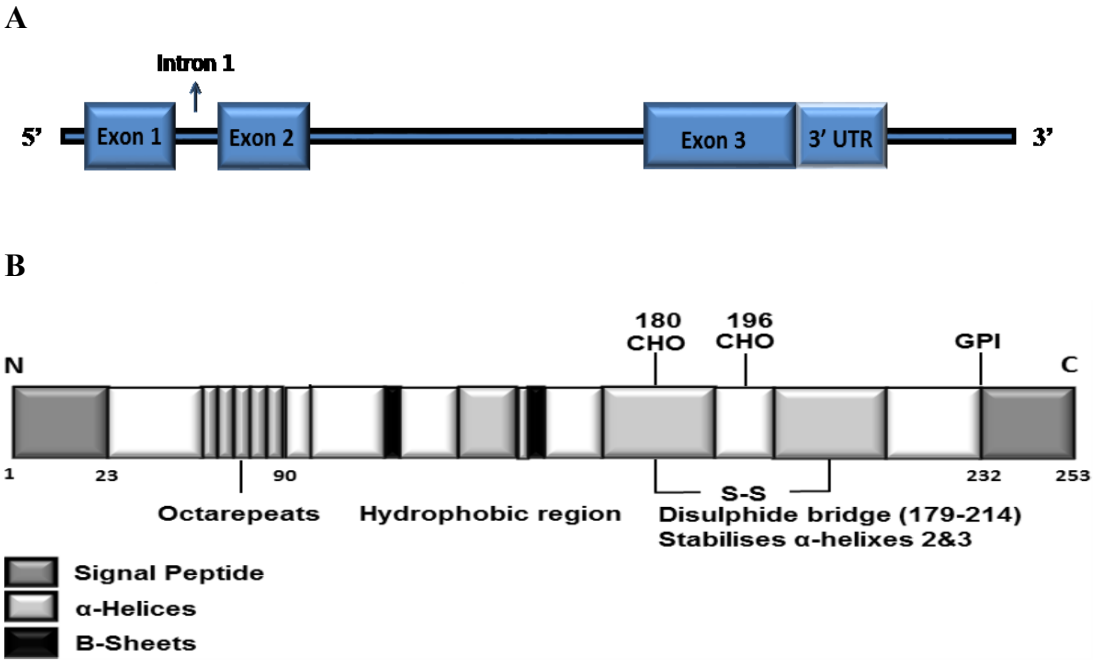

Figure 1.1: Schematic illustrations of WT mouse *Prnp* and PrP protein. (A) *Prnp* gene retains 3 exons, with the open reading frame (ORF) in exon 3. Adapted from (Shmerling et al. 1998; Moore et al. 1995). (B) Schematic diagram of murine PrP^C adapted from (Gill et al. 2000; Moore et al. 1999).

Murine PrP^C is a 253 amino acid protein with a biosynthetic pathway that is similar to that of other membrane-bound and secreted proteins including synthesis in the rough endoplasmic reticulum (ER), followed by transportation to the Golgi, on its way to the cell surface (Harris 2003).

Within the ER, PrP^C undergoes several post-translational modifications including cleavage of the N-terminal signal peptide, addition of N-linked oligosaccharide chains at two sites (180 and 196) where differential glycosylation results in un-, mono-, or di-glycosylated states of PrP^C being produced (Xanthopoulos et al. 2009), formation of a single disulphide bond, and attachment of the glycosylphosphatidylinositol (GPI) anchor following cleavage of the C-terminal hydrophobic peptide (Harris 2003; Haraguchi et al. 1989; Turk et al. 1988; Stahl et al. 1987). PrP^C locates to the outer leaflet of the lipid bilayer in regions rich in cholesterol within the cell membrane known as lipid rafts, where the protein is anchored via its GPI anchor present at the carboxyl-terminus (Harris 2003; Stahl et al. 1993; Taraboulos et al. 1995).

PrP^C structure consists of a flexible N-terminal, random coil region that is unstructured and contains five copies of an octapeptide repeat region (*Figure 1.1*). The C-terminal globular domain of PrP^C is comprised of three α-helices which make up 42% of the protein, and only 3% β-sheet structure (Pan et al. 1993). α-helixes 2 and 3 are stabilised by the presence of a disulphide bond that forms between cysteine residues at amino acids 179 and 214 in murine PrP^C (Riesner 2003). Recycling of PrP^C occurs via an endocytic pathway, where the protein is transported back into the cell by endosomes via multiple mechanisms that involve clathrin-coated pits and caveolae (Taylor and Hooper 2006; Peters et al. 2003). After internalisation, which can be influenced by the GPI anchor of PrP^C (Kaneko et al. 1997), into early endosomes, it is either recycled back to the plasma membrane via recycling endosomes or is routed to the lysosomes for degradation via late endosome/multivesicular bodies (Campana, Sarnataro, and Zurzolo 2005). The structures of human, murine, bovine and hamster PrP^C as determined by Nuclear Magnetic Resonance (NMR) are remarkably similar (Wüthrich and Riek 2001).

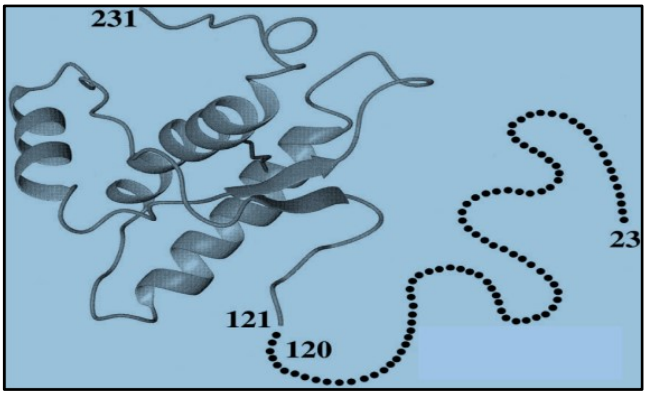

Figure 1.2: Structure of murine recombinant PrP as determined by NMR. C-terminal domain (121-231) comprises most structured region with three α-helices and two β-strands. Amino acids (23-120) make up the random coil of the protein. Sourced from (Riek et al. 1997).

1.2.3 Function of Cellular PrP (PrP^C)

The cellular isoform PrP^C is expressed most abundantly in the brain (Zomosa-Signoret et al. 2007). Early in embryogenesis (D9) it is evident that mouse brains express PrP^C mRNA and as development continues, the level of PrP mRNA increases (Manson et al. 1992). In the adult murine central nervous system, PrP^C and its mRNA are widely distributed with specific concentrations in neocortical, hippocampal and spinal cord neurons (Kretzschmar et al. 1986). Despite extensive research, the precise function of PrP^C is not yet known. Proposed roles include cell signalling, formation and maintenance of synapses, promotion of neuronal growth and survival, protection against oxidative stress and involvement in cellular uptake or binding of copper ions (Brown 2003). Other studies suggest that PrP^C plays an important role in the modulation of neuronal survival, both *in vivo* (Harris 2003; Walz et al. 1999) and *in vitro* (Chiarini et al. 2002; Kuwahara et al. 1999) supported by experimental data showing that PrP^C is a specific receptor for the C-terminal domain of the γ-1 chain of extracellular matrix laminin. After binding to the laminin γ-1 chain neuronal growth is promoted through an unknown intercellular signaling pathway (Graner, Mercadante, et al. 2000a; Graner, Mercadante, Zanata, Martins, et al. 2000).

Interestingly both the 37kDa laminin receptor precursor and the 67kDa laminin receptor have also been identified as endocytic receptors for PrP^C on the cell surface that mediate the internalisation and recycling of PrP^C through clathrin coated pits (Gauczynski et al. 2001; Rieger et al. 1997). PrP^C was also shown to be involved in the fyn kinase pathway where the protein binds to the Neural Cell Adhesion Molecule (NCAM) promoting recruitment of NCAM to lipid-rafts which also promoted neurite outgrowth further supporting a role for PrP^C in neuronal survival (Santuccione et al. 2005). Other studies have demonstrated interactions between PrP^C and cell-surface stress inducible protein 1 (STI1) which mediates neurogenesis and neuroprotection of hippocampal neurons (Zanata et al. 2002). This protective effect was shown to be dependent on the cAMP/protein kinase A (PKA) signalling pathway where PrP^C was described to function as a trophic receptor (Chiarini et al. 2002).

PrP null mice (*Prnp*$^{-/-}$) have a grossly normal neurological phenotype, however, they do have subtle abnormalities in synaptic transmission, hippocampal morphology, circadian rhythms, cognition and seizure threshold (Zomosa-Signoret et al. 2007). *Prnp*$^{-/-}$ mice are resistant to scrapie infection (Manson, Clarke, Hooper, et al. 1994; Bueler et al. 1993; Prusiner 1993) indicating an essential role for the presence of normal cellular PrP^C to establish TSE disease. Furthermore, sub-passage studies of *Prnp*$^{-/-}$ mouse brain into wild-type CD-1 mice indicated no transmission of asymptomatic disease demonstrating that the infectious agent had not been replicated during the primary passage (Prusiner 1993). Additionally heterozygous mice (*Prnp*$^{-/+}$) were shown to have enhanced resistance to disease, with extended incubation periods to clinical disease indicating a dose-dependent effect of *Prnp* expression. The heterozygous expression of *Prnp*$^{-/+}$ did not affect the distribution of either TSE associated vacuolation or PrP^{Sc} deposition observed at the clinical stage of the disease (Manson, Clarke, McBride, et al. 1994). The level of PrP^C expression therefore influences the length of incubation period in a dose-dependent manner and thus, it can be concluded that the host PrP^C is required to support TSE infection. Other studies demonstrated *Prnp*$^{-/-}$ mice to

be more resistant to the neurotoxic effect of Aβ oligomers than WT mice in both *in vivo* and *in vitro* models (Kudo et al. 2012). They found that blocking Aβ/ PrP^C binding using anti-PrP antibody or competitive PrP peptide rescues Aβ oligomer-induced neuronal cell death suggesting PrP^C is an essential co-factor in mediating Aβ oligomer neurotoxicity. Conversely, PrP^C was shown to be capable of binding and detoxifying Aβ oligomers (Biasini et al. 2011). Collectively these data demonstrate a role for PrP^C in Aβ oligomer-induced neurotoxicity however; the precise mechanisms remain to be fully elucidated.

1.2.4 Prion Hypothesis

Many hypotheses have been put forward to explain the disease mechanisms of TSEs. However over-time, and in correlation with numerous key observations carried out in the TSE scientific field, the prion hypothesis proposed by Stanley Prusiner has become the most accepted paradigm (Kuhn 1996; Prusiner 1982). This hypothesis states that the transmissible agent in TSE disease is a misfolded protein called a “prion”, a term derived from its description as being a proteinaceous infectious particle, which is able to reproduce itself in the apparent absence of nucleic acid (Legname et al. 2004; Prusiner 1998). The infectious agent according to Prusiner’s hypothesis is composed largely, if not exclusively, of a single kind of protein molecule named the protease-resistant, conformationally altered prion protein (PrP^{Sc}) which is resistant to inactivation by most procedures that modify nucleic acids (Prusiner 1982). This abnormal form of protein acts as the infectious agent in TSE disease, catalysing the conversion of the normal cellular PrP^C into the misfolded PrP^{Sc} form. Other key observations in support of this hypothesis included analysis of PrP^{Sc} concentrations in relation to titre of infection whereby results demonstrated that the majority of PrP^{Sc} was found in sucrose fractions with the highest infectivity titre (McKinley, Bolton, and Prusiner 1983). Furthermore, scrapie-associated fibrils (SAF), with amyloid-like properties identified from murine and hamster TSE models were found to be associated with infectivity (Hilmert and Diringer 1984; Merz et al. 1981). Post-mortem

analysis of tissue from infected animals using anti-SAF (Scrapie-associated fibril) antibodies also displayed accumulation of disease-associated PrP deposition in the brain (Farquhar, Somerville, and Ritchie 1989; McBride, Bruce, and Fraser 1988). All these forms of PrP^{Sc} and SAF have been identified from TSE-infected brain tissue where the prion hypothesis suggests PrP^{Sc} is the infectious agent of TSE disease (Kascsak et al. 1985; Merz et al. 1981).

In contrast studies carried out in our laboratory have questioned the correlation between PrP^{Sc} levels and titre of infectivity, showing that tissues containing minimal proteinase K-(PK) resistant PrP (PrP^{-res}) can be infectious and harbour high titres of TSE infectivity (Barron et al. 2007), and that accumulation of prion protein in the brain may not be a reliable marker of these transmissible diseases (Piccardo et al. 2007). Additionally a separate study identified the presence of low levels of detergent insoluble aggregated PrP and PrP^{-res} in uninfected human brains using sedimentation and size exclusion chromatography (Yuan et al. 2006) indicating abnormal PrP levels may be present in all brains but at very low levels. This highlights the requirement that further work must be carried out to enhance our overall understanding of these neurodegenerative diseases.

1.3 Altered forms of PrP^C and amyloid fibril generation

1.3.1 Altered isoforms of PrP

PrP^C and PrP^{Sc} have been shown to have the same primary structure (Stahl et al. 1993). Differences are found in the secondary, tertiary and quaternary structures where the abnormal PrP^{Sc} has an increase in β-sheet content (43%) and less α-helix content (30%) than the protein in its normal conformation described previously in Section 1.2.2 (Pan et al. 1993). This conformational change is thought to occur through a seeded-nucleation model where PrP^{Sc} acts as the template for the conversion of native PrP^C to an abnormal form (Kocisko et al. 1994) which is protease-resistant, and insoluble in non-denaturing detergents. After protease treatment, normal PrP^C (33–38 kDa) is completely digested (*Figure 1.3*) however, PrP^{Sc} (27–30 kDa) is partially resistant to the enzyme with only 62 N-terminal amino acids being cleaved, leaving a core fragment of 141 amino acids (Jarrett and Lansbury 1993; Oesch et al. 1985). Sodium Dodecyl Sulphate Polyacrylamide Gel Electrophoresis (SDS-PAGE) followed by immunoblotting of PK-digested brain tissue detects PrP^{Sc} banding and can be used to diagnose TSE infected tissues (Towbin, Staehelin, and Gordon 1979). PrP^{Sc} profiles are generated based on the relative amounts and molecular weights of the diglycosylated, monoglycosylated and unglycosylated forms of the protein and can inform on disease type/agent (*Figure 1.3*). These specific profiles of glycoform ratios and molecular weights have supported the probability of a bovine origin for variant Creutzfeldt-Jakob disease (vCJD), a form of CJD disease first reported in the UK in 1996 (Will et al. 1996). Profiles from sporadic or iatrogenic forms of CJD are quite different from those of vCJD and BSE (Hill et al. 1997; Collinge et al. 1996). These are examples of how differences in abnormal protein tertiary structure and post-translational modifications can be used to determine the nature and origin of prion diseases.

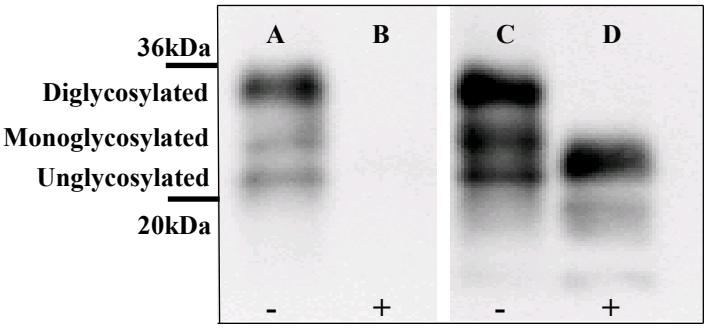

Figure 1.3: Glycosylation profiles obtained from mouse brain homogenates. (A-B) Uninfected mouse brain and (C-D) Scrapie ME7 infected mouse brain -/+ proteinase K treatment. Sodium Dodecyl Sulphate Polyacrylamide Gel Electrophoresis (SDS-PAGE), antibody7A12.

1.3.2 Different types of protein conformations

Many conformational states of native proteins may be present in a biological environment at any one time including amyloid (*Figure 1.4*). Amyloid is an extremely well structured aggregate of abnormal protein. The processes or pathways leading to amyloid formation are still poorly understood however, accumulation of these amyloid aggregates is a hallmark of many neurodegenerative disorders such as TSEs (prion protein), PD (α-Synuclein), ALS (superoxide dismutase) and AD (amyloid β peptide). From a morphological point of view protein aggregates or amyloid may be differentiated into two types; amorphous aggregates which consist mainly of disordered polypeptide chains or amyloid fibrils which are highly organised with repetitive structures where all polypeptides adopt a common fold (Invernizzi et al. 2012). Furthermore, amyloid fibrils, or plaques, are used to describe structures formed extracellularly, whereas the term intracellular inclusions refers to fibrils formed inside the cell (Westermark et al. 2005). Amyloid-associated disorders have a major impact on the elderly regarding degenerative pathologies and therefore are of huge concern in a rapidly aging world. Thus, understanding mechanisms associated with amyloid fibril formation, interactions in the brain or the failure of proteins to adopt or remain in their native functional conformational state is vital to progress our understandings of neurodegenerative diseases.

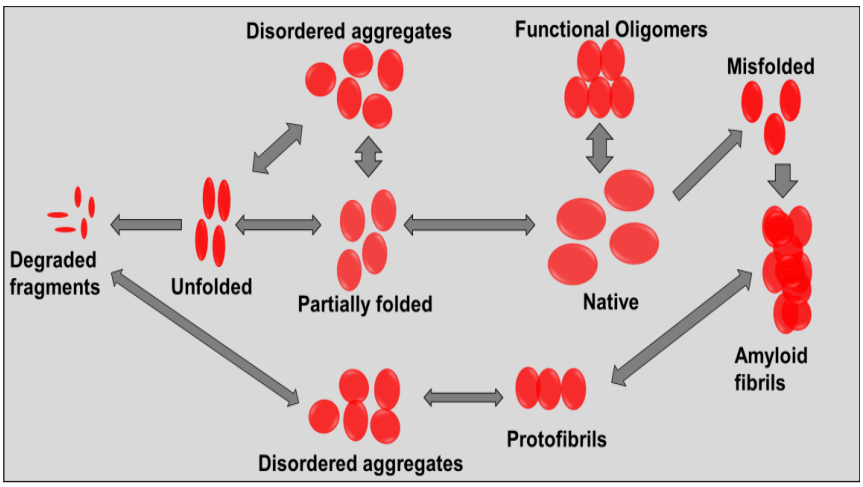

Figure 1.4: Schematic of the many complex conformational states that may be adopted from native protein. In a healthy biological environment, all of these different conformational states (refolding, ordered or disordered aggregate formation, and degradation) are constantly regulated using machinery such as molecular chaperones, degradatory systems, and quality control processes. Failure of these mechanisms triggers abnormal events, which in turn disturb factors such as axonal transport, and ion balance eventually leading to cell death. Adapted from (Chiti and Dobson 2006).

The nucleation-polymerisation model shown in *Figure 1.5* describes how the fibril amyloid assembly process occurs *in vitro* via nucleated polymerisation, where the initial nucleation step begins slowly. However after nucleation, polymerisation occurs more rapidly as the folding intermediate is capable of serving as a template (also known as a seed) for further conformational fibril growth (Jarrett and Lansbury 1993). This growth involves association of either monomers or oligomers with the nucleus (Chiti and Dobson 2006). The time required for the nuclei to form from soluble species (monomers) is referred to as the thermodynamically disfavoured lag phase and this time can be significantly shortened and ultimately abolished by the addition of a pre-formed nucleus or seed. Polymerisation and fibril growth is referred as the exponential phase, where eventually the exhaustion of monomers leads to a saturation phase where no more soluble species can associate to the ends of preformed fibrils resulting in fibril maturation (Invernizzi et al. 2012). Remarkably, it seems that all proteins which form amyloid may progress through the same intermediate steps (Kayed et al. 2003).

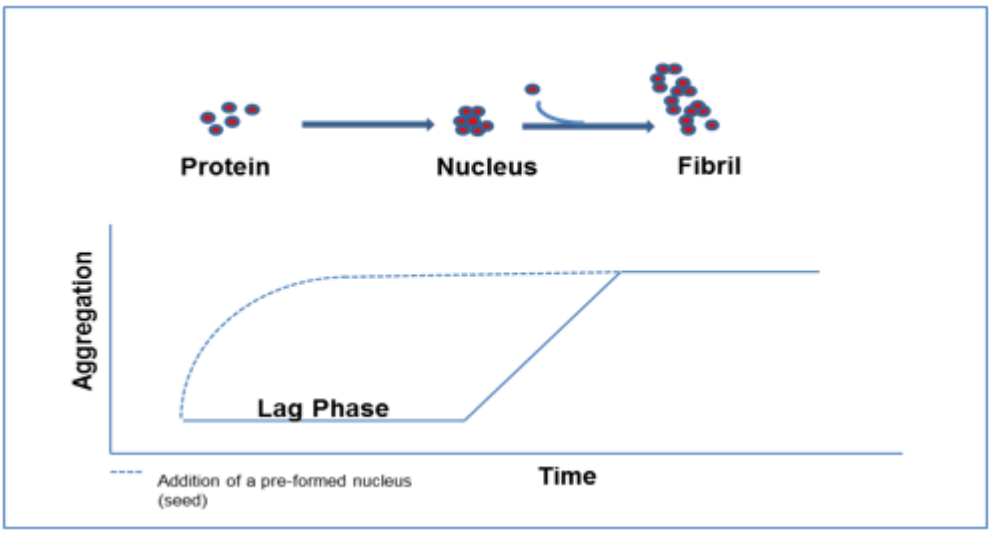

Figure 1.5: Nucleation-polymerisation model/ kinetics. Thioflavin (ThT) assays are used to measure change in fluorescence intensity of ThT upon binding to amyloid fibrils. Congo red binding, X-ray crystallography and transmission electron microscopy are other alternative techniques utilised for the examination of amyloid. Adapted from (Nilsson 2004).

Not all amyloid is pathological. Functional amyloid exists and is involved in many different biological processes, which can be physiologically useful for specific and specialised biological functions (Table 1.2). However, this is a highly regulated assembly process and if not tightly controlled could result in the occurrence of protein conformation associated diseases.

Protein	Organism	Function
Premelanosome protein (Pmel17)	*Homo sapiens*	Forms inside melanosomes, binds and orients reactive melanogenic precursors
Curlin	*Escherichia coli*	Colonise inert surfaces and mediate binding to host proteins
Neuron-specific isoform of Cytoplasmic Polyadenylation Element Binding	*Aplisia californica*	Promotes long-term maintenance of synaptic changes associated with memory storage

Table 1.2: Naturally nonpathological amyloid-like fibrils with specific functional roles (Chiti and Dobson 2006; Kocisko et al. 1994).

1.4 PrP P101L Mutation and GSS

1.4.1 Gerstmann-Sträussler-Scheinker (GSS) Disease

Human prion diseases can be hereditary or acquired or can even arise sporadically. It is estimated that between 5-15% of human prion diseases are inherited and linked to disease-specific mutations in the prion protein gene (*PRNP*). Furthermore, the methionine/valine homozygosity at the polymorphic codon 129 of *PRNP* may cause a predisposition to diseases such as sporadic and iatrogenic CJD (Salvatore et al. 1994; Brown et al. 1994; Palmer et al. 1991; Collinge, Palmer, and Dryden 1991). This association between codon 129 polymorphism and accelerated pathogenesis is not evident in familial CJD patients (codon E200K mutation) or in GSS patients with the codon P102L mutation (Hainfellner et al. 1995; Gabizon et al. 1994; Barbanti et al. 1994). GSS is defined as a rare autosomal dominant disorder characterised clinically by progressive ataxia followed by a late onset of dementia (Liberski 2012). Patients diagnosed with GSS are normally between the ages of 20-60 years old where disease duration can range from a few months to a few years. GSS is characterised by the presence of multi-centric amyloid plaques derived from abnormal PrP and is also distinguished from other human TSEs using immunoblot analysis to show the presence of N- and C-terminal truncated PrP^{Sc} fragments ranging between 6 and 10 kDa and variable numbers of bands of higher molecular weight (Ferrer et al. 2011). The majority of cases of GSS found in Japan (Doh-ura et al. 1989), Britain (Hsiao et al. 1989), Italy (Kretzschmar et al. 1992), and France (Laplanche 1994) are linked to the P102L mutation in *PRNP*, and result in the substitution of proline (CCG) by leucine (CTG), creating an additional DdeI restriction endonuclease site within exon 3 of the *PRNP* gene. One study involving a large Italian family affected by this GSS P102L mutation, showed family members to have remarkable phenotypic variability of the disease with no correlation between clinical presentation and the codon 129 genotype (Barbanti et al. 1996).

Conversely, others have proposed a genotype-phenotype relationship with the genetic polymorphism at residue 129 between methionine and valine (Bianca et al. 2003), suggesting strain specific differences in clinical manifestation were evident. Several further mutations in *PRNP* are also causative of GSS disease namely P102L^{M}, P105L^{V}, A117V^{V}, G131M^{V}, Q160X, H187R^{V}, F198S^{V}, D202N^{V}, Q212P^{M}, Q217R^{V}, Y218N, Y226X, Q227X and M232T (Valine^{V}, Methionine^{M} on same allele) (Imran and Mahmood 2011; Liberski and Budka 2004). Transmission experiments of P102L GSS disease to nonhuman primates have shown efficient transmission of infectivity to primates including squirrel monkeys, spider monkeys and marmosets (Baker et al. 1990; Tateishi et al. 1988). However to date no cases of GSS disease caused by human to human transmission have been reported (Liberski 2012).

Genotype	Age of	Duration	Clinical/Pathological signs
P102L-129M	30-62	1-10	Dementia, amyloid deposition in cerebellum, spongiosis, neuronal loss and astrogliosis, no neurofibrillary tangles (NFT's)
P102L-129M- 219K	31-34	4	Fewer plaques and no spongiosis (comparison to above)
P102L-129V	33	12	Seizures, gait difficulties, widespread plaques, no dementia/spongiosis
P105L-129V	40-50	6-12	Late dementia, amyloid plaques, neuronal loss, gliosis, no spongiform changes/ NFT's
F198S-129V*	34-71	3-12	More extensive amyloid deposits (than P102L-129M-219K). NFT's in cerebral cortex, discreet spongiosis

*Phenylalanine (TTC) to serine (TCC) substitution at codon 198 on a Val 129 allele.

Table 1.3: Genotype and corresponding phenotype of inherited GSS diseases. Adapted from (Mattson 2000).

1.4.2 101L Mutation

A number of different transgenic murine models have been produced to model the P102L (proline to leucine, corresponding mutation in murine PrP is P101L) point mutation which is the most common point mutation present in human GSS disease (Table 1.4).

Transgenic Identification	PrP^{C} Expression rate	Spontaneous disease	Reference
MoPrP-P101L Tg174 (64 times gene copy)	8-fold higher than wild-type	Yes, ataxia, low levels of PrP^{Sc}, absence of plaques (166d)	(Telling et al. 1996; Hsiao et al. 1991; Hsiao et al. 1990)
101LL (Produced by gene targeting)	WT levels of mutant protein	No signs of neurological disease (900d)	(Manson et al. 1999)
Tg196/*Prnp*$^{-/-}$ (9 copies of the transgene)	2-fold higher than wild-type	Yes in aged 400-600d mice	(Tremblay et al. 2004; Kaneko et al. 2000; Telling et al. 1996; Hsiao et al. 1994)
Tg(GSS)2*,6*,12* 22*	0.5-1, 3, 6, and 12 fold respectively	Yes, (except Tg(GSS)2 line which only expresses 2 copies of the transgene	(Nazor et al. 2005)

*Copies of transgene expressed

Table 1.4: Examples of some of the transgenic murine mouse lines developed to further our understanding of GSS disease.

As shown in Table 1.4, disease was only noted in mice overexpressing PrP^C and no signs of disease were reported in knock-in (gene replacement) 101LL transgenic mice. This may be due to the fact that 101LL mice were produced using gene targeting (not random insertion), where the 101L mutation was introduced into the endogenous murine *Prnp* gene in 129/Ola (WT) mice resulting in expression of PrP^C at the same levels as WT mice (Manson et al. 1999). This double replacement gene targeting method effectively generated 101LL transgenic mice (Manson et al. 1999; Moore et al. 1995).

All mammalian prion protein sequences (*Figure 1.6*) show a great deal of similarity and this homology could facilitate the transmission of prion disease between species.

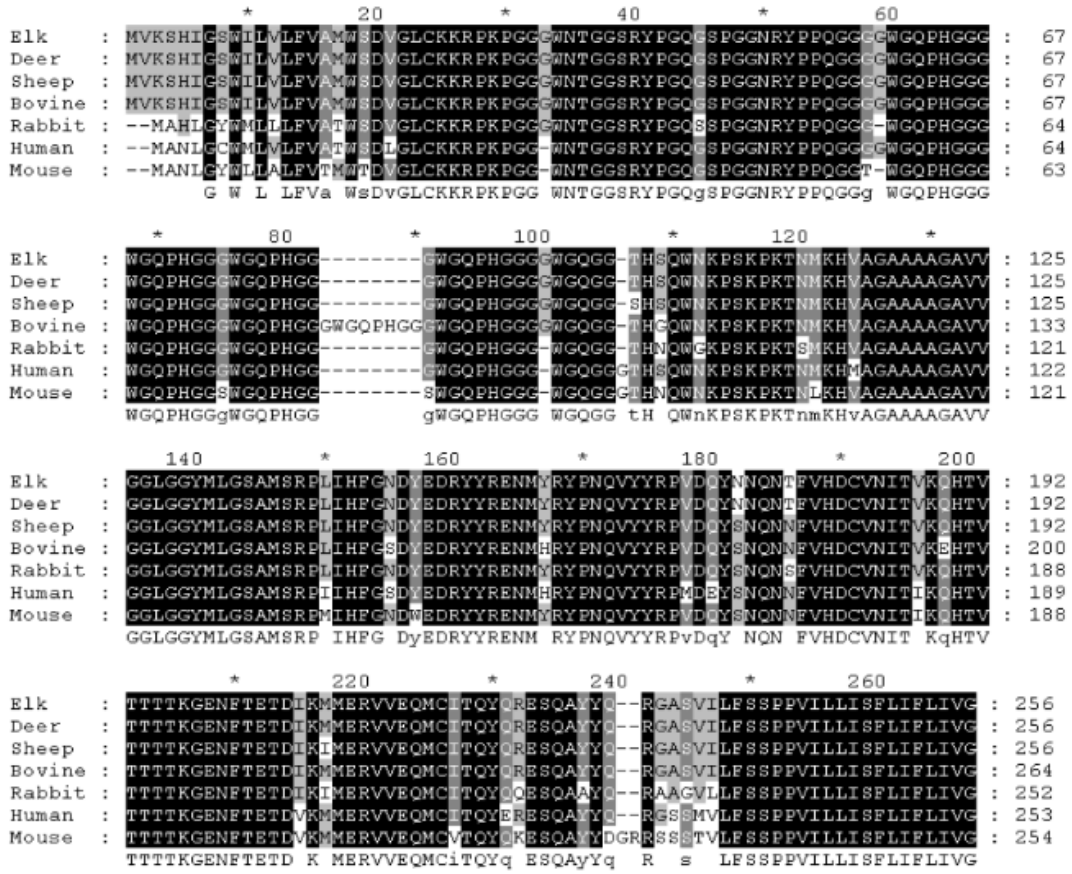

Figure 1.6: Alignment of PrP amino acids from elk, deer, sheep, bovine, rabbit, human and mouse species. Original source Pandeya et al. 2010; ISSN: 0976-1683; alignment with ClustalW.

1.5 Synthetic protein, cellular interactions and processing pathways

1.5.1 *In vitro* generated recombinant PrP and challenge experiments

Recombinant PrP can be produced in *Escherichia coli* and consequently, can be used to investigate the structure of PrP^C (Makarava and Baskakov 2008). In addition, various treatments using Guanidine-HCL (Gdn-HCl) and urea can change this predominantly α-helical structure into a structurally altered isoform that can be used to study the disease causing properties of refolded PrP in the brain in the absence of additional co-factors. Bacterially expressed recombinant PrP does however lack post-translational modifications found in eukaryotic PrP^C as it is not glycosylated and lacks a GPI anchor (Kirby et al. 2003). Previous work by our group examined whether *in vitro* generated misfolded fibril recombinant PrP was actually infectious *in vivo* and if it was capable of seeding further misfolded protein in the brain (Barron et al. 2016). To investigate this various forms of α-monomeric, β-oligomeric and fibril amyloid (both 101L and WT recombinant PrP) were inoculated by intracerebral (IC) injection into the brains of 101LL and WT mice and results indicated recombinant PrP (of any isoform) did not cause clinical TSE disease and both α-monomeric and β-oligomeric isoforms were not capable of initiating seeding of PrP aggregation in mice of both genotypes. In contrast, the recombinant PrP fibrils (both WT and 101L forms) did seed the formation of amyloid plaques in 101LL mice but not in WT. This indicated that the 101L mutation in the host PrP was the important factor in this unique proteinopathy seeding model. Additionally, it was concluded the tertiary conformation of the inoculated material and not the primary amino acid sequence was important for the initiation of a seeding pathway, which targeted the hippocampal and corpus callosum areas of the brain. Subpassage of brain material from donor 101LL challenged mice (that contained seeded PrP amyloid plaques) into host 101LL recipients displayed an overall increase in deposition load of fibril amyloid deposits in the brain in comparison to primary brain tissues but the same areas of the brain were targeted.

It was postulated that a gain in GPI anchorage increased the efficiency and capability of the subpassaged inoculum to convert more native PrP^C into its abnormal form upon subpassage. In summary misfolded PrP seeding was observed in 101LL and not WT mice. The amyloid fibrils formed did not cause an infectious prion disease, rather a proteinopathy. WT mice were capable of efficient clearance of recombinant fibrils and therefore curtailed seeding mechanisms from initiating.

Studies by other laboratories have shown TSE disease initiation and transmission was possible following intracerebral inoculation of refolded recombinant PrP in hamsters/mice (Raymond et al. 2012; Makarava, Kovacs, Savtchenko, Alexeeva, Budka, et al. 2012; Makarava et al. 2010; Legname et al. 2004) however, these studies used different transgenic models and fibrilisation methods which seemed to generate infectious fibril aggregates (Colby et al. 2010). One study clearly demonstrated that inoculation with recombinant PrP fibrils formed in 2M Gdn-HCl does not cause infection and prion disease however, challenge with a more unstable 0.5M Gdn-HCl fibril form does cause disease in Syrian hamsters (Makarava, Kovacs, Savtchenko, Alexeeva, Ostapchenko, et al. 2012). Other factors such as dose and volume inoculated were also crucial to disease generation where many experiments claiming transmission of disease were dosing at volumes of up to 50µl at variable concentrations of up to 10µg of misfolded protein (mostly not noted in publications but through personal communication) which may overload systems important for protein clearance. In comparison, our group inoculated at much lower volumes and concentrations (1.4µg/20µl), which may be more physiologically relevant to disease. Additionally further studies have used magnetic beads to deliver fibril material to the brain which maximised the impact of the inoculum by enhancing the persistence of the fibrils (Raymond et al. 2012). Taking all these data into account further examination of seeding mechanisms and PrP fibril amyloid interactions in the brain in physiologically relevant conditions will need to be carried out to broaden our knowledge and understandings of misfolding protein diseases.

Despite this, the differences in the processing of recombinant PrP fibrils in WT and 101LL mice provide us with a useful tool to determine host-causative factors that either support or curtail the formation of abnormal protein fibrils.

1.5.2 Neuronal and glial interactions with PrP

One of the key features associated with PMDs is the ability of the abnormally folded proteins to seed and propagate in a "prion-like" manner and spread from neurons to neighbouring neurons and glia (Pearce et al. 2015; Brettschneider et al. 2015). However, the mechanisms involved are poorly understood and therefore this is an area of active investigation. Highest levels of PrP^C expression are found in neurons and therefore much research has focused on the role of neuronal populations in defining mechanisms associated with protein misfolding in prion disease. Studies have shown that transgenic mice, which only express PrP^C in their neurons, are susceptible to TSEs (Race et al. 1995). Furthermore, it has been shown that manipulating PrP^C expression in neurons during specific time points of a TSE disease resulted in the reversal of spongiosis and behavioural deficits in these models (Mirabile et al. 2015; Mallucci et al. 2007; Mallucci et al. 2003). Although pre-symptomatic incubation periods could be lengthened by reducing neuronal PrP^C throughout the preclinical phase of disease, all animals ultimately developed a neurodegenerative disease (Manson 2011).

Prnp mRNA expression is also present in non-neuronal cell types in the CNS such as astrocytes and microglia (Baker, Martin, and Manuelidis 2002; Moser et al. 1995; van Keulen et al. 1995). Studies have shown abnormal PrP accumulation in astrocytes was evident in TSE models suggestive of an involvement of this cell type in replication of abnormal PrP (Diedrich et al. 1991). Additionally other reports have shown that transgenic mice expressing PrP^C only in astrocytic cell populations were susceptible to TSE disease indicating that PrP expression in these specific cell types alone was sufficient to cause neurodegeneration (Raeber et al. 1997).

Astrocytes are extremely sensitive to any changes in the homeostasis of the brain and responses to misfolded proteins can be seen early in the course of disease by up-regulation of glial fibrillary acidic protein (GFAP) alongside hypertrophy of the cell bodies (Sofroniew 2009, 2005; Schenk et al. 1999). Studies have also shown astrocytes are capable of forming numerous intracellular connections including tunnelling nanotubes, often found colocalised with endolysosomal vesicles, which are capable of cell to cell transfer of misfolded PrP (Victoria et al. 2016). Microglia are another cell type sensitive to any environmental changes in the brain and are shown to change their morphology after activation at early stages of TSE disease (Perry and Teeling 2013). Inhibition of microglial proliferation can result in increased TSE incubation times suggesting microglial response is important in disease progression (Gómez-Nicola et al. 2013). Conversely, other studies have shown microglial-dependent neurotoxicity is induced after amyloidogenic polypeptide challenge *in vitro* and is associated with the progression of neurodegenerative disorders (Thellung et al. 2017). Microglial immune responses to TSE disease are accompanied by mixed cytokine responses including mediators of both inflammatory (IL-6) and anti-inflammatory responses (*Tgfb1*) (Boche et al. 2006; Perry, Cunningham, and Boche 2002). Genetic knockout models of genes associated with these innate immune responses can influence incubation periods of TSE diseases (Bradford and Mabbott 2012) for example, knockout or knockdown of *Tgfb1* shortens disease incubation times (Tamguney et al. 2008; Lacasse et al. 2008; Thackray et al. 2004). On the other hand, studies using AD models deficient in microglial response (APP transgenic mice crossed with chemically activated microglial suicide gene) have shown that there was no effect on plaque size or number when microglia were ablated suggesting they were not critically involved in Aβ plaque formation and clearance in the brain (Grathwohl et al. 2009). Interestingly, other studies have shown stimulating bone marrow-derived macrophages using macrophage colony stimulating factor (M-CSF) cleared amyloid plaques through lysosomal-dependent mechanisms (Boissonneault et al. 2009; Majumdar et al. 2007).

Microglia are capable of both engulfment and phagocytosis of Aβ fibril material, but whether this misfolded protein can be degraded intracellularly remains controversial (Lee and Landreth 2010). Research in our lab has shown both activated microglia and reactive astrocytes were present at the periphery of amyloid plaques seeded by fibril recombinant PrP inoculation indicating these cell populations do play are role in maintaining normal brain homeostasis after recombinant fibril insult (Barron et al. 2016). The predominantly neuroprotective role of microglia suggested in prion diseases may also be applicable to other neurodegenerative disorders and could broaden our understanding of the role of neuroinflammation (Aguzzi and Zhu 2017). In summary, non-neuronal cells are also involved in neurodegeneration and are associated with misfolded protein in the brain however, it is not clear whether their activation is in response to damaged neurons, abnormal proteins or other CNS danger signals.

1.5.3 Misfolded PrP processing and degradation pathways

Protein quality control is essential for cell viability and is essential for targeting rogue proteins towards degradation pathways. Any alterations in this homeostasis can be highly detrimental to the cell eventually leading to death (Wolfe and Cyr 2011). While most misfolded aggregates can be degraded and cleared by cellular protein control, some native and mutant proteins can be resistant to all known proteolytic pathways resulting in the formation of inclusion bodies or extracellular plaques (Ciechanover and Kwon 2015). Additionally the ability of cells to deal with misfolded protein seems to decline with age and response can vary between cell types (Cuervo et al. 2005). When PrP aggregate load increases beyond the tolerance limit of a cell, various intracellular quality control mechanisms can be affected. Lysosomal quality control machinery, which acts as a terminal degradative compartment of cells, emerges as one of the primary pathways overwhelmed during the pathogenesis of TSE diseases (Majumder and Chakrabarti 2017).

Endolysosomal pathway studies have shown that the majority of abnormal PrP is found in the endolysosomal system (Yao et al. 2013; Jeffrey et al. 2010) and in prion-infected brain tissue organelles such as late endosomes, lysosomes and autophagic vesicles are increased in size and numbers (Sikorska 2004; Boellaard et al. 1991). Aberrations in the endolysosomal system have also been observed in neurons from human sporadic CJD brains (Kovacs et al. 2007) and disease was associated with blockages in lysosomal degradation where autophagosome-lysosome fusion was impaired (Majumder and Chakrabarti 2015). Interestingly, our studies have shown when the brains of 101LL mice with plaques were analysed by electron microscopy (EM), large numbers of lysosomes were found in cells surrounding mature plaques however, no intra-lysosomal PrP accumulation was evident (Barron et al. 2016). Inundation of these quality control mechanisms have also been reported in a number of other neurodegenerative diseases such as AD, PD and ALS (Majumder and Chakrabarti 2017). Studying these specific pathways after challenge with PrP fibrils may allow us to determine which conditions result in fibril amyloid generation/accumulation and which favour clearance. Routes involved in delivering misfolded proteins to lysosomes include endolysosomal, endoplasmic reticulum quality control (ERQC), Golgi QC and autophagic pathways (Saftig and Klumperman 2009). Interestingly, all of these independent pathways show signs of convergence which ensures efficient removal of unwanted cellular components (Nixon 2013). Proteins translocated directly to the endoplasmic reticulum (ER) during synthesis are monitored by specialised quality control systems within the ER lumen (ERQC), where any misfolded or defective proteins are translocated to the cytosol for degradation. This is known as the ER-associated degradation (ERAD) pathway where rogue proteins are targeted for lysosomal degradation by autophagy (Araki and Nagata 2011). Studies have shown misfolded PrP cannot be recognized and efficiently degraded by this system (Ashok and Hegde 2008). Other cellular compartments are also involved in misfolded protein clearance such as the Golgi quality control (Golgi QC) pathway which again directs abnormal proteins for lysosomal degradation (Anelli and Sitia 2008; Arvan et al. 2002).

More mature proteins associated with misfolding or aggregation are also subject to similar QC measures where degradation of soluble aggregates is aided by heat shock protein (Hsp) Hsp40, Hsp70 and Hsp100 chaperones (Kim et al. 2013). Neighbor of BRCA1 gene 1 (NBR1) and Nucleoporin p62 (p62) are common adaptor proteins, which target insoluble aggregates for degradation (Kirkin et al. 2009; Bjorkoy et al. 2005). This process involves either two pathways namely, the ubiquitin-proteasome system (UPS) or the lysosomal proteolysis/ autophagic pathway. UPS is the principal route of abnormal protein degradation where mutations in different components of the system have been identified in patients with AD, PD and HD diseases (van Leeuwen et al. 2006; Kitada et al. 1998). Rogue proteins are targeted for proteasomal degradation by covalent conjugation of ubiquitin (Ub) in a sequential reaction involving three enzymes [(ubiquitin activating enzymes (E1), ubiquitin conjugating enzymes (E2) and ubiquitin ligases (E3)] that recognise and transfer Ub to an internal lysine residue on substrate proteins. These substrates are deubiquitinated, unfolded and cleaved into small peptides and delivered to and degraded by lysosomes via the chaperone mediated autophagy (CMA) pathway. However, this pathway may be restricted to soluble misfolded proteins only (Ciechanover and Kwon 2015; Bhat et al. 2014; Goold et al. 2013). Insoluble aggregates, too large for entry into the 20S catalytic chamber, can avoid effective degradation through UPS impairment which results in an upregulation of autophagy highlighting the interplay between the two degradatory systems (Scotter et al. 2014; Hao et al. 2013; Deriziotis et al. 2011; Korolchuk, Menzies, and Rubinsztein 2010; Nedelsky, Todd, and Taylor 2008). Autophagy is a highly conserved degradation system that is capable of aggregate degradation after delivery to lysosomes and involves either macroautophagy, microautophagy or chaperone-mediated autophagy (Majumder and Chakrabarti 2017).

Macroautophagy is the most important pathway for neuronal proteostasis (Kochergin and Zakharova 2016; Yao et al. 2013) and is associated with cytosolic aggregates resistant to both UPS and the CMA that are sequestered either directly by importation into late endosomes/lysosomes or by formation of double membrane bound vesicles derived from ER membrane called a phagophore and upon closure of this isolation membrane autophagosomes are formed (Lamb, Yoshimori, and Tooze 2013; Yao et al. 2013). Autophagosomes can fuse with lysosomes to form autolysosomes and this is the site where degradation of aggregates occurs. Autophagy-related proteins include LC3 protein (microtubule-associated protein 1 light-chain 3, lapidated form LC3-II) and p62 and these proteins are used as markers for studying autophagy (Pankiv et al. 2007). Increased detection of autophagosomes of various sizes have been associated with numerous neurodegenerative diseases such as AD, PD ALS and prion. These were found located in neuronal perikarya, neurites and synapses indicating autophagy may be up-regulated in these areas in these neurodegenerative diseases (Cai et al. 2016). Increased p62 (a marker of autophagy) expression in prion-infected brains may also reflect attempts to promote clearance of aggregates by autophagy (Homma et al. 2014). Abnormalities in lysosomal systems was observed in patients with prion disease where the number and size of autophagic vessels was show to increase in affected brains (up-regulation of autophagy) possibly indicating enhanced clearance of aggregated proteins (Liberski et al. 2010; Sikorska et al. 2004; Boellaard et al. 1991). Dual-labelling of both abnormal PrP and lysosomal markers confirmed co-localisation of misfolded PrP within these organelles (Dearmond and Bajsarowicz 2010). Studies have shown that deletion of autophagy related 5 (atg5) protein in mice, which is a key autophagy intermediate in the CNS, leads to behavioural deficits and accumulation of abnormal ubiquitinated proteins which form aggregates in neurons, eventually causing neurodegeneration in these mice (Hara et al. 2006). Abnormal levels of ubiquitinated protein are also found in the brains of prion infected animals, indicating these protein degradation pathways have failed to protect the host (Kristiansen et al. 2007).

In vitro studies have also shown autophagy to be the prominent pathway for abnormal PrP delivery to the lysosomes in infected cell cultures (Yao et al. 2013; Heiseke, Aguib, and Schatzl 2010), where any interference of autophagic components results in increased abnormal PrP levels. Conversely, by increasing autophagic pathways *in vitro* there is a decrease in abnormal PrP load (Homma et al. 2014; Goold et al. 2013; Heiseke et al. 2009; Aguib et al. 2009). Overall, induction of the autophagic pathway in neurodegenerative models has shown beneficial effects through degradation of associated aggregated proteins (Ozcelik et al. 2013; Yao et al. 2013; Ravikumar et al. 2004; Ertmer et al. 2004; Webb et al. 2003). Studies using neuroblastoma cells suggest the endolysosomal pathway is the main operative pathway for rapid misfolded protein clearance (Yamasaki et al. 2014). Similar results were reported in SN56 murine cell lines and primary hamster cell cultures where abnormal PrP was internalised by late endosomes and or lysosomes but not early endocytic, or raft-derived vesicles (Magalhaes et al. 2005). Indeed, studies have also shown that culture medium from infected cells can be infectious as infected cells release shedding vesicles (extracellular vesicles up to 1μm) and exosomes (50-100nm membranous vesicles) harbouring misfolded PrP (Mattei et al. 2009). These structures are generated by invagination of endosomal membranes to form intraluminal vesicles (ILVs) with MVBs. ILV sorting to lysosomes leads to degradation however, fusion of MVBs with plasma membrane followed by exocytosis leads of release of these extracellular infectious vesicles (Hartmann et al. 2017; Alais et al. 2008; Vella et al. 2007). It is possible that due to abnormal PrP overwhelming cellular internal protein QC mechanisms, an increase of ILV fusion with plasma membrane occurs resulting in increased exosomal release of abnormal PrP. Interestingly, exosomal PrP^{C} can also display protective properties in other PMDs by binding and detoxifying Aβ oligomers in AD (Biasini et al. 2011), which indicates under normal homeostatic conditions this may be a beneficial process.

Although the UPS pathway has also been shown to be involved in abnormal PrP degradation in infected cultured cells (Goold et al. 2013) *in vivo* studies have shown that ubiquitination of abnormal PrP was restricted to larger aggregates present at late stages of disease (Kovacs et al. 2005; Kang et al. 2004) and with low levels of colocalisation (Cammarata and Tabaton 1992), suggesting abnormal PrP is not ubiquitinated to a significant degree. These data highlight the intricacy of mechanisms of intracellular protein processing and clearance demonstrating the difficulty in underpinning specific defects induced by abnormal protein accumulation and also explain why to date, no therapeutic treatments are currently available for prion or other neurodegenerative diseases.

One novel approach involving targeting the unfolded protein response (UPR) pathway, which is important in prion pathology (Hetz and Mollereau 2014; Moreno et al. 2012), using a protein kinase RNA-like endoplasmic reticulum kinase (PERK) inhibitor has shown clinical improvements in prion-infected overexpressing PrP mice (Moreno et al. 2013). Eukaryotic initiation factor 2 alpha (eIF2α) is a key regulator of protein translation (Walter and Ron 2011) and is targeted by a number of signal transduction pathways involved in controlling protein synthesis (Clemens 2004; Deng et al. 2002; Harding, Zhang, and Ron 1999). Activity of eIF2α is inhibited by phosphorylation which then suppresses global protein synthesis (Walter and Ron 2011). The PERK inhibitor reduces chronic phosphorylation of eIF2α and prion toxicity by allowing neurons to tolerate a greater accumulation of abnormal PrP and these findings were evident in animals treated both at the preclinical stage and also later in disease (Moreno et al. 2012). Although these findings are encouraging the pathogenesis of prion, and other neurodegenerative diseases is multi-factorial, with many other factors contributing to toxicity which need to be examined (Aguzzi and Falsig 2012).

1.6 Thesis aims

1.6.1 Overview

Throughout this chapter, a number of unknown mechanisms and multi-factorial complexities have been associated with studying PMDs. Some studies have suggested abnormal proteins can be present at low levels in healthy brains (Yuan et al. 2006) indicating not all individuals are equally susceptible to neurodegeneration. However, the role of protein aggregates in neurodegeneration remains unclear, and early mechanisms involved in abnormal protein processing are poorly understood (Moreno-Gonzalez and Soto 2011). Due to this lack of understanding it is widely debated whether abnormal protein deposits are toxic to neurons or have a protective role (Wolfe and Cyr 2011; Treusch, Cyr, and Lindquist 2009; Haass and Selkoe 2007). Additionally, the role of alterations in protein quality control systems involved in maintaining homeostasis in the brain induced by abnormal protein challenge and age remains elusive (Gregersen and Bross 2010). It is crucial to better understand the mechanisms associated with initial processing of abnormal protein in PMDs to allow further investigation into how to promote their elimination without disturbing normal proteostasis of the cell. In addition, further understanding of the cellular interactions between neuronal and glial cells and their influence on the processing of misfolded protein are important factors that will contribute to the development of potential therapeutic treatments.

1.6.2 Thesis hypothesis and objectives

The main aim of this thesis is to gain more insight into these unknown mechanisms of cellular and molecular processing of abnormal protein using *in vitro* models composed of both neuronal and non-neuronal cell types challenged with misfolded recombinant PrP fibrils.

Cellular interactions and response, intra-cellular trafficking of abnormal protein, protein-protein interactions and molecular response will be analysed in genotypes which either support amyloid seeding and formation (101LL) or curtail its production (WT) to further understand factors that determine efficient clearance of abnormal protein.

Hypothesis: WT and 101LL mice have different mechanisms of intracellular processing of abnormal protein that determine clearance versus the seeding of amyloid plaques.

Objectives: The use of easily accessible cell cultures from transgenic mouse models that support the formation of amyloid plaques upon challenge with abnormal recombinant PrP (101LL) in comparison to cultures from mouse models that can clear abnormal recombinant PrP (WT) will allow the investigation of mechanisms involved in abnormal protein clearance that may be relevant to multiple PMDs. This project will focus on early cellular fibril interactions and the roles of multiple cell types involved in response to and processing of misfolded protein. Processing of misfolded protein will be further assessed at both the molecular and subcellular levels within these cultures.

Objective 1: Generation of appropriate *in vitro* brain culture models using both WT and 101LL genotypes.

Objective 2: Full characterisation of these cultures at a morphological, biochemical, and immunocytochemical level focusing on neuronal and glial cell populations.

Objective 3: Production and characterisation of both WT and 101L monomeric recombinant PrP.

Objective 4: Fibrillisation of monomeric recombinant PrP followed by labelling with a fluorescent tag.

Objective 5: Challenge *in vitro* models with fibrils and monitor early subcellular pathways associated with processing using various cell specific and organelle markers.

Objective 6: Transcriptomic comparison of gene expression profiles associated with WT and 101LL *in vitro* cultures pre/post challenge to distinguish pathways involved in misfolded protein processing.

CHAPTER 2

Materials and methods

2.1 Mouse Lines

All experiments were conducted under home office project licence (2010-2015 PPL 60-4125; 2015-2017 PPL 70-8523) within the regulations of the Animals (Scientific Procedures) Act 1986. Study numbers A820 and A821 were approved by Roslin's Animal Welfare and Ethical Review Body. CD-1 albino mice were obtained from Charles River, 129/Ola (WT/101PP) mice from Jackson laboratories, $PrP^{-/-}$ and 101LL knock in transgenic mice were generated in-house. WT mice were homozygous for the wild type PrP gene (101PP) and 101LL were homozygous for the P101L mutation (Manson et al. 1999; Manson, Clarke, Hooper, et al. 1994).

2.1.1 Housing

Mouse lines were maintained in a conventional animal facility with a 12 hour light and 12 hour dark cycle under specific pathogen free conditions at The Roslin Institute with access to food and water at all times.

2.1.2 In-House mice

101LL mice and $PrP^{-/-}$ were obtained from breeding colonies already established in-house. 101LL transgenics were generated as described in Chapter 1 (Section 1.4.2) using a double replacement gene targeting strategy (Manson et al. 1999; Moore et al. 1995), PrP-/- mice were generated as described previously (Manson, Clarke, Hooper, et al. 1994).

2.1.3 DNA extraction

Deoxyribonucleic acid (DNA) was extracted and purified from either mouse tail or ear punched tissues using the Qiagen DNeasy blood and tissue kit (Qiagen) according to manufacturer's instructions. DNA was eluted in a final volume of 100-200µl AE buffer then was stored at 4°C until further analysis.

2.1.4 Genotyping WT (101PP) and 101LL PrP transgenic mice

Mouse genotype was confirmed through a process of genomic amplification by polymerase chain reaction (PCR) and restriction enzyme digestion, which produced a lower banding pattern for the mutated 101L PrP gene. Two methods were used for amplification of the mouse genomic DNA.

Method One: PCR reaction buffer was prepared to the final concentrations: 1X PCR buffer (Invitrogen), 1.5mM magnesium chloride ($MgCl_2$, Invitrogen), 0.2mM dNTP's (Promega solution containing ATP, CTP, GTP, TTP), 2pmol/µl oligonucleotides A044<>A045:
A044:(5'-TCATCCCACGATCAGGAAGATGAG-3')
A045:(5'-ATGGCGAACCTTGGCTACTGGCTG-3'); 2 units DNA Taq polymerase (Invitrogen, 500 U). Isolated mouse genomic DNA (1-2µl) was added to the PCR reaction buffer and the reaction tube was placed in a T3 or T3000 Thermo-cycler (Biometra). PCR conditions for amplification of the mouse DNA were: 94°C for 3 minutes, followed by 30 cycles of 94°C for 30 seconds, 62°C for 30 seconds and 72°C for 1 minute. A 10 minute incubation at 72°C completed the reaction and DNA was stored at 4°C.

Method Two: Type-IT Mutation Detect PCR Kit (Qiagen). PCR reaction buffer was prepared to the final concentrations: 1X Type-IT mastermix, 0.3pmol/µl oligonucleotides A044<>A045 [20µl mixed stock oligonucleotides (1:1) prepared in 500µl TE Buffer (10mM Tris/HCl, 1mM EDTA, pH 8.0)] to a total volume of 25µl distilled water (dH_2O). Genomic DNA (1-2µl) was amplified using the following PCR conditions on the T3 or T3000 Thermo-cycler (Biometra): 95°C for 5 minutes followed by 35 cycles of 95°C for 30 seconds, 60°C for 90 seconds, 72°C for 30 seconds, 68°C for 10 minutes then cooled to 4°C.

2.1.5 Restriction Enzyme Digest

The amplified DNA product was digested with restriction enzyme *Dde*I (Promega, 1000 U) which identifies the leucine containing allele 101L due to the presence of an extra restriction site (101 mutation changes CCC-Proline to CTC-Leucine creating an additional *DdeI* site within exon 3) that is absent from proline allele 101P (Manson et al. 1999). The PCR product was digested with 0.1U *DdeI* (1000 U) in the presence of 1X Buffer D (final concentrations 6mM Tris/HCl, 6mM $MgCl_2$, 150mM NaCl and 1mM DTT) and 0.1mg/ml BSA (Promega) for 3 hours or overnight at 37°C. The digested PCR product was mixed with loading buffer (0.25% bromophenol blue (w/v), 0.25% xylene cyanol FF (w/v) in 20% ficoll solution, v/v) and gel electrophoreses was carried out using a 1.5% agarose gel (ThermoFisher Scientific) containing 1X concentration of SYPRO SAFE (Invitrogen) prepared with 1X TBE buffer (89mM Tris, 89mM boric acid and 3mM EDTA). A 1Kb ladder (Invitrogen) was used for sizing and quantification of DNA fragments and a positive and negative control were included for each reaction. DNA carrying the 101L allele produced a lower band of 464 base pair length whilst 101P produced a higher band of 614 base pair. The DNA banding pattern was visualised under UV light and photographed (Imager; Appligene Oncor).

2.1.6 Genotyping $PrP^{-/-}$ mice

PCR reaction buffer was prepared to the final concentrations: 1X PCR buffer (Invitrogen), 1.5mM $MgCl_2$ (Invitrogen), 0.2mM Deoxyribonucleotide triphosphate (dNTP's, Promega solution containing ATP, CTP, GTP, TTP), 2pmol/µl oligonucleotides Null A1<> Null A2:
Null A1: (5'- GCCATCACGAGATTTCGATT -3')
Null A2: (5'- ATCCCACGATCAGGAAGATG -3'), 2 units DNA Taq polymerase (Invitrogen, 500 U). Isolated mouse genomic DNA (1-2µl) was added to the PCR reaction buffer and the reaction tube was placed in a T3 or T3000 Thermo-cycler (Biometra).

The PCR conditions for amplification were: 94°C for 3 minutes, followed by 30 cycles of 94°C for 30 seconds, 62°C for 30 seconds and 72°C for 1 minute. A 10 minute incubation at 72°C completed the reaction before the sample was cooled to 4°C. This reaction did not require restriction digest. The PCR sample was analysed by gel electrophoresis and the 1.2Kb PCR product was visualised under UV light and photographed (Imager; Appligene Oncor).

2.2 Production and characterisation of primary neuronal cultures

Primary hippocampal neuronal cultures were prepared based on previously described methods (Seibenhener and Wooten 2012; Beaudoin et al. 2012; Chen et al. 2011; Kaech and Banker 2006; Bate, Reid, and Williams 2001; Gage, Ray, and Fisher 1995; Banker and Cowan 1977). Overnight breeding pairs of mice were set-up and pregnancies were monitored by animal staff. After 17 days from plug formation (plug formation = day 0) the pregnant mouse was culled (Schedule 1 termination by cervical dislocation). A non-Schedule 1 termination of embryos proceeded which involved cooling of embryos on ice followed by immersion in chilled Basal Medium Eagle (BME, Gibco) buffer.

2.2.1 Embryo brain removal and hippocampal dissection

Each embryo was individually removed from BME buffer and decapitated. The embryo brain was removed from the skull according to previous protocols (Beaudoin et al. 2012; Fath et al. 2009). The tissue was placed fully submerged into a sterile petri dish containing Hanks/Hepes dissection buffer [Hank's balanced salt solution (HBSS, Invitrogen), 10mM Hepes (Biochrom)]. Under a dissecting microscope, a sagittal cut along the brains midline allowed for separation of the two hemispheres. The cerebellum was discarded and the meninges were removed completely. The hippocampus was identified by its C-shaped structure and opacity, which differed from the surrounding cortical tissue. Hippocampi were dissected and placed immediately into a 15ml corning tube containing approximately 6mls of chilled Hanks/Hepes dissection buffer.

2.2.2 Cell dissociation and plating

In a laminar flow cell culture hood the hippocampi were transferred into 2ml dissection buffer containing 222µl Trypsin (2.5% 10X, Life Technologies) and 20µl Deoxyribonuclease I (5mg/ml, Sigma). Samples were then incubated at 37^{o}C for 20 minutes.

The medium was aspirated off and the samples were washed twice in 10ml pre-heated growth media [500ml BME (Gibco), 50ml heat inactivated Horse Serum (Gibco), 8ml 32.5% Glucose solution (Sigma), 5ml Sodium Pyruvate 100mM (Gibco), 5ml N2 Supplement (Gibco) and 5ml Penicillin-Streptomycin (10,000 U/ml, Gibco)]. Samples were then placed in 2ml pre-heated growth media containing 20µl Deoxyribonuclease I and cells were triturated using a fire-polished glass pipette (230mm, Volac). 8µl of the dissociated cells was taken to estimate cell density using a haemocytometer. Cell viability was checked using 0.4% Trypan Blue (Sigma, v/v). At this stage the desired number of cells were plated at standard plating densities on either in-house or commercially pre-labelled platforms where a number of substrates were investigated including Poly-L-Lysine (PLL, Sigma-Aldrich), Poly-D-Lysine (PDL, Sigma-Aldrich), and Fibronectin (Gibco). Approximately 400,000 cells were plated per well on Poly-L-Lysine 6 well plates (BD Biocoat), 150,000/ 75,000 cells per coverslip on pre-labelled glass 14mm PDL coated coverslips (Neuvitro) and 30,000 cells per well on pre-labelled 96 well plates (Thermo Scientific). Plates were incubated at 37ºC/ 5% CO_2 for 4 hours. In-house coating of different platform types involved numerous steps. 14mm glass coverslips (Thermo Scientific) were placed into a heat-resistant glass container and rinsed in dH_2O to remove any dust, submerged in 70% nitric acid (v/v) for 18-36 hours then washed in sterile dH_2O three times for 10 minutes followed by three 30 minute washes. The coverslips were allowed to soak for 2 hours in fresh dH_2O, the remaining dH_2O was aspirated off and the coverslips were allowed to air-dry. Finally the glass container holding the dried coverslips was placed into a dry heat oven at 220°C for 12-16 hours. Once baked the coverslips were stored at room temperature for one month ready for labelling. Glass coverslips and Corning/Nunc plates were coated in 2ml of PLL (50µg/ml) or PDL (100µg/ml) for a minimum of 2 hours then washed with numerous washes in PBS or dH_2O. Fibronectin (100µg/ml) was added after this step (optional) for 1 hour or overnight followed by additional washes in PBS or dH_2O.

Finally the remaining PBS/ dH_2O was aspirated off, coverslips/plates were either allowed to air-dry then stored at 4°C until use or were stored in a fresh covering of distilled dH_2O at 4°C until use.

2.2.3 Culture Maintenance

After cells were incubated for 4 hours, proficient cell settlement and attachment was confirmed by microscopy. Growth media was removed and replaced with an equal volume of serum free media [500ml neurobasal media (Gibco), 10ml B27 supplement 50X (Gibco), 5ml L-Glutamine (200mM, Gibco), 5ml Penicillin-Streptomycin (10,000 U/ml, Gibco)]. One-third of media was replaced with fresh pre-warmed serum free media twice a week to maintain a healthy culture. Supernatants were retained from each media change for analysis by SDS-PAGE and Lactate Dehydrogenase Assay (LDH).

2.2.4 Cytotoxicity Assay (LDH Assay)

The CytoTox 96 assay (Promega) quantitatively measures lactate dehydrogenase and was used according to manufacturer's instructions. Supernatants were collected over a number of time points between 0-20 days *in vitro* (DIV0–DIV20) and stored at 4°C until subsequent analysis. Fluorescent values were normalized to Triton X-100 treated lysis cells that represent the maximum amount of LDH available for release. Samples were examined in duplicate or triplicate and data was analysed using GraphPad Prism package.

2.2.5 Cell lysis and protein extraction

For cell lysis preparations the cell culture dish was placed on ice and cells were washed twice in ice cold Dulbecco's Phosphate Buffered Saline (DPBS, Gibco).

200µl of NP40 lysis buffer [1% NP40 (Abcam, v/v), 0.5% Sodium Deoxycholate (Sigma, w/v), 150mM NaCl (Fisher), 50mM Tris/HCL (Fisher) plus 1mM Phenyl Methyl Sulfonyl Fluoride (PMSF 200mM, Sigma)] was added to each well (6 well plate) and cells were lysed using a cell scraper (Corning) along with gentle pipetting. The resulting cell suspension was transferred to a pre-cooled microfuge tube and incubated at 4°C under constant agitation for 30 minutes. The sample was then centrifuged at 4°C for 20 minutes at 12,000 rpm. The supernatant was aspirated off and stored for further analysis whilst the pellet was discarded. For the preparation of control brain homogenates, whole mouse brains were taken post mortem from either day 17 embryos, day 6 pups or adult mice and were snap frozen immediately then stored at -80°C until use. Brains were weighed and homogenized (100mg/ml) in glass dounce homogenisers using NP40 lysis buffer. The homogenate was centrifuged at 4°C for 10 minutes at 10,000 rpm (Benchtop microcentrifuge) to aid cellular debris removal. The supernatant was aspirated off, aliquoted and stored at -80°C until further analysis whilst the pellet was discarded.

2.2.6 Micro BCA kit and SDS-PAGE immunoblotting

Protein concentrations were obtained using the micro BCA assay (Bicinchoninic acid assay, Thermo Scientific) according to manufacturer's instructions. Optical density (562nm) was manually recorded, readings were plotted in excel and protein concentrations were calculated from XY scatter graph using standard control readings. To allow equal loading for SDS-PAGE, protein concentration adjustments were made using dH_2O to produce final protein concentrations of 5µg. Tris-Glycine SDS sample buffer (10µl, Invitrogen) was added to each sample which was then denatured at 90°C for 20 minutes. Samples were loaded onto either 10, 12 or 15 well pre-cast Novex® 12% Tris-Glycine Gels (Invitrogen) with the appropriate Seeblue plus 2 pre-stained protein standard (Life Technologies). SDS-PAGE running buffer was made (0.02M Tris, 0.19M Glycine, 3.5mM SDS) and Tris-glycine gels were run at 130V for approximately 120 minutes.

Gels were removed from their cassettes and prepared for semi-dry protein transfer. Briefly, pre-cut polyvinylidene fluoride (PVDF) membranes (Millipore) were washed in methanol for 30 seconds, then dH_2O for 2 minutes and finally immersed in transfer buffer (40mM Glycine, 48mM Tris, 1mM SDS and 20% methanol, v/v) for a minimum of 5 minutes. Each individual gel was placed in a sandwich of 6 pieces of filter paper (pre-soaked in transfer buffer), PVDF membrane, polyacrylamide gel and 6 pieces of filter paper then placed inside the semi-dry blotter (Bio-Rad) and a current of 125mA was applied ($2mA/cm^2$) per gel for 90 minutes (limited to 25V) for efficient transfer of proteins to the PDVF membrane. The membrane was then placed in a 50ml conical tube and blocked for 30 minutes in 5ml of Odyssey® Blocking Buffer (LI-COR) where constant rotation was continually achieved by placing the tubes on a tube roller. The PVDF membrane was incubated overnight at room temperature with primary antibody 6H4 (Prionics) at 0.1µg/ml in 5ml Odyssey® Blocking Buffer (LI-COR) plus 5µl Tween 20. The following day the PVDF was washed six times in freshly prepared PBS then incubated with IRDye®680RD Goat anti-mouse secondary antibody (LI-COR) at 0.2µg/ml in 5ml Odyssey® Blocking Buffer (LI-COR) plus 5µl Tween 20 for 1 hour 45 minutes (protected from the light). The PVDF was washed six times in PBS then finally the PVDF was scanned and analysed using Odyssey® imaging system and LI-COR software.

2.2.7 Cell lysis and RNA extraction

Ribonucleic acid (RNA) was extracted from both cell cultures and Day 6 mouse hippocampal tissues using the RNeasy Plus Micro Kit (Qiagen). Day 6 hippocampal tissues were dissected similarly to embryonic mice however, after the brain was isolated it was placed immediately in RNAlater RNA stabilisation Reagent (Qiagen). The hippocampal areas were then dissected and placed in a pre-weighed tubes containing 1ml of RNA stabilisation reagent. The kit recommended using tissues < 30mg in weight so occasionally larger tissues were split between two separate tubes for processing.

RNA stabilisation buffer was removed and 600µl of Buffer RLT Plus (with ß-mercaptoethanol) was added to each tube followed by an initial homogenisation step using disposable pestles (VWR) and a handheld pellet mixer (VWR). For cell cultures a starting volume of 350µl of Buffer RLT Plus (with ß-mercaptoethanol) was used for initial lysis. A QIAshredder was employed for both cell and tissue preparations which aided in a uniform homogenate preparation (samples spun at full speed for 2 minutes). The remaining steps were carried out according to the kit's protocol and for the final elution 30µl of RNase free water was used to wash the RNeasy column membrane. After centrifugation this wash step was repeated again and RNA purity was measured using the Nanodrop (Thermo Scientific) spectrophotometer. Samples were stored at -80°C until further analysis.

2.2.8 Immunostaining of primary cultures

Cell media was removed and cells were incubated with 4% paraformaldehyde (PFA, v/v) serum free medium mix (1:1) for 2 minutes at room temperature. This media mix was removed and 1-2 ml of 4% PFA (v/v) was placed on cells for 15 minutes at room temperature followed by three 5 minute washes with DPBS containing Ca^{2+} and Mg^{2+} (Gibco). 1-2ml of ice-cold methanol was added to the cells for 10 minutes with incubation at -20^{o}C followed by a 5 minute incubation with 0.3% Triton-X (Sigma, v/v) at room temperature. Again wells were washed three times in DPBS at 5 minute intervals then blocked for 1 hour at room temperature using Fc Block (purified recombinant Fc protein that blocks non-specific binding of Fc receptor expressing cells, CD16/32, BioLegend). Primary antibodies were incubated overnight in 5% Goat serum (Gibco, v/v) at 4^{o}C (concentrations listed in Table 2.1). Cells were washed three times in DPBS (Gibco) and secondary antibodies diluted in 5% goat serum (v/v, Table 2.1) were added for 1 hour at room temperature in complete darkness followed by a further three washes as above. For the final wash a 4', 6-Diamidino-2-Phenylindole, Dihydrochloride (DAPI, 300nM, Molecular Probes) counterstain was carried out.

Pre-labelled PLL 6 Well plates (Biocoat Cell Environments) were imaged using a live confocal microscope (Nikon). For glass coverslips preparations (14mm Neuvitro Corporation) 20µl of prolong diamond antifade mountant (Life Technologies) was placed on specialised cavity glass slides (Marienfeld). Using a forceps coverslips were removed from their specific well and placed inverted onto the antifade mountant (Life Technologies) and were allowed to dry for 4 hours at room temperature then overnight at 4^{o}C. Coverslips were sealed using CoverGrip coverslip sealant (Cambridge BioScience) then imaged using the LSM710 inverted confocal microscope (Zeiss). Slides were stored at 4^{o}C for several weeks without substantial loss of fluorescence.

Primary Ab	Marker/ Concentration	Secondary/ Concentration	Supplier
Anti-MAP2 (Ab5392)	Dendritic, 1/2000	Goat Anti-Chicken IgY (Alexa Fluor 488) 1/500	Both Abcam
Anti-GFAP (18-0063)	Astrocyte, 1/100	Goat Anti-Rabbit IgG (Alexa Fluor 594) 1/200	Both Thermo Scientific
Anti-GFAP (Ab53554)	Astrocyte, 1/500	Donkey Anti-Goat IgG (Alexa Fluor 555) 1/500	Both Abcam
Anti-GFAP (Ab4674)	Astrocyte, 1/500	Goat Anti-Chicken IgY (Alexa Fluor 488) 1/500	Both Abcam
Anti-Sox9 (Ab5535)	Astrocyte, 1/500	Donkey Anti-Rabbit IgG (Alexa Fluor 488) 1/500	Millipore Abcam
Anti-ALDH1L1 (Ab87117)	Astrocyte, 1/500	Goat Anti-Rabbit IgG (Alexa Fluor 647) 1/200	Both Abcam
Anti-Tau (Ab64193)	Axonal Marker, 1/100	Goat Anti-Rabbit IgG (Alexa Fluor 594) 1/200	Abcam
6H4 (01-010)	PrP amino acids 143-151, 1/500	Goat Anti-Mouse IgG (Alexa Fluor 647) 1/200	Prionics Life Tech.
7A12*	PrP amino acids 90-145, 1/500	Goat Anti-Mouse IgG (Alexa Fluor 647) 1/200	Gift* Life Tech.
Synapsin 1 (Ab64581)	Pre-synaptic, 1/200	Goat Anti-Rabbit IgG (Alexa Fluor 594) 1/200	Both Abcam
PSD-95 (Ab99009)	Post-synaptic, 1/200	Goat Anti-Mouse IgG (Alexa Fluor 647) 1/200	Both Abcam
Anti-Iba1 (019-19741)	Microglia, 1/1000	Goat Anti-Rabbit IgG (Alexa Fluor 594)	Wako Abcam
Anti-Iba1 (Ab139590)	Microglia, 1/500	Goat Anti-Chicken IgY (Alexa Fluor 488) 1/500	Both Abcam
CD11b Alexa Fluor 647 (Ab197702)	Macrophages/ monocytes, 1/200	n/a	Abcam
Myelin Basic Protein (Ab62631)	Myelin, 1/500	Goat Anti-Mouse IgG (Alexa Fluor 647) 1/200	Abcam
Anti-LAMP1 (Ab24170)/ LAMP2 (108501)	Lysosome, 1/1000	Goat Anti-Rabbit IgG (Alexa Fluor 594) 1/200	Abcam BioLegend
Anti-EEA1 (Ab2900)	Early Endosome, 1/200	Goat Anti-Rabbit IgG (Alexa Fluor 594) 1/200	Both Abcam
Anti-Rab9 (Ab179815)	Late Endosome, 1/250	Goat Anti-Rabbit IgG (Alexa Fluor 594) 1/200	Both Abcam
Transferrin 488 (T13342)	Endosome, 1/125	n/a	ThermoFisher
Cholera toxin Subunit B 488 (C34775)	Lipid-Raft, 1/200	n/a	ThermoFisher
Anti SQSTM1 p62(ab109012)	Autophagosome, 1/1000	Goat Anti-Rat IgG (Alexa Fluor 594) 1/200	Both Abcam

*Gift from Man-Sun Sy (Case Western Reserve University, Cleveland, USA)

Table 2.1 Antibodies and markers used for immunolabelling experiments.

2.2.9 IMARIS software analysis of immunolabelled hippocampal cultures

IMARIS software (Bitplane) allowed for data visualisation, analysis and interpretation of microscopy datasets. Various modules in IMARIS allowed for complex image processing to be carried out on ".czi" images obtained from confocal microscopy. For each image or channel within an image the intensities of all voxels are analysed using default standard IMARIS formulas that calculate mean, standard deviation and sum intensities (intensities do not have any units) and therefore these values can be used for relative comparison of targets of interest in different images. Slice View module allows for more robust image analysis and is a user integrative module that allows for accurate measurements of a particular structure, cell, or dendrite to be obtained based on the datasets scale bar parameters. FilamentTracer module allowed for the automatic detection of neurons and dendrites in 3D and supplied a vast range of morphological information including diameter, volume, area, length, width, and branching angle, all of which can be visualised in IMARIS Vantage. This analysis method was occasionally subjective to falsely identifying some structures and therefore semi-automatic detection or manual methods were predominantly used here. Briefly, for semi-automatic tracing the image was opened in IMARIS and a Filament object was created and the option Calculate Diameter of Filaments from Image was turned off. Region of interest was defined using the wizard and estimated diameters for the Starting points and Seed points were entered using measurements obtained in Slice View module. The next step involved setting the upper and lower threshold values to 0, starting points were added manually using shift-key + ctrl + left mouse button, and Seed points were added using shift-key + left mouse button. The image could be rotated to confirm correct placement of Seed points. At this stage All done could be selected or to Apply settings to the whole image Entire Image option was selected. For manual tracing a Filament object was created and skip automatic creation, edit manually was selected. Draw tab was displayed which provided tools for manually creating filaments.

Two options may be selected here AutoPath recommended for 2D data sets and AutoDepth (uses a FastMarching algorithm) recommended for 3D data sets which was predominantly used here. Using shift-key + left mouse button and drag, a new Filament was drawn. Pencil diameter could be changed using mouse wheel for accuracy. All algorithms employed by IMARIS software have been described previously (Meijering et al. 2004). To investigate localisation of PrP^C to neurons and astrocytes an adaption of previous methods was carried out (Fogarty et al. 2013). In this analysis, Surface tool was used to build a computer-generated representation of the area of interest in the data set. In Surpass mode Create surface was selected for the channel of interest, Smoothing option was disabled and Background subtraction was enabled. Switching to Slice mode allowed for accurate measurements to be obtained for background correction. Voxel threshold graph was altered to map the signal with precision and finished surface creation was selected. The next stage involved filtering signals of interest. The newly created surface layer was selected followed by edit tab. The options Mask all and marker of interest were selected and the option Duplicate channel before applying mask was enabled and Constant inside/outside selected with Voxels OUTSIDE surface 0.0. These steps were repeated however “Set voxels INSIDE surface 0.0” was selected. Stage three involved creating spot layers from the previous filtering step. A new spot layer was created and the marker channel of interest (neuron/astrocyte) was selected whilst ensuring Background subtraction was enabled. Stage four entailed measuring total number of PrP^C adjacent to the neuron or astrocyte. Neuron/astrocyte surface was selected followed by the Tools tab. Find spots close to surface was selected and MatLab in IMARISXT (multi-functional two-way interface) was automatically launched. Here a spot layer was chosen alongside a distance threshold for analysis. This resulted in the creation of two new spot layers, one with all the spots within the selected distance and the other containing all the more distant spots.

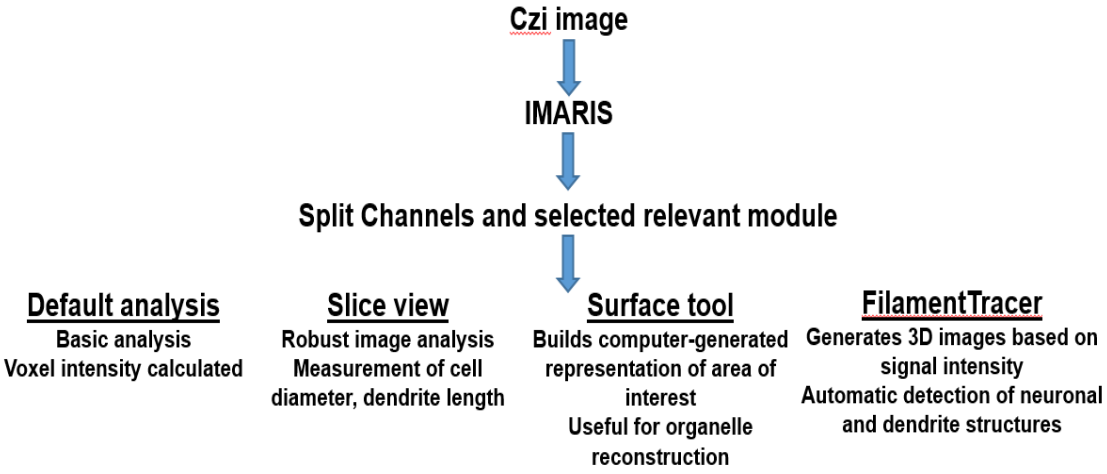

Figure 2.1: Flow chart summarising image analysis options available when using IMARIS software.

2.3 Production and purification of recombinant protein

WT and 101L PrP protein was expressed from glycerol stocks (gift from Dr. Andy Gill) of *Escherichia coli* (*E. coli*) strain (Rosetta DE3) expressing a pTrcHis B vector containing PrP open reading frame from codons 23-230 (Kirby et al. 2003). Briefly, full length murine PrP of *Prnp* genotype was amplified from genomic DNA using relevant primers (Locht et al. 1986). Alongside this the 6-histidine tag was removed from plasmid pTrcHis B (Invitrogen; http://www.lifetechnologies.com/order/catalog/product/V36020) by digestion with restriction enzymes NcoI/EcoRI. PCR fragments were digested with these specific enzymes followed by ligation into the altered pTrcHis B vector. These specific vectors are designed for efficient recombinant protein expression and purification in *E. coli* where high levels of expression are achieved. The resultant recombinant vector encoded untagged PrP (23-230). *E. coli* were then transformed with the recombinant vectors and the resulting strains (pTrcHis B vector in Rosetta DE3) were plated overnight at 37°C on Luria-Bertani (LB, Sigma) culture plates to generate glycerol stocks.

2.3.1 Bacterial expression and induction using the pTrc expression system

Recombinant PrP expression protocols were adapted based on previous tested methods (Makarava and Baskakov 2008). Both WT and 101L PrP stocks (gift Dr. Andy Gill) were used here to produce fresh glycerol bacterial stock. Luria-Bertani (LB, Thermo-scientific) plates were prepared under sterile conditions containing ampicillin (0.1mg/ml, Sigma) and/or chloramphenicol (0.05mg/ml, Sigma). WT cultures required both antibiotics whilst 101L only required ampicillin. Plates were streaked with bacteria from WT or 101L glycerol stocks then incubated at 37°C overnight. The following day a bacterial colony was selected from each plate and was used to inoculate 10ml of LB broth (Thermo-scientific) containing either ampicillin (0.1mg/ml) and/or chloramphenicol (0.05mg/ml). The inoculated broths were incubated at 37°C overnight in an orbital shaker (200rpm).

For the production of fresh glycerol plasmid stocks 100μl of overnight culture was added to 10ml LB broth containing ampicillin and/or chloramphenicol. This culture was incubated at 37°C for 4 hours in an orbital shaker (200rpm). 500μl of this culture was added to 500μl of 30% glycerol/LB (v/v) and was immediately snap frozen and stored at -80°C until further use. For further bacterial growth 4ml of overnight culture was added to 400ml of terrific broth (Sigma-Aldrich) containing the relevant antibiotics. Incubation was carried out in a conical flask at 37°C for 3 hours in an orbital shaker (200rpm). The cultures were grown to an OD_{600} of between 0.6-0.8 at which point PrP expression was induced by the addition isopropyl ß-D-1-thiogalactopyranoside (IPTG, Sigma-Aldrich) to a final concentration of 1mM. Induced cultures were incubated overnight at 37°C overnight in an orbital shaker (200rpm). Induction of recombinant protein was confirmed by SDS-PAGE. 20μl of either plus/minus IPTG sample was added to 10μl NuPage LDS sample loading buffer (Invitrogen) followed by protein denaturation at 90°C for 5 minutes. Samples were pulse centrifuged at 12,000rpm then loaded onto either a 10 or 15 well Nu-PAGE 12% Bis-Tris Gels (Life Technologies) along with the appropriate Seeblue plus 2 pre-stained protein standard (Life Technologies). Gel electrophoresis was carried out at 180V for 45 minutes in 1X NuPage running buffer (Invitrogen). The cassette was removed from gel tank, dismantled and the exposed gel was stained in instant blue buffer (Expedeen) for visualisation of the isolated protein. This confirmed PrP of the anticipated size was produced.

2.3.2 Pellet harvesting and bacterial lysis

Bacterial cells were harvested by centrifugation at 12,000rpm for 15 minutes using a Sorvall Lynx 4000 centrifuge and SLA1500 rotor. Cell pellets were stored at -80°C until lysis. Bacteria were lysed using 9ml of lysis buffer (50mM Tris pH8, 1mM EDTA, 100mM NaCl) per gram of cell pellet.

After this 20μl lysozyme (10mg/ml, Sigma-Aldrich) per ml of lysis buffer was added to degrade the bacterial cell wall and this mix was incubated with constant stirring at 4°C for 40 minutes. Solid sodium deoxycholate was added to a final concentration of 1mg/ml to disrupt the cell membrane and release recombinant protein contained in inclusion bodies. To reduce the viscosity of the solution, after incubation of 1.5 hours, 5μl of Deoxyribonuclease I from bovine pancreas (DNase) was added at 2mg/ml along with approximately 500μl of 2M $MgCl_2$. This mix was stirred for 1.5 hours then centrifuged in a Sorvall Lynx 4000 centrifuge (SLA1500 rotor) at 15,000 rpm for 15 minutes. The resulting pellets contained the inclusion bodies and were stored at -80°C until purification.

2.3.3 Immobilized-Metal Affinity Chromatography (IMAC) PrP purification

Stock buffers were prepared as follows:

- 9M Urea (Sigma-Aldrich) was prepared and then mixed with amberlite (Sigma-Aldrich) overnight at room temperature. This mix was then filtered through a 0.45μm filter (Millipore).
- IMAC A: 8M Urea, 0.1M Sodium phosphate dibasic (Na_2HPO_4, Sigma-Aldrich), 10mM Tris-HCL, 10mM reduced glutathione (Sigma-Aldrich), pH 8.0.
- IMAC B: IMAC A buffer pH 4.5.

Inclusion bodies were solubilised in IMAC A buffer using 10ml of buffer per gram of pellet. Once thoroughly resuspended (approximately 2 hours) the solution was spun in a Sorvall Lynx 4000 centrifuge (SLA1500 rotor) at 15,000 rpm for 20 minutes. The resulting pellet was discarded and the supernatant was retained. Nickel-Nitrilotriacetic acid (Ni-NTA, 5ml) agarose (Qiagen) was poured into a 50ml tube, allowed to settle then was washed three times in dH_2O followed by a final wash in IMAC A buffer. The supernatant was batch bound to this resin for approximately 1.5 hours by placing tube on a 360° spinner at room temperature.

The resin was poured into an empty gravity flow cartridge (Qiagen) and the flow through was collected. The column was washed with 15ml of IMAC A then recombinant PrP was eluted using 25ml of IMAC B. To minimise protein degradation 50µls of 0.5mM Ethylene Glycol Tetraacetic Acid (EGTA, Sigma-Aldrich) was added to each fraction to give a final contraction of 5mM EGTA. The first two eluted fractions normally contained the target protein and this was validated by SDS-PAGE.

2.3.4 PrP protein concentration

Recombinant PrP fraction absorbance was measured using nanodrop spectrophotometry (Thermo Scientific) and the concentration of recombinant protein was calculated using the extinction co-efficient based on the PrP sequence (62,280), molecular weight of PrP (23,104) and the following equation:

$$\text{Protein Concentration (mg/ml)} = \left(\frac{OD\ 280 - OD\ 320}{Extinction\ co-efficient}\right) \text{ x Molecular Weight}$$

2.3.5 Reduced glutathione removal using HiPrep 26/10 Desalting column

The AKTA-Fast protein liquid chromatography (FPLC, GE Healthcare) system was utilised for filtration processing of IMAC fractions. Stock desalting buffer was prepared as follows: 6M Urea (Sigma-Aldrich) and 0.1M Tris-HCL pH 7.5. The HiPrep 26/10 desalting column (GE Healthcare) was equilibrated with desalting buffer, then the IMAC fractions containing diagnostic protein were combined and loaded on the column via a superloop. The column capacity was 13mls so this was the maximum volume loaded at one time. Flow rate was set at 1ml/minute and maximum pressure at 0.15 MegaPascal (MPa). Samples were collected immediately as the protein normally eluted in the first two fractions, monitored by UV absorbance and validated by SDS-PAGE. Fractions containing PrP protein (range of 0.5–2.5mg/ml) were pooled and diluted immediately in desalting buffer to a final concentration of 0.3mg/ml.

This step was critical in minimising the formation of dimers during oxidative refolding of PrP. A final concentration of 5mM EGTA was also added to prevent protein degradation. A disulphide bond was then made by the addition of oxidised glutathione (0.075mM) and the protein was incubated overnight at room temperature with constant stirring.

2.3.6 Reversed Phase HPLC for high purity prion protein purification

After addition of a disulphide bond recombinant PrP was further purified using a reversed phase column (Vydac 214TP101522 RP) and a Dionex HPLC UltiMate 3000 system (Thermo Scientific). Stock buffer was prepared as follows:

- HPLC Buffer A: 0.1% Trifluoroacetic Acid (Sigma-Aldrich, v/v) in 1L Milli Q dH_2O.
- HPLC Buffer B: 0.1% Trifluoroacetic Acid in Acetonitrile (Sigma-Aldrich, v/v).

The reversed phase column was equilibrated with HPLC Buffer A, whilst equilibrating the oxidised PrP was filtered through a 0.22µm filter then diluted (1:3 v/v) in HPLC Buffer A to reduce urea concentration. The diluted sample was loaded on the column via a superloop where a maximum concentration of 7mg protein was never exceeded. Flow rate (HPLC Buffer A) was increased to 1ml/minute and maximum pressure was limited to 4 MegaPascal (MPa). The sample was injected through the column and the flow through was collected immediately (approximately 40mls). Protein was eluted in HPLC Buffer B using a pre-determined multistep gradient flow program (Table 2.2). Fractions corresponding to UV peak readings were collected for SDS-PAGE analysis.

Minutes	Flow (ml/min)	%B
0	1	0
5	1	15
35	1	35
45	1	80
50	1	80
55	1	0

Table 2.2: Multistep gradient flow program for efficient protein displacement using RP-HPLC.

2.3.7 Protein lyophilisation

Fractions containing the purest target protein (validated by SDS-PAGE) were selected for immediate lyophilisation using the Savant automatic environmental Speedvac system. Each individual fraction was aliquoted into 100µl volumes. Speedvac was set to low drying rate and samples were incubated for 2 hours 15 minutes. After lyophilisation samples were stored at -80^{o}C until further use.

2.3.8 Mass spectrometry

Mass spectrometry was performed in-house by Dr. Andy Gill, The Roslin Institute on lyophilised protein samples to confirm the presence and purity of the recombinant PrP protein and analysis reports were supplied accordingly.

2.3.9 Fibrillisation of recombinant PrP

Fibrillisation of recombinant PrP was carried out according to previous published methods (Graham et al. 2010; Breydo, Makarava, and Baskakov 2008). Lyophilised recombinant PrP samples were reconstituted in 6M Gdn-HCl (pH 6.0) to a concentration of between 10-15mg/ml.

Reaction mixtures contained the following final concentrations: 2M Gdn-HCL, 50mM MES, 10mM Thiourea and approximately 0.5-1mg/ml of reconstituted recombinant protein. To monitor fibrillisation kinetics, Thioflavin T (ThT) was added at a final concentration of 10μM. The reaction mix was dispensed into a FluoroNunc 96 well flat bottom plate (Thermo Fisher) along with 3 Teflon balls (2.381mm diameter, The Precision Plastic Ball Company). The plate was sealed with a plate sealer then placed in the Fluoroskan (Thermo Scientific). The fluorescent plate reader was set to shaking at 900rpm at 37°C and incubated for 24 hours. ThT fluorescence was measured every 5 minutes for 24 hours (excitation at 444 nm, emission at 485 nm) to monitor fibril production. Data points generated were processed using a fibrillisation processor macro excel program which produced a sigmoidal kinetic curve based on ThT fluorescence readings output over-time. Fibrillisation reactions were also set up in the absence of PrP protein and were used to account for background fluorescence. Additionally, reactions were set-up without ThT to produce recombinant PrP fibrils for future challenge studies and these reactions were pooled and dialysed for storage. Dialysis was carried out against 2 litres of 10mM sodium acetate pH 5.0 with two buffer changes. Final concentrations of fibrils was estimated using the nanodrop as previously described (Section 2.3.4) then fibrils were stored at 4°C.

2.3.10 Maturation and proteinase K digestion of fibrils

Dialysed fibrils were processed according to standard protocols (Breydo, Makarava, and Baskakov 2008). Loading buffer was prepared as follows (all chemicals from Sigma-Aldrich): 125mM Trizma, 4.5M Urea, 20% (v/v) Glycerol, 1.25M β-mercaptoethanol, 4% (w/v) Sodium dodecyl sulfate, and 0.02% (w/v) Bromophenol blue. Three samples were prepared for each batch of fibrils as per Table 2.3.

Ingredient	Sample 1: Control no PK digestion (µl)	Sample 2: PK digestion (µl)	Sample 3: PK digestion with maturation (µl)
PrP (0.5mg/ml)	2	2	2
dH_2O	4.8	4.8	4.8
1M Tris pH 7.5	0.8	0.8	0.8
1% Triton-X 100	0.4	0.4	0.4
			Incubate at 80°C for 15 minutes
PK (20 µg/ml)	n/a	0.5	0.5
		PK Samples at 37°C for 1 hour	
Pefabloc 100mM	n/a	2.125	2.125

Table 2.3: Reaction mix recipes for maturation analysis of fibrils.

After preparing the samples as noted in Table 2.3, 8µl of loading buffer was added to each tube followed by a 10 minute incubation at 95°C. SDS-PAGE (12% NuPAGE Bis-Tris gel, Invitrogen) and silver staining was carried out next to aid protein visualisation (Chevallet, Luche, and Rabilloud 2006).

2.3.11 Silver staining

SDS-PAGE was carried out as described previously (Section 2.2.6) however, after electrophoresis the NuPAGE Bis-Tris gel (Invitrogen) was soaked in fixing solution (30% Ethanol, 10% Acetic acid, dH_2O 40:10:50 v/v) overnight at room temperature. The gel was then incubated for 1 hour in sensitising solution [30% Ethanol (v/v), 5% Sodium thiosulphate (w/v), 0.84M Sodium acetate, 0.5mls Glutaraldehyde (25%)] followed by four 15 minute washes in dH_2O. The gel was then stained with silver nitrate (0.25% w/v) in dH_2O with formaldehyde (0.1% w/v) for 1 hour followed by two 1 minute washes in dH_2O.

The gel was developed in 2.5% (w/v) sodium carbonate with formaldehyde (0.04% w/v) until bands were clear. After this step the gel was transferred immediately into stop solution (1.46% EDTA, w/v) and images were taken using a Typhoon scanner (GE Healthcare).

2.3.12 Transmission Electron Microscopy (TEM)

WT, 101L fibrils and WT α-helical monomeric protein samples were prepared for TEM by Stephen Mitchell, Kings Buildings, Edinburgh using formvar/carbon coated grids (Copper 200 mesh). Each grid was inserted into the single specimen holder of a JEM-1400 Plus Electron Microscope. Images of both fibrils and monomeric protein were taken at various magnifications and saved as .dm3 files. Fibril dimensions were determined using IMARIS Slice View module.

2.3.13 Labelling fibrils with Alexa Fluor Succinimidyl Esters (NHS esters)

To allow for efficient fibril labelling with Alexa fluor 555 succinimidyl ester fluorophores a buffer exchange was carried out to remove fibrils from sodium acetate pH 5.5 buffer and replace with sodium bicarbonate pH 9.0. Fibrils (1ml at 0.5mg/ml) were centrifuged at 13,200rpm for 15 minutes then the resulting pellets were washed in 0.1M sodium bicarbonate pH 9.0. This step was repeated three times, finally the pellets were reconstituted in 100µl of 0.1M sodium bicarbonate. 100µl of sterile Dimethylsulfoxide (DMSO) was added to one vial of Alexa Fluor 555 at 100µg (Molecular Probes). From this point all tubes were kept in tinfoil to protect from light. 5µl of Alexa Fluor was added to 100µl of fibrils and this mix was incubated at room temperature for 1 hour on a 360º rotator followed by overnight incubation at 4ºC with constant agitation. The following day 1.5M hydroxylamine hydrochloride pH 8.5 was added at 1:10 (v/v) and the sample was incubated for 1 hour on a 360º rotator at room temperature.

Samples were centrifuged at 13,200rpm for 15 minutes, the supernatant was removed and 200µl of 0.1% sarkosyl/PBS was added to wash pellets. This centrifuge/ washing step was repeated five times. For the final centrifuge pellets were brought up in 100µl 0.1% Sarkosyl/PBS. Labelled fibrils were stored at 4^{o}C protected from light. Sodium acetate alone (minus fibrils) was processed under exact same labelling conditions as a control for labelling. It was optional here to take 10µl for analysis by SDS-PAGE. Procedure as described previously (Section 2.2.6) however gel was protected from light and was developed in the following mix: 125ml methanol; 23ml acetic acid and 102ml dH_2O for 1 hour at room temperature. The gel was then placed in destain overnight (115ml Ethanol; 35ml acetic acid up to 500ml dH_2O). The next day the gel was imaged using a Typhoon scanner (GE Healthcare) with excitation/emission Cy3 filter to confirm effective fibril labelling of the diagnostic PrP protein.

2.4 Primary culture challenge experiments

A number of experiments were carried out using primary hippocampal cultures generated from WT or 101LL mice to access how both genotypes responded to external stimuli.

2.4.1 Generic oxidative stress study

Both WT and 101LL cultures were treated with hydrogen peroxide (30% v/v H_2O_2, Sigma) at DIV8 to induce oxidative stress. Samples were treated in duplicate at the following concentrations of H_2O_2: 0μM. 10μM, 100μM and 300μM for 24 hours. LDH samples were taken at 0hr, 2hr, 4hr, 6hr and 24hr to monitor cellular toxicity over-time. After 24 hours incubation all culture coverslips were fixed and immunostained for neuronal and astrocytic response.

2.4.2 Phagocytosis Assay

The assay was carried out according to manufacturer's instructions. Briefly all media was removed from cells and live cell media (ThermoFisher Scientific) was added to each well. Control wells contained live media alone whilst test cells contained live media with cells plus pHrodo beads added at 1mg/ml concentration. All wells were incubated for 2 hours at 37°C. Fluorescence readings were taken at 590nm using the Wallac 1420 plate reader. After this cells were fixed and imaged using LSM710 confocal microscope.

2.4.3 WT and 101LL challenge with labelled/ unlabelled fibrils

WT and 101LL cultures were challenged at specific time points with either labelled or unlabelled WT or 101L fibrils. Concentrations of fibrils used varied between the ranges 7.5μg/ml to 75μg/ml and cell densities between 30,000 and 150,000 cells.

Fibrils were pulse sonicated (Ultrasonic Processor, HERT systems) for 10 seconds (35% Pulsar) repeated three times before addition to cultures. Fibril challenge included both 6 and 24 hour incubations.

2.4.4 101L unlabelled fibril challenge for RNA-seq analysis

Both WT and 101LL cultures (400,000 cells) were challenged at DIV7 with 7.5µg/ml of unlabelled 101L fibrils for 24 hours. Challenge experiments were replicated four times per genotype. Representative LDH media aliquots were taken from cultures pre/post challenge. Before addition to cultures, fibrils were pulse sonicated (HERT systems) for 10 seconds (35% Pulsar) repeated three times. After incubation period, wells were lysed and RNA was extracted as described earlier (Section 2.2.7) from fibril treated cultures at DIV8.

2.5 Transcriptomic analysis of 101LL and WT models

RNA was isolated from:

- WT and 101LL DIV8 primary cultures minus fibril challenge
- WT and 101LL Day 6 hippocampal tissues
- WT and 101LL DIV8 primary cultures plus fibril challenge

Transcriptomic analysis comparison of WT and 101LL DIV8 primary hippocampal cultures minus fibril challenge along with WT and 101LL Day 6 hippocampal tissues was carried out using the Affymetrix Mouse Gene 2.1 ST array plate (Edinburgh Genomics). Additionally, WT and 101LL DIV8 primary cultures minus fibril challenge were compared to WT and 101LL DIV8 primary cultures plus fibril challenge using Illumina RNA-sequencing (Edinburgh Genomics). Four replicate samples per group were analysed.

2.5.1 RNA processing for transcriptomic analysis using microarray/RNA-seq

RNA was isolated from 101LL and WT *in vitro* primary hippocampal cultures pre and post-fibril challenge and from Day 6 101LL and WT *in situ* unchallenged hippocampi tissues (Materials and Methods, 2.2.7). For *in vitro* RNA extractions typically a minimum of four hippocampi were dissociated and plated at 400,000 cells per well however, occasionally only two hippocampi were plated due to shortages in embryo availability. RNA extractions were always pooled in cases where more than one well was cultured from the same batch of embryos and this was counted as one sample. Fibril challenge experiments were always carried out in duplicate wells (Section 2.4.4). Four replicate samples were produced for each genotype group for downstream processing. Day 6 hippocampi tissues were isolated each time from three pups (six tissues) from the same batch and this produced one individual sample. Again, this was replicated four times per genotype. RNA extracted samples were processed by Edinburgh Genomics.

RNA integrity was determined using the Agilent TapeStation System and a RNA integrity number equivalent (RINe) was obtained for each sample. For all samples, RINe values of 9 or above were obtained indicating high quality intact RNA was isolated (data not shown). For microarray, cDNA was produced using the Ambion WT expression kit (Invitrogen) and accordingly labelled using the GeneChip WT terminal labelling kit (Affymetrix). Approximately 3µg of fragmented, biotin-labelled cDNA was hybridised to a Mouse Gene 2.1 ST array plate (Affymetrix) using the Gene Titan instrument (Affymetrix) and standard Affymetrix protocols. The microarray results generated probe cell intensity data CEL files which were analysed in-house using various software programs such as Affymetrix expression console (Section 2.5.2, *Figure 2.2*) and Partek Genomics Suite (Partek Inc., Section 2.5.3). Illumina RNA-sequencing sample processing and preliminary analysis of RNA-seq data was carried out by Edinburgh Genomics. Both Ingenuity Pathway Analysis (Section 2.5.4) and Miru (Section 2.5.5) were used for further analysis of both microarray and RNA-seq datasets (DOI: http://hdl.handle.net/10283/3168).

2.5.2 Affymetrix Expression Console (Affymetrix)

Expression console software was free to download and was used to analyse probe intensity levels pre/post normalisation to ascertain the presence of any outliers in the microarray dataset (*Figure 2.2*). It was also used to convert raw data CEL files to TXT files which could be analysed in Miru (Bio-layout) after a secondary conversion to Expression file format. Expression console was launched and a new study was created selecting CEL files under the add intensity files tab. CEL files were giving descriptive names and the run analysis option was selected along with Gene Level [Default: RMA-Sketch (Robust Multichip Average)].

While initiating analysis the file name suffix was left blank, results were accessed under the options QC (Signal distribution generated log probe cell intensity and log expression signal boxplots). Library annotation files were downloaded from Affymetrix site under Technical Documentation; Library Files; MouseGene2.1STArray (Zip, 21MB) for CEL file conversion and probe set annotation. Analysis of data was carried out as described above, under the Edit tab select create annotation merge file; create Affymetrix gene level merge file; select annotation file; select dataset; save; export results; results with annotations to TXT. Click  icon for options; select an annotation merge file; save as TXT file. For editing purposes the TXT file was then converted to a XLS file and the following editions were carried out in excel: Find and Replace option was used to replace cells containing "---" with "N/A". Two new columns were added on left side of sheet; Gene Symbol column was cut and pasted into new blank column beside Probe Set ID. Concatenate both columns using formula "=A1&":"&B1". All data at Log_2 (RMA analysis) was delogged by copying all values to a new sheet then in a parallel new cell the formula "=2^A1" was entered and applied to all numbers. Delogged numbers were selected and copied and pasted as number only over original numbers and file was saved accordingly first as a XLS file then as Text (Tab delimited) and finally saved as a "filename.expression" file.

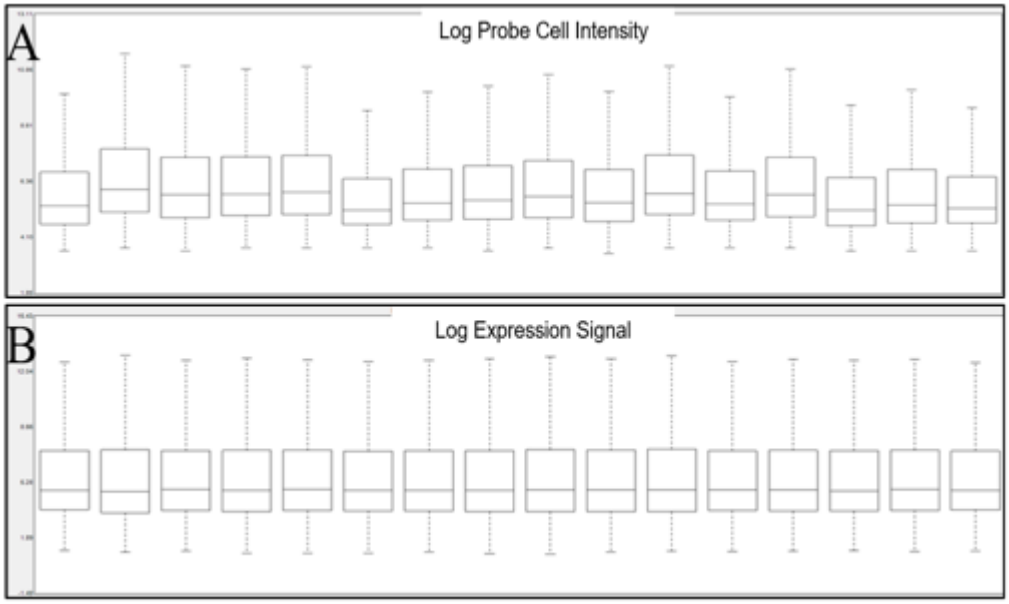

Figure 2.2: Affymetrix Expression console confirmed normal sample distribution. To examine if any outliers were present in microarray data pre and post normalisation, probe signal intensities profiles were compared across all 16 samples (Section 2.5, 8 *in vitro*, 8 *in vivo*). (A) Log raw probe cell intensity box plot created in Affymetrix Expression console, x axis 16 samples, y axis log probe cell intensity values. (B) Log Expression signal based on normalised probe set signal intensities, x axis 16 samples, y axis log expression signal. Box plots were based on CEL file probe signal intensity values of 16 samples. Prior to normalisation (A) some differences in the distributions were present however, no samples were dramatically different from other replicates in the same group. After normalisation, all samples were comparable to each other and no outliers were present. RMA (Robust Multichip Average) algorithm performed a background correction, quantile normalisation and median polish summarisation of data.

2.5.3 Partek Genomics Suite (Partek)

Partek was launched using a remote desktop connection genepool-vm.bio.ed.ac.uk and the relevant password required was entered. A new folder was created on this remote desktop and CEL files (microarray) were transferred to this folder. Partek Genomics tab was opened and Gene Expression workflow was selected and sample files were imported.

The option use RMA (Robust Multichip Average) was selected and then Import. Partek uses an robust multi-array average algorithm which performs a background correction, quantile normalisation and median polish summarisation of data. Box plots were accessed at this stage from the right panel of the Partek genomics suite. Sample attributes were selected followed by add a categorical attribute. Attribute name was Genotype and Group name was WT or 101LL. Samples were added followed by add another attribute option (selection based on group number for analysis) and option Yes was selected for save spreadsheet. From here data such as PCA (Principle Component Analysis) was accessed and saved as GIF files. Next select option detect differentially expressed genes; Genotype selected; Add factor; Contrast; Name; Add contrast level from candidate levels list; Add contrast. This provided a list of every gene that was up or down-regulated. To create a more constricted dataset a gene list was created. Select create gene list; select comparison groups (under contrast); Fold change default at > 1.5 or < - 1.5 p-value with FDR < 0.1. Filters may be altered here; create; save as; .TXT in Partek; then files were transferred to users' desktop and renamed to .xls files.

2.5.4 Ingenuity Pathway Analysis (IPA, Qiagen)

IPA was launched from the Qiagen website under the Ingenuity pathway analysis option using the appropriate password (link to website is: http://www.ingenuity.com/products/login. A new project was created and gene lists created from analysed RNA-seq data (Edinburgh Genomics) were added as per following instructions: New; New Core Analysis; Upload; File was .xls format; Select File format (Flexible); Contains column Headings (Yes); Select Identifier Type (Select All); Array platform used for experiments (Not Specified/ applicable). Column ID was selected for ID filter which recognises majority of genes in dataset. Fold change was used as Observation 1 followed by Save and Create Analysis; Choose relevant Project.

Parameters Selected as follows: General Settings: Relationships to consider (Direct and Indirect Relationships), Networks (Genes are always included: Molecules per network 35/ Networks per analysis 10), Data sources (All), Confidence (Select Experimentally observed), Species (Select all), Tissue & Cell lines (All), Mutation (All), Fold Change can be left as 0 or select a relevant value. Select run analysis; input descriptive name. A report was computed under Analyses and was headed by a Summary Tab followed by a number of tabs including Canonical Pathways, Upstream Analysis, Disease & Functions, Regulator Effects, Networks, Lists and My Pathways and Molecules. PDF summary sheets were generated and contained brief descriptions of all of the above data (Reference Table 6.5 for PDF summaries).

2.5.5 Miru (BioLayout Express)

Miru is a powerful tool specifically designed for the visualisation and analysis of large network graphs obtained from biological datasets (Theocharidis et al. 2009). Before using this software excel datasheets obtained from microarray or RNA-seq analysis were altered to display all annotation data on the left of sheet and group headings were positioned in logical order. This altered file was saved as “filename.expression” (Section 2.5.2). Miru was launched from website: http://kajeka.com/. The normalised, non-log transformed gene expression files were inputted into the Miru platform. Miru displayed Load correlation data dialog box, ID columns red, meta-data green and raw data light blue and created visual graphs based on a Pearson correlation matrix. A sample to sample correlation matrix was calculated using the pre-processing option along with the transpose option. A Correlation Value of 0.95-0.99 was selected followed by ok. The resulting analysis displayed Nodes, representing individual data sets in the form of circular balls and Edges representing connections between each node (Red lines show close relation Pearson of 1, Blue lines represent lower end of threshold) and were saved accordingly. For gene analysis no pre-processing was required.

A pairwise transcript to transcript Pearson correlation matrix was calculated based on each transcripts profile across all samples in the experiment. For Expression Graph Settings various values were altered, generally a value of 50 was entered for Filter Rows with all values less than 50 (background and or genes of little relevance) and 0.95-0.99 for Correlation Value (Nodes and Edges values are displayed accordingly). The network graph was further processed and clustered into groups of genes sharing similar profiles (unique clusters) using the Markov Clustering (MCL) algorithm, at an MCL inflation value set to 2.2 (controls granularity of clustering). Generally a value of 5-10 was selected for the Smallest Cluster Allowed then click Run MCL. Under Class Viewer  icon the content of each cluster was viewed using the various options available. To identify clusters of interest Class viewer was selected and various clusters were explored. To remove Nodes without any assigned class a “no class” node was selected followed by Ctrl+Alt+S (select all nodes) then Ctrl H (Hide). Clusters of interest were selected using Ctrl+R (reverse selection) then Ctrl H or Ctrl U to unhide nodes. Tables of data were exported as TXT files. To separate gene name from I.D number in excel, select column, Data, Text to Columns, Delimited, Tick space, Finish. Gene lists associated with clusters were cross referenced with Analysis of variance (ANOVA) lists by the following method: Copy cluster list into new tab (gene name only), highlight and name column List1 (top left box, List1 enter), in another tab named reference (ANOVA) add all genes and P-Values, LogFC data (ANOVA), don’t include headings, enter code =VLOOKUP(A1,List1,1,FALSE), A1 can be changed to link to any column for comparison, highlight the correct number of cells, Select Home, Fill, Down.

2.5.6 PANTHER, GOrilla and DAVID gene expression analysis

PANTHER (Protein Annotation Through Evolutionary Relationship), GOrilla (Gene Ontology enrichment analysis and visualisation tool) and DAVID (Database for Annotation, Visualisation and Integrated Discovery) are freely accessible bioinformatic databases (Mi et al. 2013; Eden et al. 2009; Huang, Sherman, and Lempicki 2008). PANTHER is a comprehensive system combining gene function, ontology, pathways and statistical analysis tools. GOrilla is another Gene Ontology (GO) analysis tool with fast running time and effective graphical representation. DAVID is also effective at extracting biological meaning for large gene lists. All programs were utilised here for analysing gene expression experimental data GO terms. Each tool was launched from the website link http://www.pantherdb.org/, http://cbl-gorilla.cs.technion.ac.il/ and https://david.ncifcrf.gov/. From previously created gene datasets in excel a list of candidate gene symbols were copied and pasted into relevant box and *Mus musculus* was selected where applicable for organism identification. Selected Identifiers included either Affymetrix exon gene ID or official gene symbol. Various options were then selected based on each dataset and the relevant analysis was saved accordingly.

2.5.7 BioGPS

This gene annotation portal based on existing genetic and genomic resources is freely and publicly available at http://biogps.org/ and enables users to easily integrate data within the BioGPS platform and explore the landscape of gene annotation for one or more genes of interest (Wu et al. 2009). Genes of interested were inputted into this software and results were saved accordingly.

2.5.8 Real-Time quantitative Reverse Transcription PCR (RT qRT-PCR)

Extracted RNA samples were used as a template for cDNA synthesis. RNA was diluted accordingly in RNase-free water based on nanodrop quantification values to get a final working volume of 1µg RNA. Samples were incubated with 2µl (0.5µg/µl) of Oligo (dT)15 (Promega) plus 2µl 10mM dNTP's (Invitrogen) and topped up to a final volume of 26µl using RNase-free water. Negative controls comprising RNase-free water alone were also included. The mixture was heated for 5 minutes at 65^{o}C followed by immediate incubation on ice for 1 minute. The following reaction for first strand synthesis was then carried out: 8µl of 5X First strand buffer (Life Technologies), 4µl of 0.1M DTT (Life Technologies), 1µl Superscript III (Life Technologies) and 1µl RNasin Plus RNAse Inhibitor (Promega). The thermocycler was set-up to the following program: 60 minutes at 50^{o}C followed by 15 minutes at 70^{o}C then hold at 4^{o}C. The synthesised cDNA had a concentration of 25ng/µl and was stored at -70^{o}C until further use. A standard PCR as described in Section 2.1.4 was used to confirm the presence of cDNA. 15µl of mastermix (Table 2.4) was added to each well in a 96 well plate followed by the addition of 5ng/µl of cDNA (1/5 dilution of stock). Controls included wells where cDNA was replaced with RNAse/DNAse free water. This controlled for cross contamination between wells or contamination of one or more reagents. Additionally, wells comprising the equivalent concentration of RNA (minus reverse transcription) were included as controls for genomic DNA contamination.

Components (All Primerdesign)	Per Single Reaction (µl)
Resuspended primer mix	1*
2X PrecisionPLUS mastermix	10
RNAse/DNAse free water	4
Final Volume	**15**

*Working concentration of primers was 300nM in a 20µl reaction

Components (Sigma Oligo's)	Per Single Reaction (µl)
Brilliant III Ultra-Fast SYBR Green*	10
Reference Dye (1/500 dilution)	0.3
20µM Primer A	0.4
20µM Primer B	0.4
RNAse/DNAse free water	0.9
Final Volume	**12**

*Agilent Technologies

Table 2.4: Mastermix ingredients and quantities for RT-qPCR using Primerdesign or Sigma methods. All runs were carried out using the Stratagene Mx3005p system. In these studies SYBR green mastermix (Primerdesign/ Agilent technologies) was the fluorescent dye used. 96 well PCR plates (ABgene) and optical caps (Applied Biosystems) were used for all RT-qPCR runs. Each sample was loaded in triplicate.

Primers were selected based on target genes of interest and included Transforming growth factor beta induced (*Tgfbi*), Laminin alpha 1 (*Lama1*), Transthyretin (*Ttr*), Myocyte Enhancer Factor 2C (*Mef2c*), Midline 1 (*Mid1*), Solute carrier family 9 member b2 (*Slc9b2*) and PrP (*Prnp*) all from Primerdesign. Tumor necrosis factor, alpha-induced protein 2 (*Tnfaip2*), Tumor necrosis factor (*Tnf*), Purinergic receptor P2Y, G-protein coupled, 14 (*P2ry14*), Lysosomal protein transmembrane 5 (*Laptm5)*, and neurotrophic receptor tyrosine kinase 1 (*Ntrk1*) were obtained from Sigma.

To identify suitable reference/ housekeeping genes the GeNorm PCR kit (Primerdesign, *Figure 2.3*) was used as described in manufactures protocol (http://www.protocol-online.org/forums/uploads/monthly_07_2012/post-6378-0-25922900-1342778301.ipb). The kit utilised a panel of 12 reference genes namely, *B2m* (Beta-2 microglobulin), *Ubc* (Ubiquitin C), *Gapdh* (Glyceraldehyde 3-phosphate dehydrogenase), *Actb* (Beta-actin), *18S* (Ribosomal RNA), *Ywhaz* (Tyrosine 3-Monooxygenase/Tryptophan 5-Monooxygenase Activation Protein), *Cyc1* (Cytochrome C-1), *Canx* (Calnexin), *Rpl13a* (Ribosomal protein LI3A), *Atp5b* (ATP synthase/ H^+ transporting mitochondrial F1 complex), *Eif4a2* (Eukaryotic Translation Initiation Factor 4A2) and *Sdha* (Succinate Dehydrogenase Complex). Mastermix for reactions described previously in Table 2.4 and sample cDNA was added to 96 well plate in triplicate at 5ng/µl (1/5 dilution of stock). As shown in Table 2.5, amplification conditions varied slightly between Primerdesign and Sigma and were selected according to primers used.

Cycling	Step	Time (seconds)	Temperature °C
	Enzyme activation	120	95
Cycling x40	Denaturation	10 (15)	95
	DATA Collection*	60 (30)	60

*Fluorogenic data collected through SYBR green channel.

Table 2.5: Amplification conditions for 2X PrecisionPLUS qPCR mastermix used in conjunction with the Mx3005p system (Primerdesign). Conditions in brackets were used for brilliant III Ultra-Fast SYBR Green mastermix (Sigma). The result of each run was saved as both MXP and TXT format.

To analyse results, MxPro software was launched and SYBR Green (with dissociation curve) option was selected followed by relevant saved mxp file. The plate was labelled according to sample identification and the all tab was selected followed by the analysis and the results tab.

Under the Amplification plots option all Ct (Cycle threshold) values were viewed to confirm reproducibility and variability between replicates (< 0.5 difference in Ct values acceptable). Consolidated reports were generated and saved as bmp files. Text report option was selected and the following parameters were chosen: Well, Well name, Dye, Well type, Ct (dR), and Quantity (copies) and this information was exported as a Text file. Text files were saved as xlsx for standard analysis. Results from the GeNorm PCR kit were analysed using the Biogazelle qbase^{+} analysis software. This software included a module for GeNorm analysis. The software was launched and a new project was created followed by next tab. The relevant TXT files were imported under manual import option. Manual import configuration had the following parameters – Mx3000xP, Open Runs (Never), Extract well Info (Selected) and Sample (Selected). The next options were variable depending on sample analysis type where maximum replicate variability (Difference in Cq) was set to 0.5 and default settings were selected for the rest of the available parameters. Quality control outputs demonstrated 100% pass rates. Analysis results produced a graph showing average expression stability of 12 reference targets ranking according to expression stability (left of graph least stable, right most stable).

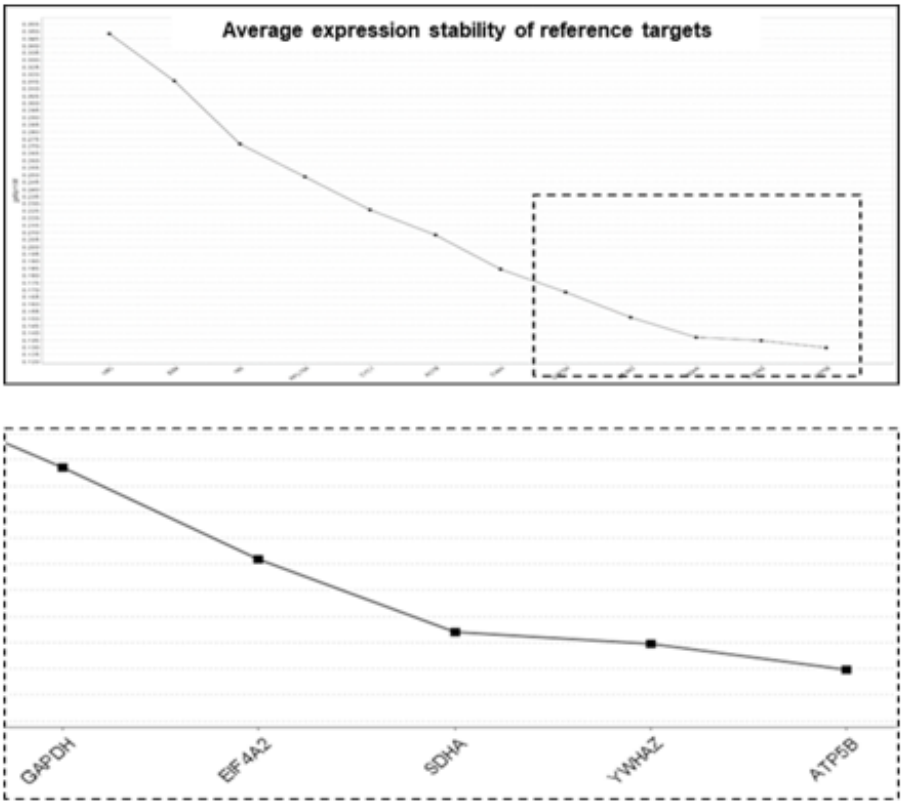

Figure 2.3: Identification of the most stable reference/housekeeping genes. The GeNorm kit was used to identify genes that would be stably expressed across all samples, to provide suitable reference/ housekeeping genes for normalisation to be carried out of all RT-qPCR runs. The top graph shows expression stability of 12 individual reference targets (Section 2.5.8) generated using Biogazelle qbase (geNorm technologies) software based on MxPro (Stratagene) obtained data. Least stable genes are to the left of the graph (bottom) and increase in stability to the right. Enlarged image (dotted line box) clearly demonstrates that Succinate dehydrogenase complex (*Sdha*), Tyrosine 3-monooxygenas/tryptophan 5-monooxygenase (*Ywhaz*) and ATP synthase/ H^+ transporting mitochondrial F1 complex (*Atp5b*) were stably expressed across all 16 microarray untreated samples and therefore were selected as reference/housekeeping genes for all RT-qPCR runs. Y axis geNorm M-value, calculated by GeNorm is a measure of stability of gene expression, lower M-values show increased stability. X axis, genes were ranked starting with least stable genes on left.

Relative changes in gene expression were calculated using the Delta Delta Ct ($\Delta\Delta C_T$) method using the formula shown in Table 2.6 (Livak and Schmittgen 2001).

Sample	Gene	
	Target (Gene of interest)	Reference
Calibrator (WT)	C_T(target, calibrator)	C_T(reference, calibrator)
Test (101LL)	C_T(target, test)	C_T(reference, test)

Table 2.6: Relative Quantification using the Livak, or $\Delta\Delta C_T$ method. Normalisation was carried out against the most stable reference gene. Three stages were carried out in excel based on the average of C_T readings: 1. Normalise C_T (target gene) to C_T (reference gene); 2. Normalise ΔC_T of test sample to ΔC_T of calibrator [$\Delta\Delta C_T$ = C_T (test) - ΔC_T (calibrator)]; and 3. Calculate expression ratio, or fold difference [$2^{-\Delta\Delta C_T}$].

2.6 Organotypic brain slice culturing

Brain organotypic brain slice cultures (BOSC) were developed based on a modified version of the original protocol described by Stoppini (Stoppini, Buchs, and Muller 1991). Organotypic brain slices were obtained from brains of mice at postnatal Days 6-7 (Cho, Wood, and Bowlby 2007). A non-Schedule 1 termination of each individual postnatal pup involved decapitation followed by immediate brain removal and immersion into oxygenated artificial cerebrospinal fluid (aCSF). The aCSF was prepared as follows and mixture was cooled until slush like appearance: 125mM NaCl, 26mM $NaHCO_3$, 25mM Glucose, 2.5mM KCl, 1.25mM $NaH_2PO_4H_2O$, 1mM $CaCl_2$ and 4mM $MgCl_2$ pH 7.4. The aCSF slush was then oxygenate using 95% O_2 / 5% CO_2 gas (BOC). After a 3 minute incubation in oxygenated aCSF the brain sample was placed on the Mcilwain tissue chopper and 400µm thick coronal brain sections were cut. The sectioned brain was carefully placed in aCSF buffer and slices were dissected under a dissection microscope which aided efficient separation. Both full brain slices and hippocampal only slices were taken for culturing. The freshly prepared slices were placed on pre-warmed 6 well culture plates containing sterile 0.4µm pore 30mm membrane inserts (Millipore) and 1ml of culture medium.

Organotypic slice culture medium ingredients were obtained from Invitrogen and the formula was as follows: 49.6ml Minimum Essential Medium (1X) liquid (with Earle's Salts, 25mM HEPES, without L-Glutamine), 24.8ml Hank's balanced salt solution, 24.8ml Horse serum (heat-inactivated), 1ml Penicillin-Streptomycin (10,000 U/ml, Gibco) and 0.25% L-Glutamine 100X (200mM). Plates were incubated at 37^{o}C in 5% CO_2. Organotypic slice culture medium was replaced twice a week with fresh pre-warmed medium to maintain a healthy culture. Fixation of organotypic slices for immunolabelling was carried out as follows: organotypic slices were incubated with 4% PFA (w/v) for 45 minutes at room temperature. The PFA was removed and slices were washed three times with DPBS containing Ca^{2+} and Mg^{2+} (Gibco). 1-2ml of ice-cold methanol was added to the cells for 10 minutes at -20^{o}C followed by a 5 minute incubation with 0.3% Triton-X (v/v, Sigma-Aldrich) at room temperature. Cells were blocked for 2 hours at room temperature using Fc Block (Anti-mouse CD16/32 BioLegend). Primary antibodies (Table 2.1) were incubated overnight in 5% Goat serum (v/v, Gibco) at 4^{o}C, then were washed three times in DPBS containing Ca^{2+} and Mg^{2+} (Gibco). Incubation in secondary antibodies listed in Table 2.1 followed for 1.5 hours at room temperature in complete darkness. Slices were washed three times again in DPBS, for the final wash and a DAPI (Molecular Probes) counterstain was carried out (300nM). Using a scalpel the membrane supporting the tissue slice was dissected from the insert and was placed in 40µl of Prolong Diamond Antifade Mountant (Life Technologies) which was previously loaded onto a specialised cavity glass slide (Marienfeld). Coverslips were placed over membranes and were allowed to dry for 4 hours at room temperature then overnight at 4^{o}C. Coverslips were sealed using CoverGrip Coverslip Sealant (Cambridge BioScience) and imaged using the LSM710 inverted confocal microscope (Zeiss). Slides were stored at 4^{o}C for several weeks without substantial loss of fluorescence.

CHAPTER 3

Development and characterisation of primary hippocampal neuronal culture model

3.1 Abstract

An *in vitro* system was established at the Roslin Institute with which to study the cellular and molecular mechanisms of prion-induced neurodegeneration. The hippocampal area of the brain is vulnerable in a range of protein misfolding diseases, therefore primary mixed neuronal cultures were prepared from murine hippocampi and characterised for cell representation and synapse formation. This model system contained readily accessible neurons and important supportive cells such as astrocytes and microglia. Cultures were established from wild type animals and a number of different transgenic animals with altered PrP^C production. This study mainly focused on two genotypes, PrP 101LL mice (101LL) that support PrP fibril formation and 129/Ola mice (WT) that do not. The cultures developed highly branched neuronal networks supported by glia. In-depth analysis of immunolabelled cell populations was carried out using IMARIS modelling software and no obvious morphological differences were noted between WT and 101LL genotypes. Neuronal maturity was confirmed by the presence of both pre and post-synaptic protein markers and cultures were maintained for up to twenty days. PrP^C was detectable in cultures from DIV3 (Days *in vitro*) and biochemical analysis confirmed a similar glycosylation profile to murine brain suggesting PrP^C in this model was processed similarly to the *in vivo* environment. In conclusion, this system provided an excellent *in vitro* model for investigating early misfolded protein processing.

3.2 Introduction

The brain is the most complex organ of the body therefore the development of more simplified easily accessible but still appropriately representative *in vitro* models is paramount for studying neurodegeneration. Currently there are no effective treatments for neurological disorders such as Alzheimer's disease (AD), Parkinson's disease (PD) and Prion disease all of which are associated with misfolding proteins. A well characterised *in vitro* model system may provide mechanistic insights of misfolded protein metabolism relevant to the development of new therapeutic strategies for these diseases. Currently there are numerous cell lines used in the neurodegenerative field to study neurodegeneration including PC12 (rat adrenal medulla pheochromocytoma cells), SH-SY5Y (human neuroblastoma cells), N2a (mouse neuroblastoma cells) and GT1 (mouse hypothalamic cells), however each of these cell lines have their limitations in their overall representation of the brains cellular make-up (Schlachetzki, Saliba, and Oliveira 2013; Bosque and Prusiner 2000). Primary neuronal cells are more biologically relevant and can be used to culture neurons and other supporting cells from numerous mouse lines relevant to the study of neurodegenerative disease. In this chapter, a primary hippocampal neuronal system was developed based on previous published work (Kaech and Banker 2006; Banker and Cowan 1977). The hippocampus is associated with cognition, learning and memory and is one of the first regions to suffer damage in AD (Mu and Gage 2011), is implicated in cognitive dysfunction observed in PD's (Calabresi et al. 2013) and also is a target area associated with early synaptic loss in some Prion diseases (Hilton et al. 2013; Cunningham et al. 2003). Furthermore, our previous studies have indicated that this specific area of the brain is a target for abnormal protein seeding in 101LL mice and therefore may play a major role in protein misfolding diseases (Barron et al. 2016). Studying subcellular distribution and misfolded protein interactions in the hippocampus *in vivo* is extremely difficult due to its position within the brain. Thus, this area is the focus for *in vitro* modelling in this study.

The development of a primary culturing system from the hippocampus can help to address this to a certain extent whilst providing an easily accessible and manipulatable system for studying misfolded protein trafficking and degradation pathways. Hippocampal cultures were prepared from late-stage mouse embryos (Day 17). There were a number of considerations that influenced this choice of time point including but not limited to, the presence of pyramidal neurons, ease of tissue dissociation, and comparatively low presence of glial cells. However, the trade-off for these positive factors is that the generation of dentate granule neurons has not yet begun (Banker and Cowan 1977). Traditionally an astrocyte feeder layer system was used to provide trophic support to the neurons. Here an alternative strategy was employed where neurons were maintained in growth medium containing N2 and B27 supplements that enhanced and promoted neuronal growth and maintenance (Kaech and Banker 2006; Brewer et al. 1993). To summarise, previous studies by our group have shown that WT mice were able to curtail protein misfolding seeding mechanisms whilst 101LL mice supported it. Both WT and 101LL mouse lines therefore provided excellent tools for investigating misfolded protein interactions. Thus, primary hippocampal neuronal models were generated from these genotypes providing an excellent *in vitro* platform to enable the investigation of neuronal and neuroglia interactions when challenged with misfolded protein. Any processing pathways found here might also be relevant to other neurodegenerative diseases.

3.3 Results

3.3.1 Optimising conditions for hippocampal dissection and cell dissociation

CD-1 mice were initially used to develop the workflow and establish a reproducible hippocampal dissection and processing methodology as these mice are reliable breeders and provided large numbers of embryos. After this optimisation WT, 101LL and PrP knockout line ($PrP^{-/-}$) were used for generating primary hippocampal cultures. In accordance with Home Office non-schedule 1 procedures, the embryos were chilled on ice until a complete lack of responsiveness was observed and then immersed into ice-cold BME buffer (Materials and Methods, 2.2). As shown in *Figure 3.1* each embryo head was removed and the brain isolated. A tail snip was also retained from each embryo (applicable to all genotypes) and PCR was subsequently used to confirm genotype.

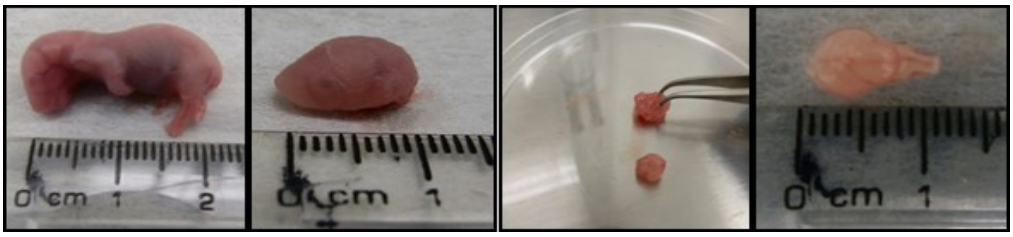

Figure 3.1: Illustration of the technique to remove brains from Day 17 embryos. Each embryo was approximately 2cm in length. The head was decapitated and using a fine scissors, a midline incision at the skin surface was made and the skull was separated into two halves. The brain was carefully removed and was placed into a 35mm culture dish containing ice-cold Hanks/Hepes buffer. Hippocampi were then isolated with the aid of a dissection microscope.

To facilitate efficient dissociation of hippocampal cells, trypsin from two manufactures Worthington Biochemical Corporation and Life Technologies were initially investigated.

Cells needed less trituration using Life Technologies Trypsin minimising damage during cell dissociation and therefore this brand was used for all subsequent hippocampal dissociation procedures. Cell density was calculated using a hemocytometer and cell viability was determined using 0.4% Trypan Blue solution. In all cases where Trypan blue was used to test cellular viability the majority of cells tested were colourless indicating minimal presence of damaged cells in relation to cell dissociation methods. Approximately 400,000 cells were isolated per embryo and cells were plated at concentrations relevant to the culture platform used (Materials and Methods, 2.2.2). Cells were initially plated overnight in growth medium however, this generated surplus debris in the cultures, which contributed to cell stress and neuronal deterioration within a couple of days in culture. To overcome this problem initial incubation time in growth medium was decreased from 24 hours to 4 hours allowing adequate time for cellular adherence to the relevant attachment factor. This also allowed for rapid removal of unwanted cellular debris from the cultures. After this step, cells were maintained in serum-free medium. Two different recipes of media were investigated to determine which would provide maximum neuronal support and growth *in vitro* (Table 3.1). These recipes were made with either GS21 (Sigma) or B27 (Gibco) supplements and culture growth and sustainability was monitored accordingly. GS21 claimed to be superior to B27 regarding long-term neuronal viability however, when cellular viability was measured using a Lactate dehydrogenase (LDH) cytotoxicity assay (Section 3.3.2), B27 cultures showed better neuronal viability (*Appendix Figure 3a*). Light phase contrast microscopy of cultures confirmed the development and morphological characteristics of neuronal-like cells. This was useful in determining if cells were present but was limited in its overall contributions to understanding the development and viability of these cultures over-time. Other characterisation methods were therefore employed to help with these investigations.

Original Serum-Free Medium	Improved Serum-Free Medium
Basal Medium Eagle 500ml (Gibco)	Neurobasal Medium 500ml (Gibco)
B27 50X 10ml (Gibco)	B27 50X 10ml (Gibco)
32.5% Glucose 8ml (Sigma)	L-Glutamine 200mM 5ml (Gibco)
Penicillin-Streptomycin 5ml (Gibco)	Penicillin-Streptomycin 5ml (Gibco)
Sodium Pyruvate 100mM 5ml (Gibco)	
N2 supplement 5ml (Gibco)	

Table 3.1: Different formulas for supporting primary cultures were investigated. Initially cultures were incubated with original serum-free medium recipe however, due to various problems incurred during culturing this formula was changed to the improved serum-free medium, which supported long-term viable neuronal growth.

3.3.2 Monitoring neuronal viability in normal and stressed environments

To assess the suitability of different culturing protocols it was necessary to determine the viability of cellular preparations to identify to most sustainable and optimal methods for maintaining primary neuronal cultures *in vitro*. Thus, cellular viability of WT and 101LL cultures was evaluated using a commercially available CytoTox 96 Non-Radioactive cytotoxicity LDH Assay (Materials and Methods, 2.2.4). This assay quantitatively measures a stable cytosolic enzyme LDH that is released from damaged cells into the medium and is therefore used to determine cellular health (Smith et al. 2011). Supernatants removed during routine culture maintenance were retained for LDH analysis (Materials and Methods, 2.2.3). Initial experiments indicated retained supernatants could not be frozen for long term storage as recommended by the supplier, instead they were stored at 4^{o}C (LDH consists of five isoenzymes which have varied responses to different storage conditions, LDH 4 and LDH 5 are sensitive to freezing). LDH readings in WT cultures were minimal indicating neuronal cells were viable in their new *in vitro* environment (*Figure 3.2*). Low concentrations of LDH measured over-time suggested that WT cell cultures were viable up to eight days *in vitro*.

101LL neuronal cultures displayed a similar LDH response trend but were more susceptible to cellular stress after initial plating (*Appendix Figure 3.a*). To determine how long viable primary hippocampal cultures could be maintained for, longer time point experiments were carried out and results confirmed cells were stable up to DIV20 (*Appendix Figure 3.b*). Similar studies were also carried out using a PrP knockout line ($PrP^{-/-}$). $PrP^{-/-}$ mice lack the presence of PrP^{C} protein, which has been proposed to have neuro-protective properties suggesting these cells may be more susceptible to stresses from *in vitro* culturing. LDH studies showed minimal stress levels were evident in $PrP^{-/-}$ cultures even after initial plating indicating PrP^{C} may not play an important role in neuroprotection (data not shown).

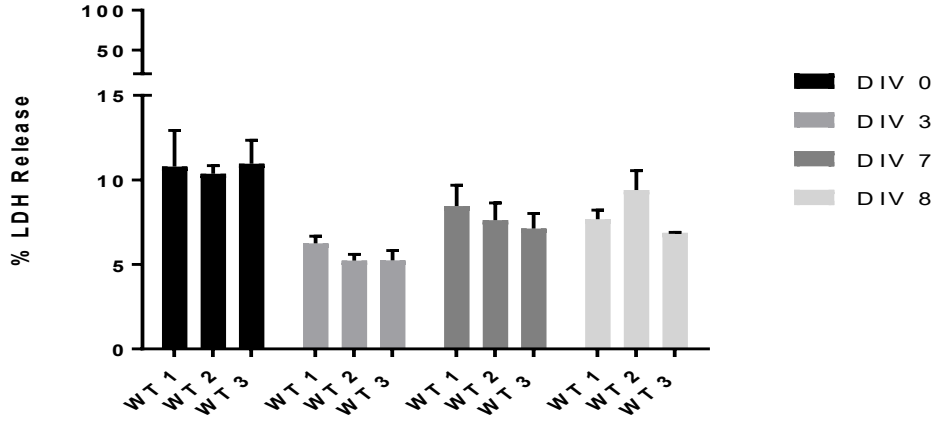

Figure 3.2: Minimal levels of Lactate Dehydrogenase (LDH) were found in primary hippocampal cultures. LDH was measured in the supernatant of primary cultures prepared from WT mice at 0, 3, 7 and 8 days *in vitro* (DIV) and was used to monitor cellular viability over-time and cell viability was maintained up to DIV8. Individual sample readings also confirmed viability was reproducible in cultures. Fluorescent values were normalized to Triton X-100 treated lysis cells that represent the maximum amount of LDH available for release. WT cells plated at 400,000 cells per well on pre-coated PLL 6 well plates, Graph mean plus standard deviation, n=3 triplicate technical replicates.

3.3.3 Characterisation of neuronal development

Cell growth was initially characterised based solely on the morphological appearance of cells under phase contrast microscopy, in conjunction with LDH analysis (*Figure 3.2, 3.3*). Further insight on cell development was gained from live cell imaging where neurons developed as expected and were seen to be constantly monitoring their environment by either contracting or extending their processes. Snapshots obtained from live imaging (*Figure 3.3*), show early neuronal developmental as previously described by other groups (Beaudoin et al. 2012). These stages were determined by morphological alternations and included; DIV0-1 cell attachment to the chosen substrate followed by extension of lamellopodia; DIV1-2 emergence of several minor/short neuronal processes known as neurites; DIV2-3 individual neurite growth forming long axons and DIV3 axon development where dendrites started to grow and branch. Further development involved synapse formation and neuronal maturation, which will be discussed later in this chapter (Section 3.3.5). Based on phase contrast image analysis from both WT and 101LL cultures it was concluded that both neuronal cultures develop in a similar manner, reflective of that reported in the literature (Beaudoin et al. 2012; Kaech and Banker 2006). Some individual cellular variation in cell maturity was seen within cultures but by DIV6, all cells were at equivalent stages of growth. Phase contrast microscopy showed the development of neuronal-like cells from primary hippocampal cultures however, this was not an absolute identification of these cell types. To address this, immunofluorescent labelling of neuronal specific proteins was used to confirm neurons were present and allowed for in-depth morphological analysis to be carried out. Immunolabelling for both MAP2 and Tau confirmed the presence of neurons in culture (*Figure 3.4*). MAP2 is commonly used as a marker for neuronal cells and their dendritic processes. Tau is expressed abundantly in neurons and to a lesser extent in astrocyte and oligodendrocyte cell populations. Both markers highlighted the complexity of these neuronal communication networks however, the intensity of Tau immunolabelling was too complex for any additional computational analysis to be carried out.

Therefore, MAP2 was predominantly used for future morphological analysis studies using IMARIS image analysis software (Materials and Methods, 2.2.9). IMARIS software was developed to explore and analyse complex datasets and was used throughout the characterisation of primary hippocampal cultures. Initial analysis employed IMARIS filament tracer, which reconstructed MAP2 immunolabelled confocal images and showed some 3D characteristics were maintained after fixation of cultures using specialised concave microscope slides (*Figure 3.5*). Additional analysis allowed for the detailed examination of neuronal population morphologies from both WT and 101LL genotypes, that were shown previously to have contrasting responses to abnormal protein insult *in vivo* (Barron et al. 2016). No differences were seen in dendrite area (sum of the generated surfaces of a frustum or truncated cone) and dendrite branching angle (angle directly at a branch point) parameters in both genotypes (*Figure 3.6;* mean dendrite area WT 34.56; 101LL 35.40; mean dendrite branching angle WT 16.12; 101LL 15.95). However, differences in dendrite length (the sum of the length of all edges, which compose a dendrite) were detected (*Figure 3.6*; mean dendrite length WT 6.02; 101LL 4.98). Further investigations determined variation in this parameter occurred between cultures even of the same genotype and therefore, any significant morphological differences between genotypes should be viewed cautiously as these results may not be of biological significance. Additionally, the intricacy of the neuronal networks were challenging to the algorithms employed in the IMARIS software, which may have introduced some misconstructions. Overall, it was concluded no obvious differences were evident in the intrinsic properties of 101LL cultures that might support abnormal protein production after fibril challenge. Monitoring the development of primary neurons over-time by immunocytochemistry was important in determining growth, development and survival *in vitro*. MAP2 staining was used to investigate this at a number of time points. Neuronal growth was evident and constantly developing over-time (*Figure 3.7*). At DIV20, a noticeable decrease in neuronal staining was evident which complemented previously obtained LDH results (*Appendix Figure 3.b*) suggesting a loss of neuronal viability from this time point.

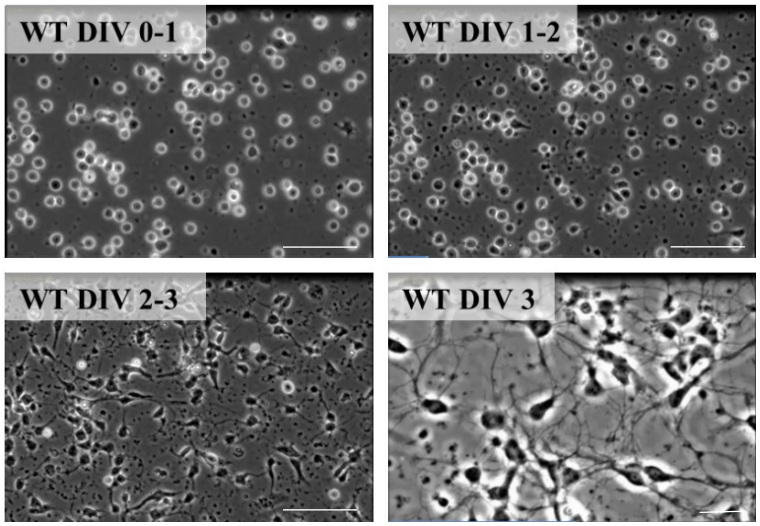

Figure 3.3: Morphological development of dissociated cells into neuronal-like cells. *In vitro* development of dissociated neuronal cultures was visualised using the live cell observer and snapshots from live imaging videos were taken from 0-3 days *in vitro* (DIV) to confirm neuron-like cells were developing normally. Neuronal-like processes were evident from DIV2-3, confirming normal growth of cells. Scale bar WT DIV 0-1; 1-2; 2-3 50µm, WT DIV 3 30µm Zeiss live cell axiobserver.

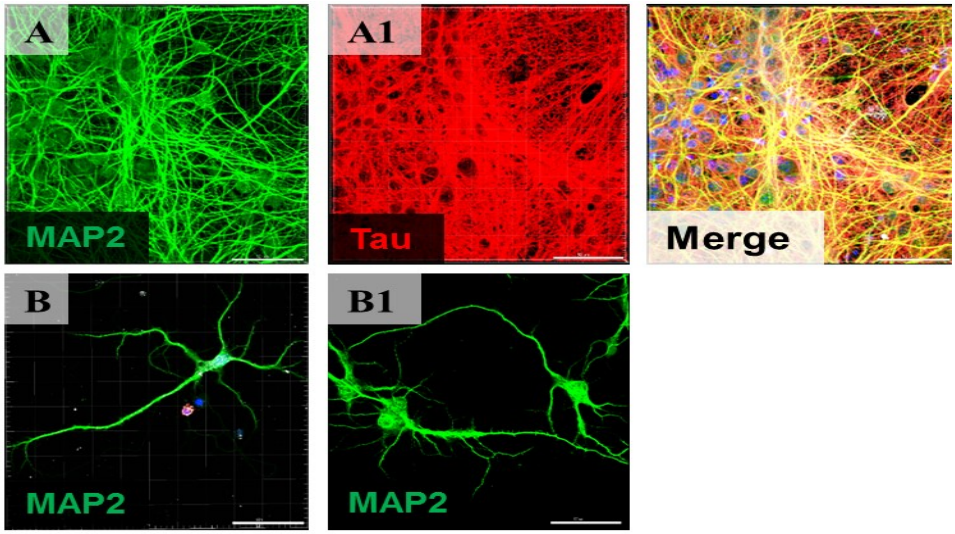

Figure 3.4: Immunolabelling of neuronal specific proteins confirmed neurons were present in cultures. Primary cultures labelled with (A) Dendritic marker Microtubule Associated Protein 2 (MAP2/Green) and (A1) Neuronal marker Tau (Red). Tau immunolabelled images displayed less definition in comparison to MAP2. (B-B1) Plating at low cell density was advantageous for studying neuronal morphology. Hippocampal cultures (A) 150,000 (B) 75,000 cells, plated on PDL/Fibronectin glass coverslips, Scale bar 50µm, Zeiss LSM 710.

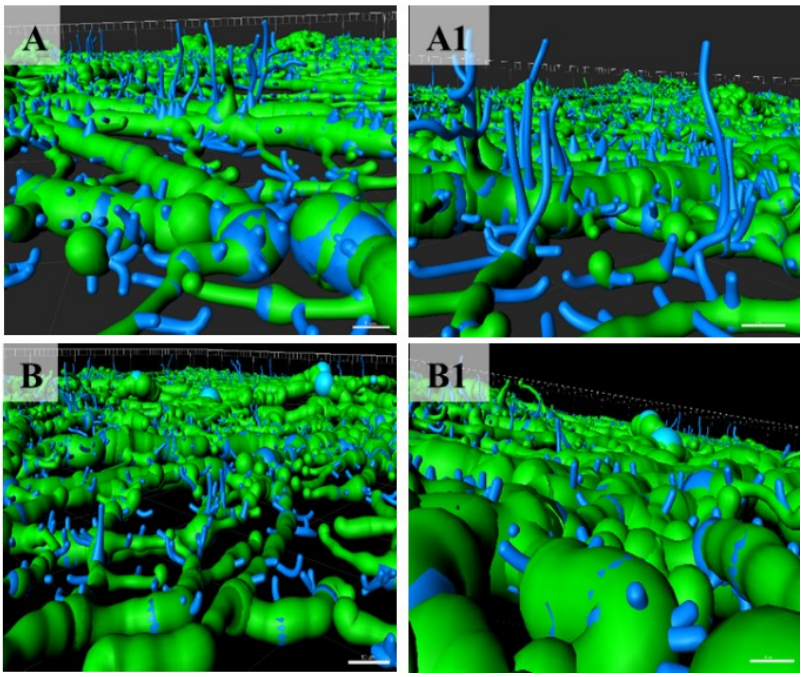

Figure 3.5: Concave mounting of cultures conserved neuronal architecture. IMARIS reconstructions of MAP2 (neuronal) immunolabelled images were generated for concave and flat mounting methods. (A-A1) Concave coverslip mounting and (B-B1) Flat coverslip slip mounting. Concave images displayed abundant 3D processes throughout sections, highlighted in blue. Flat mounting showed limited 3D processes present in the sections therefore, concave mounting was always used for imaging which helped maintain neuronal structures. 101LL DIV8 cultures 75,000 cells, plated on PDL/Fibronectin glass coverslips, Scale bar (A, B) 10µm, and (A1, B1) 5µm, Zeiss LSM 710.

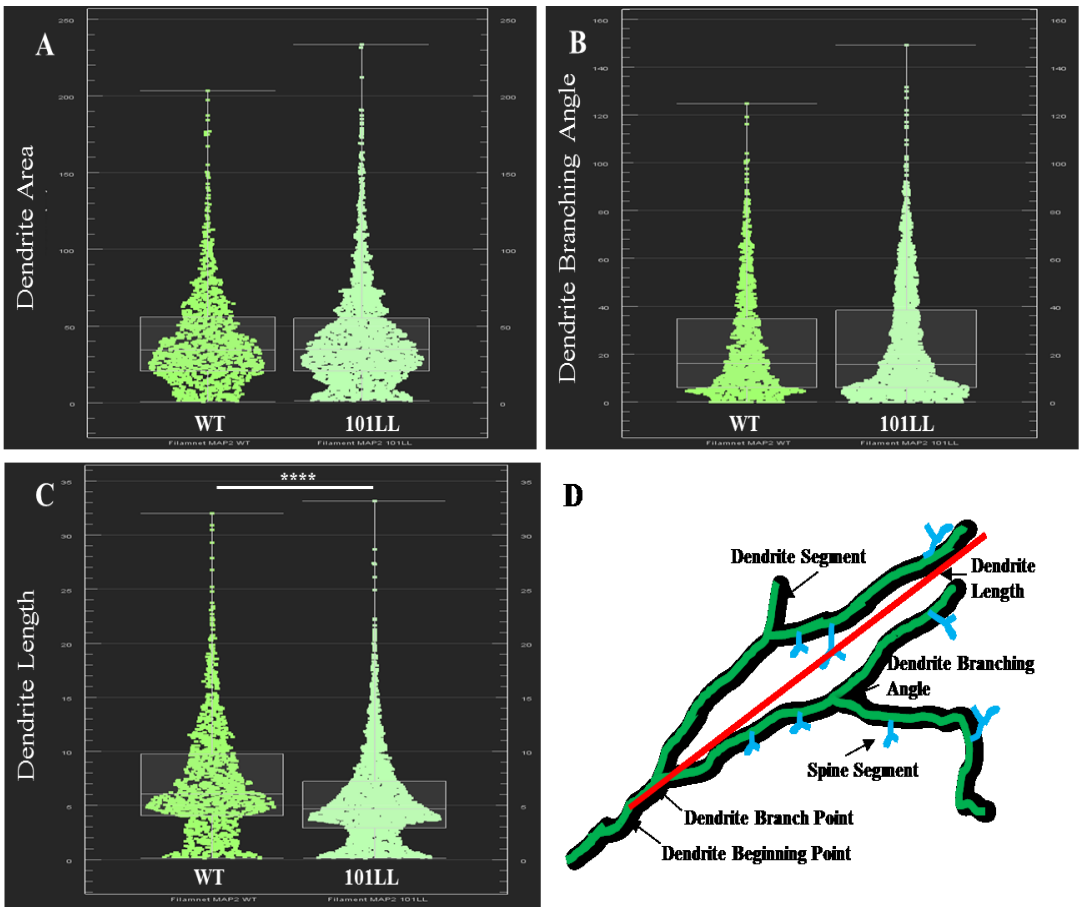

Figure 3.6: Morphological comparison of neuronal networks from both genotypes. Neuronal structure of WT and 101LL cultures were compared using IMARIS software to identify if any differences were apparent which might explain how one genotype curtails abnormal PrP production (WT) whilst the other supports it (101LL). Additionally, morphological analysis provided baseline data of neuronal cells pre-fibril challenge. IMARIS Vantage (Materials and Methods, 2.2.9) produced visual representative graphs based on IMARIS filament tracer datasets obtained from MAP2 immunolabelled images of WT and 101LL DIV8 cultures. (A) Dendrite area (µm^2, sum of the generated surfaces of a frustum), (B) Dendrite branching angle (Âo, angle directly at a branch point) and (C) Dendrite length (µm, the sum of the length of all edges which compose a dendrite) were compared. (D) Schematic diagram of different areas of the neuron. No differences were evident between genotypes when comparing dendrite area and dendrite branching angle however, significant differences were obtained for dendrite length (P-Value <0.0001), suggesting both similarities and differences were evident between WT and 101LL comparisons. GraphPad Prism was used to analyse IMARIS Vantage readings, unpaired t test.

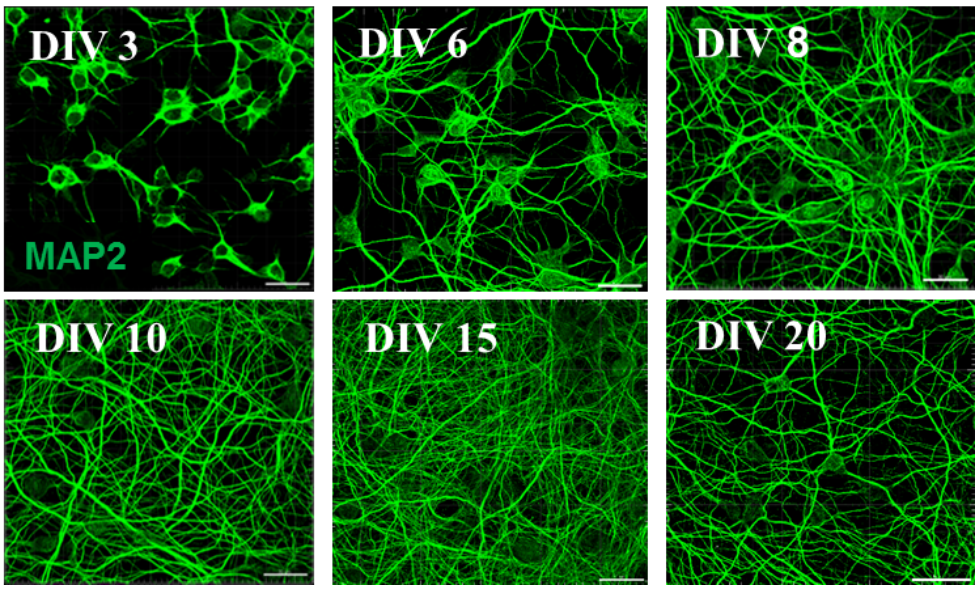

Figure 3.7: Neuronal growth was constantly developing over-time *in vitro*. Immunolabelling with neuronal marker MAP2 (Green) was used to monitor neuronal growth and neurons were still present in cultures at DIV20. 101LL cultures 150,000 cells, plated on PDL/Fibronectin glass coverslips, Scale bar 30µm, Zeiss LSM 710.

3.3.4 Characterisation of non-neuronal cells

As primary cultures are derived from hippocampal mixed brain cell origins, neurons may not be the only cell populations present in these cultures. Thus, the presence of other non-neuronal supporting cells and their abundance, form and degree of interaction at the morphological level was explored. Immunolabelling using the marker Anti-Glial Fibrillary Acidic Protein (GFAP) for astrocytic cells was positive suggesting these supporting glial cells were present *in vitro* and were shown here to be interlinked with neurons (*Figure 3.8*). GFAP is however expressed in numerous cell types in the CNS including astrocytes and ependymal cells. Therefore, to determine if GFAP specifically labelled astrocytes within these cultures two additional markers were used namely; Aldehyde dehydrogenase 1 family, member L1 (ALDH1L1) and Sry-related HMG-box (Sox9). ALDH1L1 is a marker that selectively labels astrocytes in the presence of neurons and microglia (Yang et al. 2011).

ALDH1L1 positive immunolabelling suggested cells identified in primary cultures were astrocytes (data not shown). Anti-Sox9 antibody is a member of the Sry-related HMG-box gene family of transcription factors and is a more definitive astrocytic marker as it is almost selectively expressed by astrocytes in the brain except for ependymal cells and in the neurogenic regions where it is also expressed by neural progenitor cells (Sun et al. 2017). As shown in *Figure 3.9*, GFAP positive cells also expressed Sox9 confirming accurate identification of astrocytes. Gene expression studies described in Chapter 6 (Section 6.3.2) provided transcriptomic data that was mined here to investigate gene expression levels of astrocytic associated cells in cultures to distinguish if genotypic differences were present. No differences in gene expression values for both *Gfap* and *Sox9* as assessed by microarray were evident between genotypes suggesting similar numbers of astrocytes were present in both WT and 101LL cultures (*Figure 3.9*). Morphologically, astrocytes appeared in the form of star shaped glial cells (*Figure 3.10*). The presence of highly ramified processes enable cellular interactions and extracellular homeostasis (Agarwal and Bergles 2014). Importantly, no morphological differences were identified between genotypes and astrocytes appeared to be in surveillance mode pre-fibril challenge.

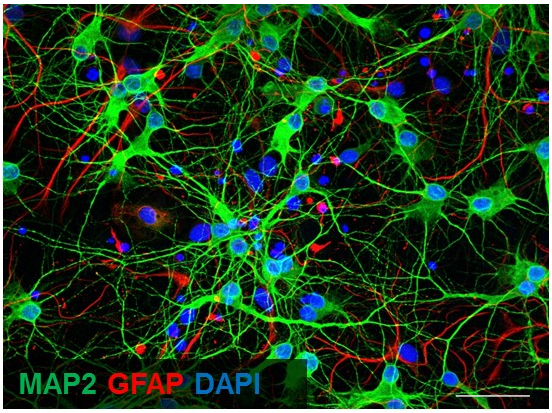

Figure 3.8: Dual-immunolabelling of neurons and astrocytic cells in culture. To investigate if non-neuronal cells were present in primary cultures, dual-immunolabelling for neurons and supporting astrocytic cells were carried out. Anti-Glial Fibrillary Acidic Protein (GFAP/Red) positive immunolabelling suggested astrocytes were present *in vitro* and were interlinking with neuronal (MAP2/Green) populations. WT DIV6 cultures 75,000 cells, Scale bar 20µm.

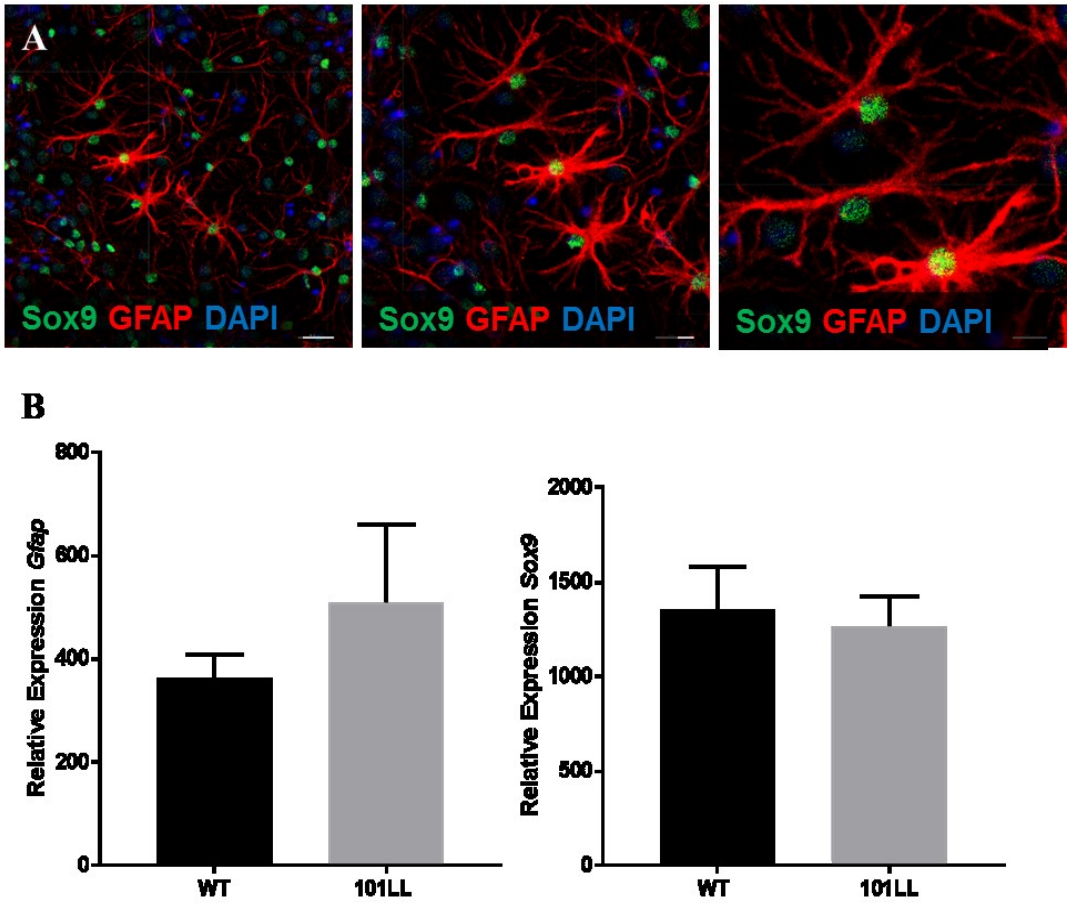

Figure 3.9: Astrocytic populations were present in cultures. To confirm GFAP positive cells were actually astrocytes, dual-immunolabelling with additional astrocyte specific antibodies was carried out. Transcriptomic data obtained from analysis presented in Chapter 6 (Section 6.3.2) was also used to compare astrocytic expression levels in both WT and 101LL cultures to ascertain if these glial cell populations were present in similar numbers in both genotypes. (A) Anti-Sox9 antibody (Sox9/Green) and (GFAP/Red) immunolabelling confirmed GFAP positive populations were astrocytes. (B) Transcriptomic data was mined to examine gene expression profiles of both *Gfap* and *Sox9* in WT and 101LL DIV8 cultures and confirmed no significant differences were evident between genotypes suggesting similar numbers of astrocytes were present in both genotypes. An increase in GFAP signal would represent increased number of astrocytes or activation of gliosis. WT cultures 30,000 cells, plated on PDL plastic plates, Scale bar 100, 30 and 20µm, Zeiss LSM 710. Graph mean plus standard deviation, n=4, n=individual cultures, *Gfap* P-Value 0.11 and *Sox9* P-Value 0.53, unpaired t test.

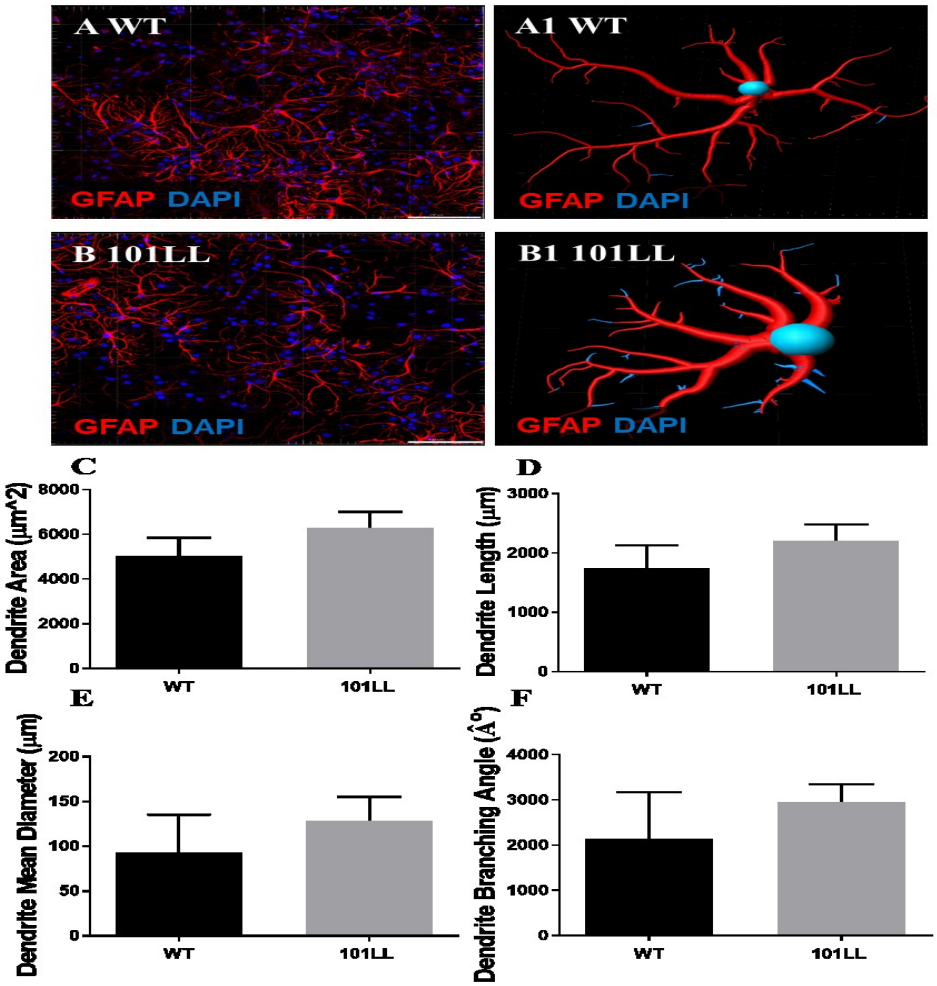

Figure 3.10: Morphological similarities in astrocytic structure were evident between WT and 101LL cultures. Astrocyte morphologies in WT and 101LL cultures were compared using IMARIS software to provide a baseline characterisation of these supportive cells in both genotypes. IMARIS Vantage (Materials and Methods, 2.2.9) was used to reconstruct astrocytic populations based on GFAP immunolabelled images. (A) WT and (B) 101LL primary cultures immunolabelled with astrocytic marker (GFAP/Red) and DAPI (Nuclear/Blue). (A1) WT and (B1) 101LL IMARIS astrocyte reconstructions. (C-F) Comparison between WT and 101LL astrocytic morphologies based on IMARIS generated data-set analysis, which included the following parameters; dendrite area (µm^2, sum of the generated surfaces of a frustum), length (µm, the sum of the length of all edges which compose a dendrite), mean diameter (µm) and branching angle (Âo, angle directly at a branch point). Immunolabelled cells and reconstructions displayed a multiple process phenotype in both genotypes indicating astrocytes were in surveillance mode. No significant differences of any parameters were evident between WT and 101LL genotypes suggesting astrocytic morphologies were comparable between genotypes pre-fibril challenge. GraphPad Prism was used to plot and analyse IMARIS data-set values, P-Values C-F; 0.05, 0.09, 0.20, 0.18, unpaired t test. Scale bar 100µm, Zeiss LSM 710.

Microglia are another type of glial cell involved in maintaining the homeostasis of the brain. Immunocytochemistry studies using two microglial markers namely Cluster of differentiation molecule 11b (CD11b) and Ionized calcium-binding adapter molecule 1 (Iba1) confirmed the presence of these resident macrophages in primary hippocampal cultures (*Figure 3.11*). Microglial populations appeared ramified with long processes, suggestive they were in surveillance mode. Increased immunolabelling of CD11b and Iba1 was detected in $PrP^{-/-}$ cultures suggesting higher numbers of microglia were present in these cultures in comparison to those in WT or 101LL (data not shown). This indicated microglial levels might vary dependent on PrP genotype. This could not be effectively assessed by immunocytochemistry therefore, transcriptomic data presented in Chapter 6 (Section 6.3.2), was mined to investigate gene expression levels of microglial associated cells in both WT and 101LL cultures. As indicated in *Figure 3.11*, no differences in gene expression of microglial-associated genes, Growth arrest specific 6 (*Gas6*) and MER proto-oncogene tyrosine kinase (*Mertk*) were apparent suggesting WT and 101LL cultures had similar levels of microglial present in culture.

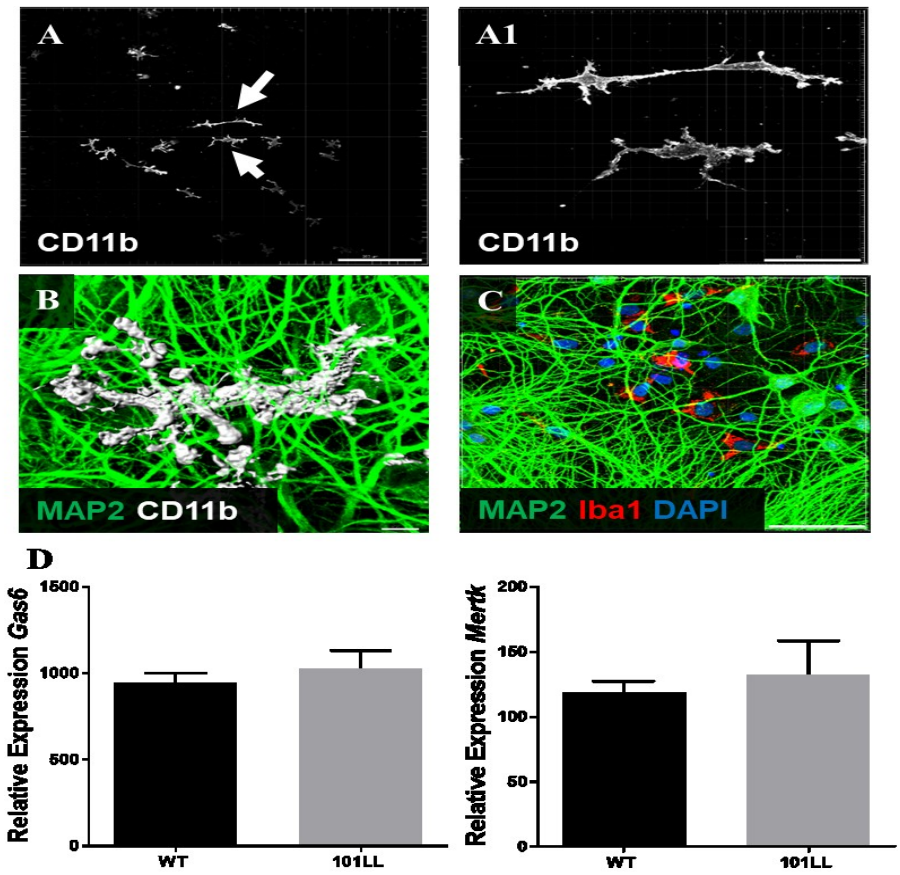

Figure 3.11: Microglial populations were present and in surveillance mode. Immunolabelling for microglial specific markers was carried out to identify if microglial cells were present in primary cultures. Transcriptomic data obtained from analysis presented in Chapter 6 (Section 6.3.2) was used to compare microglial specific gene expression levels in both WT and 101LL cultures to ascertain if these glial cell populations were present in similar numbers in both genotypes. (A-A1) Microglial markers included Cluster of differentiation molecule 11b (CD11b/White) and (C) Ionized calcium-binding adapter molecule 1 (Iba1/Red). (A1) Higher magnification of CD11b positive cells. (B) IMARIS reconstruction of CD11b positive cell displaying integration with neurons (MAP2/Green). (D) Transcriptomic data was mined to examine gene expression profiles of genes uniquely expressed in microglial populations, namely Growth arrest specific 6 (*Gas6*) and MER proto-oncogene tyrosine kinase (*Mertk*) (Butovsky et al. 2014). Immunolabelling for microglial populations confirmed these resident macrophages were present in cultures and IMARIS reconstructions indicated a multiple process phenotype suggesting microglia were in surveillance mode. *Gas6* and *Mertk* expression was present in WT and 101LL DIV8 cultures and no significant differences were evident between genotypes suggesting similar numbers of microglia were present in WT and 101LL cultures. WT cultures 30,000 cells, plated on PDL plastic plates, Scale bar (A) 200µm, (A1 and C) 50 µm, (B) 5µm, Zeiss LSM 710. Graph mean plus standard deviation, n=4, n=individual cultures, *Gas6* P-Value 0.20 and *Mertk* P-Value 0.34, unpaired t test.

3.3.5 Investigating neuronal maturation

To determine the functional maturity of neurons in culture the presence of both pre and post-synaptic markers were determined using immunocytochemistry. Anti-synapsin I antibody was used as a pre-synaptic marker and Anti-Postsynaptic Density protein 95 (PSD-95) as a post-synaptic marker. Synapsin 1 is first expressed in Day 17 embryos in growing axonal and dendritic processes and PSD-95 is associated with the formation and maturation of excitatory synapses (Sheng and Kim 2011; Mason 1986). Both pre and post-synaptic markers were detectable in primary cultures and IMARIS analysis confirmed similar levels of staining were present in both genotypes as shown in *Figure 3.12*. These findings were important as they highlighted no differences in synaptic populations were evident between genotypes pre fibril challenge. These data also confirmed the primary hippocampal neuronal cultures developed into an intricate network of structurally mature synapses relatively comparable to that found in the brain.

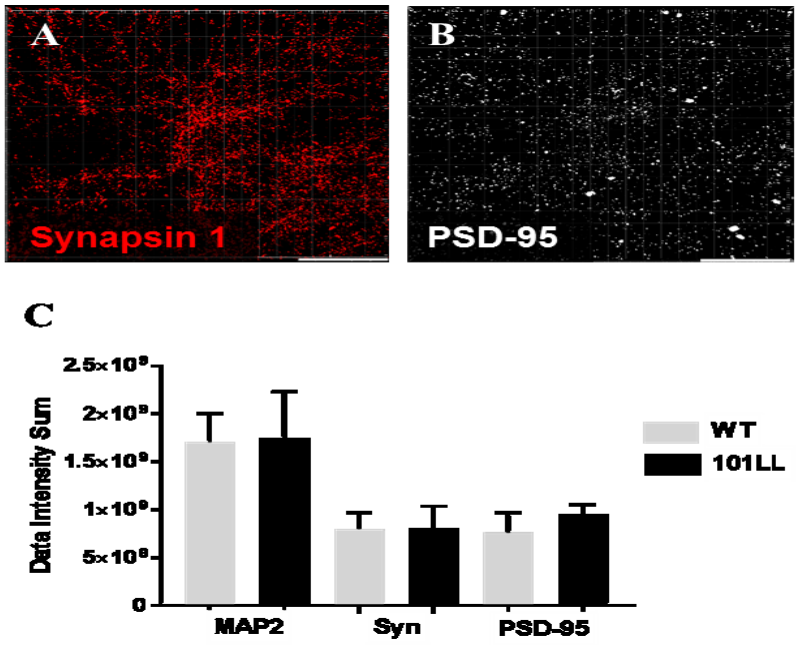

Figure 3.12: Primary cultures developed into structurally mature neuronal synaptic networks. To confirm cultures were developing synaptic networks in culture, labelling with pre and post-synaptic markers was carried out. (A) Pre-synaptic marker, Synapsin 1 (Syn1/Red) and (B) Post-synaptic marker, Anti-Postsynaptic Density protein 95 (PSD-95/White). (C) Data intensity sums generated in IMARIS (Materials and Methods, 2.2.9) based on neuronal (MAP2), pre-synaptic (Syn1) and post-synaptic (PSD-95) labelling were plotted from both genotypes. Labelling of pre and post-synaptic markers confirmed the presence of mature neuronal synaptic networks, and IMARIS analysis showed levels of synapses present in WT and 101LL cultures were comparable. These data provided baseline synaptic profiles of both genotypes pre-fibril challenge. WT and 101LL cultures 30,000 cells, plated on PDL plastic plates, Scale bar 50µm, Zeiss LSM 710. Graph mean plus standard deviation, n=4, n=individual WT culture images, P-Values MAP2 0.60; Syn 0.53 and PSD-95 0.12, unpaired t test.

Collectively, data from these characterisation experiments suggest that WT and 101LL hippocampal cultures were differentiated into highly branched neuronal networks supported predominately by astrocyte populations with a smaller contribution from microglial cells. Additionally synaptic markers were present from DIV8 indicating neuronal maturity from this time point. LDH assays in combination with immunocytochemical analysis concluded these neuronal cultures were viable up to twenty days *in vitro*. At this point, no obvious differences between genotypes were apparent that might explain how one model is capable of supporting fibril formation whilst the other is not.

3.3.6 Cellular associations with PrP^C

Normal cellular PrP^C can be converted into an abnormal isoform resulting in the formation of amyloid fibrils, and addition of abnormal PrP fibril seeds can enhance this process as reported in previous studies (Barron et al. 2016). The presence of normal PrP^C is essential for this seeding mechanism to occur. The presence of PrP^C in primary cultures was therefore analysed by immunocytochemistry using anti-PrP antibodies 6H4 (recognises amino acids 143-151) and 7A12 (recognises amino acids 90-145) to determine PrP protein levels and cellular associations in culture. PrP^C was associated with both neuron and astrocyte cell populations, and where confocal images were analysed using IMARIS tool function (Materials and Methods, 2.2.9), PrP^C detection was predominantly associated with neurons (*Figure 3.13*). Genotype specific profiles were also created by IMARIS based on neuronal, astrocytic and PrP^C signals (*Figure 3.14*). Based on these profiles it can be concluded no obvious differences regarding cell or PrP^C expression were apparent when comparing WT and 101LL cultures.

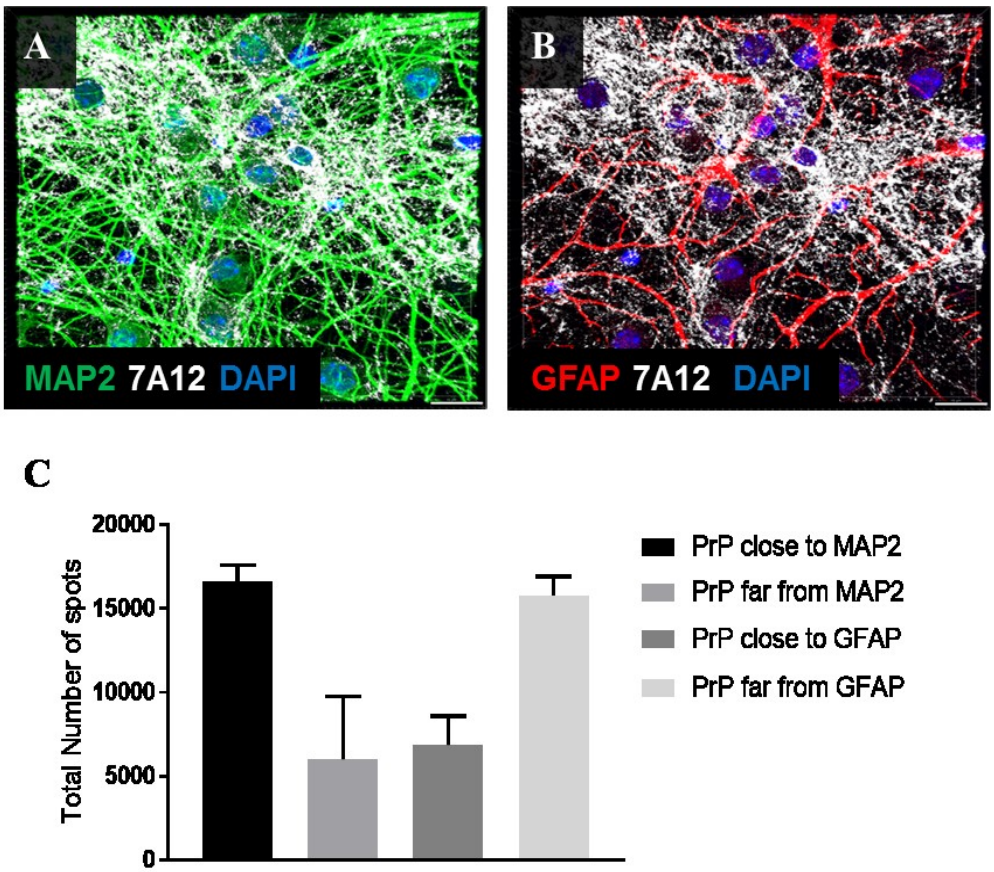

Figure 3.13: PrP^C was detectable on both neuronal and astrocytic cells. To investigate if PrP^C protein was present and detectable in cultures and to identify cellular associations with this protein, immunocytochemistry using an anti-PrP antibody was carried out. (A) Anti-PrP antibody 7A12 (PrP^C/White), neurons (MAP2/Green) and DAPI (Nuclear/Blue). (B) 7A12 (PrP^C/White), astrocytes (GFAP/Red) and DAPI (Nuclear/Blue). (C) IMARIS tool function analysis (Materials and Methods, 2.2.9), of PrP^C cellular localisation. Close to parameters were within 1µm distance of cell and far from parameters were greater than 1µm distance from cell. PrP^C was associated with both neuron and astrocyte cell populations however, IMARIS localisation analysis showed PrP^C detection was predominantly associated with neurons (within 1µm) whilst astrocytic PrP^C localisation was further away (> 1 µm). 101LL cultures 30,000 cells, plated on PDL plastic plates, Scale bar 15µm, Zeiss LSM 710. Graph mean plus standard deviation, n=2, n=individual culture images.

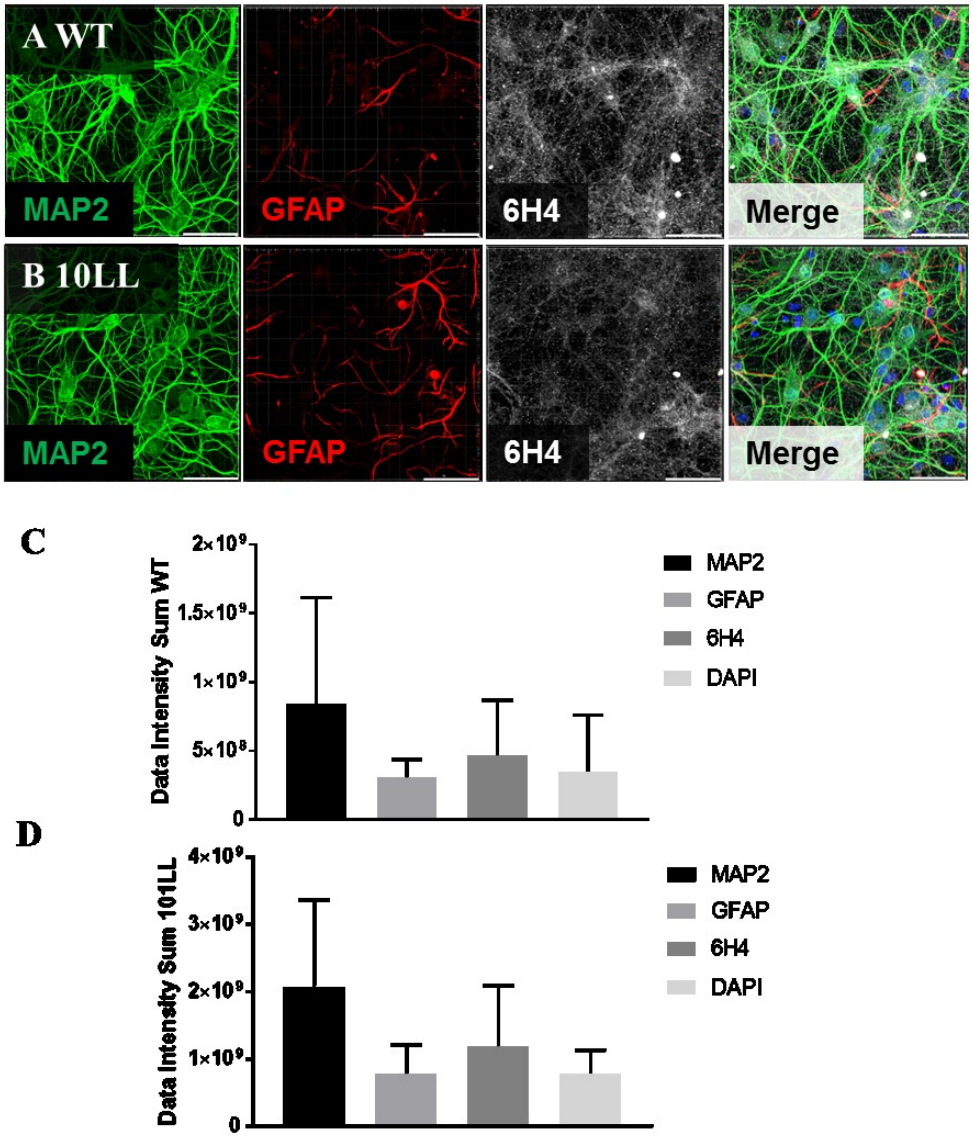

Figure 3.14: WT and 101LL cultures have similar cellular profiles. To investigate if WT and 101LL cultures were comparable based on predominant neuronal and astrocytic cell populations, including PrP^C expression, genotype specific profiles were generated in IMARIS for genotype comparisons to be carried out. These investigations provided baseline profiles of WT and 101LL cultures pre-fibril challenge. (A) WT and (B) 101LL immunolabelling for neurons (MAP2/Green), astrocytes (GFAP/Red) and PrP^C (6H4/White). (C) WT and (D) 101LL IMARIS data intensity sums based on immunolabelled images. Note DAPI images not included. Based on immunolabelling and IMARIS generated profiles no obvious differences regarding cell or PrP^C expression were apparent when comparing WT and 101LL culture. WT and 101LL cultures DIV8, Scale bar 50µm, Zeiss LSM 710. Graph mean plus standard deviation, n=2, n=individual culture images.

Immunocytochemistry was invaluable for confirming the presence of PrP^C protein in culture however, this technique was limited in providing information about post-translational modifications of PrP^C. To address this point and to gain more information with regards to PrP glycoform profiles, immunoblotting experiments were carried out (Materials and Methods, 2.2.6). Immunoblotting validated immunolabelling results whilst providing additional information on the glycoform patterns associated with the protein. PrP^C can either be un-, mono- or di-glycosylated during post-translational modification (Xanthopoulos et al. 2009) and as shown in *Figure 3.15*, WT and 101LL cultures showed all three glycosylated states of PrP^C were present and were at comparable levels suggesting normal PrP^C processing was occurring in primary cultures. Additionally, di-glycosylated higher molecular bands appeared more prominent in *in vitro* lysates which was comparable to adult brain profiles obtained suggesting again similar translational modifications of PrP^C were been carried out in both systems. In comparison, lower levels of detectable PrP^C were shown in embryonic brain lysates where unglycosylated banding appeared extremely faint. Immunocytochemical results have previously show an increase in neuronal growth over-time in culture (*Figure 3.7*), and as PrP^C is predominantly expressed by neurons, an increase in protein production would be expected, as shown by immunoblot (*Figure 3.15*). These results suggested levels of PrP^C were increasing with neuronal development in culture, which was confirmed by immunocytochemical labelling of PrP^C over-time in culture (*Appendix Figure 3.c*). These observations were also similar to previous studies monitoring PrP^C mRNA expression during embryogenesis that showed as the embryo develops the levels of PrP^C mRNA also increase (Manson et al. 1992). In conclusion, both immunocytochemical and biochemical analysis confirmed the presence of PrP^C in primary cultures and both WT and 101LL cultures had similar expression levels of the protein. Furthermore, expression levels of the *Prnp* gene based on transcriptomic data presented in Chapter 6 (Section 6.3.2), confirmed no significant differences in *Prnp* expression were evident between genotypes pre-fibril challenge.

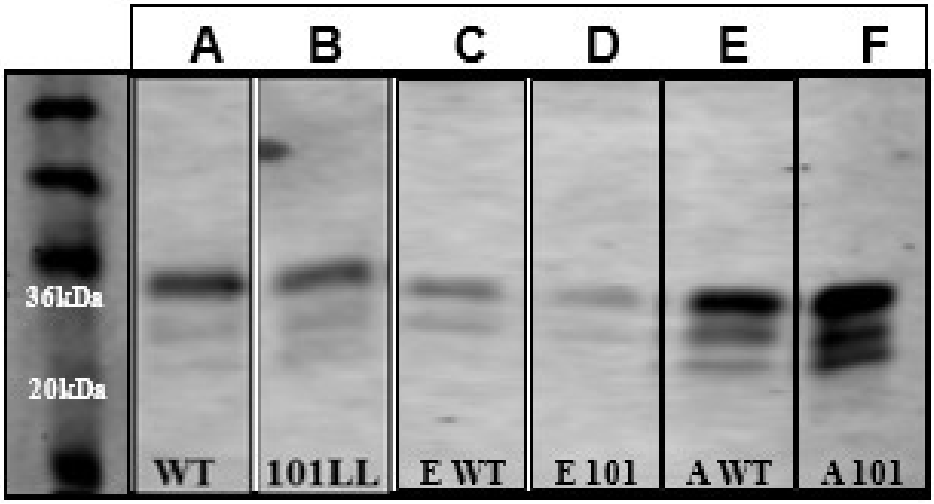

Figure 3.15: Typical glycosylated forms of PrP^C were present in primary culture lysates. Biochemical analysis of primary culture lysates was carried out to investigate if PrP^C glycoform patterns found in cultures were similar to that found in an *in vivo* brain. (A-B) Immunolabelling of PrP^C cell culture lysates, (C-D) Whole embryo (Day17) murine brain lysates and (E-F) Adult murine brain homogenates. All three glycoform bands were present at anticipated sizes in WT and 101LL primary culture lysates and both genotypes showed similar banding intensities, suggesting normal PrP^C processing was occurring in primary cultures in both genotypes. Furthermore, di-glycosylated molecular bands appeared more prominent in culture lysates which was comparable to adult brain profiles used here to show diagnostic PrP^C banding, suggesting again similar translational modifications of PrP^C were been carried out in both *in vitro* and *in vivo* systems. Equal protein loading at 5µg based on micro BCA assay (Thermo Scientific), 12 well Tris/ Glycine gel, 6H4 antibody.

In order to evaluate intracellular processing of PrP^C it was important to be able to detect intracellular organelles crucial to this process. A number of organelle markers were used to label cultures such Early Endosome Antigen 1 (EEA1/ early endosomes), Ras-related protein Rab9 (late endosomes) and Lysosomal-Associated Membrane Protein 1 (LAMP1/ lysosomes). Additionally, cholera toxin Ganglioside GM1 ligand Subunit B was used to label lipid-rafts (Nichols et al. 2001) which are involved in membrane protein trafficking (Taylor and Hooper 2006). Co-localisation of PrP^C and cholera toxin Subunit B was detected indicating some PrP^C protein was present on lipid-rafts (*Figure 3.16*). These domains are known to be involved in the membrane localisation and recycling of PrP^C and trafficking of misfolded PrP.

Thus, identifying and studying these membrane microenvironments will be important to determine their involvement in conformational conversion processing of abnormal protein after fibril challenge. PrP^C immunolabelling also co-localised with EEA1, Rab9 and LAMP1 showing PrP^C protein was present in early/ late endosomes and in lysosomes (*Figure 3.16*). Cellular PrP^C is known to be recycled from the cell membrane via an endocytic pathway, where the protein is transported back into the cell by endosomes (Peters et al. 2003) or it is routed to the lysosomes for degradation via late endosomes (Campana, Sarnataro, and Zurzolo 2005). The presence of PrP^C within these structures confirmed normal PrP^C processing was occurring within these cultures, which was evident in both genotypes and these data supported biochemical analysis (*Figure 3.15*), showing normal glycoform profiles. Immunocytochemical analysis (*Appendix Figure 3.d*), suggested predominant organelle association with neuronal cell populations. Analysing these organelles will be key in identifying pathways involved in misfolded PrP processing after cultures are challenged with misfolded PrP fibrils.

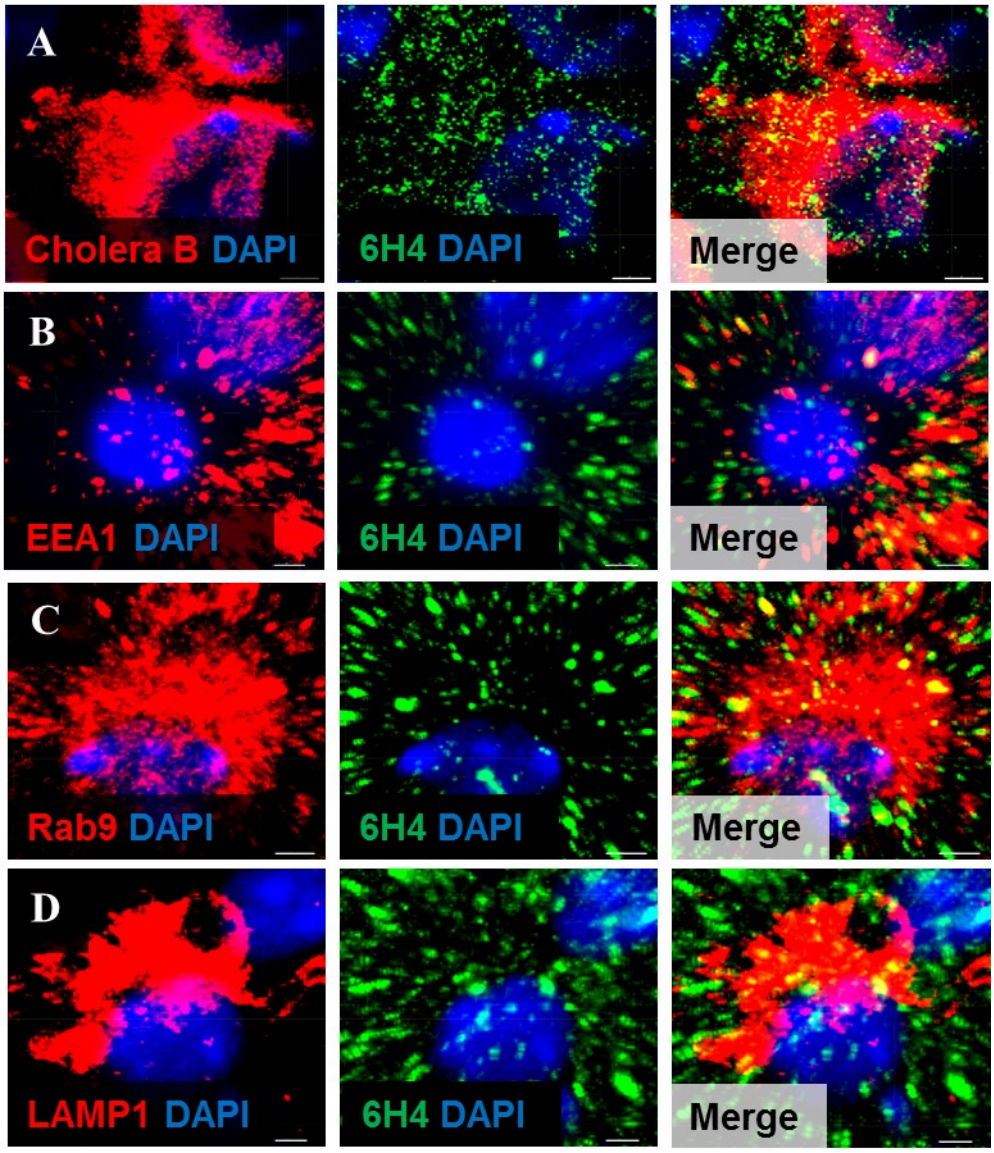

Figure 3.16: PrP^C localisation with lipid-rafts and endolysosomal organelle domains. To ascertain if PrP^C was undergoing normal processing in primary cultures, a number of endolysosomal associated organelles were labelled using various markers. (A) Lipid-rafts were labelled with Cholera Toxin B (Cholera B/Red), (B) Early endosomes with Early Endosomal Marker 1 (EEA1/Red), (C) Late endosomes with Ras-related protein 9 (Rab9/Red) and lysosomes with Lysosomal-Associated Membrane Protein 1 (LAMP1/Red). PrP^C was immunolabelled with 6H4 (Green). Merged images displayed co-localisation (Yellow) was evident between lipid-rafts, early and late endosomes, lysosomes and PrP^C indicative that PrP^C was undergoing normal recycling via an endolysosomal pathway. Scale bar 2µm, Zeiss LSM 710.

3.3.7 Genotype specific response to chemically induced stress

Both WT and 101LL cultures displayed similar characteristics after a range of immunocytochemical and biochemical tests were carried out. The next stage of characterisation involved investigating if any differences were present between genotypes regarding their response to chemically induced stress. Thus, both WT and 101LL cultures were exposed to increasing concentrations of hydrogen peroxide (30% w/w H_2O_2, Materials and Methods, 2.4.1) and cellular response stress levels were monitored over a 24 hour time frame using the LDH assay. Immunocytochemistry was carried out at end point to ascertain cytotoxic effects on neuronal and astrocytic populations. $PrP^{-/-}$ cultures were also tested to distinguish if PrP^{C} actually does have neuroprotective properties as claimed in the literature (Roucou, Gains, and LeBlanc 2004). LDH analysis included cell supernatants harvested at 0hr, 2hr, 4hr, 6hr, and 24hr time points (*Figure 3.17, Appendix Figure 3.e*). Results of the LDH assay indicated 101LL cultures were more susceptible to stress than WT. Interestingly $PrP^{-/-}$ cultures maintained a high percentage of cell viability after 24hrs at 100μM H_2O_2 (*Appendix Figure 3.e*), indicating that PrP^{C} may not be actively involved in neuroprotection. End point immunocytochemistry results reflected LDH data showing neuronal and astrocytic populations were reduced in cultures in a dose dependent manner in response to H_2O_2 (*Figure 3.18*). A noticeable reduction of 101LL neuronal cells in comparison to WT was evident at 100μM and 300μM H_2O_2 concentrations, again complementing LDH results. Positive immunolabelling for 101LL astrocytic populations was evident at 300μM H_2O_2 however, these cells did not appear healthy. In conclusion, 101LL cultures appeared more susceptible to hydrogen peroxide induced oxidative stress than WT cultures.

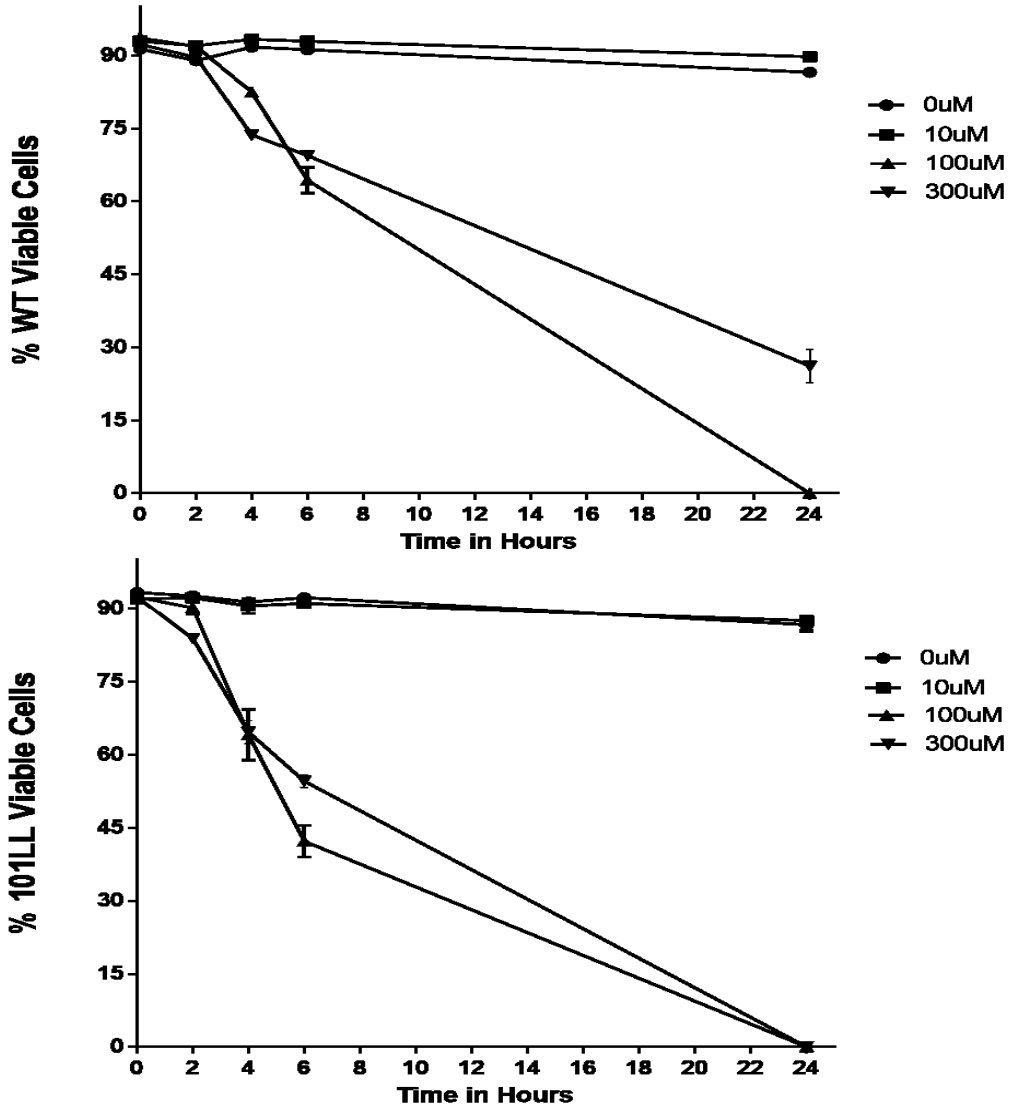

Figure 3.17: 101LL cultures were highly susceptible to chemically induced stress. Although WT and 101LL cultures shared similarities based on morphological and immunocytochemical profiling, it was unknown if both genotypes would respond in a similar manner to chemically induced stress. To investigate this further, WT and 101LL cultures were exposed to increasing concentrations of H_2O_2 (0, 10, 100, 300µM) and cellular response was measured using the LDH cytotoxicity assay. (A) WT stressed cultures and (B) 101LL stressed cultures. Culture supernatants were sampled at 0, 2, 4, 6 and 24hrs and LDH activity measurements were plotted accordingly. 101LL cells appeared more susceptible to oxidative stress than WT cultures and displayed earliest cytotoxic effects. Fluorescent values were normalized to Triton X-100 treated lysis cells that represent the maximum amount of LDH available for release, then the percentage of viable cells were calculated by percentage LDH release value minus 100. WT and 101LL cells plated at 150,000 cells per well on PDL/Fibronectin glass coverslips, Graph mean plus standard deviation, n= 2 duplicate technical replicates.

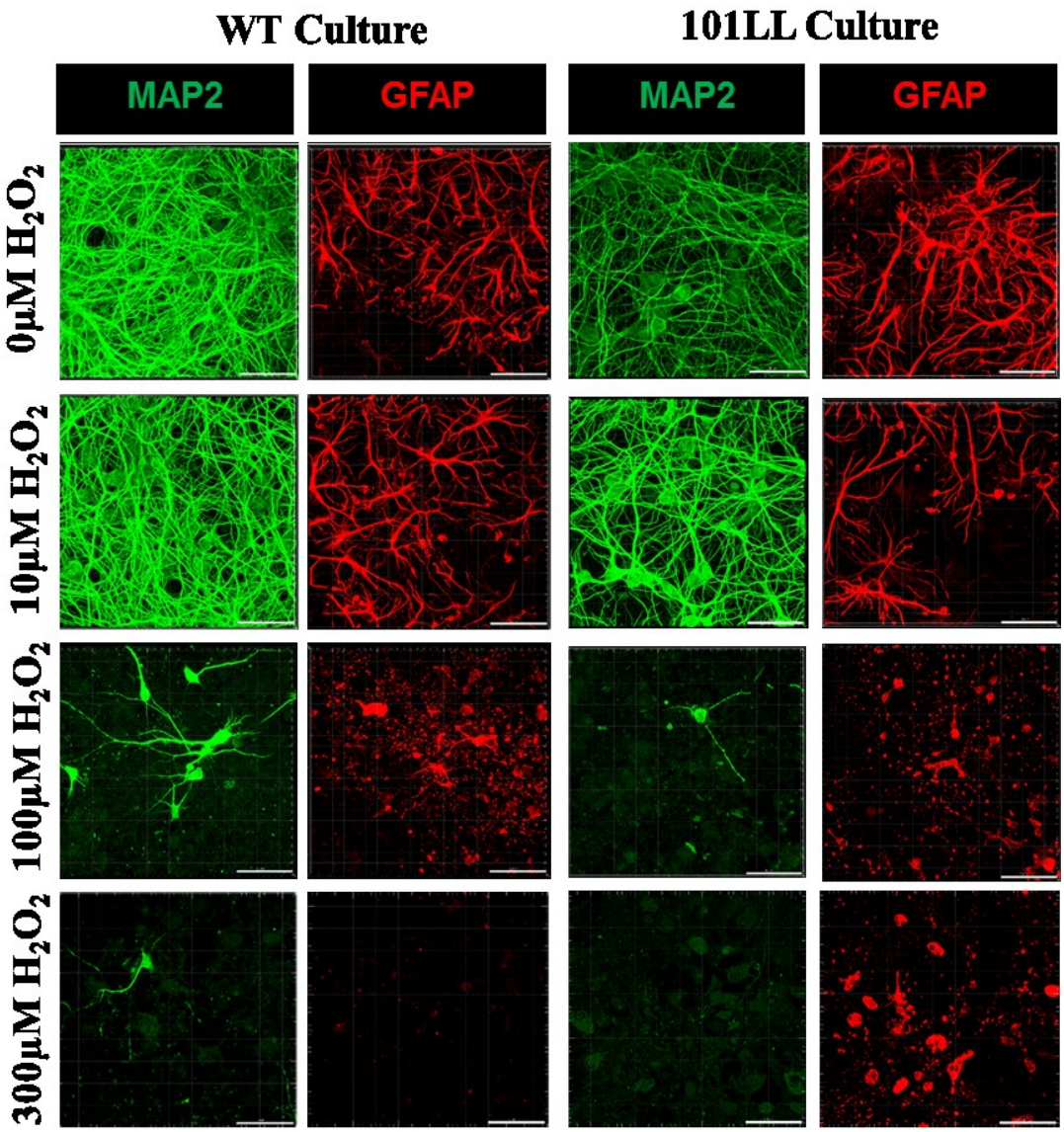

Figure 3.18: Induced oxidative stress leads to neuronal and astrocytic decline in both WT and 101LL cultures. To monitor the effect of oxidative stress on cellular populations in primary cultures, immunolabelling of neurons and astrocytes was carried out after 24-hour exposure to various concentrations of H_2O_2 (0, 10, 100, 300μM). Immunolabelling of neurons (MAP2/Green) and astrocytes (GFAP/Red) in both WT and 101LL primary cultures showed a clear reduction of MAP2 (neurons) and GFAP (astrocytes) immunolabelling at both 100μM and 300μM concentrations in both genotypes confirming both cellular populations and genotypes were susceptible to oxidative stress. Neuronal populations appeared more susceptible in 101LL cultures. Astrocytic immunolabelling was evident in 101LL cultures at 300μM concentration however, these cells did not look healthy. Scale bar 50μm, LSM710.

3.4 Discussion

The overall aim of this study was to develop a representative model of the brain to study neuron-glia interactions after challenge with misfolded PrP fibrils. Murine primary neuronal cultures were therefore established and characterised at the morphological, biochemical and immunocytochemical level. Previous studies by other groups have focused more on the initial practical preparation procedures involving isolating neuronal cells from the brain but have failed to further characterise the resulting cultures in more detail (Seibenhener and Wooten 2012; Beaudoin et al. 2012; Kaech and Banker 2006). Other studies have characterised their cultures to a better extent however, this was from neuronal cultures isolated from adult rat brains and again was limited regarding validation experiments (Ray et al. 2009). The work described in this chapter provided a well characterised and optimised model system to study abnormal protein interactions in a controlled easily accessible system.

The hippocampal area of the brain is a prime target for misfolded protein accumulation and was therefore selected to provide cells for primary culture. The initial procedures for dissecting hippocampal areas from Day 17 embryo brains were developed in accordance with both Home office and Roslin veterinary staff. Initially embryos from each individual mother were removed and immediately decapitated however, when embryo numbers were high (above four) this method proved inefficient and resulted in rapid tissue degradation in embryos that were culled last. The method established in this chapter provided a more effective, efficient and ethically sound way of using all the embryos from a single pregnancy. Once tissues were isolated and dissociated, a number of options for further processing were available. Previous methods have shown that hippocampal cultures need to be co-cultured with an astrocyte feeder layer (Gardner, Jukkola, and Gu 2012; Kaech and Banker 2006).

This method was not employed here, instead trophic support of neurons was provided using various co-factor supplements which proved to be a quicker less complicated method of establishing viable primary neurons (Brewer and Price 1996; Brewer et al. 1993).

Morphologically the primary hippocampal neurons differentiated into highly branched synaptically connected neuronal networks characterised using Tau, MAP2, PSD-95 and Synapsin 1 immunolabelling. These neurons were supported by astrocytic and microglial populations. These glial cells play an important role in maintaining neuronal networks and protect neurons from toxicity reflected here by the fact that cells were viable in culture for over twenty days *in vitro* (Boehler, Wheeler, and Brewer 2007; Ye and Sontheimer 1998). The hippocampus also contains other subsets of neuroglial cells such as oligodendrocytes which are involved in axon myelination which enhances the speed and efficiency of axon conduction. Myelin basic protein (MBP) is expressed exclusively in these myelinating glia. Limited MBP immunoreactivity was evident in both WT and 101LL cultures (data not shown) which confirmed previous reports which showed co-culture with seeded oligodendrocytes dissociated from the cerebellum and brain stem was needed to achieve efficient myelination *in vitro* (Gardner, Jukkola, and Gu 2012). It should be noted however that these co-culturing methods resulted in some but not all neurons undergoing myelination and therefore were limited regarding myelination studies. Studying myelination of axons and related mechanisms was not essential to this study therefore, no further investigations were carried out.

Biochemical studies showed PrP^C glycosylation profiles obtained from primary cell lysates were comparable to adult brain lysates. This confirmed the presence of PrP^C in these cultures and showed the same biosynthetic pathway found *in vivo* must also be occurring in the primary neuronal models.

PrP^C expression was validated using immunolabelling and organelle localisation of PrP^C confirmed normal trafficking and recycling of the protein via an endolysosomal pathway. Endolysosomal pathways are also involved in delivering misfolded proteins to lysosomes (Yamasaki et al. 2014; Saftig and Klumperman 2009) therefore, identifying these pathways in primary cultures was important as it will allow for the monitoring of fibril processing after challenge in cultures.

Genotypes used in this study were selected based on previous studies which showed 101LL mice supported misfolded PrP seeding *in vivo* whilst WT mice were capable of curtailing this process after challenge with recombinant PrP fibrils (Barron et al. 2016). Generating *in vitro* cultures from these mice allowed for a novel, more accessible system to study early misfolded PrP cell interactions in detail. Additionally, a $PrP^{-/-}$ primary line was used in some studies as a control for PrP antibodies and to gain insight into neuronal activity in the absence of PrP^C which is thought to have neuroprotective properties. Generic stress studies indicated $PrP^{-/-}$ cultures were less susceptible to oxidative stress than WT and 101LL genotypes indicating that expression of the PrP^C protein did not guarantee neuroprotection. This study also highlighted the fact that after induction of oxidative stress, 101LL cultures appeared more susceptible to changes in culture homeostasis than WT (*Figure 3.17, 3.18*). This preliminary data was the first indication that differences may exist between WT and 101LL cultures regarding response to external stimuli.

IMARIS software was used to perform novel in-depth analysis of immunostained cells in both WT and 101LL genotypes and no obvious differences were apparent between cultures pre-fibril challenge that could explain how one curtails and the other supports protein misfolding. 3D neuronal matrixes were maintained even after coverslip mounting (*Figure 3.5*) protecting the intricacy of neuronal networks formed. These techniques resulted in generating neurons comparable to that found *in vivo* (*Figure 3.4*).

IMARIS analysis showed PrP^C was expressed predominantly by neurons (*Figure 3.13*) however, PrP^C expression was also associated with astrocytes and microglia to a lower degree (data not shown). Both WT and 101LL cultures had similar composition profiles regarding the proportions of neurons, astrocytes and PrP^C based on data intensity sum plots generated in IMARIS (*Figure 3.14*). Importantly, astrocyte morphological profiles and expression of astrocyte-associated genes were similar between WT and 101LL cultures and astrocytic populations appeared to be in surveillance mode in both genotypes in these unchallenged cultures. Microglial phenotypes analysed using IMARIS reconstruction were shown to be integrated with neuronal populations and morphological appearances showed they were ramified in appearance exhibiting long processes (*Figure 3.11*). This suggested microglia were in surveillance mode as opposed to an amoeboid state where cell bodies are large and processes are short and thick, a phenotype correlated with microglial activation in response to neuronal injury (Arcuri et al. 2017; Ling and Wong 1993). Collectively, these analyses provided a baseline neuronal and non-neuronal profile pre-fibril challenge where any changes overserved after fibril insult would be attributed to the addition of recombinant PrP fibrils.

Another means of characterisation of *in vitro* cultures is by electrophysiological studies. Cellular electrophysiological activity is critical for neurons and action potentials can be monitored *in vitro* using patch clamp technologies (Bourke et al. 2014). Although patch clamp analyses could not be performed on these cultures due to logistical issues, the presence of both pre and post-synaptic markers in these cultures was shown (*Figure 3.12*) indicating a complex neuronal communication network was present and structurally mature. Importantly, baseline profiles pre-fibril challenge indicated similar synaptic populations were present in both genotypes.

To summarise, the data presented in this chapter confirm a well-established primary hippocampal neuronal culture model has been developed. After a number of characterisation steps no obvious differences were noted between genotypes pre-fibril challenge that would support different processing capabilities of misfolded PrP. Additionally, transcriptomic analysis confirmed similar *Prnp* expression levels between genotypes indicating the point mutation in the 101LL's was not effecting the levels of PrP^{C} present. 101LL cultures were however more susceptible to oxidative stress than WT cultures, which was also observed in LDH response after initial plating of 101LL cells. In conclusion, this model provides an essential tool to investigate the intricacy of early misfolded PrP interactions with neuronal, astrocytic, microglial and synaptic populations in cultures from both WT and 101LL genotypes.

CHAPTER 4

Recombinant PrP production, refolding and fluorescent labelling

4.1 Abstract

Abnormal PrP protein processing and accumulation can be studied either *in vivo* or *in vitro* using recombinant PrP fibrils as a seed to initiate further protein misfolding however, tracking fibrillar protein cellular interactions and processing proves difficult. One way to circumvent this is to label recombinant fibrils with a fluorescent dye. In this study both WT and 101L PrP protein was expressed in *Escherichia coli* (Rosetta DE3) from a pTrcHis B derived vector containing codons 23-230 of the PrP open reading frame. PrP expression from bacterial cells was carried out using the Isopropyl ß-D-1-thiogalactopyranoside (IPTG) induction pTrc expression system. Further purification involved a multistep process including Immobilised Metal Affinity Chromatography (IMAC) using Nickel-Nitrilotriacetic acid (Ni-NTA); size exclusion chromatography and Reverse Phase High Performance Liquid Chromatography (RP-HPLC). Recombinant PrP displaying the highest purity validated by Sodium Dodecyl Sulfate Polyacrylamide Gel Electrophoresis (SDS-PAGE) and Mass Spectrometry (MS) was selected to produce fibrils using the prion fibrillisation assay. Silver staining and electron microscopy confirmed the presence of these refolded forms of PrP which were then labelled with Alexa Fluor Succinimidyl Esters (NHS esters) to aid visualisation of fibril trafficking *in vitro*. Fibrils generated in this chapter displayed similar characteristics to fibrils isolated from infected brains and therefore provided a useful surrogate of *in vivo* generated misfolded PrP, which was amenable to fibril based challenge experiments in primary hippocampal neuronal cultures.

4.2 Introduction

PMD's such as AD, PD, HD and TSEs or prions are associated with the accumulation of abnormally folded proteins in specific regions of the brain (Knowles, Vendruscolo, and Dobson 2014; Braak et al. 2003; Caughey and Lansbury 2003; Forloni et al. 2002; Bucciantini et al. 2002). The generation and spread of these misfolded protein aggregates or fibrils is common to all PMD's, and it is widely debated whether these abnormal fibrillar deposits are toxic to surrounding neurons or if they are generated as a protective mechanism to sequester smaller soluble forms of misfolded protein (Treusch, Cyr, and Lindquist 2009; Haass and Selkoe 2007). Additionally, early mechanisms involved in fibril processing are poorly understood (Moreno-Gonzalez and Soto 2011). Pervious work by our group has shown both WT and 101L recombinant PrP fibrils are capable of seeding misfolded PrP amyloid in the brains of 101LL mice but not in WT. Therefore, both of these genotypes were employed in order to study the different processing pathways associated with misfolded fibril interactions. Furthermore, *Prnp* fibril genotype was irrelevant to seeding occurrence however, genotype of the challenged host was important. To confirm no differences existed between fibrils due to genotype, fibrils were produced and characterised from both WT and 101L *Prnp* plasmid vectors. These fibrils will be used to challenge primary hippocampal neuronal cultures generated from both WT and 101LL genotypes, and the results of this challenge will be discussed in Chapters 5 and 6.

Recombinant PrP protein generated from *E. coli* has been used extensively in prion research however; producing protein of high purity is difficult. This may be due to traditional methods of recombinant PrP production utilising a fusion of PrP to histidine tags, or other methods which resulted in PrP that was partially degraded or of insufficient purity (Rezaei et al. 2000; Jackson et al. 1999; Hornemann et al. 1997; Zahn, von Schroetter, and Wüthrich 1997).

The methods used here were based on published protocols generated from various groups and allowed for the expression of tag-free recombinant PrP of the highest purity (Makarava and Baskakov 2008; Kirby et al. 2003). Fibrils generated from recombinant PrP using the prion fibrillisation assay were then labelled with a fluorescent dye which was advantageous for tracking fibril interactions with neuronal, astrocytic and microglial cell populations along with monitoring general trafficking and organelle processing. Some fibrils were left unlabelled to act as controls for challenged experiments.

4.3 Results

4.3.1 Bacterial growth and induction using the pTrc system

Recombinant PrP was produced from *E. coli* bacteria carrying the plasmid containing the mouse *Prnp* gene. Bacterial glycerol plasmid stocks were kindly gifted by Dr. Andy Gill and were used here to produce both WT and 101L recombinant PrP based on the pTrc expression system (Materials and Methods, 2.3.1). As shown in *Figure 4.1*, protein expression was effectively induced by the addition of isopropyl ß-D-1-thiogalactopyranoside (IPTG), resulting in the production of recombinant PrP of anticipated size (23,104kDa).

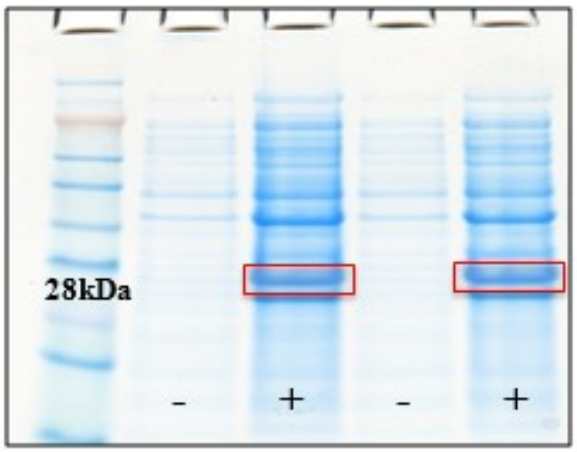

Figure 4.1: Bacterial cultures were induced using the pTrc expression system. SDS-PAGE was used to confirm recombinant PrP expression. Pre IPTG induction (-) and post IPTG induction (+). Red boxes show diagnostic PrP bands were present in IPTG treated samples confirming efficient induction of recombinant PrP. Novex 12% Bis-Tris Protein Gels, 1.0 mm, 15-well; SeeBlue Plus 2 Pre-Stained Standard, gel stained with Instant blue.

4.3.2 Bacterial lysis and IMAC PrP protein purification

The next processing step involved crudely purifying inclusion bodies containing the recombinant protein from induced bacterial culture cell pellets by bacterial lysis. Immobilized-Metal Affinity Chromatography (IMAC) purification followed and eluted recombinant PrP fractions were collected accordingly (*Figure 4.2*).

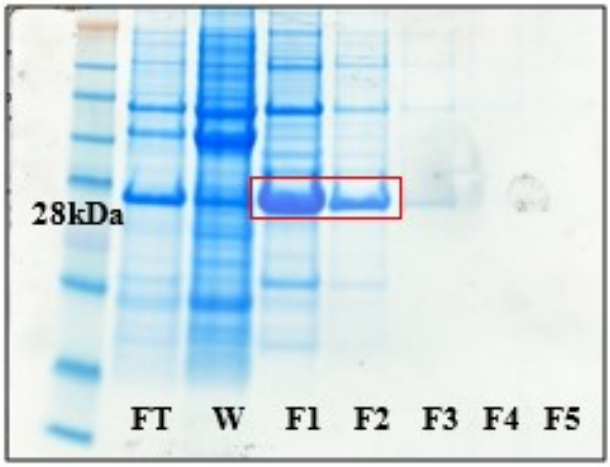

Figure 4.2: Immobilized-Metal Affinity Chromatography (IMAC) purified fractions were visualised using SDS-PAGE stained gel. IMAC purification allowed for elution of non-specifically bound proteins whilst recombinant PrP was retained bound to Nickel-Nitrilotriacetic acid agarose. SDS-PAGE was used to confirm what fraction recombinant PrP eluted in. FT= Flow through, W= Wash, F= Fraction. Majority of recombinant PrP was eluted in fractions F1 and F2 (Red Box). NuPAGE Novex 12% Bis-Tris Protein Gels; SeeBlue Plus 2 Pre-Stained Standard, gel stained with Instant blue.

4.3.3 AKTA-Fast Protein Liquid Chromatography

IMAC buffer processing resulted in binding of recombinant PrP with reduced glutathione which aided protein solubilisation and prevented the formation of disulphide bonds in the denatured protein during IMAC purification (Zahn, von Schroetter, and Wuthrich 1997).

For further downstream purification of IMAC fractions shown *in Figure 4.2*, reduced glutathione was removed using a size exclusion column (HiPrep 26/10) which allowed large proteins to elute first before smaller substances such as salts and other small molecules. As shown in *Figure 4.3* the majority of PrP of expected size eluted in a single fraction.

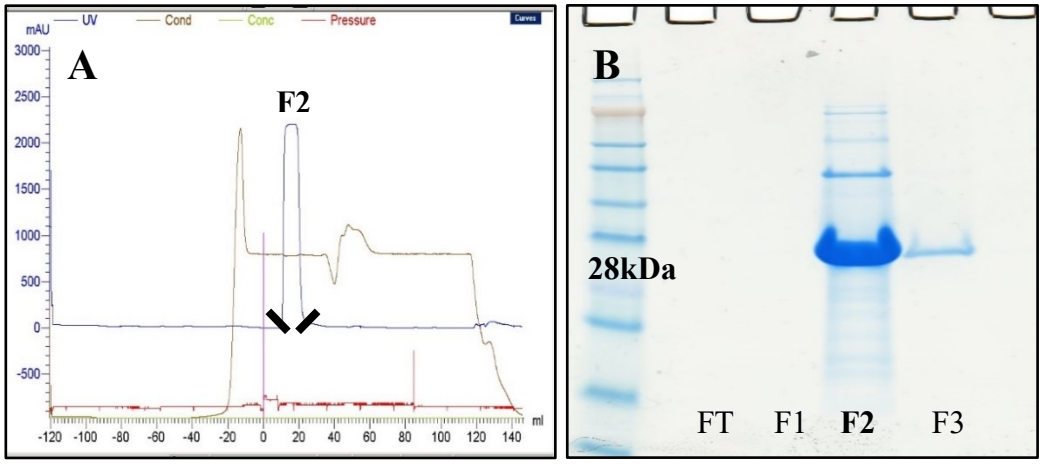

Figure 4.3: Recombinant PrP was further purified using a desalting method. AKTA-Fast protein liquid chromatography (FPLC) separation method was employed for protein filtration. (A) Ultraviolet (UV) measurements (mAU units) were recorded in conjunction with fraction collection and an isolated peak was identified and obtained for Fraction 2, **(\ /)** symbols denote where fraction began/ended. (B) SDS-PAGE confirmed majority of protein eluted in F2. NuPAGE Novex 12% Bis-Tris Protein Gels; SeeBlue Plus 2 Pre-Stained Standard, gel stained with Instant blue.

4.3.4 Reversed Phase HPLC for high purity prion protein purification

After FPLC filtration, solubilised recombinant PrP fractions were refolded using oxidised glutathione. This resulted in the formation of a disulphide bond analogous to the *in vivo* PrP^C protein, where α-helixes 2 and 3 are stabilised by the presence of this disulphide bond (Riesner 2003). Further purification was carried out using Reversed Phase High Performance Liquid Chromatography (RP-HPLC).

Recombinant PrP protein is hydrophobic and therefore attaches to the reverse phase column tightly. An organic solvent can then subsequently elute the hydrophobic PrP bound to the column. PrP was eluted and collected in individual fractions, each displaying highly pure PrP protein (*Figure 4.4*).

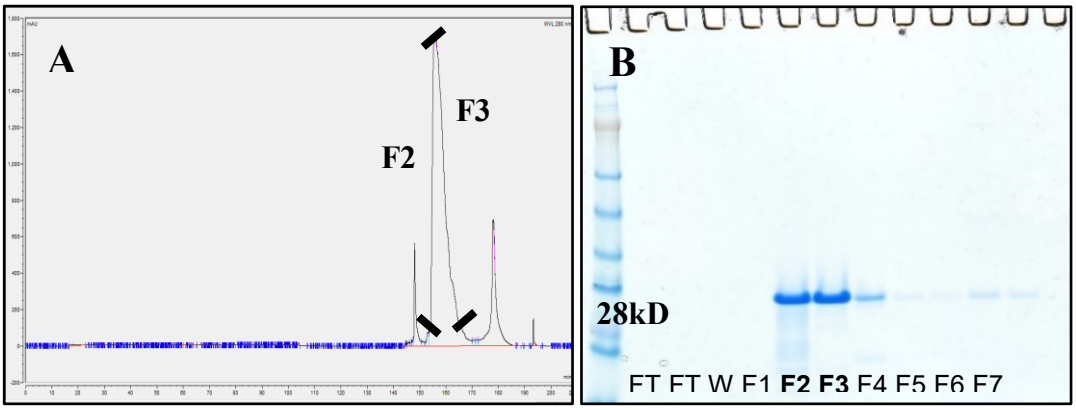

Figure 4.4: Reversed Phase HPLC produced highly pure PrP fractions. Recombinant PrP purity was analysed using Ultraviolet (UV) and SDS-PAGE. (A) UV measurements (mAU units) were recorded in conjunction with fraction collection, **(\ /)** symbols denote where fractions began/ended. (B) SDS-PAGE confirmed protein presence and purity in F2 and F3. NuPAGE Novex 12% Bis-Tris Protein Gels; SeeBlue Plus 2 Pre-Stained Standard gel stained with Instant blue.

Protein concentrations varied from fraction to fraction and were calculated accordingly (Materials and Methods, 2.3.4). Highly pure fractions were lyophilised immediately using the Savant SPD2010 SpeedVac (Section 2.3.7) and stored at -80°C until further use. Mass Spectrometry (Section 2.3.8) validated PrP purity (*Appendix Figure 4.a*) and any recombinant PrP samples displaying protein modifications were discarded.

4.3.5 PrP fibrillisation assay

The principle of this step was to take soluble, monomeric recombinant PrP and convert it into a fibril form by shaking the protein vigorously in the presence of Gdn-HCL and Thiourea reaction mixtures. This fibril conversion was monitored in real time using both an amyloid binding dye, Thioflavin T (ThT), and a fluorescence plate reader. The presence of fibrils was confirmed by increased fluorescence from ThT, monitored in real time by the fluorescence reader (*Figure 4.5*). Increased ThT fluorescence indicated the fibrillisation assay was efficiently converting monomeric forms of recombinant PrP into fibril conformations.

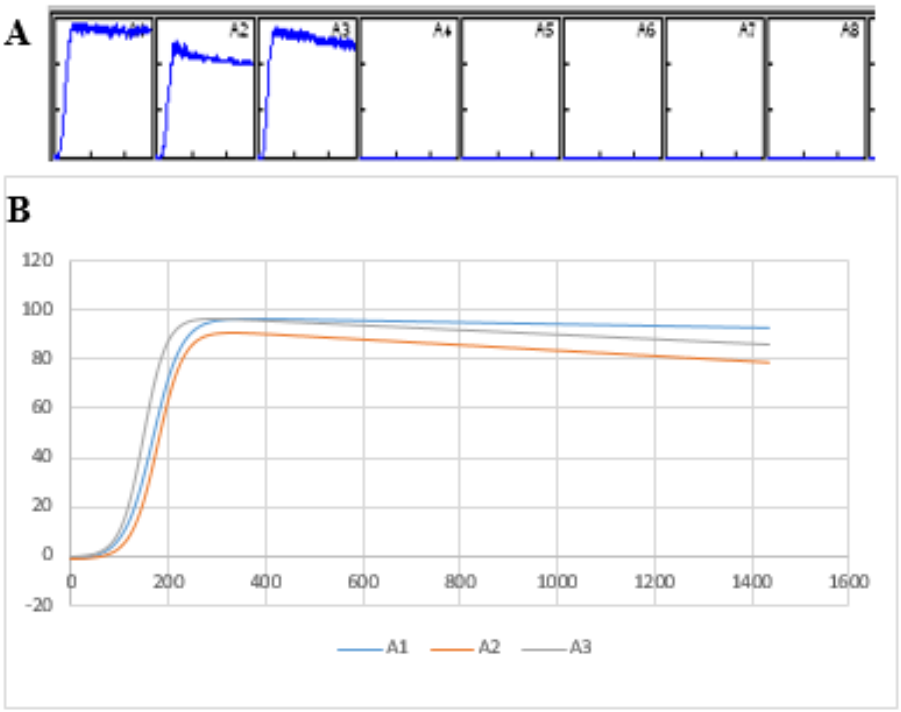

Figure 4.5: Recombinant PrP conversion to fibril form. Fibrillisation of recombinant PrP was monitored in real time by fluorescence and data generated was plotted accordingly. (A) Real-time fluorescent monitoring of ThT increase was visualised over-time using the Fluoroskan. Samples were loaded in triplicate, first three contained protein plus ThT, the next protein alone and finally ThT alone. (B) An excel macro analysed all readings collected over 24 hour period and produced a plot of Fluoroskan reading (485 nm) against time (minutes). Both readings displayed typical sigmoidal kinetic curves as expected confirming fibril production.

4.3.6 Maturation and proteinase K (PK) digestion of fibrils

Fibrils produced from recombinant PrP present proteinase K (PK) resistant bands at 10 and 12 kilodaltons (kDa) when examined using SDS-PAGE, however so do non-specific aggregates of recombinant PrP (Breydo, Makarava, and Baskakov 2008). To distinguish between both types, samples obtained from the PrP fibrillisation assay were heated at 80ºC a method known as maturation. Upon this maturation the pK resistant core of amyloid fibrils expand to 16 kDa, a characteristic which is not evident in non-fibrillar aggregates. The presence of this diagnostic band was validated by SDS-PAGE which confirmed efficient and specific amyloid fibril generation (Figure 4.6).

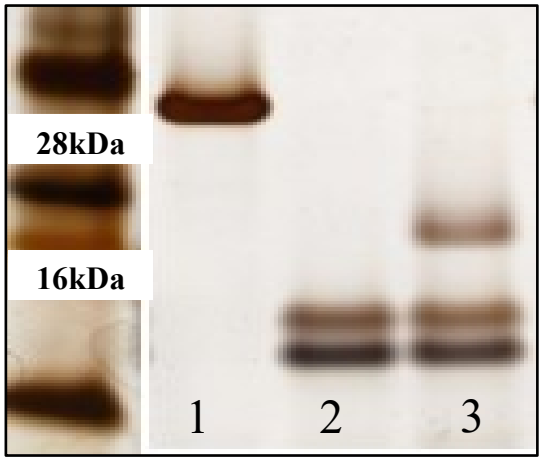

Figure 4.6: Silver stain of proteinase K (PK) treated fibrils confirmed specific amyloid fibril generation. Maturation and PK digestion of fibrils was carried out and analysed using SDS-PAGE and silver staining. Sample 1: Control no PK digestion, Sample 2: PK digested sample, Sample 3: PK digestion with maturation. As shown in lane 3, the characteristic 16kDa diagnostic band associated with amyloid fibrils was present confirming fibril generation. NuPAGE Novex 12% Bis-Tris Protein Gels.

4.3.7 Transmission electron microscopy

To determine if recombinant fibrils from different *Prnp* genotypes had similar morphological characteristics, transmission electron microscopy (TEM) was carried out. Samples were prepared for TEM by Steve Mitchell (Materials and Methods, 2.3.12). A JEM-1400 Plus electron microscope was used to image fibrils to investigate their structures. TEM images confirmed fibrils were successfully produced and were morphologically similar between genotypes (*Figure 4.7*). Diluted fibril preparations allowed for measurements of fibril length and width to be obtained using the Slice View module in IMARIS software (Materials and Methods, 2.2.9) which allowed accurate measurements of fibrils based on scale bar parameters to be obtained. IMARIS results confirmed fibrils were morphologically similar between genotypes and no significant differences were noted between length and width parameters measured. In conclusion, no differences in fibril structure were apparent by TEM/IMARIS analysis of fibrils produced from WT or 101L *Prnp*. These data support previous literature suggesting that fibril genotype does not influence how PrP fibrils are processed and instead host *Prnp* genotype is the more important determining factor.

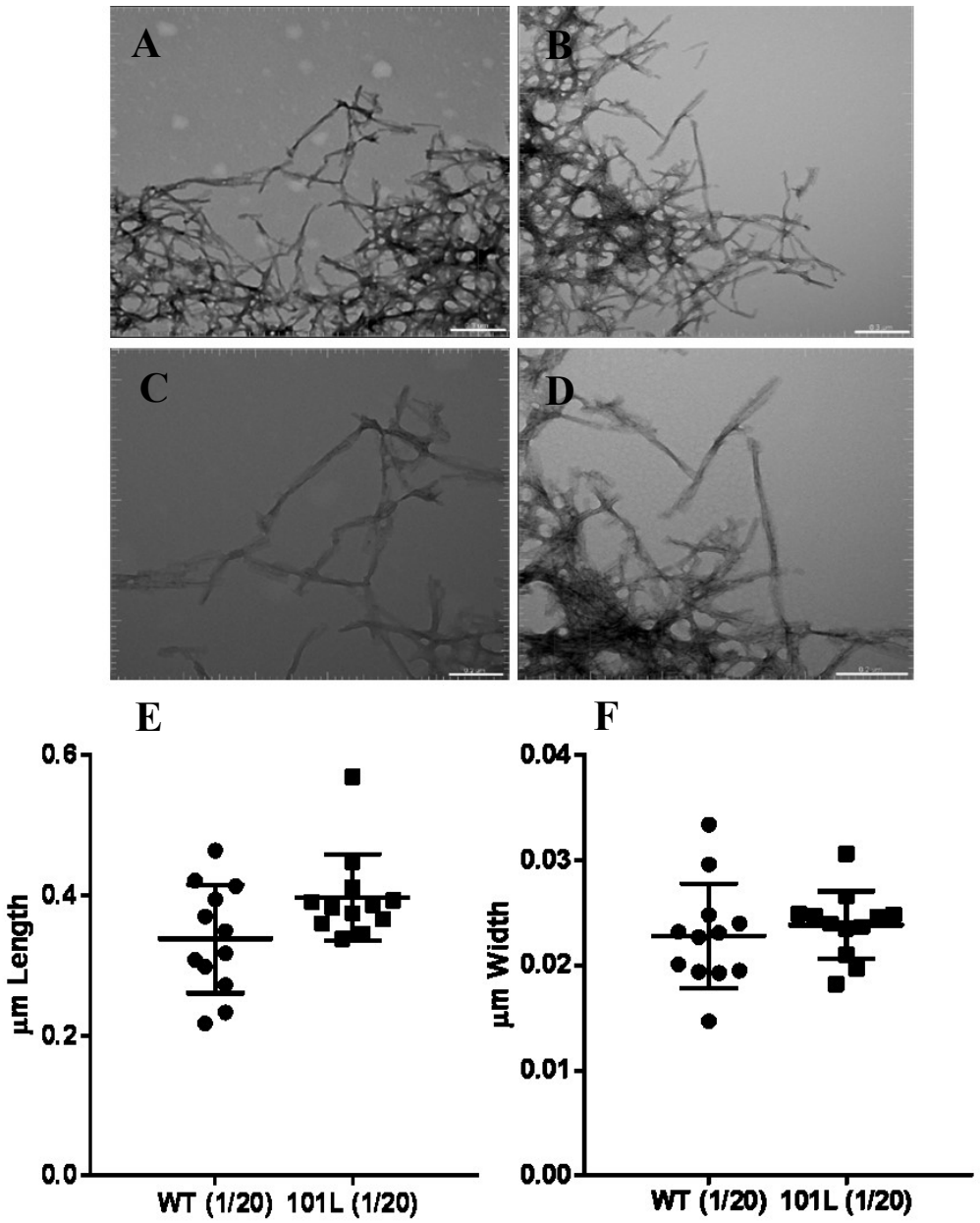

Figure 4.7: Transmission Electron Microscopy (TEM) used for visualisation of fibril structures. To confirm fibril presence and gain insights into fibril structures, TEM imaging of both WT and 101L fibrils was carried out. (A)-(B) WT, (C)-(D) 101L diluted fibril preparations and (E)-(F) Measurements of fibril length and width calculated using IMARIS software based on WT and 101L (1/20 dilution) EM images. Fibril presence was confirmed and no significant differences were noted between genotype dimensions: WT versus 101L fibril length P-Value 0.0502, WT versus 101L fibril width P-Value 0.5485. Scale Bar (A) and (C) 0.3µm, (B) and (D) 0.2 µm. Graph mean plus standard deviation, n=12, n= individual fibrils, unpaired t test.

4.3.8 Labelling fibrils with Alexa fluor succinimidyl esters (NHS esters)

To allow tracking and visualisation of fibrils in *in vitro* experiments, fibrils were labelled with a fluorescent dye. Alexa Fluor 555 NHS (N-HydroxySuccinimid) Ester (Succinimidyl Ester) was selected to label fibrils due to the dyes superior fluorescence emissions and greater photostability in comparison to other spectrally similar fluorophores. Additionally, the Succinimidyl esters (NHS esters) of Alexa Fluor dyes are easily conjugated to primary amines (R-NH2) located on proteins. Fibrils produced from both WT and 101L *Prnp* genotypes were labelled with Alexa Fluor 555 NHS esters. Fluorescent labelling was confirmed using a Typhoon scanner in conjunction with SDS-PAGE (*Figure 4.8*). To check labelled fibrils would be detectable by confocal microscopy aliquots of labelled fibrils were placed on a 96 well culture plate and were imaged using a Zeiss LSM710 confocal microscope. As shown in *Figure 4.8*, fibrils were detectable by confocal microscopy. Confocal images were measured using IMARIS software which provided a baseline measurement of the size of labelled fibrils before any challenge experiments were carried out. In summary, recombinant PrP fibrils were successfully produced from both WT and 101L *Prnp* genotypes and no differences in fibril structure were apparent between genotype. Fibrils were effectively conjugated to Alexa Fluor 555 which will allow *in vitro* tracking of fibril processing upon primary hippocampal culture challenge.

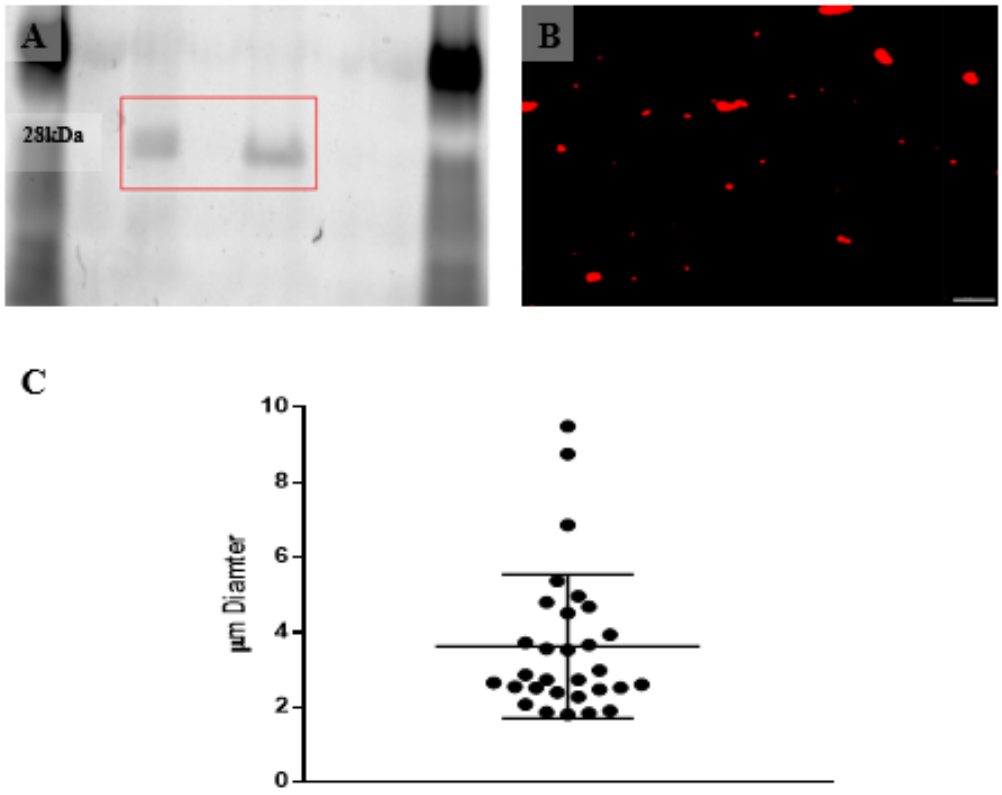

Figure 4.8: Fibrils were efficiently labelled with detectable fluorescent tags. Fluorescent labelling of fibrils was confirmed using two visualisation methods, the typhoon scanner and confocal microscopy. (A) Typhoon image using Cy3 filter of labelled fibrils at 5 and 0.5 mg/ml concentrations. (B) Confocal image of 3µl of labelled fibrils (7.5µg/ml). (C) Images of labelled fibrils obtained using the confocal microscope were analysed in IMARIS Slice view module to give an approximation of overall size. Typhoon scanner identified fluorescent bands of expected size for recombinant PrP and fibrils were detectable by confocal microscopy. IMARIS analysis of labelled fibrils generated baseline measurements before challenge experiments (mean size of 3.61 µm). (A) Typhoon image: NuPAGE Novex 12% Bis-Tris Protein Gel, 1.0 mm, 15-well; SeeBlue Plus 2 Pre-Stained Standard. Images obtained from Typhoon FLA9500 scanner, Cy3. (B) Scale Bar 10µm. (C) Graph mean plus standard deviation 1.92, n=30, n= individual labelled fibrils.

4.4 Discussion

In this chapter the production and characterisation of recombinant PrP fibrils was optimised, and the misfolded recombinant PrP generated will be used to challenge primary neuronal cultures *in vitro*. WT and 101L recombinant PrP was produced, refolded into fibril form and labelled with a fluorescent tag. Previous studies from our group have shown both WT and 101L recombinant PrP fibrils seeded plaque formation in 101LL mice but not in WT mice indicating that the primary sequence of recombinant PrP fibrils does not influence seeding mechanisms (Barron et al. 2016). Data in this chapter showed both WT and 101L generated fibrils share similar physical dimensions by EM (*Figure 4.7*) irrespective to PrP sequence complimenting previous results by our group. Both WT and 101L fibrils were generated however, from characterisation data and previous *in vivo* studies, the *Prnp* genotype used to generate fibrils should have no influence on challenge outcome.

Improvements to traditional methods were introduced throughout recombinant PrP production. Immobilized-Metal Affinity Chromatography (IMAC) was one of the first alternative steps involved in producing highly pure recombinant PrP from crude lysates. The principle of this purification step is that proteins that bind to metal ions will adhere to an IMAC column which is composed of nickel ions chelated by beads. For recombinant PrP there was no need to append a His-tag to the protein as the N-terminal copper binding domain of PrP can be used in the absence of a His-tag for efficient binding to the immobilised nickel ions (PrP contains 10 endogenous histidines). As shown in *Figure 4.2*, this was an effective method of binding recombinant PrP which was then easily eluted off the column using specific buffers. Another important step for recombinant PrP purification involved reduced glutathione removal which was present in protein-containing fractions isolated from the IMAC step. Efficient removal and purification of PrP using a desalting method was shown in *Figure 4.3*. Recombinant PrP was then further purified using Reversed Phase High Performance Liquid Chromatography (RP-HPLC).

Here substances were separated by hydrophobicity and as recombinant PrP protein is relatively hydrophobic it attached to the column tightly and efficiently. An organic solvent was then used to progressively elute the hydrophobic PrP which was collected in numerous fractions and SDS-PAGE confirmed highly pure PrP was obtained (*Figure 4.4*). All processing steps were fully characterised using SDS-PAGE, MS and EM all of which confirmed highly pure recombinant PrP fibrils were generated free of PrP adducts normally generated from spontaneous oxidation or degradation (Makarava and Baskakov 2012). Studies by other groups have shown fibrils isolated from infected tissue are resistant to PK digestion (Parchi et al. 2000; Collinge et al. 1996), appear fibrillar and "rod-like" in structure when imaged by EM (Prusiner et al. 1983) and have a width measurement of between 0.003-0.0035μm (Caughey et al. 2009). The artificially "*in vitro*" created fibrils described in this chapter share similar characteristics (*Figure 4.6, 4.7, 4.8*) and therefore provide a suitable synthetic surrogate of *in vivo* generated misfolded PrP for fibril challenge experiments.

Fibrillisation of recombinant PrP was carried out according to previously published methods (Graham et al. 2010; Breydo, Makarava, and Baskakov 2008). Initially lyophilised recombinant PrP samples were reconstituted in 6M Gdn-HCl pH 6.0 to a concentration of 3mg/ml however this was later increased to between 10-15mg/ml which aided in the production of highly concentrated fibrils whilst reducing the volume needed for fibril challenge studies in primary neuronal cultures. The conditions associated with the refolding of monomeric recombinant PrP to produce fibril material vary between laboratories and involve using different concentrations of denaturant and buffering along with variations in speed of agitation (Raymond et al. 2012; Makarava et al. 2010; Novitskaya et al. 2006; Legname et al. 2004). Our group have previously shown that fibrils produced as described in this chapter can seed further fibril aggregation in the brain in the absence of disease.

These results also agreed with other published data irrespective of how the fibrils were generated (Makarava, Kovacs, Savtchenko, Alexeeva, Ostapchenko, et al. 2012; Makarava et al. 2011; Makarava et al. 2010).

Fluorescent analysis using SDS-PAGE and a typhoon scanner in conjunction with confocal microscopy confirmed efficient labelling of fibrils with Alexa Fluor dye. The dye is water soluble and pH insensitive from pH 4-10 which was advantageous for working in biological environments. Additionally, succinimidyl esters attach to amine-containing molecules forming amide bonds which are as stable as peptide bonds (Banks and Paquette 1995). Studies have demonstrated using TEM that these small extrinsic fluorescent tags do not interfere with the formation of amyloid fibrils and can therefore be used as a marker for studying protein aggregation (Anderson and Webb 2011). Additionally, other groups have shown cell lines and primary cultures were capable of cellular internalisation and processing of Alexa fluor labelled misfolded proteins again confirming fluorescent labelling of fibrils will be a suitable method for the visualisation of misfolded protein uptake and processing in primary cultures (Hollister et al. 2015; Magalhaes et al. 2005).

In summary, highly pure recombinant WT and 101L PrP fibrils were produced from bacterial cultures and then fluorescently labelled allowing for easy detectability of fibrils when added to primary neuronal cultures *in vitro*. This was important as it will allowed direct visualisation of abnormal protein trafficking and interactions in mixed cellular populations, crucial to understanding the mechanisms of misfolded protein processing in neuronal cultures.

CHAPTER 5

Monitoring fluorescently labelled fibril trafficking and cellular processing in primary hippocampal cultures

5.1 Abstract

Accumulation and spread of misfolded protein is common to all protein misfolding diseases (PMDs) however, mechanisms involved in abnormal protein trafficking and spreading remain unclear and non-neuronal cellular responses are poorly understood. To characterise pathways involved with the uptake and trafficking of misfolded protein, fluorescently labelled PrP fibrils were used to challenge primary neuronal hippocampal cultures and cellular response associated with both neuronal and non-neuronal cells was examined. Primary cultures generated from the 101LL genotype, which supports abnormal fibril seeding, and the WT genotype, which curtails abnormal protein formation, provided ideal candidates for these investigations to be carried out based on the hypothesis that both have different mechanisms of intracellular processing of abnormal protein that determine clearance versus the seeding of amyloid plaques. Fibril interactions with neurons and PrP^C protein in both 101LL and WT cultures were apparent however, no significant neuronal loss was evident over a 24-hour exposure period indicating fibril concentrations investigated were not initially neurotoxic. Fibril internalisation by cells trafficked fibrils into early and late endosomes in both genotypes indicating early sorting and recycling of fibrils was occurring and was been mediated via an operative endocytic pathway. Intracellular labelling of lysosomal vesicles in WT cultures indicated cells were capable of internalising fibrils proficiently for degradation however, 101LL cells did not. This impeded lysosomal processing of fibrils in 101LL cultures may explain how this genotype is capable of supporting the aggregation of abnormal protein in the brain. Non-neuronal cellular processing of fibrils was evident in both cultures. WT astrocytic populations appeared hypertrophic in comparison to 101LL astrocytes indicating glial cells were responding to fibril challenge whilst playing an active role in fibril uptake and processing in WT challenged cultures. Microglial response was evident in both 101LL and WT cultures and microglia appeared to be actively phagocytosing fibrils.

Synaptic fibril associations were evident in both genotypes and 101LL cultures had significant reduction in post-synaptic marker PSD-95 after fibril challenge suggesting 101LL neurons were more susceptible than WT to fibril challenge. These experiments visualise and characterise the initial steps associated with misfolded protein uptake and processing, and show evidence of associations with both neuronal and non-neuronal cells in two divergent genotypes. The results presented here highlight misfolded proteins in this case fibrils can interact with numerous cells types not just neurons. Additionally, abnormalities in endolysosomal degradation pathways identified in the 101LL cultures that impede fibril degradation provides insights into abnormal protein processing and provides test targets for further investigations for intervention in PMDs.

5.2 Introduction

One of the key features associated with PMDs is the ability of the abnormally folded proteins to propagate in a “prion-like” manner (Section 1.5.2) and spread from neurons to neighbouring neurons and glia however, the cellular mechanisms involved are poorly understood (Pearce et al. 2015; Brettschneider et al. 2015). Studies in prion infected neuroblastoma cells indicated that once abnormal PrP is formed on the cell surface or in endosomes, it can be sequestered in lysosomes (Magalhaes et al. 2005; Caughey et al. 1991). In prion infected brains, abnormal PrP usually accumulates in extracellular deposits but can also be located in late endolysosomal vesicles in neurons (Laszlo et al. 1992). Additionally, glial response to environmental changes in the brain can include astrocytic and microglial cell activation characterised by a notable change in cell morphology at early stages of neurodegeneration (Perry and Teeling 2013). Abnormal proteins can induce these glial responses, characterised by the presence of hypertrophic cell bodies (Sofroniew 2009, 2005; Schenk et al. 1999), and studies have shown both astrocytes and microglia cell types are capable of phagocytosis of Aβ fibril material (Jones et al. 2013; Lee and Landreth 2010). More recently, astrocytic endolysosomal vesicles were found to be capable of cell-to-cell transfer of misfolded PrP (Victoria et al. 2016). These observations suggest both neuronal and non-neuronal cells play important roles in PMDs and endolysosomal vesicles may be a major route for abnormal protein degradation. To gain further insights into these associations, initial responses to misfolded PrP fibril challenge were investigated using primary hippocampal cell cultures. Fluorescently labelling PrP fibrils allowed for the visualisation of trafficking and processing associated with abnormal fibrils. Additionally, hippocampal cultures were generated from mice with PrP genotypes that were capable of supporting PrP misfolding or that curtailed it and thus, provided a means for gaining further insights into possible different mechanisms associated with efficient or deficient misfolded protein processing.

Genotype specific responses were characterised using immunocytochemistry in conjunction with IMARIS software which provided a novel platform for performing detailed analysis of cellular interactions with fluorescently-labelled fibrils *in vitro*.

5.3 Results

5.3.1 Neuronal response to fibril challenge in primary hippocampal cultures

Recombinant PrP fibrils were produced and fluorescently labelled (Chapter 4, *Figure 4.8*) for use in fibril challenge experiments. Primary neuronal cultures are capable of cellular internalisation and processing of Alexa fluor labelled misfolded proteins (Hollister et al. 2015; Magalhaes et al. 2005) therefore, primary hippocampal cultures generated from WT and 101LL embryos (Chapter 3, Section 3.3.3) were used in these fibril challenge experiments to allow visualisation of abnormal protein uptake and processing *in vitro*. Initial challenge studies indicated fibrils were not neurotoxic at 7.5µg/ml concentrations over a 24-hour time period as measured by LDH release (*Figure 5.1*). IMARIS analysis of immunolabelled images supported these findings and showed no significant differences between unchallenged and fibril-challenged cultures were evident based on neuronal marker MAP2 (*Appendix Figure 5.a*) confirming a lack of neurotoxicity within these parameters (6 and 24-hours, 7.5µg/ml). This was an important finding as it provided baseline parameters for future investigations. To examine if fibril insult could induce cytotoxicity at higher concentrations, a range of fibril concentrations (0-45µg/ml) were applied to cultures over a 24-hour period and cellular cytotoxicity was monitored. A correlation with increased fibril concentration and cellular cytotoxicity measured by LDH release was evident (*Figure 5.1*). At 30µg/ml approximately 40% cells were showing signs of cellular stress confirming fibrils were capable of inducing cellular toxicity in primary cultures in a dose dependant manner. Similar cytotoxic effects were evident using unlabelled fibrils (*Figure 5.1*) suggesting labelling with a fluorescent tag was not effecting cellular response to fibrils. and also confirmed studies by other groups that have shown labelling with extrinsic fluorescent tags can be used to study protein aggregation (Anderson and Webb 2011).

Throughout the investigations presented in this chapter, cultures were challenged for either 6 or 24-hours at fibril concentrations of 7.5 or 30µg/ml, parameters that were deemed sufficient for eliciting limited cellular degradation (7.5µg/ml) whilst possibly stimulating a strain on organelle clearance pathways (30µg/ml). WT and 101L fibrils were used as previous results showed both shared similar physical dimensions (Chapter 4, *Figure 4.7*) and previous data from our group demonstrated that both fibril types were capable of seeded plaque formation in 101LL mice but not in WT mice, indicating the primary sequence of recombinant PrP fibrils does not influence seeding mechanisms (Barron et al. 2016). Super-resolution studies using the Zeiss AiryScan 880 confocal microscope were performed to examine the precise location of fibrils after addition to cultures, and to investigate if fibrils were localising with PrP^C. The AiryScan 880 has a 32-channel gallium arsenide phosphide photomultiplier tube area detector that collects a pinhole-plane image at every scan position which improves resolution and signal-to-noise ratio, and can resolve structures of 120 nm in x,y and 350 nm in z dimensions (Huff 2015). As shown in *Figure 5.2*, fibrils were directly localising with neuronal dendritic processes and around neuronal cell bodies and IMARIS reconstructions (*Figure 5.2*), highlighted these associations. Furthermore, fibrils localised with PrP^C and this may be an indication of initial mechanisms associated with fibril conversion of normal cellular PrP^C to the abnormal form, a process known as seeding-nucleation conversion (Prusiner 1996; Kocisko et al. 1994). These data also show fibril detection can be distinguished from normal PrP^C immunolabelling when using anti-PrP antibody 6H4. Unfortunately, only limited super-resolution studies were carried out due to lack of AiryScan confocal resources.

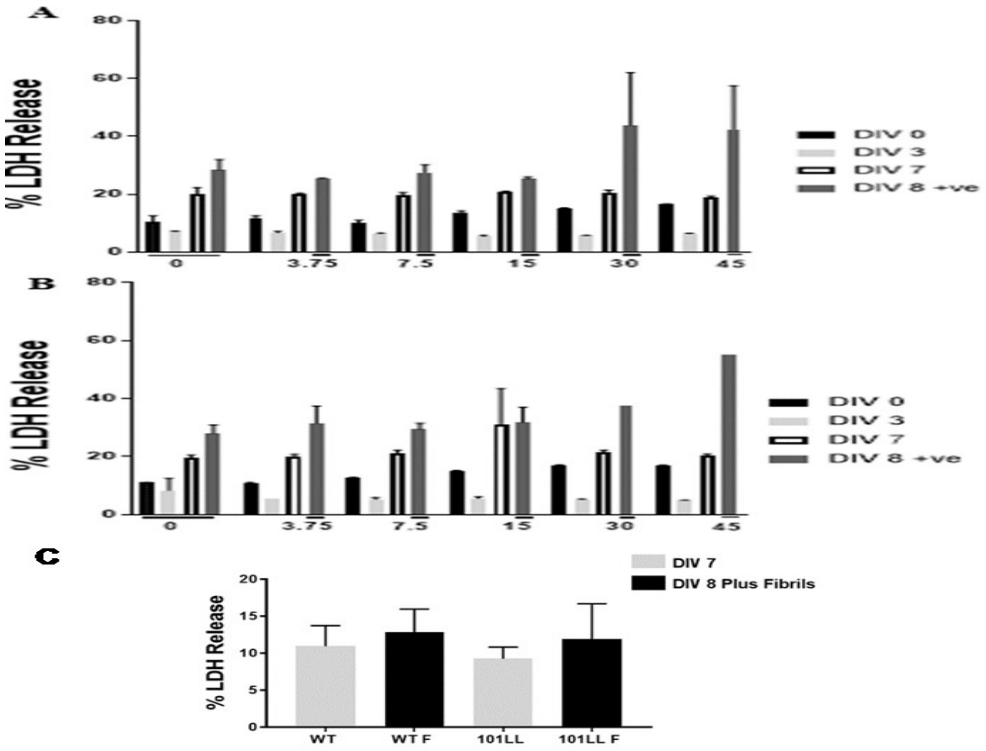

Figure 5.1: Cellular response to fibrils was dose dependant in primary cultures. To investigate if fibrils were capable of inducing neurotoxicity in cultures, a range of fibril concentrations (0-45µg/ml) were applied to cells over a 24-hour timeframe. The effect of fluorescently labelling fibrils was also examined to ascertain if this fluorescent tag was influencing toxicity in cultures. (A) LDH readings from WT cells challenged with Alexa Fluor 555 WT fibrils and (B) WT cells challenged with unlabelled WT fibrils. A correlation between cytotoxicity and increased fibril concentration was evident in labelled and unlabelled challenged groups confirming fibrils were capable to inducing cellular toxicity at higher concentrations. Additionally, LDH profiles were comparable between groups, for example at 30µg/ml, approximately 40% cells were showing signs of cellular stress in both labelled and unlabelled challenged cultures. These data suggest labelling fibrils with a fluorescent tag does not affect cytotoxicity. (C) Fibrils did not induce neurotoxicity in either WT or 101LL primary cultures. LDH assay was used to monitor cytotoxicity associated with fibril challenge in both WT and 101LL cultures. LDH readings showed no significant increase after challenge (WT F, 101LL F) in comparison to control readings (WT, 101LL) indicating fibrils were not neurotoxic at this concentration and incubation timeframe. (A-B) WT cells plated at 30,000 cells per well on pre-coated PDL plates, Graph mean plus standard deviation, n=2 duplicate technical replicates. Note only one value available for both 30 and 45µg/ml readings in (B) due to pipetting error. (C) 400,000 cells challenged with 7.5µg/ml of 101L fibrils for 24-hours at DIV7, Graph mean plus standard deviation, WT n=10, WT F n=12, 101LL n=8, 101LL F n=8, n= duplicate technical replicates of individual wells, unpaired t test. Fluorescent values were normalized to Triton X-100 treated lysis cells that represent the maximum amount of LDH available for release.

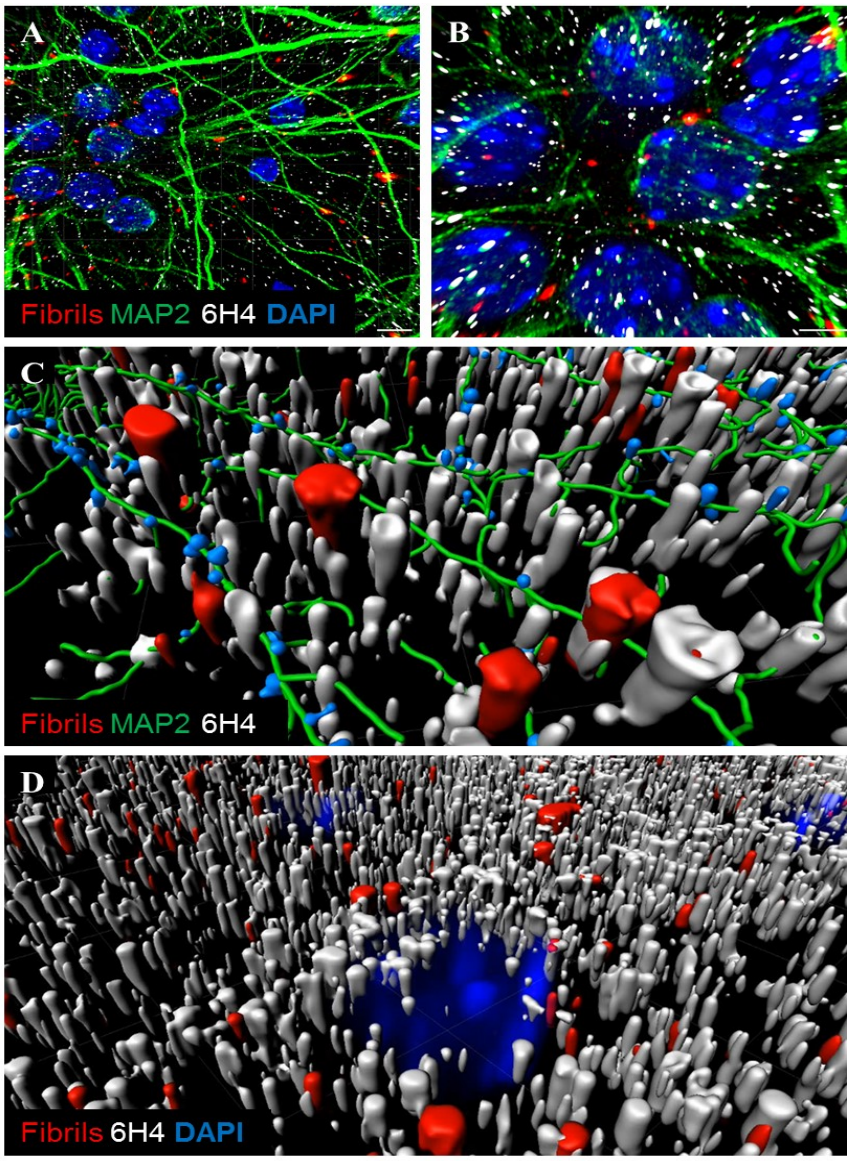

Figure 5.2: Fluorescence image analysis of fibril-challenged cultures. Super-resolution imaging using the Zeiss AiryScan 880 allowed for detailed image reconstructions to be carried out using IMARIS which allowed for efficient fibril interaction analysis. These analysis were used to investigate whether fibrils were localising with neuronal cells and PrP^C and whether anti-PrP antibody labelling could be distinguished from fibril labelling. (A) and (B) Fibrils (Red) appeared to be interacting with neuronal processes (MAP2/Green), neuronal cellular bodies (MAP2/Green; Nuclear/DAPI/Blue) and PrP^C (6H4/White). (C) and (D) IMARIS reconstructions confirmed these observations and clearly show fibrils were interacting with PrP^C along dendritic processes and around neuronal nuclear bodies. These data confirmed fibril detection can also be distinguished from normal PrP^C immunolabelling when using anti-PrP antibody 6H4. 101LL cultures 75,000 cells, challenged with 7.5µg/ml WT fibrils, glass coverslip. Scale bar (A) 5µm, (B) 3µm, (C), (D) 2µm, Confocal AiryScan 880.

5.3.2 Non-Neuronal response to fibril challenge in primary hippocampal cultures

To ascertain if neuronal and or non-neuronal cells were capable of fibril endocytosis, a phagocytosis assay was initially carried out using pHrodo red *S.aureus* bioparticle conjugates (Materials and Methods, 2.4.2). When beads are internalised by cells acidification of the pHrodo dye conjugated to the particles increases fluorescence as the pH of its surroundings becomes more acidic and this signal can be detected using a plate reader or can be visualised by confocal microscopy. Neurons, astrocytes and microglia were capable of phagocytosing pHrodo bioparticles (data not shown) implying these cellular populations should be able to actively process fibrils in a similar manner. Thus, fibril aggregate diameter (FAD) measurements were obtained using IMARIS (Section 2.2.9) before and after addition to WT and 101LL cultures to ascertain if changes in fibril size were evident after challenge indicative of active cellular fibril processing. A significant decrease in fibril size was noted in both WT and 101LL cultures after 6 hours (*Figure 5.3*). Longer incubation timeframes did not result in significantly more degradation of fibrils indicating both genotypes were rapidly responding to fibril insult within a few hours suggesting cells were actively trying to reduce fibril burden in primary cultures. Results obtained from the pHrodo phagocytosis assay, confirmed both neuronal and non-neuronal cells were capable of phagocytosis of unwanted materials and as fibril challenge was not causing any obvious morphological changes in neuronal populations (*Appendix Figure 5.a*), the possibility that other non-neuronal cells could be actively interacting with and possibly degrading fibrils to protect neuronal populations was investigated. Thus, both astrocytic and microglial response was monitored after fibril challenge in primary cultures as studies have shown these glial cells maintain neuronal networks and protect neurons from toxicity (Boehler, Wheeler, and Brewer 2007; Ye and Sontheimer 1998).

Previous immunolabelling characterisation results (Chapter 3, *Figure 3.10*), confirmed astrocytic populations were present in WT and 101LL cultures and were morphologically comparable displaying multiple process phenotypes pre-fibril challenge. Astrocytes in both genotypes were interacting with fibrils however, only WT challenged cultures exhibited a change in astrocytic morphology (*Figure 5.4*). This hypertrophic astrocytic response to misfolded protein has been previously described in other studies that showed reactive astrocytes played a role in restricting inflammation and protecting neurons, therefore reducing CNS degeneration (Sofroniew 2009, 2005; Schenk et al. 1999) suggesting WT astrocytic response was neuroprotective. Conversely, other studies have shown reactive astrogliosis response may contribute to neurodegeneration via loss of normal astrocyte function or gain of abnormal effects (Sofroniew and Vinters 2010). Neuronal populations present in WT fibril-challenged primary cultures did not show any signs of degradation suggesting reactive astrocytes were neuroprotective in this case and were possibly actively phagocytosing fibrils. No evidence of astrocytic activation in 101LL cultures indicated either a delayed response, a lack of response or an inactivated response due to the 101LL point mutation however, this did not cause any obvious neuronal toxicity over the timeframes investigated. Increasing fibril load or challenge time may result in a reactive astrocytic response or may even induce cellular toxicity however, this was not explored further due to time constraints. As described in Chapter 3 (*Figure 3.13*) PrP^C was also associated with astrocyte cell populations, although to a lower degree than neurons and fibril localisation with PrP^C on astrocytic bodies was evident in both WT and 101LL cultures (*Figure 5.4*). Studies have shown astrocytic involvement in replication of abnormal PrP protein (Diedrich et al. 1991). Further reports indicated TSE infection was evident in transgenic mice expressing PrP^C only in astrocytes indicating that PrP^C expression in these specific cell types alone was sufficient to cause neurodegeneration (Raeber et al. 1997). Due to the short timeframe associated with fibril challenge experiments in this study, it could not be concluded if abnormal PrP replication was happening in this cell type.

However, initial investigations of PrP^C immunolabelling after challenge (*Appendix Figure 5.f*) showed no significant differences pre and post-challenge in both genotypes, indicating that within a 24-hour timeframe no PrP^C conversion was occurring nevertheless, this would have to be confirmed biochemically in future investigations as discussed in Section 7.3.1. Fibril localisation with astrocytic PrP^C protein does however indicate normal cellular function may be altered in these cell types which could lead to abnormal PrP replication. Microglia were also present in unchallenged primary cultures (Chapter 3, *Figure 3.11*), however, their presence was less abundant than astrocytic cell populations. Microglial cells in unchallenged cultures appeared ramified exhibiting long processes indicating they were in surveillance mode as opposed to an amoeboid state where cell bodies are large and processes are short and thick, a phenotype correlated with microglial activation in response to neuronal injury (Arcuri et al. 2017; Ling and Wong 1993). After fibril challenge, microglial cells appeared short and thick indicating microglia were activated after fibril insult (*Appendix Figure 5.b*). High magnification imaging confirmed localisation between fibrils, microglia and PrP^C and enlarged images showed many smaller fibril structures were present in these activated phagocytic cells suggesting phagocytosis was occurring possibly to aid fibril degradation and this was evident in both WT and 101LL cultures. Localisation of fibrils with PrP^C suggest the possibility of fibrils acting as seeds for the conversion and misfolding of normal host PrP protein however, this was not investigated here. More so, previous studies have shown by EM that activated microglial are normally absent where abnormal PrP is confined solely to membranes indicating microglia were not essential for conversion of normal PrP to the abnormal disease form (Jeffrey et al. 2012). Overall, activation of microglia in both genotypes indicated this was a generic response to fibril challenge that was limiting neuronal damage in primary cultures.

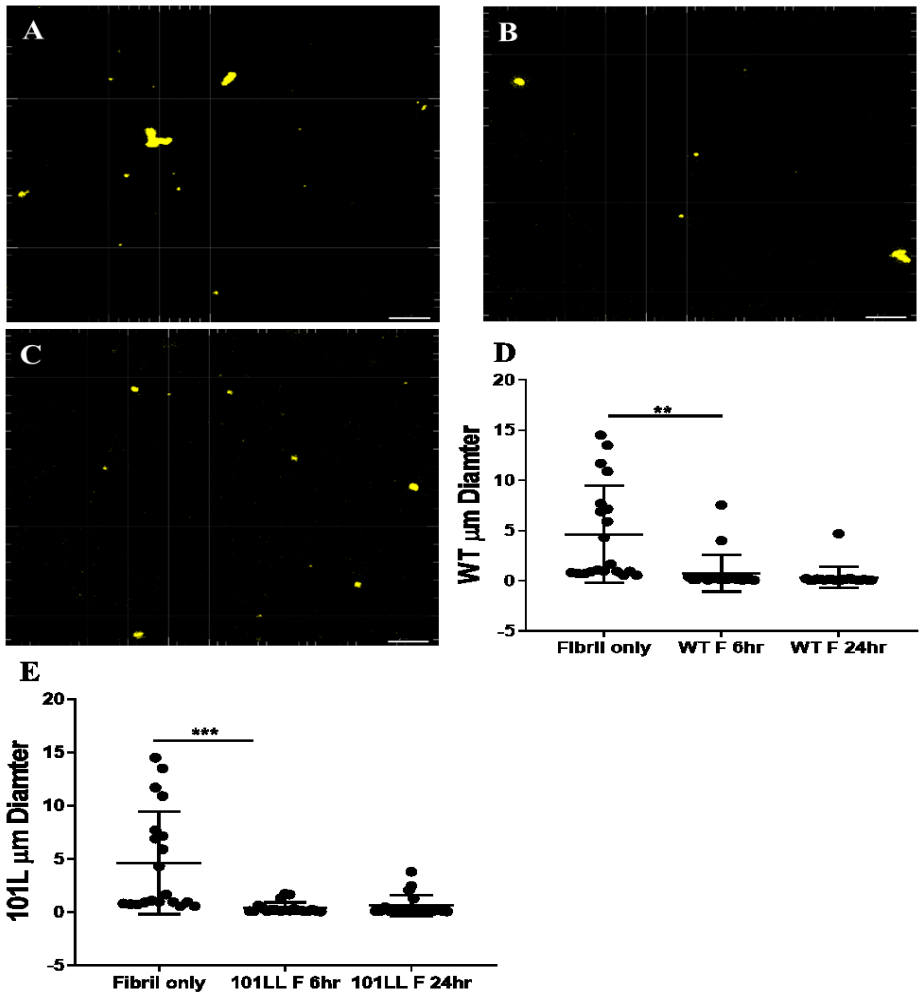

Figure 5.3: Fibril size was reduced after addition to cultures. To investigate if fibrils were been degraded in cultures, fibril aggregate diameter measurements before and after addition to cells were taken at two time points. (A-C) Representative images of (A) Fibrils only, (B) Fibrils plus cells (WT culture, 6-hour fibril challenge) and (C) Fibrils plus cells (WT culture, 24-hour fibril challenge). (D) and (E) Measurements of fibril diameter were calculated using IMARIS software for both WT (Mean diameter fibrils only 4.63; fibrils plus cells 6-hour 0.76, 24-hour 0.36 µm) and 101LL (Mean diameter fibrils only 4.63; plus cells 6-hour 0.40; 24-hour 0.61 µm) cultures. Significant differences in diameter readings were noted in both WT (P-Value 0.001) and 101LL (P-Value 0.0004) cultures indicating fibril size was been reduced after addition to primary cultures. Timeframes show this happened rapidly within a 6-hour period. No significant differences in readings were evident between WT and 101LL 6-hour culture fibril values (P-Value 0.40). Longer incubation timeframe (24-hour) did not result in significantly more degradation of fibrils (P-Value 0.40, 0.40), indicating both genotypes were rapidly responding to fibril insult and were actively trying to reduce fibril burden. WT and 101LL cultures 30,000 cells, challenged with 7.5µg/ml WT fibrils for 6 or 24-hours, Scale Bar 20µm, Confocal LSM710. Graph mean plus standard deviation, n=20, n= individual fibril diameter, unpaired t test.

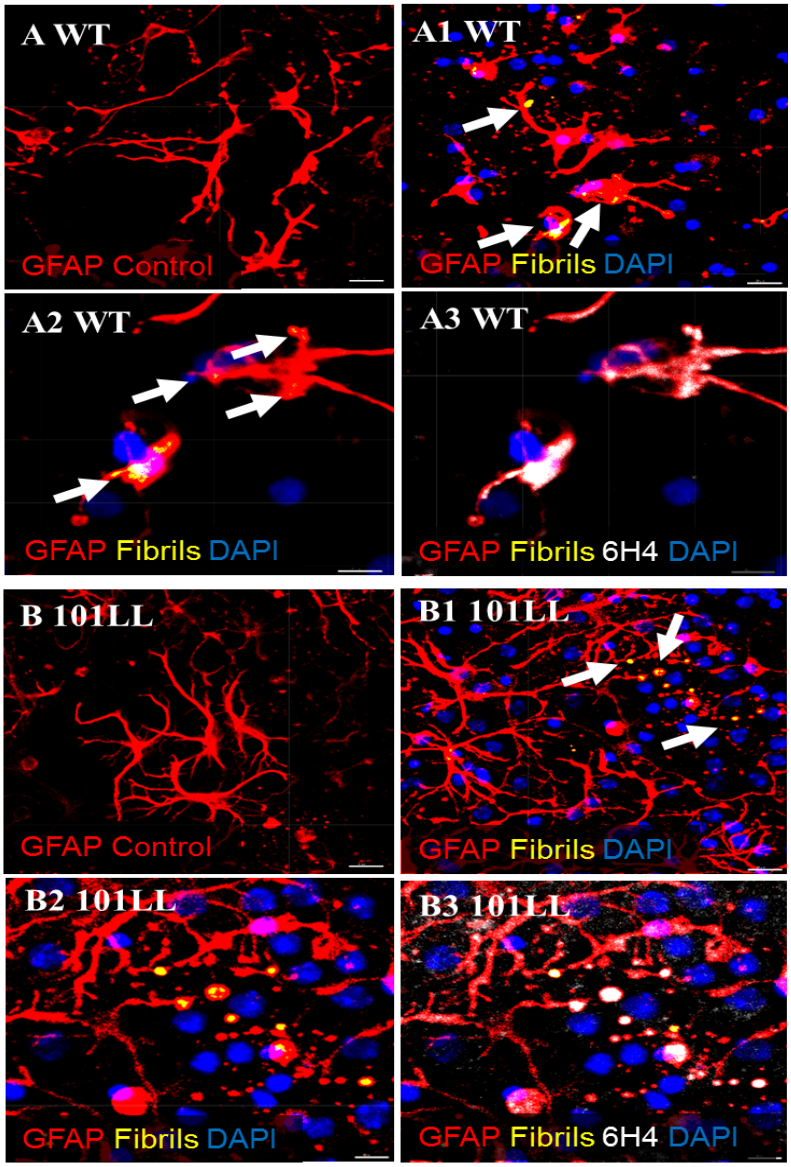

Figure 5.4: Astrocytic response differed between fibril-challenged genotypes. Immunolabelling of astrocytes after fibril challenge was carried out to investigate if glial cells were interacting and responding to fibrils. (A) and (B) Unchallenged WT and 101LL controls; (A1-A3; B1-B3) WT and 101LL challenged cultures with fibrils (Yellow), astrocytic marker (GFAP/Red), PrP^{C} (6H4/White), and DAPI (Nuclear/Blue). Localisation of fibrils with astrocytes was evident (Arrows) in both genotypes however, only WT challenged astrocytes displayed a change in morphology (A1,A2,A3) in comparison to unchallenged controls. This hypertrophic change characterised by a shortening and thickening of processes indicated a reactive astrogliosis response was occurring in WT cultures which was absent in 101LL cultures. Localisation of fibrils with PrP^{C} on astrocytic bodies was also evident in both WT and 101LL cultures. WT and 101LL cultures 75,000 cells, challenged with 7.5µg/ml WT fibrils, Scale bar (A-B) 15µm, (A1-A3; B1-B3) 10µm, Confocal LSM710.

5.3.3 Synaptic response to fibril challenge in primary hippocampal cultures

Previous studies have shown the hippocampus is a target area associated with early synaptic loss in prion diseases which precedes neuronal death (Hilton et al. 2013; Cunningham et al. 2003). Synapsin 1 (Syn) is a pre-synaptic vesicle-associated protein, involved in the regulation of axonogenesis and synaptogenesis (Qin et al. 2004; Chin et al. 1995). PSD-95 is the most abundant scaffold protein localised in post-synaptic terminals of excitatory neurons and has a critical role in post-synaptic function and plasticity (Yuki et al. 2014). The presence of both pre and post-synapses were evident in both WT and 101LL cultures (Chapter 3, *Figure 3.12*) and IMARIS data intensity value comparisons confirmed similar levels of synaptic populations were evident between genotype comparisons based on Synapsin 1 and PSD-95 labelling pre-fibril challenge. Fibril localisation with synapses was evident in both genotypes however, only 101LL cultures showed a significant reduction in PSD-95 labelling after fibril challenge and this reduction was occurring before any detectable neuronal loss (*Figure 5.5*). WT cultures did not show any changes in synaptic markers after fibril challenge indicating they were less susceptible to fibril synaptic interactions over a 24-hour period. Studies have shown early synaptic loss precedes neuronal death (Hilton et al. 2013) and this would explain the lack of correlation between neuronal loss and PSD-95 reduction observed here. AD hippocampal studies have also shown neuronal loss was disproportionate to initial decrease in synaptic number and density (Davies et al. 1987). Collectively, the initial fibril effects reported in this chapter support the hypothesis that synaptic loss is an early event and precedes neuronal loss. It also indicates results obtained using primary hippocampal cultures compliment *in vivo* data obtained from investigations into neurodegenerative diseases such as AD (Scheff et al. 2006; Masliah et al. 2001) indicating this *in vitro* system was providing a suitable model for studying neurodegeneration.

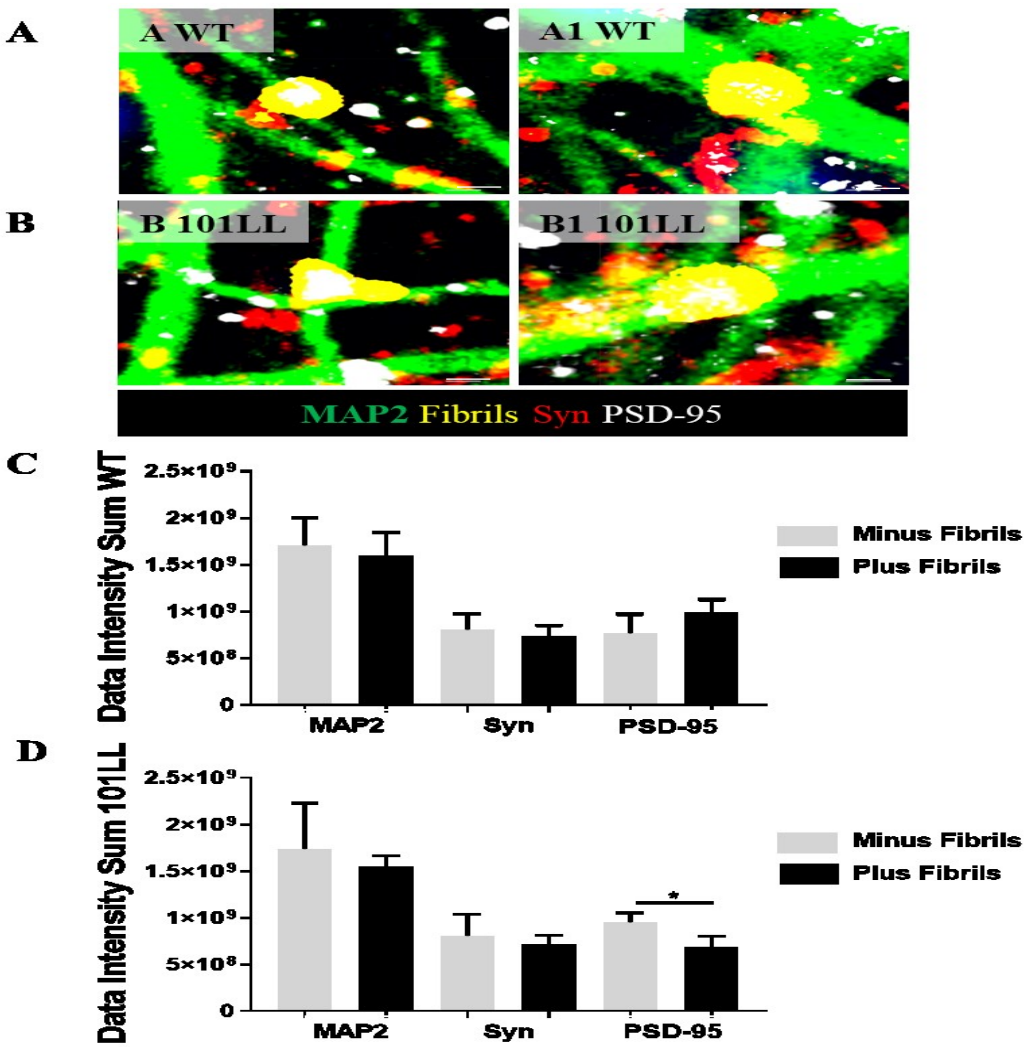

Figure 5.5: Fibril challenge reduced PSD-95 in 101LL cultures. After fibril challenge, pre and post-synaptic protein and fibril interactions were investigated to ascertain if fibrils were localising and possibly disrupting neuronal synapses. (A-A1) WT and (B-B1) 101LL images showed interactions between fibrils (Yellow); neurons (MAP2/Green); Synapsin 1 pre-synaptic marker (Syn/Red) and post-synaptic marker (PSD-95/White) were evident in both cultures. (C) WT and (D) 101LL IMARIS analysis of data signal intensities obtained from MAP2, Syn and PSD-95 immunolabelling. No significant differences were noted in neuronal immunolabelling after challenge and between synaptic markers in WT cultures however, as shown in (D) a significant reduction in PSD-95 was evident in 101LL cultures (P-Value 0.02). These data confirm fibrils were interacting with synapses in both genotypes however, no changes in MAP2 signalling suggested neurons were not affected over the 24-hour challenge period. In 101LL cultures, a significant reduction in PSD-95 confirmed fibrils were actively reducing this scaffold protein. WT and 101LL cultures 30,000 cells, challenged with 7.5µg/ml 101L fibrils for 24-hours, Scale Bar (A,A1-B,B1) 1µm, Confocal LSM710. Graph mean plus standard deviation, n=4, n= data intensity sum of individual wells, unpaired t test.

5.3.4 Fibril trafficking and organelle associations

To identify the subcellular compartments involved in uptake and trafficking of fibrils in primary hippocampal cultures, co-staining with a variety of organelle markers (Chapter 3, *Figure 3.16*) was carried out. Previous studies have indicated abnormal PrP localisation with raft membranes and these associations may provide a means of cellular internalisation of fibrils via clathrin-coated pits (Taylor and Hooper 2006; Vey et al. 1996). Cholera toxin Ganglioside GM1 ligand Subunit B was used to label lipid-rafts to explore if fibril interactions were associated with these glycolipoprotein microdomains. Image analysis (*Appendix Figure 5.c*), indicated some fibrils were localising to these areas in both genotypes however these observations were rare. Lipid-rafts have been shown to be more abundant in mature hippocampal neurons than other cell types such as astrocytes (Malchiodi-Albedi et al. 2010) indicating fibrils were mainly internalised by neurons via this route however, specific cells types were not immunolabelled in these studies. As fibril lipid-raft domain localisation was only evident in some cases, internalisation via this route may also be limited. These findings support studies that have shown if abnormal PrP formation occurred outside of raft domains they may lack raft associations (Magalhaes et al. 2005). Misfolded proteins and exogenous abnormal PrP can also be taking up by cells in a relatively nonselective process such as macropinocytosis, which delivers internalised substances to endosomal or lysosomal organelles (Silverman et al. 2016; Swanson and Watts 1995). This uptake may also be occurring in primary cultures as vesicular structures associated with macropinocytosis called macropinosomes range in size from 0.2 to 5μm therefore, would be capable of internalising fibrils which were within this size range (*Figure 5.3*) (Lim and Gleeson 2011). It is also known recycling of normal PrP^{c} occurs via an endocytic pathway, where the protein is transported back into the cell by endosomes (Peters et al. 2003) or it is routed to the lysosomes for degradation via late endosome/multivesicular bodies (MVB) (Campana, Sarnataro, and Zurzolo 2005) and therefore, this pathway was important for trafficking investigations.

To establish if cells were actively involved in the uptake and further organelle processing of fibrils, similar endolysosomal routes as described above were investigated by co-staining with Early Endosome Antigen 1 (EEA1/ early endosomes), Ras-related protein Rab9 (Rab9/late endosomes) and Lysosomal-Associated Membrane Protein 1 (LAMP1/ lysosomes) (Chapter 3, *Figure 3.16*). Both WT and 101L fibrils were localising in neuronal early endosomal domains in both WT and 101LL cultures (*Figure 5.6*). This indicated early sorting and recycling via an endocytic pathway was operative in neurons. These results also confirmed no differences were apparent in initial fibril processing routes associated with either WT and 101L fibrils, complementing previous results that showed both shared similar physical dimensions (Chapter 4, *Figure 4.7*). Further visualisation of fibril trafficking (*Figure 5.7*) using late endosomal marker Rab9, confirmed fibrils (both WT and 101L) were associating with neuronal late endosomal organelles (astrocytic associations were also noted in both genotypes, data not shown) confirming maturation of early endosomes into late endosomes was occurring. Ras-related protein Rab5 localises to early endosomes and is involved in recruiting Rab7 and Rab9 associated with maturation of these compartments to late endosomes (Kaur and Lakkaraju 2018; Pollard 2017). These data confirmed fibrils were on route for lysosomal degradation in both genotypes and studies by others have shown fibril material can be cleared through acidification of lysosomes (Boissonneault et al. 2009; Majumdar et al. 2007). The internalisation of fibrils into lysosomal vesicles was investigated using lysosomal marker LAMP1 (*Figure 5.8*). IMARIS reconstruction clearly showed fibrils (WT and 101L) were internalised by WT neuronal lysosomal organelles. This processing of fibrils in WT cultures suggested cultures were actively trying to degrade fibrils in these acidic lysosomal organelles. Interestingly, and as mentioned in the introduction, studies have shown astrocytes are capable of cell-to-cell transfer of misfolded PrP often found colocalised with endolysosomal vesicles (Victoria et al. 2016). WT astrocytic cells were hypertrophic and co-staining with LAMP1 showed fibrils were also internalised into lysosomal vesicles in this cell type (*Appendix Figure 5.d*).

Additionally, as this process was occurring beside what appears to be a neuron, it could be conclude that astrocytes were playing a neuroprotective role however, because of this close proximity, cell-to-cell transfer of fibril materials may also be possible as studies have shown insufficient acidification of astrocytic lysosomes can result in inadequate digestion of material (Loov et al. 2012). When lysosomal-fibril associations were investigated in 101LL cultures, no evidence of fibril internalisation was found in neuronal lysosomal organelles (*Figure 5.9*) or astrocytic lysosomal organelles (data not shown). This failure to traffic fibrils through lysosomal compartments in 101LL neuron and glia was the first indication of a major difference in fibril processing between genotypes and avoidance of lysosomal degradation may explain how the 101LL genotype is capable of supporting misfolded protein seeding in the brain. An alternative hypothesis would be that rapid lysosomal processing was occurring in 101LL cultures and the 24-hour time-point used for analysis was too late for detection however, this was doubtful as fibrils were clearly localising and were detectable in early and late endosomes after the 24-hour fibril challenge. To validate lysosomal results further additional co-staining using LAMP2 was carried out. Both LAMP1 and LAMP2 are estimated to contribute to half of all proteins of the lysosome membrane (Eskelinen 2006). LAMP2 staining confirmed fibrils were associating with lysosomes in WT cultures but not in 101LL cultures (*Appendix Figure 5.e*). Pervious work in our laboratory has also indicated no intra-lysosomal abnormal PrP accumulations were noted in the brains (end-point) of 101LL mice inoculated with recombinant fibrils suggesting *in vitro* observations presented here were accurate (Barron et al. 2016). Defects in endocytic sorting have been associated with enlarged endosomes in AD (Kaur and Lakkaraju 2018) and accumulation of amyloid-β by astrocytes can also result in enlarged endosomes (Söllvander et al. 2016). To address if size or structure of early/late endosome and lysosome organelles was changing after fibril challenge in primary cultures which may account for differences noted between genotypes, a number of control versus fibril treated organelle confocal image comparisons were carried out alongside IMARIS organelle signal analysis (Section 2.2.9).

As shown in *Figure 5.10* no obvious differences based on visual inspection were evident in all organelle size comparisons between control and fibril treated groups and between genotypes. This indicated no obvious changes in organelle structures were apparent after 24-hour challenge that might account for different fibril processing between genotypes. However, IMARIS data intensity analysis based on organelle staining did show a significant reduction in LAMP1 staining in 101LL cultures was evident after fibril challenge (*Figure 5.10*), suggesting less lysosomal activity was occurring in this genotype. Recent studies have confirmed that promoting LAMP1 or lysosomal organelle degradation of Aβ using a small molecular URMC-099 (lineage kinase type 3 inhibitor), was crucial in restoring synaptic integrity and hippocampal neurogenesis in AD mice. Hence, endolysosomal clearance via lysosomes provided a neuroprotective role and this degradation route was evident in WT cultures following fibril challenge (Kiyota et al. 2018). The reduction in LAMP1 activity and the lack of localisation of fibrils within lysosome structures evident in 101LL fibril-challenged cultures indicated fibril degradation was impeded in this genotype. These results highlighted the 101LL point mutation was influencing the endolysosomal pathway potentially resulting in the seeding of fibril aggregates in this genotype.

Throughout these investigations PrP^C associations with fibrils, lipid-rafts and organelles was evident. These associations could be involved in the conformational conversion of PrP^C to the abnormal form for example, studies have shown lipid-rafts appear to be involved abnormal protein conversion as these structures provide favourable environments for the process to occur (Taylor and Hooper 2006). Additionally, experimetal evidence also suggests the involvement of recycling endosomes as potential intracellular sites for this conversion (Marijanovic et al. 2009). As discussed previously in Section 5.3.2, confomational coversion of PrP^C was not investigated in this chapter however, initial investigations for changes in PrP^C immunolabelling levels after challenge (*Appendix Figure 5.f*) indicated that within a 24-hour timeframe no PrP^C conversion was occurring in both genotypes.

Additional preliminary studies investigated if fibrils were associating with other processing pathways such as autophagy. Studies have shown p62 binds to ubiquitin and targets abnormal proteins for degradation through the autophagolysosomal pathway (Homma et al. 2014), therefore increased levels of p62 is used as an indicator of autophagy (Bartolome et al. 2018). Using p62 as an autophagosome marker (Materials and Methods, Table 2.1) fibril autophagosome localisation was explored in primary cultures. Preliminary results indicated fibrils were localising with these autophagic vacuoles in WT cultures which would possibly result in fibril degradation over longer periods of time however, no evidence of fibril localisation was noted in 101LL cultures (*Appendix Figure 5.g*). Due to limited time full investigation of this pathway could not be carried out however, these data do indicate that an autophagy pathway was also evident in WT cultures which would further contribute to fibril degradation. A summary of the significant findings in this chapter can be found in *Figure 5.11* and *Figure 5.12*. These figures detail the differences in fibril processing pathways in WT and 101LL primary neuronal hippocampal cultures and highlight the possible changes/failures in these pathways that ultimately lead to the seeding of PrP amyloid plaques in fibril-challenged 101LL mice.

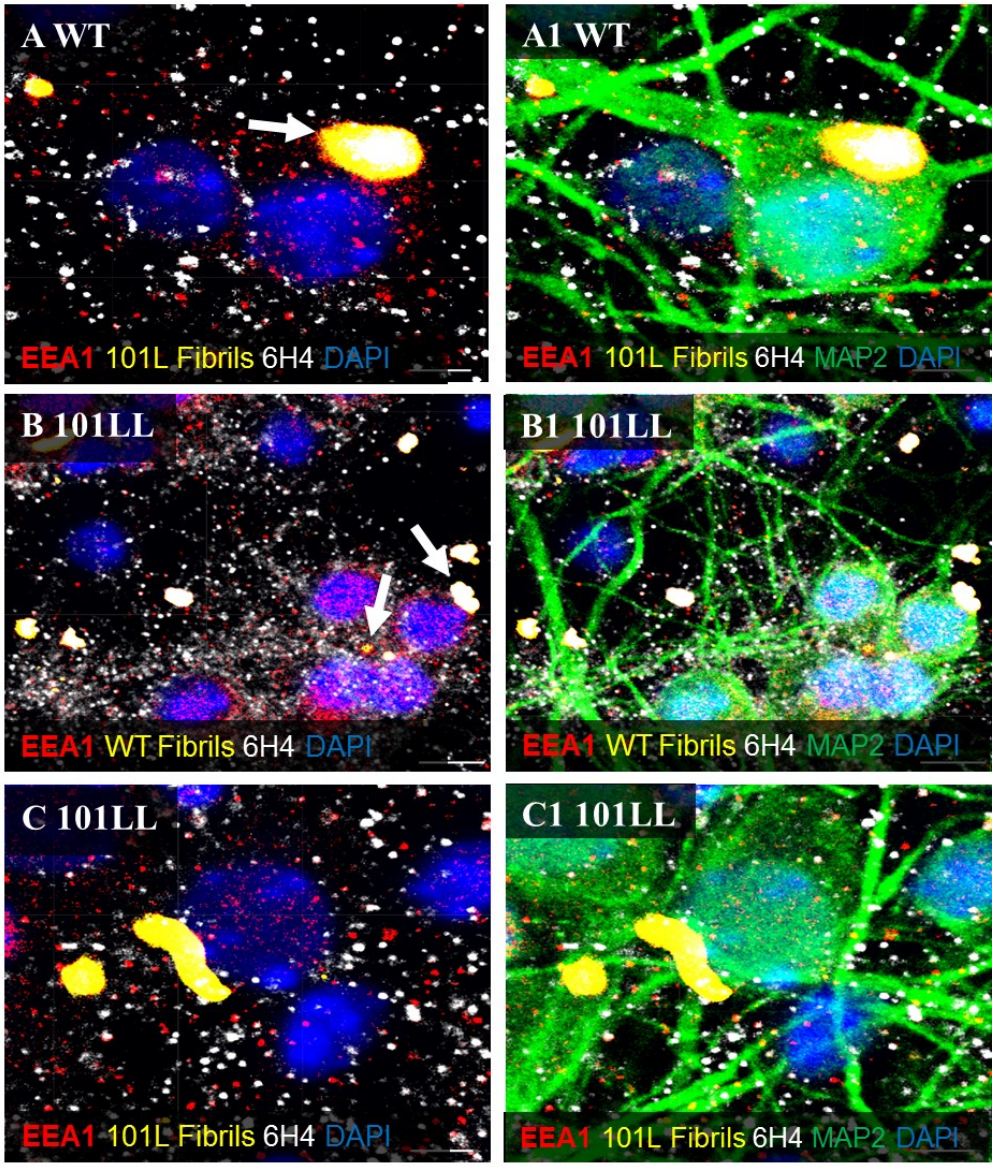

Figure 5.6: Intracellular trafficking of fluorescent-tagged fibrils. Organelle markers were used to investigate if fibrils were been internalised into cells via an endosomal mechanism and to ascertain if WT and 101L fibrils were trafficked in a similar manner in cultures. (A-A1) WT cultures challenged with 101L fibrils (Yellow/Arrows), Early endosomal marker (EEA1/Red), PrP^{C} (6H4/White) and DAPI (Nuclear/Blue). (B-B1) 101LL cultures challenged with WT fibrils (Yellow/Arrows) and (C-C1) 101LL cultures challenged with 101L fibrils. Arrows indicate both large are small fibril interactions with early endosomes were evident. WT and 101L fibrils were possibly internalised into neurons in both WT and 101LL cultures and were localising with early endosomal organelle domains indicating an endocytic processing pathway was operative. No differences in uptake were evident between the two fibril types or between genotypes. WT and 101LL cultures 30,000 cells, challenged with 30µg/ml of WT or 101L fibrils for 24-hours, Scale Bar (A-A1; C-C1) 5µm, (B-B1) 10µm, Confocal LSM710.

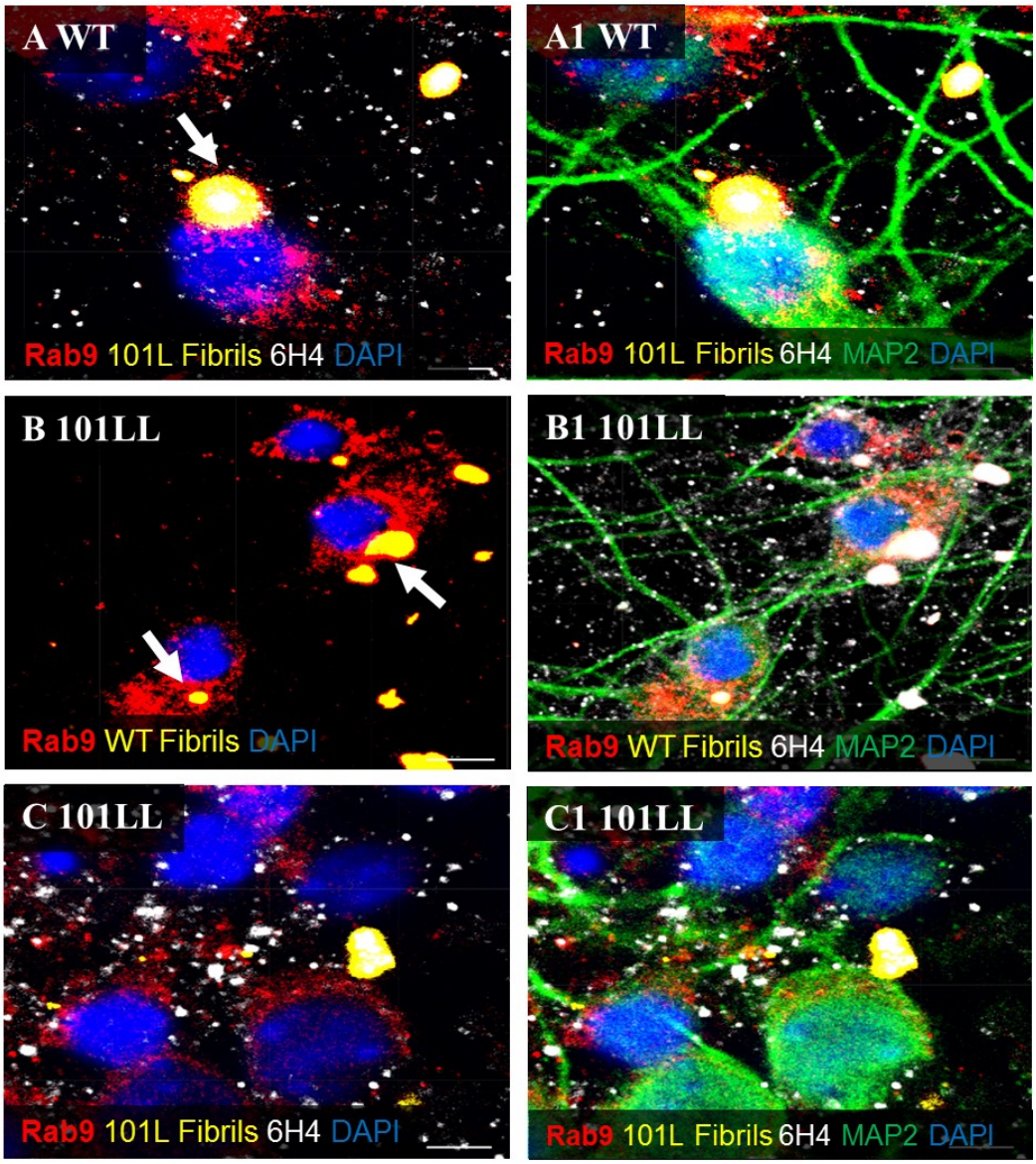

Figure 5.7: Targeting of fibrils to late endosomal organelles. To investigate if fibrils were been trafficked to late endosomes which would be indicative of a functional and operative endosomal pathway, cultures were labelled with a late endosomal marker. (A-A1) WT cultures challenged with 101L fibrils (Yellow/Arrows), Late endosomal marker Rab9 (Red), PrP^{C} (6H4/White) and DAPI (Nuclear/Blue). (B-B1) 101LL cultures challenged with WT fibrils (Yellow/Arrows) and (C-C1) 101LL cultures challenged with 101L fibrils. Arrows indicate both large are small fibril interactions with late endosomes were evident. Localisation of both WT and 101L fibrils with late endosomal organelles was evident in both WT and 101LL neuronal cultures confirming maturation of early endosomes into late endosomes was occurring. No differences were evident between processing routes of the two fibril types or between genotypes. WT and 101LL cultures 30,000 cells, challenged with 30µg/ml of WT or 101L fibrils for 24-hours, Scale Bar (A-A1; C-C1) 5µm, (B-B1) 10µm, Confocal LSM710.

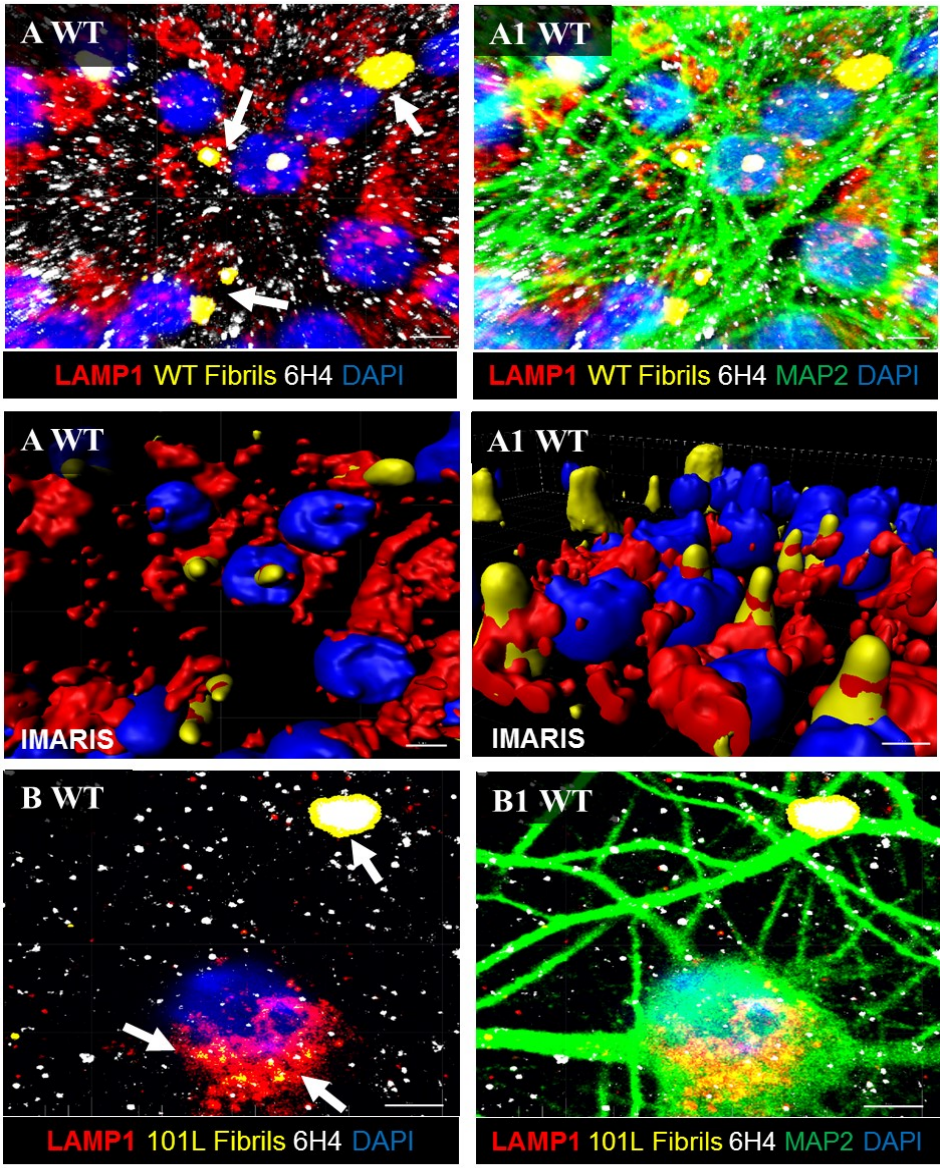

Figure 5.8: Fibrils were localising in lysosomes in WT cultures. To examine if fibrils were been trafficked to lysosomal domains, WT cultures were labelled with a lysosomal marker to examine if lysosomal degradation pathways were operative in this genotype. (A-A1) WT cultures challenged with WT fibrils (Yellow/Arrows), labelled with Lysosomal marker LAMP1 (Red), PrP^{C} (6H4/White) and DAPI (Nuclear/Blue). Panel below shows IMARIS reconstructions of fibril and organelle interactions. (B-B1) WT cultures challenged with 101L fibrils (Yellow/Arrows). Arrows indicate both large are small fibrils were present however, only smaller fibrils appeared to localise with lysosomes. Lysosomal labelling in WT cultures showed both WT and 101L fibrils were present in these acidic organelle domains. IMARIS reconstructions confirmed WT fibrils were clearly embedded in organelle structures. PrP^{C} localisation with fibrils was also evident. WT cultures 30,000 cells, challenged with 30µg/ml WT or 101L fibrils for 24-hours, Scale bar 10µm, Confocal LSM710.

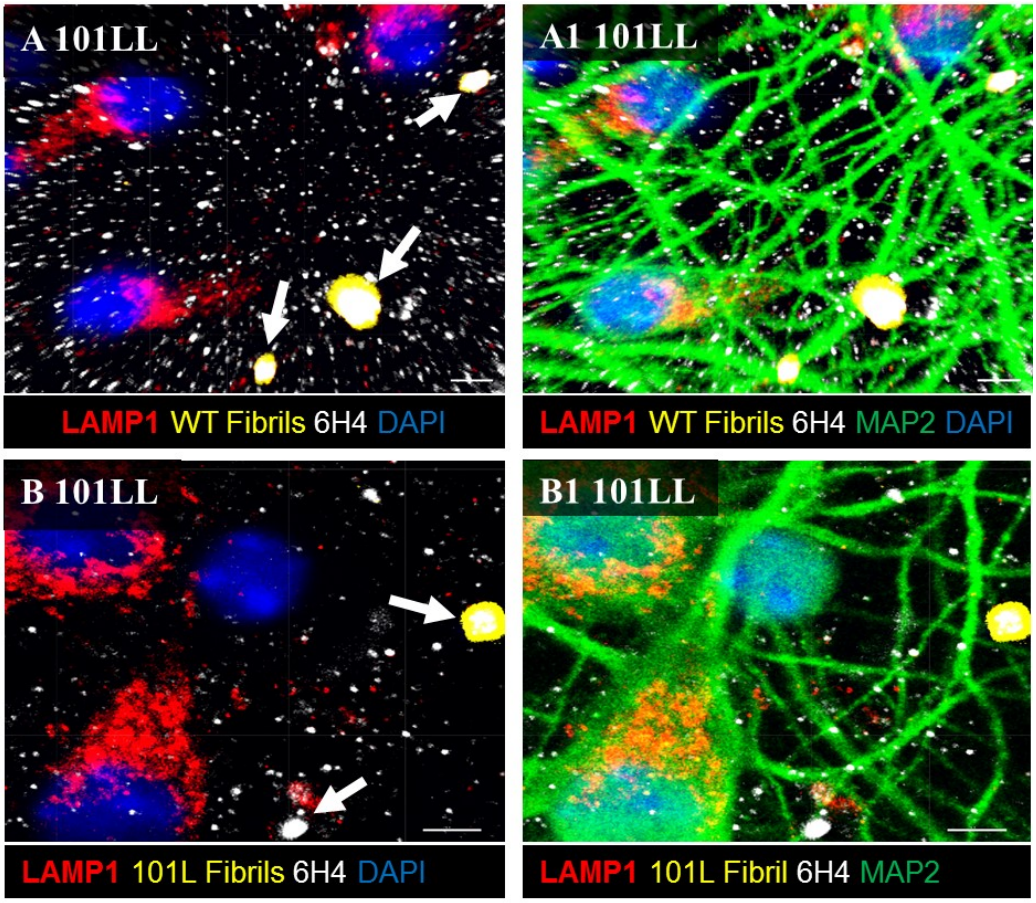

Figure 5.9: Lack of localisation of fibrils in 101LL cultures. To investigate if fibrils were been targeted to lysosomal domains for degradation in 101LL cultures, dual-labelling with a lysosomal marker was carried out. (A-A1) 101LL cultures challenged with WT fibrils (Yellow/Arrows), Lysosomal marker LAMP1 (Red), PrP^{C} (6H4/White) and DAPI (Nuclear/Blue). (B-B1) 101LL cultures challenged with 101L fibrils (Yellow/Arrows). Arrows indicate lack of interactions was evident with both large and small fibrils. Lysosomal labelling showed both WT and 101L fibrils were not localising in lysosomal organelle domains in 101LL cultures and therefore, fibrils were avoiding lysosomal degradation, possibly supporting protein misfolding and seeding. 101LL cultures 30,000 cells, challenged with 30µg/ml WT or 101L fibrils for 24-hours, Scale bar 5µm, Confocal LSM710.

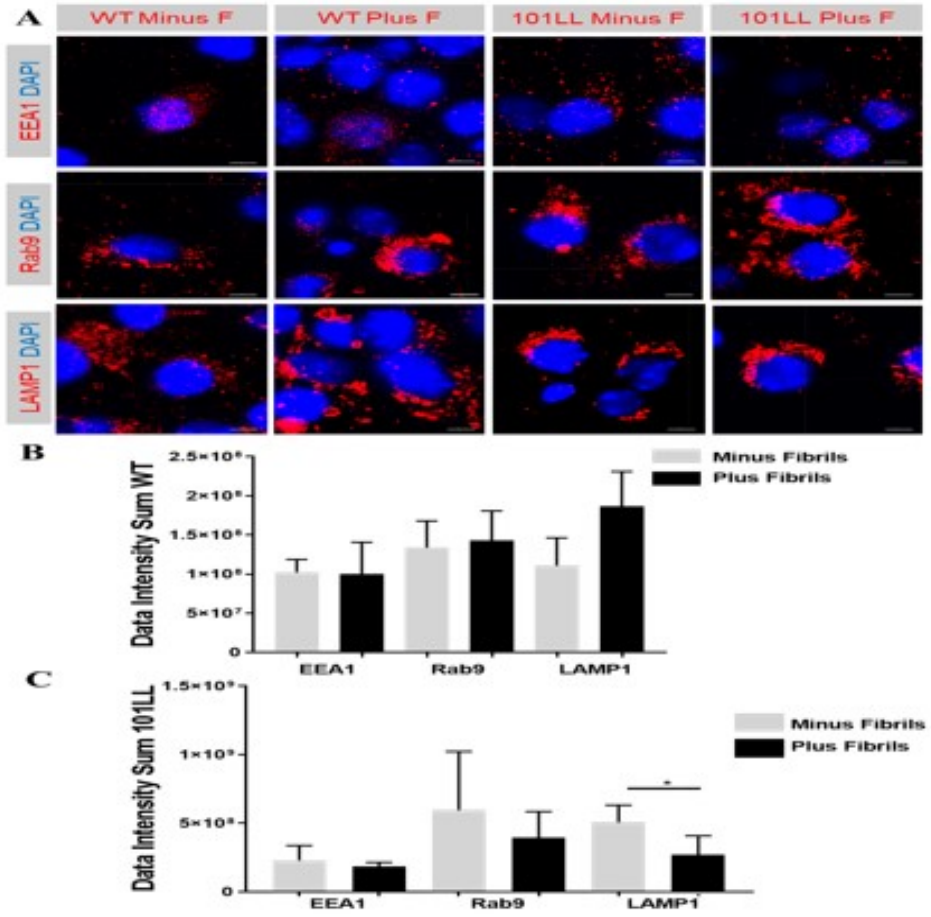

Figure 5.10: Reduced lysosomal activity was evident in 101LL challenged cultures. Defects caused by accumulation of abnormal proteins can enlarge organelles therefore, organelle size before and after fibril challenge were compared to investigate if any changes were occurring in primary cultures which might account for the irregularities noted in 101LL fibril lysosomal processing pathways. (A) Panel of organelle images from WT and 101LL challenged cultures (Plus F) including controls minus fibrils (Minus F) labelled with Early endosomal marker (EEA1), Ras-related protein Rab9 (Rab9) and Lysosomal-Associated Membrane Protein 1 (LAMP1) all in red. (B) and (C) IMARIS analysis of data signal intensities obtained from organelle markers EEA1, Rab9 and LAMP1 minus or plus fibrils in WT and 101LL cultures. No noticeable differences were noted in organelle size and structure after fibril challenge. IMARIS analysis in WT cultures showed no significant changes from organelle comparisons however analysis of 101LL cultures indicated a significant reduction in LAMP1 staining after fibril challenge (P-Value 0.02) suggesting less lysosomal activity was occurring in the genotype. WT and 101LL cultures 30,000 cells, challenged with 30µg/ml 101L fibrils for 24-hours, Scale Bar 5µm, Confocal LSM710. Graph mean plus standard deviation, (B) Controls minus fibrils n=2, plus fibrils n=5 for all markers, (C) Controls minus fibrils n=3, plus fibrils EEA1 n=5, Rab9 n=7 and LAMP1 n=9. n=data intensity sum of individual wells, unpaired t test.

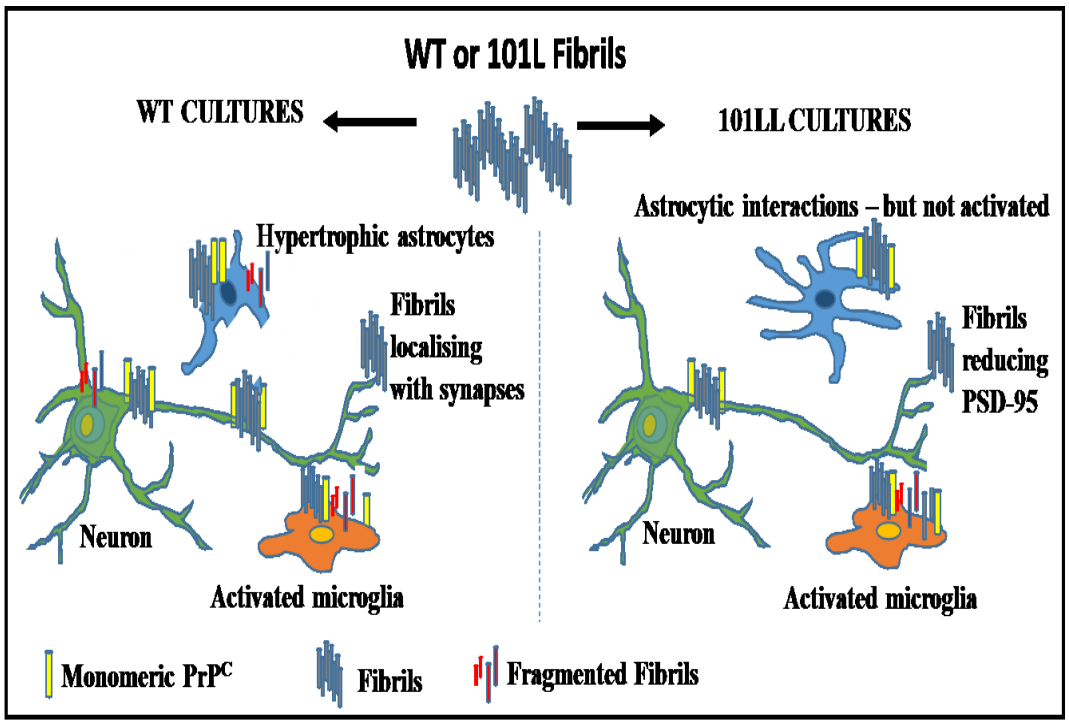

Figure 5.11: Summary of cellular response to fibril challenge observed in primary hippocampal neuronal cultures. Fibrils were localising along the entire neuronal cell including synapses in both genotypes. Although fibrils were not inducing a neurotoxic effect over a 24-hour period at 7.5µg/ml concentrations, a significant reduction in PSD-95 was evident in 101LL cultures showing synaptic loss preceded neuronal loss and this result highlighted 101LL neurons were more susceptible than WT to fibril insult. WT astrocytes became activated and hypertrophic after fibril challenge and fibrils were localising within lysosomal organelles suggesting cells were actively degrading these abnormal conformations. Fibril localisation with 101LL astrocytes was also evident however, glial cells did not appear activated and no lysosomal interactions were apparent. Fibrils were internalised by activated microglia in both genotypes and reduced fibril sizes detected indicated degradation was occurring in these cells. PrP^C was detected in all cell types and localisation with fibrils indicated normal monomeric PrP^C could be targeted for conversion to fibril aggregates however, after 24-hour challenge no significant reduction in PrP^C was evident indicating this conversion was not occurring within this timeframe.

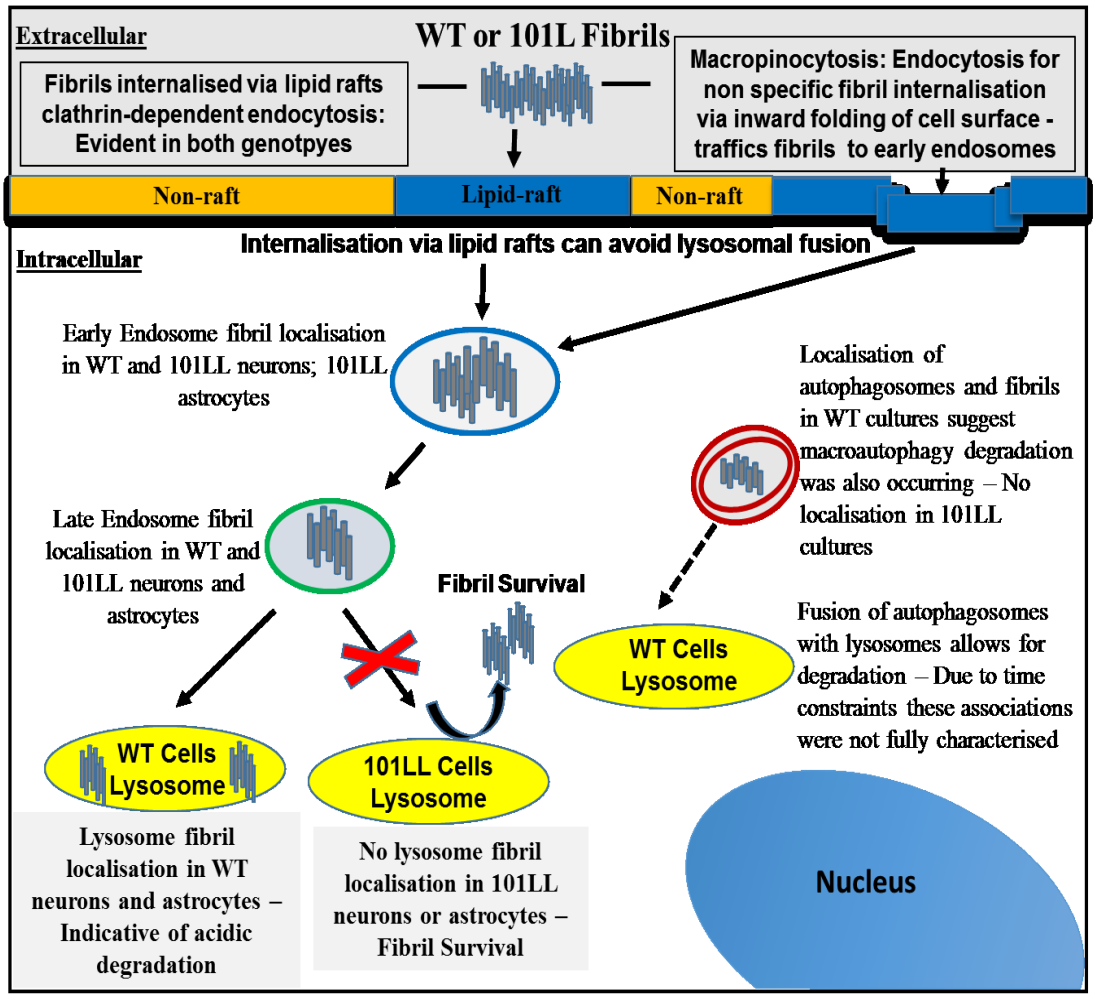

Figure 5.12: Summary of organelle processing results obtained after fibril challenge. Minimal lipid-raft localisation of fibrils was evident suggesting limited fibrils were been internalised into cells via clathrin-coated pits. Macropinocytosis provided a possible alternative route of internalisation which delivers internalised substances to endosomal or lysosomal organelles. Fibrils were detected in both early and late endosomal organelles in both genotypes indicating an operative endocytic pathway and early sorting and recycling of fibrils was occurring after cellular uptake. Neuronal and astrocytic processing of fibrils in late endosomes in both genotypes confirmed fibrils were on route for lysosomal degradation through acidification. In WT cultures, fibrils were internalised by neuronal and astrocytic lysosomal organelles indicative that active degradation was occurring. No fibril lysosomal localisation was evident in 101LL cultures and a significant reduction in lysosomal organelle activity after challenge suggested fibrils would survive and possibly propagate further in this genotype. A second lysosomal marker was used to confirm these observations and validated the results presented here. Autophagy was also evident in WT cultures only and provided another degradation pathway by fusion of autophagic vacuoles with lysosomes however, due to time constraints of this project these associations were not fully explored in this chapter.

5.4 Discussion

The initial interactions of misfolded protein with neuronal and non-neuronal cells is poorly understood however, the presence of misfolded protein is common to all PMDs. The data presented in this chapter provide insights into initial neuronal interactions with misfolded PrP fibrils and also highlight the involvement of supporting glial cells such as astrocytes and microglia which appeared to play neuroprotective roles (*Figure 5.11, 5.12)*. Additionally, fluorescently labelling fibrils proved advantageous for the visualisation of uptake and trafficking of misfolded protein within primary cultures. Fibrils were shown to localise along entire neuronal dendrites within the 24-hour fibril exposure timeframe and no significant neuronal loss was evident at lower fibril concentrations indicating fibrils were not neurotoxic within this timeframe at lower concentrations. Interestingly, as initial mechanisms involved in misfolded protein processing are poorly understood (Moreno-Gonzalez and Soto 2011), it is widely debated whether abnormal protein deposits are toxic to neurons or if they are generated as a protective mechanism to sequester smaller soluble forms of misfolded protein (Wolfe and Cyr 2011; Treusch, Cyr, and Lindquist 2009; Haass and Selkoe 2007). Although the data presented here demonstrate lack of toxicity (*Figure 5.1c*), increasing fibril dose did escalate toxicity of fibrils (*Figure 5.1a,b*) either by gain of toxic function of fibrils or loss of native function of surrounding cells. Additionally, increasing timeframes of fibril challenge may also induce neurotoxicity however, due to time constraints of this project these thresholds were not investigated further here. Fibril insult did however, significantly reduce PSD-95 in 101LL cultures, confirming reports that synaptic loss precedes neuronal loss (Hilton et al. 2013) and these results show 101LL neurons were more susceptible than WT. Interestingly, similar loss of PSD-95 was reported in AD patients before any neuronal loss was evident (Yuki et al. 2014), and in mouse models of HD (Smith et al. 2014), suggestive that this protein may be a vulnerable target associated with many PMDs.

Indeed, a recent study in AD has shown Aβ oligomer-induced loss of PSD-95 could be recovered in mouse hippocampal slices using compounds isolated from medicinal plants (Zolezzi et al. 2018). These data highlight synapse loss can be recovered and identification of PSD-95 vulnerability in the 101LL fibril-challenged primary culture model provides potential future targets for studying effects of novel compounds that could impede or recover synaptic decline. Although understandings of misfolded protein induced synaptic reduction and dysfunction are incomplete, data presented in the chapter indicate primary hippocampal cultures would provide a suitable model for further investigations of initial synaptic response to fibrils. Future studies examining these interactions and consequences thereafter would improve our understandings of the mechanisms contributing to synapse dysfunction leading to possible therapeutic targets to halt neurodegeneration associated with PMDs.

Early responses to misfolded proteins include activated morphological response by astrocytic and microglial cell populations and these changes can be detected at early stages of TSE disease (Perry and Teeling 2013; Sofroniew and Vinters 2010). Research in our lab has also shown activated microglia and reactive astrocytes were present at the periphery of amyloid plaques in 101LL mice challenged with recombinant PrP fibrils (Barron et al. 2016), indicating glial cell populations play a role in maintaining brain homeostasis in response to misfolded protein insult. However, these results were based on analysis of animals approximately 500 days after inoculation with fibrils and therefore do not represent initial responses to abnormal protein insult. In this study, astrocytic cell populations in WT primary cultures appeared hypertrophic in comparison to 101LL astrocytes and controls. These data indicate that WT astrocytes were rapidly responding to fibril insult and possibly inducing early fibril degradation. As activated astrocytes were observed prior to any neuronal or synaptic defects in WT cultures, it was suggestive of a neuroprotective role.

This response may also be applicable to other neurodegenerative disorders and can be further studied using primary neuronal cultures derived from other mouse models to broaden our understandings of fibril induced neuroprotective astrogliosis. As mentioned already, previous *in vivo* work in our lab has shown reactive astrocytes were associated with amyloid plaques in 101LL fibril-challenged mice. Contrasting results shown here where 101LL cultures were showing no astrocytic activation although fibrils were in their proximity suggest this response must either be dose dependant or time dependant, and this could be explored in future experiments however, the focus of this study was investigating initial cellular response to fibril challenge. Studies have shown microglia are capable of both engulfment and phagocytosis of Aβ fibril material (Lee and Landreth 2010) and when investigated here, microglia were responding rapidly to fibril insult and appeared both activated and phagocytic in both genotypes. Conversely, Alzheimer models using APP transgenic mice crossed with a chemically activated microglial suicide gene have shown that when microglial cells were ablated there was no effect on plaque size or number suggesting microglia were not critically involved in plaque formation and clearance in the brain. Microglial fibril engulfment and possible phagocytosis were shown here (*Appendix Figure 5.b*) in both genotypes and as no changes in neuronal populations were evident after fibril challenge (*Figure 5.a*), this response was deemed neuroprotective. This activated microglial response could change with increased fibril insult or challenge timeframe leading to over activated microglial states resulting in the release of reactive oxygen species (ROS) that could cause neurotoxicity (Block, Zecca, and Hong 2007). Although time constraints did not allow such analysis to be performed during this project, this could be a focus of future study. Microglial responses observed here suggest modulating microglial cellular and or inflammatory responses could provide possible therapeutic targets for removal of misfolded proteins in PMDs however, further characterisation of microglial activation states and the mechanisms by which these states may be modulated to decelerate neurodegeneration would have to be carried out first.

Recent studies have however highlighted, there is a lack of relevant microglial cell model systems available which has precluded progress in this area (Ginhoux 2016). The fibril-challenged primary neuronal culture model described in this chapter could bridge this gap and could be used for future investigative experiments for the identification of possible therapeutic targets for the modulation of microglial response in PMDs.

Localisation of fibrils with neuronal, astrocytic and microglial PrP^C was evident in fibril-challenged cultures and could represent pathways for generating further misfolded protein (Kocisko et al. 1994) however, within the 24-hour exposure timeframe no significant reduction in PrP^C was evident (*Appendix Figure 5.f*) indicating conversion was not occurring within this timeframe. Abnormal forms of PrP are known to utilise and manipulate various intracellular quality control mechanisms during neurodegeneration (Chapter 1, Section 1.5.3) and the lysosomal quality control machinery emerges as one of the primary targets (Majumder and Chakrabarti 2017). The lysosomal pathway acts as a terminal degradative compartment of cells and routes involved in delivering misfolded proteins to lysosomes include; endolysosomal, ERQC, Golgi QC and autophagic pathways (Saftig and Klumperman 2009). In this study, endolysosomal and autophagic pathways were investigated as alterations in both, due to blocked vesicular fusion or lack of cargo loading in the vesicles have been associated with a number of neurodegenerative diseases (Chapter 1, Section 1.5.3). Multiple organelle markers were used (*Figures 5.6, 5.7, 5.8 and 5.9*) in the assessment of neuronal lysosome distribution and trafficking as current research has indicated lysosomal labelling used alongside various endolysosomal markers is more accurate than relying on lysosomal staining alone (Cheng et al. 2018). As summarised in *Figure 5.12*, intracellular labelling of lysosomal vesicles in WT cultures indicated both neuronal and astrocytic cells were capable of internalising fibrils proficiently for degradation via a endolysosomal pathway and this was evident using either WT and 101L fibril preparations.

Additionally, fibril associations with p62 in WT cultures showed autophagy was also an activated pathway in WT cultures. Studies have shown the autophagy-related protein p62 can be used for monitoring autophagy activity (Pankiv et al. 2007) and increased levels of p62 in prion-infected brains is linked to the promotion of aggregate clearance by autophagy (Homma et al. 2014). Conversely, fibrils were only associating with early and late endosomal organelles in 101LL cells indicating lysosomal pathways were been impeded and this inefficient processing of fibrils for degradation may explain how this genotype is capable of supporting abnormal protein seeding in the brain. Studies have shown deficient fusion between endosomes and lysosomes may be due to impaired ability of endosomes to recruit Ras-related protein Rab7, a GTPase required for endosome-lysosome fusion and this impairment may also be occurring in 101LL cultures (Urwin et al. 2010; Rink et al. 2005). Indeed, recent studies confirmed Rab7 is a main regulator of membrane trafficking at late endosomes and membrane fusion of late endosomes to lysosomes and autophagosomes to lysosomes (Modica and Lefrancois 2017) however, how cells regulate these interactions is not well understood. The model presented in this chapter provides a system to allow further investigations into Rab7 function. Gathering more insights into these proteins and how they regulate fusion to acidic organelles is crucial for the modulation of effective and efficient abnormal protein degradation. Collectively these data suggest possible pharmacological enhancement of lysosomal activity may encourage abnormal PrP clearance and that proteins such as p62 and Rab7 could be potential targets for therapeutic control of misfolded proteins associated with PMDs. Treatment with autophagy-inducing compounds such as lithium and rapamycin can reduce abnormal PrP in cultured neuroblastoma cells (Heiseke et al. 2009), and studies have shown rapamycin activation *in vivo* delayed disease onset, reduced plaque burden in the brain and improved survival of GSS prion-infected A116V mice (Cortes et al. 2012). However, activation of the autophagic pathway alone may not be enough to eliminate intracellular abnormal PrP aggregates from within cells (Browman and Zurzolo 2013).

Therefore, further extensive research into autophagy and related pathways will be required before establishing a possible pharmacological approach for treatment of PMDs and the fibril-challenged model presented in the chapter provides a means of preforming these investigations.

In conclusion, the data described in this chapter provide visual evidence of important pathways associated with misfolded protein trafficking, processing and possible degradation involving both neuronal and non-neuronal cells in two divergent genotypes. Currently studies involving manipulating quality control lysosomal degradation pathways in neurodegenerative diseases are been carried out and the data presented in this chapter support targeting these pathways for efficient removal of unwanted cellular components (Majumder and Chakrabarti 2017; Nixon 2013; Saftig and Klumperman 2009).

CHAPTER 6

Transcriptomic analysis provides molecular insights to cellular responses pre/post-fibril challenge

6.1 Abstract

Accumulation and spread of misfolded protein is common to all PMDs however, the mechanisms initiating these processes are poorly understood. The aim of this study was to use transcriptomic profiling to gain mechanistic insights into cellular responses to misfolded PrP protein. The 101LL genotype supports seeding of misfolding by fibrils in the brain whilst the WT genotype curtails abnormal protein formation after fibril challenge therefore; both provided ideal models for studying misfolded protein interactions. Transcriptome analysis comparing hippocampal brain tissue with primary hippocampal neurons established both systems were broadly similar. Gene expression profiles were also similar in primary hippocampal cultures form both genotypes indicating the 101LL point mutation was not influencing gene expression levels pre-fibril challenge. Post-fibril challenge transcriptomic analysis indicated both 101LL and WT cultures exhibited changes in gene expression. In WT fibril-challenged cultures, an increase in gene expression of genes associated with endocytosis, macrophage engulfment and ER-associated misfolded protein catabolic processes, all of which would encourage fibril degradation was observed. These pathways were not induced in 101LL cultures. This suggests the induction of these processes is required to curtail abnormal protein folding after fibril challenge and highlights possible targets to investigate further for intervention in PMDs.

6.2 Introduction

PMDs such as AD, PD, HD and TSE are associated with the accumulation of abnormally folded proteins in specific regions of the brain such as the hippocampus. However, the mechanisms involving seeding, processing and degradation of these rouge proteins are poorly understood (Holmes and Diamond 2012; Moreno-Gonzalez and Soto 2011). In this chapter, the response of primary hippocampal cultures to fibril challenge was investigated on a transcriptome level. This provided insights into molecular mechanisms associated with misfolded protein handling using cultures that either support misfolded protein generation (101LL) or that curtail its production (WT). Primary hippocampal cultures were used for this analysis as they provided a readily accessible defined system for fibril challenge and rapid extraction of RNA for transcriptome analysis. Differentially expressed genes (DEGs) identified after fibril challenge were investigated using several software platforms to provide insights into the phenotypic variations in fibril response of 101LL and WT animals (Barron et al. 2016). As primary cultures were generated from hippocampal tissue, the transcriptomic data presented in this chapter is specific to a brain area vulnerable to disease. Initial baseline transcriptome profiles were generated by microarray analysis however, over the course of the project, a more comprehensive analysis using RNA-sequencing (RNA-seq) for pre and post-fibril challenge transcriptome analysis was carried out.

101LL versus WT *in vitro* (hippocampal culture) and 101LL versus WT *in vivo* (hippocampal tissue) comparisons were made by microarray analysis to ascertain if the P101L mutation was causing any gene expression changes in the 101LL genotype. Using standard analysis parameters no DEGs were identified in these genotype comparisons indicating that the point mutation had no effect on basal gene expression in comparison to the WT genotype.

These data also provided baseline gene expression profiles where any changes after challenge would be fibril-specific responses. Microarray analysis was also carried out to compare *in vitro* hippocampal cultures and *in vivo* hippocampal tissues to establish if *in vitro* cultures would provide a genetically comparable model to the brain. Transcriptome results indicated gene expression profiles in primary cultures were comparable and grossly similar to acutely dissected hippocampal tissue. Thus, primary hippocampal cultures would provide an appropriate *in vitro* representation of the hippocampal area of the brain for studying misfolded protein interactions. To establish the genotype-specific response to fibril challenge, cultures from WT and 101LL animals were challenged at DIV7 with 7.5µg/ml of unlabelled 101L fibrils for 24 hours, after which point total RNA was isolated (Materials and Methods, 2.4.4). DEG lists specific to each genotype were then identified by RNA-seq analysis. WT cultures had double the amount of DEG changes than 101LL cultures after fibril challenge (WT versus WT plus fibrils 1,080 DEGs, 101LL versus 101LL plus fibrils 545 DEGs). DEG lists identified were analysed further using Ingenuity Pathway Analysis (IPA) and Miru software along with PANTHER and DAVID platforms to gain insights into processes associated with these specific gene expression changes. In WT cultures, fibril challenge induced initiating mechanisms associated with misfolded protein degradation such as endocytosis and macrophage engulfment. These mechanisms were not induced in 101LL cultures suggesting fibrils may be processed inefficiently in this genotype which could explain how 101LL mice are unable to curtail and degrade abnormal misfolded protein *in vivo* (Barron et al. 2016). Furthermore, genes associated with amyloid beta clearance, microglial and glial cell activation were down-regulated in 101LL fibril-challenged cultures suggesting mechanisms involved in fibril processing and clearance were dampened in this genotype. In conclusion, the emphasis of this study was to investigate early cellular responses in primary cultures after fibril challenge. Biological processes associated with protein degradation whilst reducing inflammatory responses were associated with WT response after fibril challenge, but not in 101LL cultures.

Processes identified here provide a number of possible test targets that can be further explored in future experiments and developed for potential therapeutics against PMDs. These findings may also be applicable to other neurodegenerative diseases involving abnormally formed proteins such as Aß, tau and α-synuclein.

6.3 Results

6.3.1 Methodology for sample transcriptomic analysis

RNA isolation, processing and quality control from 101LL and WT cultures and tissues (*Figure 6.1*) was described previously in Materials and Methods (2.2.7, 2.4.4 and 2.5.1). Microarray analysis was carried out on unchallenged 101LL and WT primary hippocampal cultures (derived from Day17 embryos), and 101LL and WT Day 6 hippocampal tissues (*Figure 6.1*). The same unchallenged 101LL and WT primary hippocampal culture samples (used for microarray) and fibril-challenged 101LL and WT primary cultures (Materials and Methods 2.4.4) were analysed using Illumina RNA-sequencing. Additional workflows based on producing good quality data (Fuller et al. 2016) included data filtering and validation of results (*Figure 6.1*).

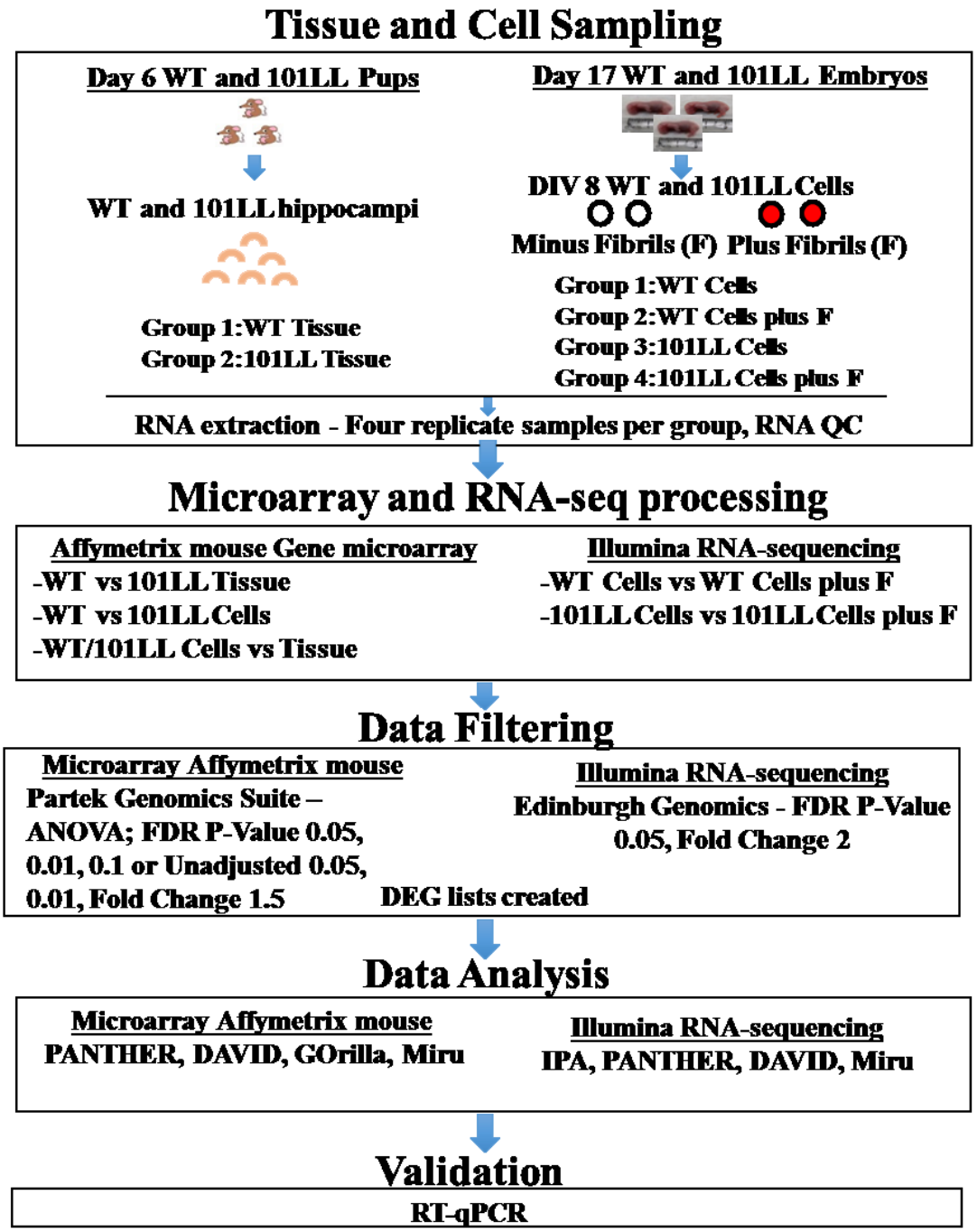

Figure 6.1: Experimental design and workflow. Overview of methodology from origin at Tissue and Cell Sampling through to Validation of data produced from microarray and RNA-seq. Stringent data filtering and unbiased transcriptomic analysis allowed for the generation of good quality data.

6.3.2 WT versus 101LL gene expression in primary cultures and acutely dissected tissue

Does the 101LL point mutation influence gene expression levels pre fibril challenge? To address this question, microarray analysis of unchallenged WT versus 101LL primary hippocampal cultures and WT versus 101LL Day 6 hippocampal tissues which both contain a mixed population of cells was carried out. These comparisons generated probe cell intensity data (CEL) files which were evaluated using Partek Genomics Suite software (Materials and Methods, 2.5.2, 2.53) and Principal Component Analysis (PCA) plots were generated to emphasise variation and bring out strong patterns in the datasets. As shown in *Figure 6.2*, there was a clear separation in sample distribution between *in vivo* and *in vitro* systems suggesting all samples were correlating correctly and both hippocampal dissection and RNA extraction methods were reproducible for both systems. Further processing of CEL files using Partek Genomics Suite and one-way analysis of variance (ANOVA) based on various contrasts (comparisons) selected (Materials and Methods, 2.5.3) was used to generate DEG lists from both WT versus 101LL primary hippocampal cultures and WT versus 101LL Day 6 hippocampal tissues comparisons. False Discovery Rate (FDR) parameters were applied for generating more constricted datasets. FDR reduces the number of false positives and increases the chances of identifying all the differentially expressed genes in a dataset. The principles of FDR are that P-Values are first sorted and ranked, the smallest value gets rank 1, the second rank 2, and the largest gets rank N, each P-Value is multiplied by N and divided by its assigned rank to give the adjusted P-Values (Benjamini and Hochberg 1995). Using standard parameters (FDR P-Value < 0.05 or 0.1) no DEGs were identified when comparing genotypes in unchallenged 101LL versus WT *in vitro* cultures and 101LL versus WT *in vivo* tissues, indicating the 101LL point mutation was not influencing gene expression levels pre-fibril challenge in either system (Table 6.1).

Using less stringent parameters (Unadjusted P-Value of < 0.01) including Fold Change (FC, < 1.5 or > 1.5) a limited number of DEGs (Tables 6.2, 6.3) were detected when comparing 101LL versus WT genotypes in both *in vitro (*19 DEGs*)* and *in vivo* systems (16 DEGs). For validation of DEG lists (Tables 6.2, 6.3), a number of genes were processed by RT-qPCR and expression trends obtained confirmed (*Figure 6.3, 6.4, 6.5, 6.6*) microarray data was accurate. Transforming growth factor, beta induced (*Tgfbi*) which plays an important role in cell proliferation (Zhang et al. 2009) and Laminin, alpha 1 (*Lama1*) which is involved in neuronal differentiation, migration and survival (Graner, Mercadante, et al. 2000b) and can inhibit fibril formation (Monji et al. 1998) were confirmed to be up-regulated in 101LL cultures (*Figure 6.3*) suggesting cells may be primed to inhibit fibril formation whilst encouraging neuritogenesis. Conversely, Myocyte Enhancer Factor 2C (*Mef2c*) which is a central regulator of neuronal differentiation and survival (Cho et al. 2011) was shown to be down-regulated in 101LL cultures indicating variability in gene expression relating to neuronal survival was evident in this genotype. In tissue, Transthyretin (*Ttr*) which inhibits Aβ aggregation and detoxifies cell-damaging conformers (Wang et al. 2014) was shown to have Increased expression in WT tissue (*Figure 6.5*) suggesting this genotype may be capable of inhibiting abnormal PrP aggregation processes. Increased expression in both tissue and cells, of Midline1 (*Mid1*) which is associated with microtubule stabilisation (Aranda-Orgillés et al. 2008) and has been associated with the pathogenesis of Alzheimer's disease (AD) where it binds to and regulates translation of BACE1 mRNA implicated in generation of amyloid plaques (Hettich et al. 2014) was evident in the 101LL genotype (*Figure 6.2*). This suggested neurons may be less stable in the 101LL genotype and therefore, require higher expression levels of *Mid1* to stabilise neuronal microtubule structures. *Prnp* which is involved in cell signalling, formation and maintenance of synapses and promotion of neuronal growth and survival (Harris 2003; Walz et al. 1999) was confirmed to be consistently expressed across all genotypes and systems (*Figure 6.2*).

These data confirmed the 101LL mutation was not influencing PrP expression and supported the use of the primary culture system to provide a suitable *in vitro* model for investigating abnormal PrP protein interactions. For completeness, validation of genes was also assessed in both *in vivo* and *in vitro* systems to investigate if gene expression profiles were similar between systems and some discrepancies were evident (*Figure 6.3, 6.4, 6.5*). For example, although *Tgfbi* was confirmed to be significantly up-regulated in 101LL cultures (*Figure 6.3a*), this was not evident in 101LL tissues. These findings showed gene expression may vary between systems and this will be addressed further in Section 6.3.3. RNA-seq of unchallenged 101LL versus WT *in vitro* cultures using standard parameters (FDR P-Value < 0.05, FC 2) identified only 3 DEGs to have increased expression in the 101LL genotype namely, *Tnfaip2*, *Tgfbi* and *Gm21742*. *Tgfbi* was previously identified and validated to have increased expression in 101LL cultures (*Figure 6.3*) and *Gm21742* is an unprocessed pseudogene that had no count readings for WT groups. Tumor necrosis factor, alpha-induced protein 2 (*Tnfaip2*) is involved with cell differentiation and is also associated with amyotrophic lateral sclerosis (ALS) disease where overexpression increased cell death, inflammatory processes and TNF signalling (Brohawn, O'Brien, and Bennett 2016; Kurji et al. 2010) making cells more susceptible to neurodegeneration. The increased expression of *Tnfaip2* identified by RNA-seq in 101LL cultures suggests these cells maybe more susceptible to stressors in comparison to WT cultures however, RT-qPCR analysis did not validated these differences (*Figure 6.6*). In summary, microarray analysis using standard parameters (P-Value FDR < 0.05 or 0.1) showed no differences in gene expression was evident when comparing WT versus 101LL genotypes in either *in vitro* or *in vivo* systems, indicating both genotypes had similar baseline gene expression profiles pre-fibril challenge. Additionally, *Prnp* expression levels were shown not to be influenced by the 101LL point mutation. RNA-seq analysis of WT versus 101LL cultures did identify three DEGs however, only one was validated to be accurate.

Thus, both microarray and RNA-seq results complimented each other and any changes in baseline gene expression profiles described after fibril challenge would be a genotypic specific response.

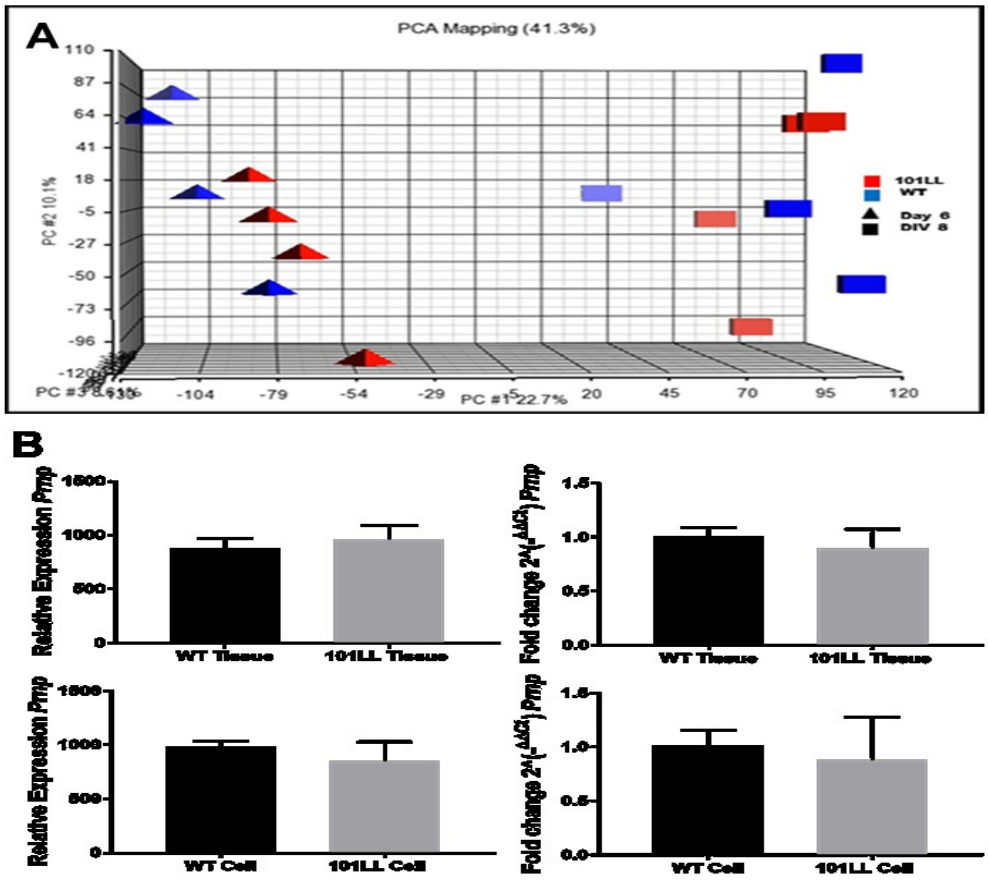

Figure 6.2: Principal Component Analysis (PCA) showed a clear separation between culture and tissue samples. A PCA plot generated from microarray analysis of all 16 *in vivo* and *in vitro* samples was used to visualise patterns associated with *in vivo* and *in vitro* datasets. This visualisation plot generated using Partek genomics suite confirmed a clear separation and pattern was evident between cell (square symbol) and tissue (triangle) groups of arrays analysed by principal component suggesting all samples were correlating correctly and sample-to-sample processing was reproducible for both systems. (B) Genes showing similar expression across both systems were validated using RT-qPCR. Relative expression values and RT-qPCR results are shown from *in vivo* (tissue) and *in vitro* (cell) systems. Expression values obtained from microarray generally matched with RT-qPCR results validating transcriptomic results. *Prnp* expression in both tissue (P-Value 0.37; 0.31) and culture (P-Value 0.20; 0.56) showed no significant differences in expression values validating microarray results. Reference gene *Ywhaz*, Graph mean plus standard deviation, n=4, n=individual samples, unpaired t test. Fold changes from RT-qPCR were calculated using 2-ΔΔCt method (Materials and Methods, 2.5.8) and relative expression values were obtained from microarray data.

Partek Analysis	101LL vs WT Culture	101LL vs WT Tissue
P-Value FDR < 0.05	Negative*	Negative*
P-Value FDR < 0.1	Negative*	Negative*
Unadjusted P-Value < 0.01, FC 1.5	19 DEGs	16 DEGs

*Nothing passed.

Table 6.1: Standard filtering of microarray datasets showed no differences in gene expression were evident between WT and 101LL groups. Partek analysis of microarray datasets from 101LL and WT genotypes in culture (*in vitro*) and tissue (*in vivo*) systems using standard FDR parameters showed no DEGs were identified in genotype comparisons. However, unadjusted analysis showed a limited degree of variation was present regarding gene representation between genotype comparisons in both systems.

Gene (Protein Coding)	Function	Fold Change
Nescient Helix-Loop-Helix 1 (***Nhlh1***)	DNA binding protein/ controlling cell type determination	-1.99
Cortistatin (***Cort***)	Inhibits cAMP (Cyclic adenosine monophosphate) production	-1.73
Myocyte Enhancer Factor 2C (***Mef2C***)	Crucial for normal neuronal development, distribution and electrical activity	-1.63
Reelin (***Reln***)	Regulates microtubule function in neurons and neuronal migration	-1.57
Collagen Type III Alpha 1 Chain (***Col3a1***)	Encodes pro-alpha1 chains of type III collagen	2.90
Biglycan (***Bgn***)	Collagen fibril assembly/ regulation inflammation and innate immunity	3.27
Ectonucleotide Pyrophosphatase/Phosphodiesterase 1 (***Enpp1***)	Broad specificity and cleaves a variety of substrates	3.86
Nidogen 1 (***Nid1***)	Distributed in basement membranes and tightly associated with laminin	4.03
Collagen Type I Alpha 1 Chain (***Col1a1***)	Fibril-forming collagen found in most connective tissues	4.08
Laminin, alpha 1 (***Lama1***)	PrP^C is a specific receptor for laminin	4.20
Collagen Type I Alpha 2 Chain (***Col1a2***)	Fibril-forming collagen	4.49
T-Box 18 (***Tbx18***)	Embryonic development	5.00
Cytochrome P450 Family 1 Subfamily B Member 1 (***Cyp1b1***)	Involved in synthesis of cholesterol and other lipids	5.27
Transforming growth factor, beta induced (***Tgfbi***)	Cell proliferation	5.50
Apolipoprotein D (***Apod***)	Protein binding/ lipid transporter activity	5.93
Lumican (***Lum***)	Protein/ Collagen fibril organisation	6.32
Alanyl Aminopeptidase, Membrane (***Anpep***)	Degrade neurotransmitters at synaptic junctions	6.64
LOC101055644 Midline1 (***Mid1***)	Metal ion/ protein/ zinc ion binding/ Microtubule-associated ubiquitin ligase	7.53
Solute Carrier Family 6 Member 13 (***Slc6a13***)	In presynaptic terminals regulates GABA signalling termination through GABA uptake	7.69

*Ensembl genome ID

Table 6.2: Limited gene expression differences were evident between 101LL and WT cultures. Partek comparisons of 101LL and WT cultures using unadjusted P-Value of < 0.01 and FC < -1.5 or > 1.5, identified a limited number (19) of DEGs. Negative FC values indicate down-regulated genes in 101LL whilst remaining numbers were all up-regulated in 101LL cultures.

Gene (Protein Coding)	Function	Fold Change
Transthyretin (***Ttr***)	Transports thyroid hormone thyroxine and retinol, can inhibit Aβ aggregation	-2.30
Cytochrome P450 Family 2 Subfamily C (***Cyp2c69***)	Synthesis of cholesterol and other lipids, iron ion binding and epoxygenase P450 pathway	-1.90
Lysyl Oxidase (***Lox***)	Cross-linking of extracellular matrix proteins	-1.81
Olfactory receptor 420 (***Olfr420***)	G-protein coupled receptor activity, olfactory receptor activity	-1.76
Collectin Subfamily Member 12 (***Colec12***)	Scavenger receptor, may play role in clearance of amyloid beta in Alzheimer disease	-1.61
Olfactory receptor 420 (***Olfr390***)	Olfactory receptor activity	-1.55
Complement Factor HH (***Cfh***)	Regulation of complement activation	-1.53
Olfactory receptor 420 (***Olfr960***)	Olfactory receptor activity	-1.52
Ribonucleoprotein (***Nop56***)	Part of a large pre-ribosomal ribonucleoprotein (RNP) complex	1.52
Mitochondrial Encoded TRNA Proline (***Mt-tp***)*	RNA gene affiliated with the non-coding RNA class	1.56
Heat Shock Protein Family A (Hsp70) Member 8 (***Hspa8***)	Functions as a chaperone and binds to nascent polypeptides to facilitate correct folding	1.59
RAB6B, Member RAS Oncogene Family (***Rab6b***)	Retrograde transport in neuronal cells	1.63
Calcineurin Like EF-Hand Protein 1 (***Chp1***)	Mediates the association between microtubules and membrane-bound organelles of the endoplasmic reticulum and Golgi apparatus	1.70
Ribosomal Protein L13 (***Rpl13***)	RNA binding, protein binding	1.70
Mitochondrial Encoded TRNA Glutamine (***Mt-tq***)*	RNA Gene affiliated with the non-coding RNA class	2.50
LOC101055644 Midline1 (***Mid1***)**	Metal ion/ protein/ zinc ion binding/ Microtubule-associated ubiquitin ligase	3.84

*RNA gene **Ensembl genome ID

Table 6.3: Limited differences in gene expression were evident between 101LL and WT tissues. Partek comparisons of 101LL and WT tissues using unadjusted P-Value of < 0.01 and FC < -1.5 or > 1.5, identified a limited number (16) of DEGs. Negative FC values indicate down-regulated genes in 101LL whilst remaining numbers were all up-regulated in 101LL cultures.

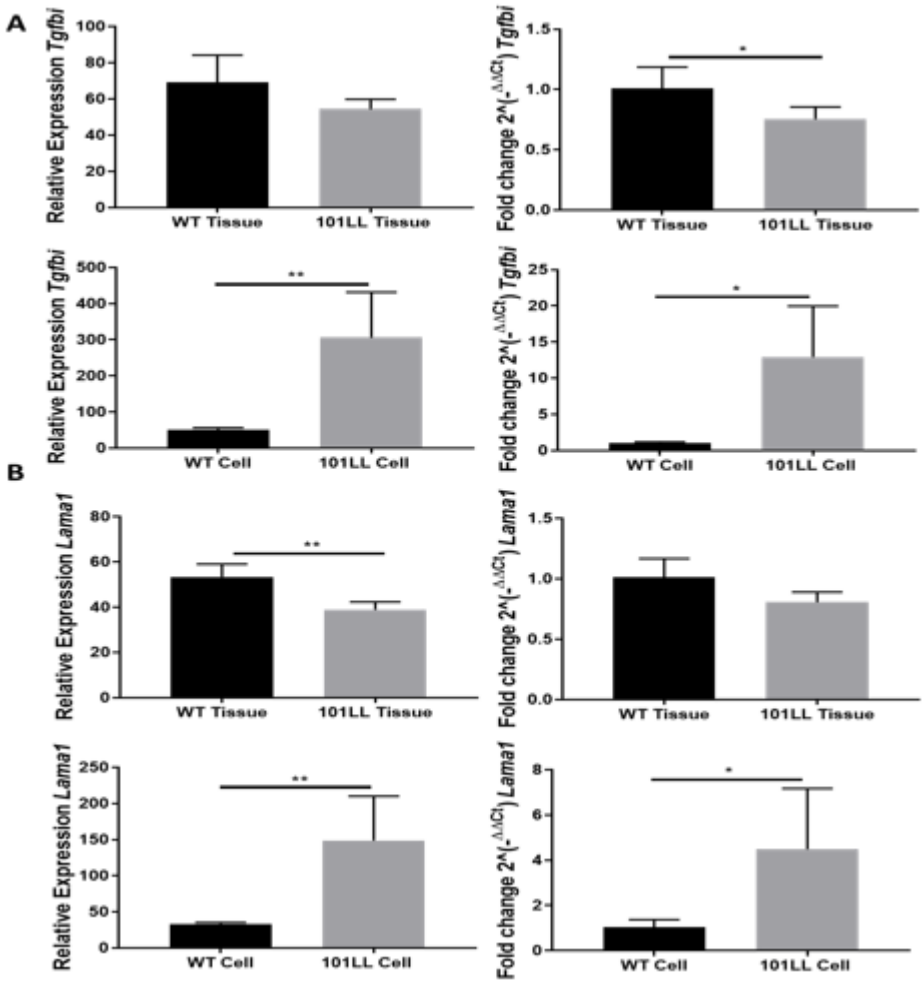

Figure 6.3: Microarray data from cell culture was validated using RT-qPCR. Relative expression values and RT-qPCR results are shown from both *in vivo* (tissue) and *in vitro* (cell) systems for general comparisons. (A) Transforming growth factor, beta induced (*Tgfbi*) and (B) Laminin, alpha 1 (*Lama1*). Expression values obtained from microarray matched with RT-qPCR results validating transcriptomic results. (A) *Tgfbi* showed no expression differences in tissue (P-Value 0.11) however, RT-qPCR did show significant differences were evident (P-Value 0.04). Significant differences were noted and comparable in cell comparisons (P-Value 0.006; 0.01). (B) *Lama1* microarray expression showed significant differences between tissue groups (P-Value 0.004) however, corresponding RT-qPCR did not show significance (P-Value 0.06). Significant differences were noted in cell comparisons (P-Value 0.009; 0.04). Differences in gene expression were also evident between systems. RT-qPCR normalisation reference gene *Ywhaz*, Graph mean plus standard deviation, n=4, n=individual samples, unpaired t test. Fold changes from RT-qPCR were calculated using 2-ΔΔCt method (Materials and Methods, 2.5.8) and relative expression values were obtained from microarray data.

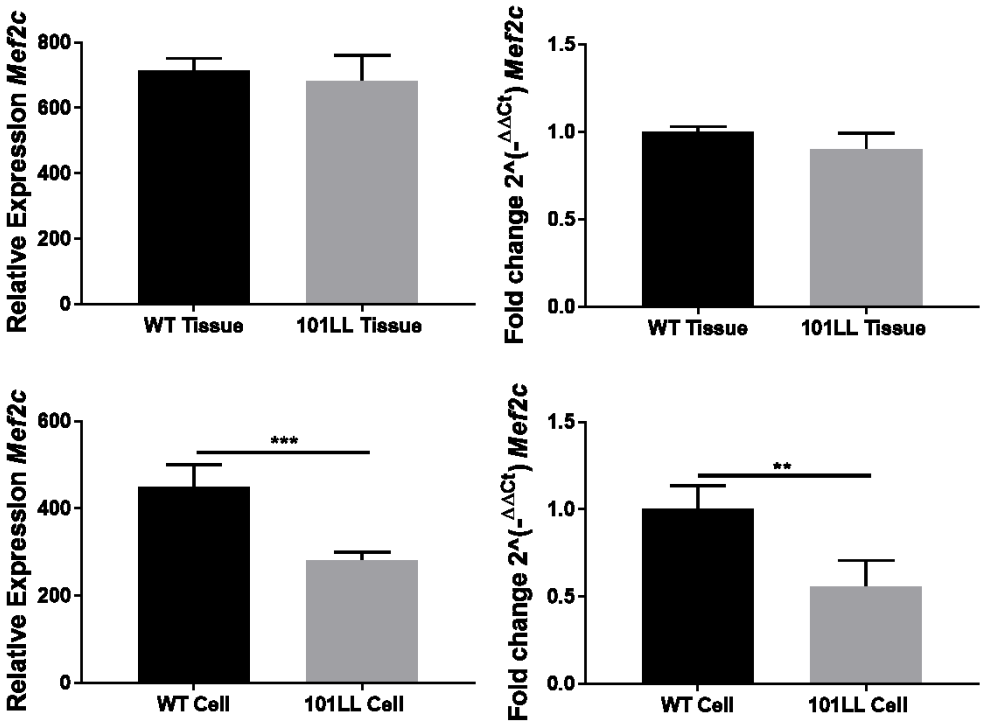

Figure 6.4: Validation of microarray data from cell culture using RT-qPCR. Relative expression values and RT-qPCR results are shown from *in vivo* (tissue) and *in vitro* (cell) systems for general comparisons of Myocyte Enhancer Factor 2C (*Mef2c*) expression. Expression values obtained from microarray matched with RT-qPCR results validating transcriptomic results. *Mef2c* gene expression showed no differences in tissue (P-value 0.46; 0.07) but was significantly down-regulated in 101LL cell cultures (P-Value 0.0007; 0.003). Reference gene *Ywhaz*, Graph mean plus standard deviation, n=4, n=individual samples, unpaired t test. Fold changes from RT-qPCR were calculated using 2-ΔΔCt method (Materials and Methods, 2.5.8) and relative expression values were obtained from microarray data.

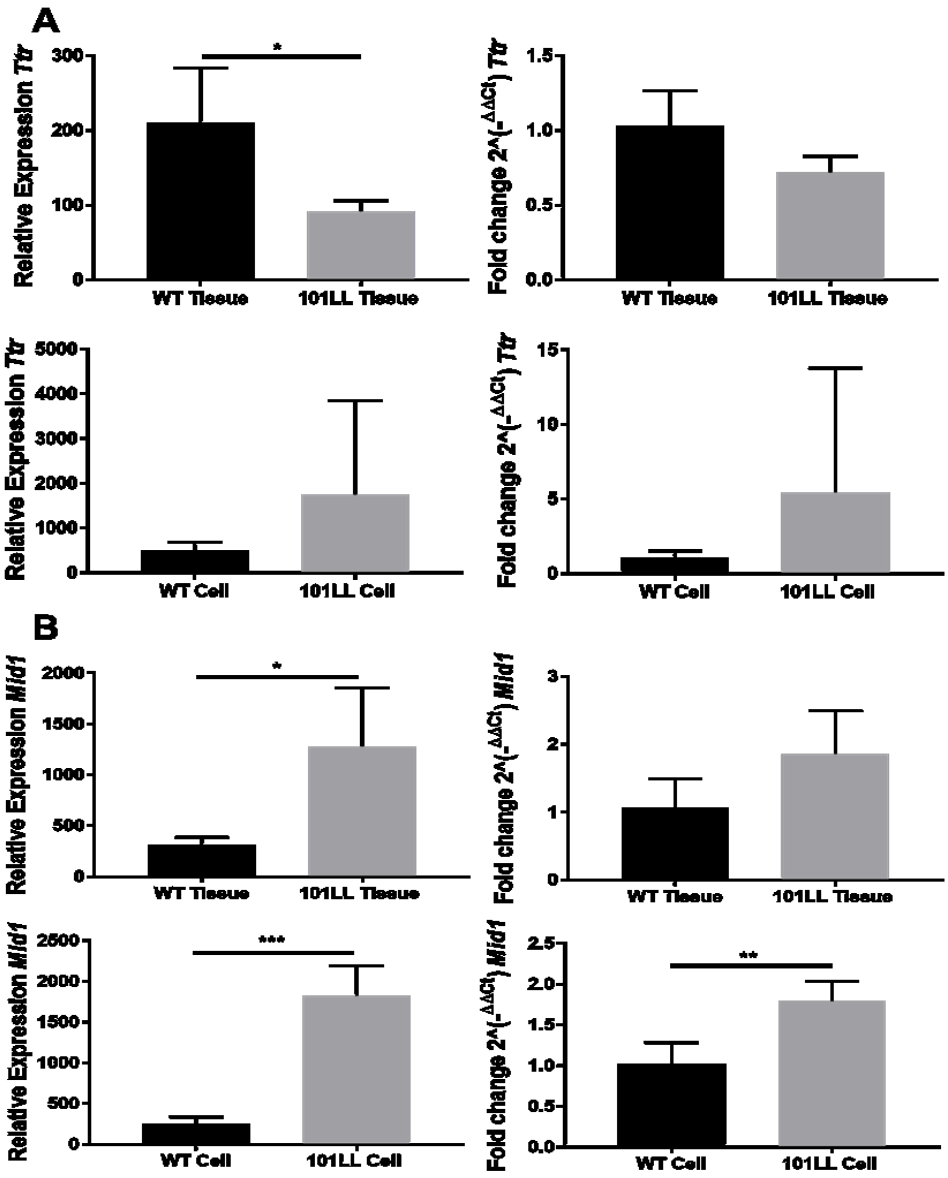

Figure 6.5: Validation of Transthyretin (*Ttr*) and Midline 1 (*Mid1*) expression from tissue using RT-qPCR. Relative expression values and RT-qPCR results are shown from *in vivo* (tissue) and *in vitro* (cell) systems for comparisons. *Ttr* and *Mid1* expression values obtained from microarray generally matched with RT-qPCR. (A) In tissue, *Ttr* microarray expression was shown to be significantly down-regulated (P-Value 0.02). RT-qPCR confirmed down-regulation was evident however; the P-Value obtained although borderline was not significant (P-Value 0.05). No expression differences were noted in cell comparisons (P-Value 0.28; 0.33). (B) *Mid1* was up-regulated in 101LL tissue (P-Value 0.01; 0.08) and cultures (P-Value 0.0002; 0.005). Additionally this data confirm that *Mid1* as identified by Ensembl genome was correct. Reference gene *Ywhaz* for *Ttr* and *Sdha for Mid1*, Graph mean plus standard deviation, n=4, n=individual samples, unpaired t test. Fold changes from RT-qPCR were calculated using 2-ΔΔCt method (Materials and Methods, 2.5.8) and relative expression values were obtained from microarray data.

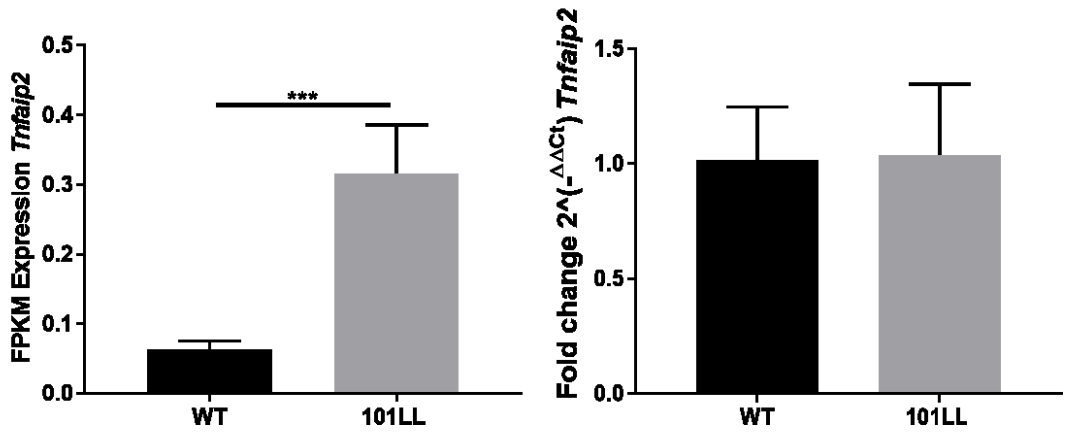

Figure 6.6: Tumor necrosis factor, alpha-induced protein 2 (*Tnfaip2)* expression was not validated by RT-qPCR. RNA-seq comparisons of WT and 101LL cultures identified *Tnfaip2* to be significantly up-regulated in 101LL cultures (P-Value 0.0004) however; RT-qPCR could not validate this observation. Reference gene *Sdha*, Graph mean plus standard deviation, n=4, n=individual samples, unpaired t test. Fold changes from RT-qPCR were calculated using 2-ΔΔCt method (Materials and Methods, 2.5.8) and Fragments Per Kilobase of transcript per Million (FPKM) values were obtained from RNA-seq data.

6.3.3 Is gene expression analogous between primary cultures and acutely dissected tissues?

To investigate the comparability between both *in vitro* and *in vivo* systems in more detail (*Figure 6.1*), direct comparisons of microarray datasets from both was carried out using Partek. As primary hippocampal cells were been cultured *in vitro*, some changes in gene expression between both systems were to be expected. Using standard parameters (P-Value FDR <0.01, FC 1.5) differences were apparent and genes were predominantly down-regulated in cultures (*Figure 6.7*). Similar numbers of DEGs identified between WT (330 DEGs) and 101LL (380 DEGs) comparisons (*Figure 6.7*) was expected as previous results confirmed both genotypes had comparable gene expression profiles (Table 6.1). Relevant functions of DEG lists identified in *Figure 6.7*, were investigated using various bioinformatic databases (Materials and Methods, 2.5.6) including, PANTHER, GOrilla and DAVID (Mi et al. 2013; Eden et al. 2009; Huang, Sherman, and Lempicki 2008). PANTHER analysis of up and down-regulated gene lists from 101LL DEGs (121 up-regulated and 259 genes down-regulated in culture in comparison to tissue), WT DEGs (95 up, 235 down, graph not included) and overlap or common DEGs (54 up, 280 down, graph not included) was carried out (*Figure 6.8*). Majority of genes were associated with cellular and metabolic processes in all gene lists and similar GO profiles from both up and down-regulated gene lists were obtained indicating although majority of genes were down-regulated in culture they shared similar GO enrichment profiles to up-regulated genes. Additionally, all groups were associated to a lesser extent with other functions such as response to stimulus, immune system, biological and developmental processes (graphs not shown). Cellular and metabolic processing may be the dominant functions identified as they relate to a number of processes, for example, cellular processing includes cell communication, cell-cell signalling, synaptic signalling, trans-synaptic signalling, cellular component organisation, membrane organisation and regulation of membrane lipid distribution.

Metabolic processing includes positive regulation of cellular metabolic processes, regulation of dephosphorylation, regulation of phosphorus metabolic processes and regulation of phosphorylation. To gain more clarity on gene enrichment associations with DEGs identified both GOrilla and DAVID platforms were used. GOrilla results were limited and no GO enrichment results were obtained for up-regulated genes in 101LL and WT groups and for the down-regulated overlap group (data not shown). DAVID GO enrichment for biological processes provided more informative results (*Figure 6.9*). Genes up-regulated in both WT and 101LL system comparisons were associated with lipid metabolic processes indicating cultures were involved in synthesis and degradation of lipids for energy. Lipids can be broadly classified into five categories including fatty acids, triacylglycerols (TAGs), phospholipids, sterol lipids and sphingolipids (Tracey et al. 2018). The data presented in *Figure 6.9*, indicate sterol lipid involvement. Cholesterol is a sterol lipid, is vital to cell membrane structure and functions as a precursor to fat-soluble vitamins and steroid hormones. Cholesterol is also a major constituent of the brain, and is tightly regulated between the major brain cells (neurons, astrocytes, microglia) and is essential for normal brain development (Orth and Bellosta 2012). These findings along with other associations identified such as cell differentiation and positive regulation of neuron differentiation indicate cells were actively encouraging neuronal growth in culture and energy required for this development was acquired from lipid processing. This data supports neuronal development characterisation studies described in Chapter 3 (*Figure 3.3, 3.7*) showing active neuronal growth was occurring in cultures. Down-regulated genes had associations with signal transduction, which is described as the movements of electrical potentials from neuron to neuron. As cells were cultured *in vitro*, it was possible that a reduction in neuronal stimulation and electrical impulses would be observed in comparison to *in vivo* tissue. Additionally, this principle would apply to other processes identified such as feeding behaviour.

In conclusion, DEGs were identified when comparing *in vitro* versus *in vivo* systems. PANTHER analysis showed both up and down-regulated genes from all *in vitro* and *in vivo* system comparisons (*Figure 6.8*) shared similar GO enrichment profiles indicating none of the processes identified were dominant regarding gene expression. In contrast, DAVID GO enrichment showed up and down-regulated gene lists were associating with different processes indicating PANTHER and DAVID platforms can produce variance in GO analysis and therefore, more than one system for investigating gene expression should always be used to avoid bias. Importantly, biological processes identified in DAVID suggest an environmental adaptation of cells was occurring *in vitro,* which was a normal observation as cells were removed from *in vivo* and were adapting accordingly by promoting neuronal growth. Thus, although DEGs were identified between both system comparisons, biologically no major differences were identified suggesting both systems were comparable.

An alternative approach to compare both *in vitro* and *in vivo* systems involved using Miru (Materials and Methods, 2.5.5). Miru is a complex pattern recognition software, designed specifically for the integration, visualisation and analysis of network graphs derived from whole biological datasets in a non-bias manner (Theocharidis et al. 2009) and therefore, was used to compare both systems without any filtering of datasets. Miru generated a visual network graph consisting of clusters of co-expressed genes (*Figure 6.10*). These cluster profiles were visualised in Miru to compare both *in vitro* and *in vivo* systems and as shown in *Figure 6.11,* Cluster 001 was comprised of 539 genes which were all up-regulated *in vivo* in both 101LL and WT genotypes (99% of genes identified had a P-Value of < 0.05). GO enrichment of these genes confirmed associations with cellular and metabolic processes similar to comparison results previously obtained using PANTHER (data not shown). DAVID enrichment (Cluster001) for biological processes ranked gene associations to angiogenesis, signal transduction, chemical synaptic transmission, ion transport and feeding behaviour (data not shown).

Interestingly, all these processes were identified previously using Partek analysis and DAVID enrichment (*Figure 6.9*) and were associated with down-regulated genes *in vitro* supporting Miru observations. Angiogenesis is a physiological process through which new blood vessels form and therefore, associations identified here were expected, as cells grown *in vitro* would have no need for a blood supply. Signal transduction and feeding behaviour have been discussed already and synaptic transmission may be related to higher numbers of neurons present in the tissues. Importantly, results shown here support DAVID enrichment results obtained from Partek generated DEG lists (*Figure 6.9*). Cluster 005 was comprised of 34 genes, which were all up-regulated in both 101LL, and WT cultures (*Figure 6.11*). Go enrichment of this cluster showed genes association with post-embryonic development, multicellular organism growth and axon guidance. All these processes were important in enhancing and maintaining the growth of isolated embryonic neuronal cells *in vitro*, which was also reflected in PANTHER analysis, presented earlier (*Figure 6.8*). The remaining clusters identified did not show any major differences between both systems and collectively showed many similarities were evident (*Appendix Figure 6.a*). These clusters were associated with a range of processes identified in DAVID including, protein transport, proteolysis, response to metal ion and lipid metabolic processes, protein targeting to mitochondria, intracellular protein transport, tumor necrosis factor-mediated signalling pathway, G-protein coupled receptor signalling pathway, myeloid cell differentiation, cell surface receptor signalling pathway, actin cytoskeleton organisation and regulation of canonical Wnt signalling pathway. Collectively these data show numerous clusters of genes were identified with similar expression profiles in both *in vitro* and *in vivo* systems associated with a range of functions, suggesting both systems were grossly comparable. To summarise, when entire datasets were processed in Miru, only a small subset of genes (Cluster 001) were identified to be collectively up-regulated *in vivo* in comparison to *in vitro* systems and gene enrichment showed processes identified were rational to each systems requirements.

Remaining clusters showed both systems were comparable across a broad range of functions. This analysis approach supported Partek results and although gene expression was not analogous between cultures and tissues, the differences identified were limited. In conclusion, primary hippocampal culture models were grossly comparable to *in vivo* tissue and therefore, provided a realistic neuronal cell model for studying misfolded protein interactions *in vitro*.

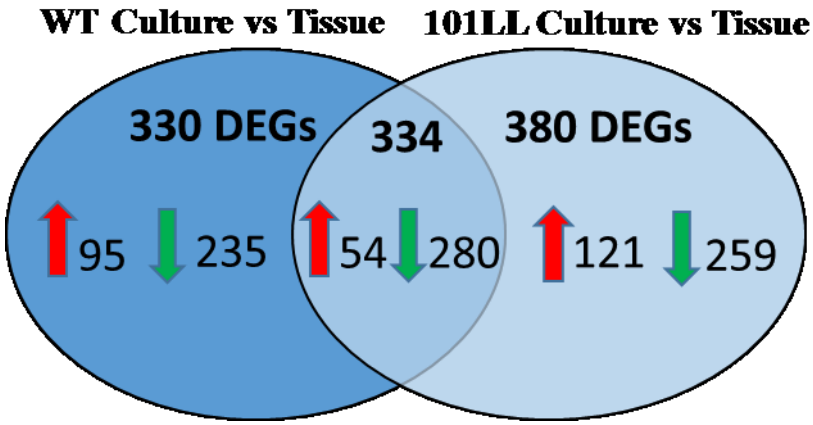

Figure 6.7: Limited differences in gene expression were evident between systems. Partek analysis of microarray data was used to compare *in vitro* (culture) with *in vivo* (tissue) systems in both genotypes. Partek filtering using P-Value FDR <0.01, FC 1.5; identified 330 DEGs from WT culture versus tissue (235 down-regulated and 95 up-regulated); 380 DEGs from 101LL culture versus tissue (259 down-regulated and 121 up-regulated) and an overlap of 334 DEGs (280 down-regulated and 54 up-regulated) common to both with similar up or down-regulated patterns in both genotypes (two genes were borderline for FC common comparisons so were removed from list). Red arrows up-regulated genes and green arrows down-regulated genes in culture.

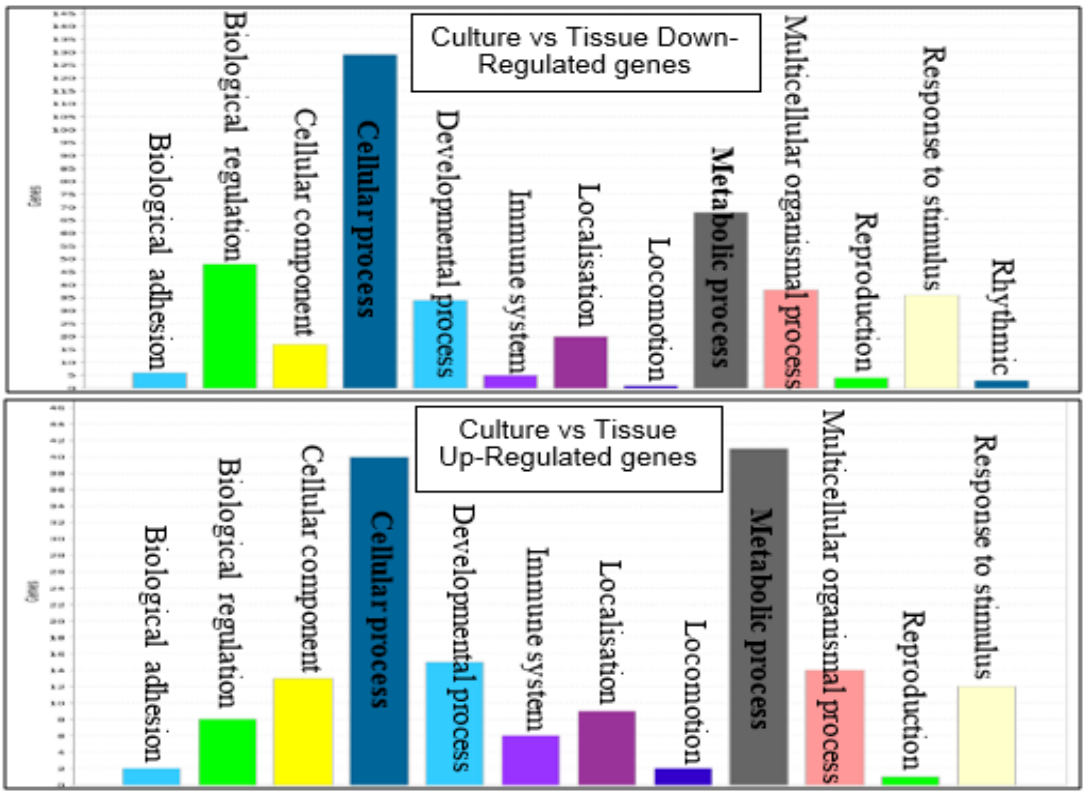

Comparisons *in vitro* vs *in vivo* systems (DEGs)	% genes associated with cellular processing	% genes associated with metabolic processing
WT 235 Down	27%	18%
WT 95 Up	25%	25%
101LL 259 Down	31%	16%
101LL 121 Up	24%	25%
Overlap 280 Down	29%	18%
Overlap 54 Up	29%	22%

Figure 6.8: Similar GO enrichment profiles from system comparisons were evident between up and down-regulated gene lists. DEG lists from system comparisons were enriched for gene ontology using PANTHER. Down-regulated (259 DEGs, 101LL culture versus tissue) gene associations are shown in top graph, of which 31% were associated with cellular processing and 16% with metabolic processing. Bottom graph represents up-regulated genes (121 DEGs, 101LL culture versus tissue) and shows a similar profile to down-regulated genes (rhythmic process not identified). Y-axis equals numbers of genes. PANTHER analysis of all WT, 101LL, and overlap DEG groups is highlighted in table underneath showing DEG lists were predominantly associated with cellular and metabolic processing.

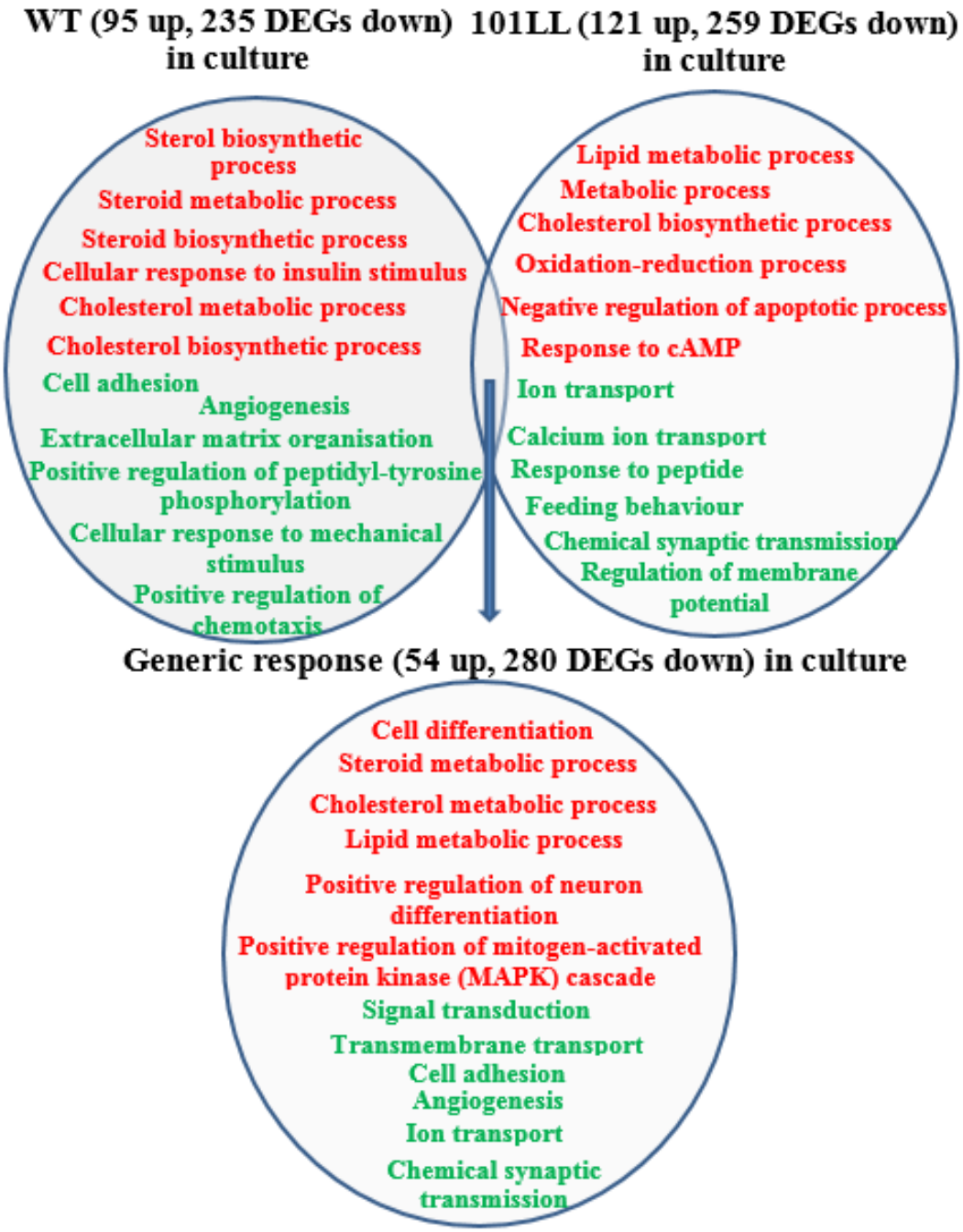

Figure 6.9: Summary of DAVID enrichment of biological processes. Data obtained from comparisons of *in vitro* (culture) with *in vivo* (tissue) systems in both genotypes using microarray identified DEG lists from *Figure 6.7*. Top six hits arranged according to significance (P-Values not included). Biological processes identified in each genotype showed comparability between groups and processes identified in generic response were also comparable to each genotype indicating biological processes identified in DAVID were not genotype specific. GO enrichment for up-regulated genes shown in red text, down-regulated gene associations in green text.

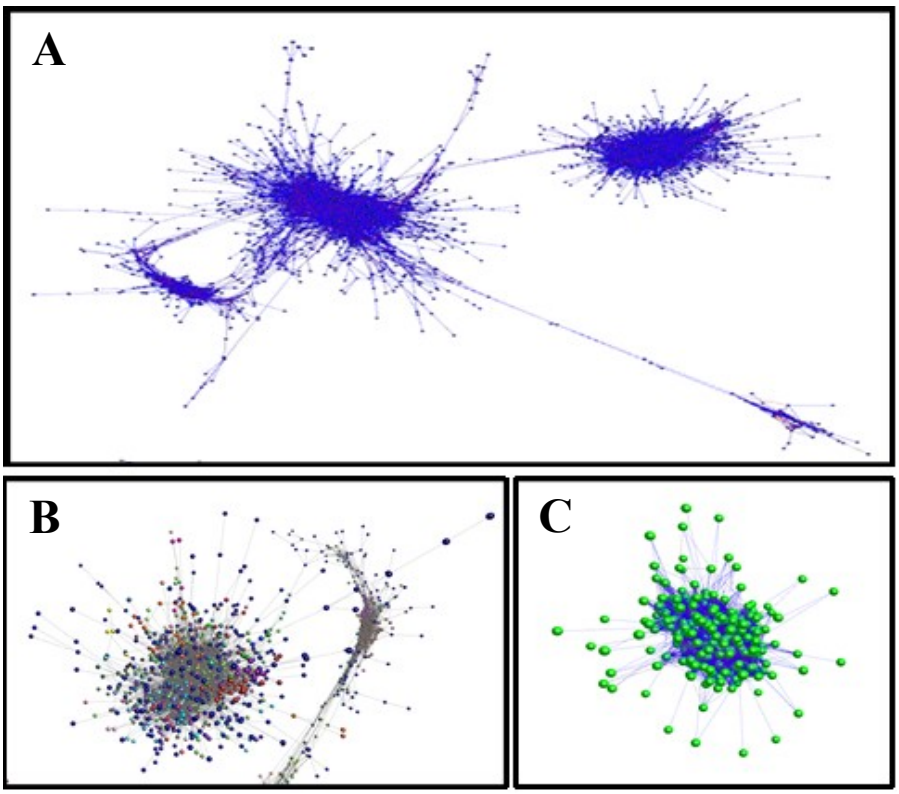

Figure 6.10: Miru generated visual graphs showing spatial representation of genes orientated accordingly to their correlation to one another. Network analysis was carried out on WT and 101LL microarray transcriptomic data from both *in vivo* and *in vitro* systems. (A) Miru created a complete graph based on entire gene lists and correlation values inputted. (B) Markov clustering algorithm divided main graph into clusters of co-expressed transcripts, represented as different colors in the graph. (C) A representative single cluster of genes identified in Miru. Correlation Value (R) 0.95, Filter 50, MCL 2.2, 10 smallest cluster allowed.

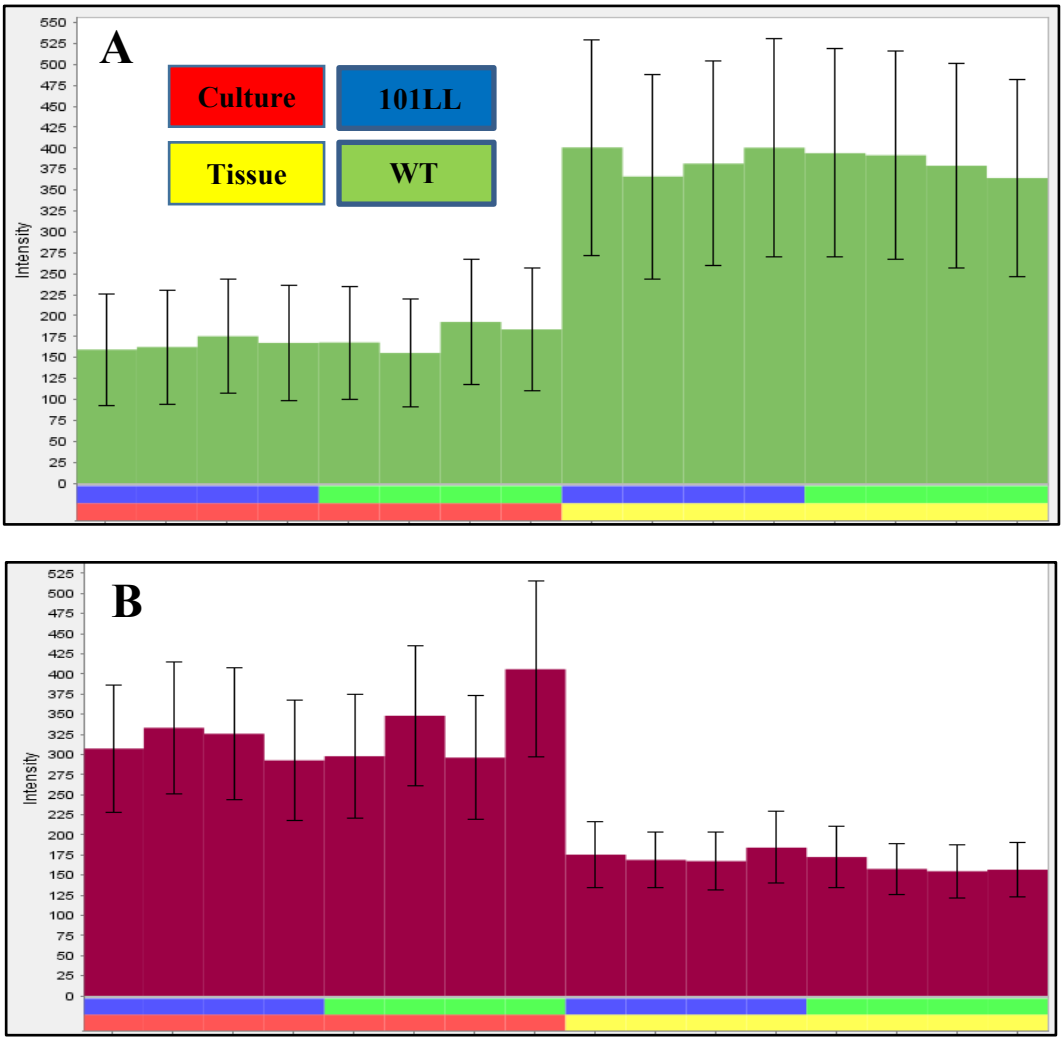

Figure 6.11: Cluster profiles were visualised in Miru to compare both *in vitro* and *in vivo* systems. (A) Cluster 001 comprised 539 related genes, 99% of these genes identified had a P-Value of < 0.05 when compared to ANOVA lists. These genes were all up-regulated in both 101LL and WT tissue samples (yellow bar) in comparison to culture (red bar). DAVID GO enrichment of this dataset showed cellular and metabolic processes to be major biological processes identified. (B) Cluster 005 comprised 34 genes all up-regulated in both 101LL and WT cell culture samples. GO enrichment of this dataset showed associations with post-embryonic development, multicellular organism growth and axon guidance. Y-axis equals normalised expression intensity values.

6.3.4 Do fibril-induced molecular responses vary between genotypes?

To address this question, RNA-seq analysis was carried out on RNA extracted from unchallenged and fibril-challenged WT and 101LL primary cultures (7.5µg/ml of unlabelled 101L fibrils for 24 hours, 2.4.4) at Edinburgh Genomics. A principal components analysis was undertaken on normalised filtered expression data to explore observed patterns with respect to experimental factors analysed (*Appendix Figure 6.b*). Unchallenged 101LL samples displayed more variable global expression profiles than WT samples however, both genotypes exhibited strong responses to fibril challenge in such a way as to make their expression patterns consistent with one another and their clusters to converge (*Figure 6.12*). As discussed in Section 6.3.2, increased expression of *Tnfaip2* and *Tgfbi* was identified in unchallenged 101LL cultures (RT-qPCR did not validate *Tnfaip2* observation *Figure 6.6*). As shown in *Appendix Table 6.a*, after fibril challenge, *Tnfaip2* was significantly down-regulated in 101LL cultures, no significant changes were noted in WT cultures, and this was validated by RT-qPCR (*Figure 6.13*). As discussed previously (Section 6.3.2), *Tnfaip2* overexpression can make cells more susceptible to neurodegeneration (Brohawn, O'Brien, and Bennett 2016; Kurji et al. 2010), therefore reduced expression of this gene after fibril challenge in 101LL cultures may be a survival response to lower susceptibility of cells to fibril insult. *Tgfbi* which is involved in cell proliferation (Zhang et al. 2009), showed a significant increase in expression in WT fibril-challenged cultures and no changes were noted in 101LL fibril-challenged cultures (*Appendix Table 6.a*) suggesting cell proliferation was increasing in the WT genotype in response to fibril challenge. This cell proliferation may be associated with microglial activation (Monif, Burnstock, and Williams 2010) which was shown by immunocytochemical analysis in Chapter 5 to be occurring in WT fibril-challenged cultures (Appendix *Figure 5.b*), and involved possibly in fibril degradation. Collectively, initial results confirmed fibril insult was causing strong responses in cultures and preliminary investigations suggest fibril response may vary between genotypes.

To investigate the possibilities of variance in fibril responses between genotypes, a heatmap of the top 50 most differential genes between WT and 101LL fibril-challenged groups identified by FDR was generated (*Figure 6.14*), and confirmed genotype specific responses were evident. The gene Lipoprotein receptor-related protein 1b (*Lrp1b*) was identified as the top most differential gene up-regulated in 101LL genotype. *Lrp1b* has been associated with neuroprotective roles in AD, where it interacts with APP and reduces the processing of Aβ by regulating endocytic trafficking (Cam and Bu 2006). *Lrp1b* is also a central mediator of complement protein C1q-induced neuroprotection against Aβ in AD mice (3xTg) and this neuroprotective response was triggered early on in the progression to AD before the accumulation of plaques and ensuing complement activation and inflammation (Benoit et al. 2013). This early neuroprotective response may also be occurring in 101LL cultures exposed to PrP fibrils and may have important applications for future PMD therapies. Cathepsin Z (*Ctsz*) was identified as the top most differential gene down regulated in 101LL fibril-challenged cultures or conversely, up-regulated in WT fibril-challenged cultures. This gene belongs to the C1 family of lysosomal cysteine proteases, is restricted to immune system cells including macrophages and dendritic cells and is involved in normal intracellular protein degradation (Santamaria et al. 1998). Variations in lysosomal pathways in 101LL cultures have already been highlighted in Chapter 5 by immunocytochemistry (*Figure 5.9*). The reduction in lysosomal associated gene expression identified here in 101LL fibril-challenged cultures support these findings and highlight a means by which fibrils may be maintained due to irregularities in lysosomal degradation pathways. GO enrichment of all 50 DEGs using DAVID showed processes identified such as oligodendrocyte development and astrocyte differentiation were associated with down-regulated genes in 101LL fibril-challenged cultures and therefore were up-regulated in WT fibril-challenged cultures.

As shown in Chapter 5 (*Figure 5.4*) fibrils induced a hypertrophic astrocyte response in WT fibril-challenged cultures only, suggesting increased astrocyte

differentiation processes identified here could be actively increasing the presence of normal functional astrocyte populations to compensate for abnormal fibril-induced astrogliosis.

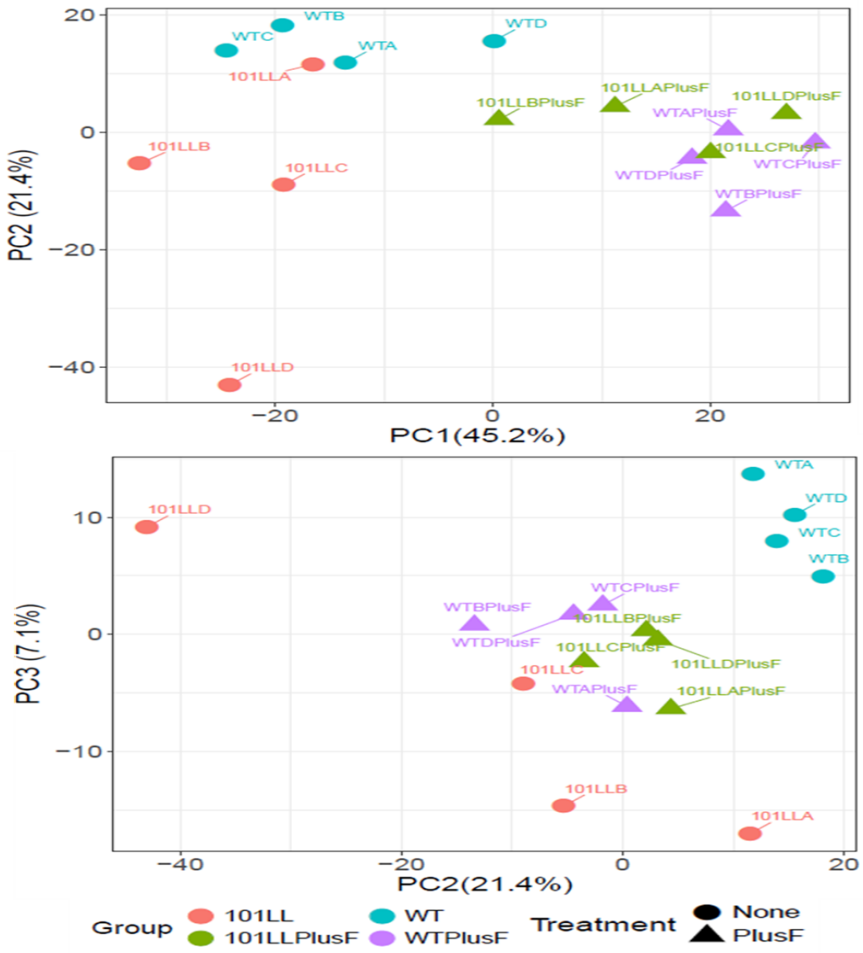

Figure 6.12: Both genotypes show similar response to fibril challenge. PCA plots of first, second and third components from PCA analysis using all 16 WT and 101LL samples pre and post-fibril challenge. 101LL displayed more global expression profiles than WT samples however, both 101LL and WT responded similarly to fibril challenge. PC 1 was associated with 2 factors: Group (P Value 1.92e-05) and Treatment (P-Value 1.38e-06), PC 2 was not associated with any experimental factors, PC 3 was associated with 2 factors: Group (P Value 0.0354) and Type (P Value 0.03). P-Values were generated in Edinburgh Genomics ANOVA report, Reference *Appendix Figure 6.b*.

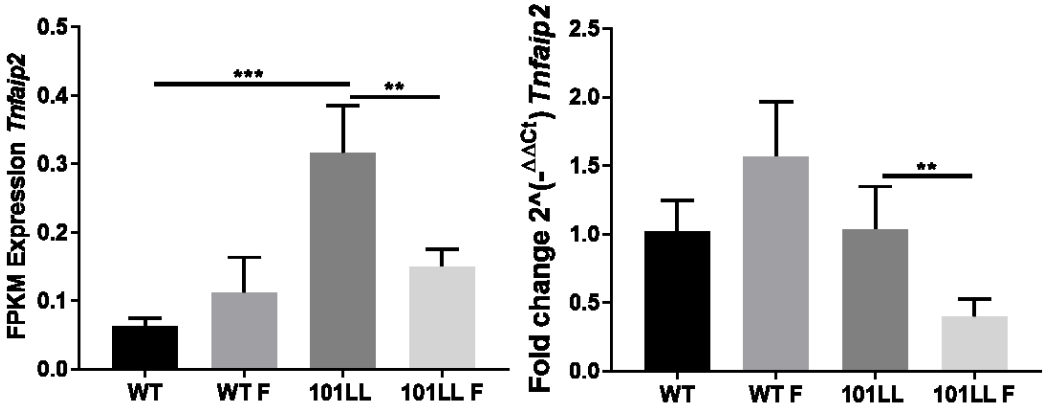

Figure 6.13: Tumor necrosis factor, alpha-induced protein 2 (*Tnfaip2)* expression changes after fibril challenge were validated by RT-qPCR. Relative expression values and RT-qPCR results are shown from *in vitro* unchallenged and fibril-challenged cultures. Expression values obtained from RNA-seq generally matched with RT-qPCR results validating transcriptomic results. *Tnfaip2* was confirmed to be significantly down-regulated in 101LL fibril-challenged cultures (101LL F, P-Value 0.008) and no changes were evident in WT cultures although this was borderline (P-Value 0.05). Reference gene *Sdha,* Graph mean plus standard deviation, n=4, n=individual samples, unpaired t test. Fold changes from RT-qPCR were calculated using 2-ΔΔCt method (Materials and Methods, 2.5.8) and Fragments Per Kilobase of transcript per Million (FPKM) values were obtained from RNA-seq data.

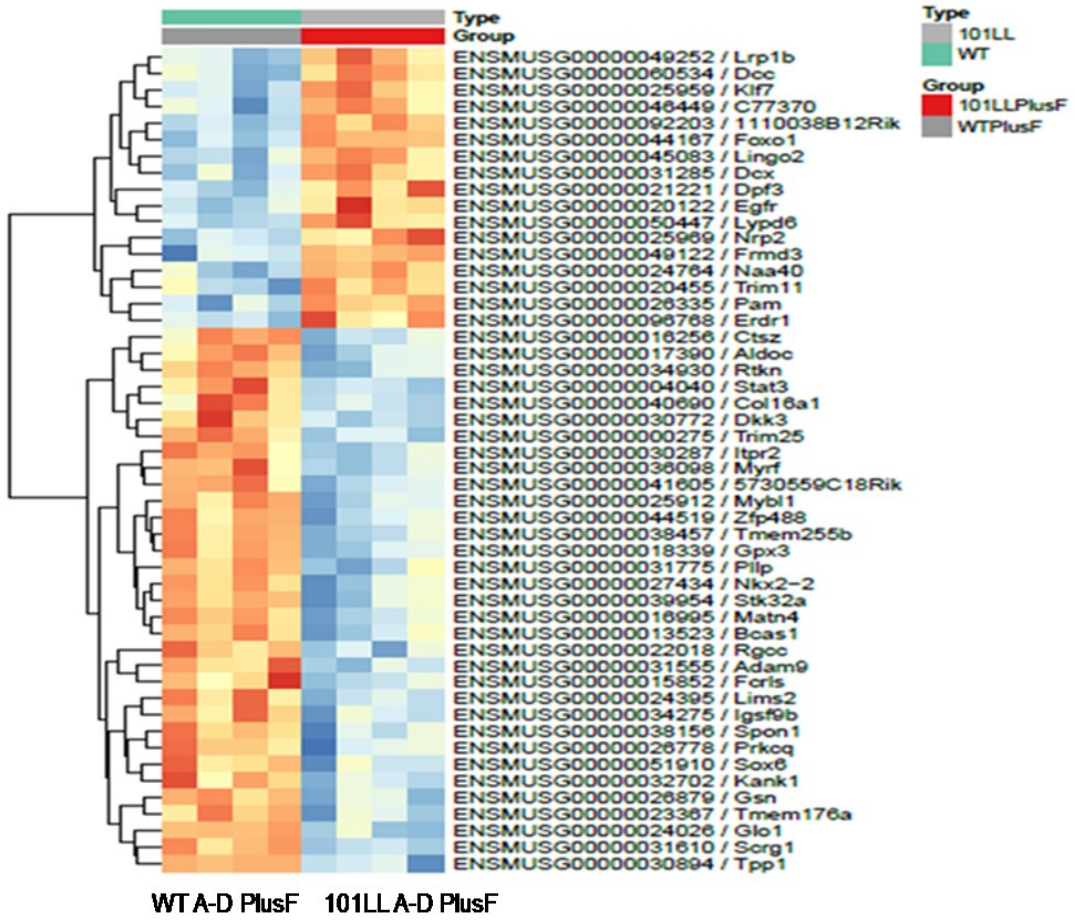

DAVID GO enrichment (DEGs up-regulated in 101LL Plus Fibrils)	Gene Count	P-Value
Nervous system development	5	1.6E-4
Neuron migration	3	4.0E-3
Axon guidance	3	5.8E-3
DAVID GO enrichment (DEGs down-regulated in 101LL Plus Fibrils)	Gene Count	P-Value
Oligodendrocyte development	3	6.8E-4
Astrocyte differentiation	2	1.6E-2
Membrane protein ectodomain proteolysis	2	2.8E-2

Figure 6.14: Top 50 most differential genes identified by FDR between WT challenged (WTPlusF) and 101LL fibril-challenged groups (101LLPlusF). Heatmap generated with the pheatmap package (Edinburgh Genomics) showed genotype differences to fibril response were evident. GO enrichment of these DEGs using DAVID provided some insights into these responses and identified processes such as proteolysis which is involved in misfolded protein degradation to be down-regulated in 101LL Plus fibrils or conversely up-regulated in WT Plus fibrils cultures therefore, was either impeding (101LL) or supporting (WT) fibril degradation in fibril-challenged cultures.

6.3.5 Fibril influence on *Prnp* expression in WT and 101LL cultures

RNA-seq data highlighted *Prnp* expression was highly variable in unchallenged 101LL cultures and highly consistent in WT cultures (*Appendix Figure 6.c*), which might explain variable global expression noted by PCA (*Figure 6.12*). However, as previously shown (*Figure 6.2*) no significant expression differences were noted between WT and 101LL unchallenged groups. After fibril challenge, *Prnp* expression was shown to be significantly up-regulated in WT fibril-challenged cultures although this was a subtle increase (LogFC 0.20, FC 1.15, FDR 0.02) and no significant changes were noted in 101LL fibril-challenged cultures (LogFC -0.33, FC 0.79, FDR 0.59). RT-qPCR validated expression profiles however, did not show any significant differences between groups (*Figure 6.15*). As the FC increase for WT fibril-challenged cultures was minimal, it was concluded no relevant biological differences in *Prnp* expression were apparent in fibril-challenged WT and 101LL cultures. Interestingly, these data compliment previous immunolabelling studies shown in Chapter 5 (*Appendix Figure 5.f*), that showed fibrils were not changing levels of PrP^{C} protein in WT and 101LL cultures after 24-hour fibril challenge. Collectively these data also suggest abnormal PrP fibrils may not be inducing immediate conformational changes of normal PrP^{C} to the abnormal form, as this would have resulted in noticeable changes in either *Prnp* expression or detectable PrP^{C}.

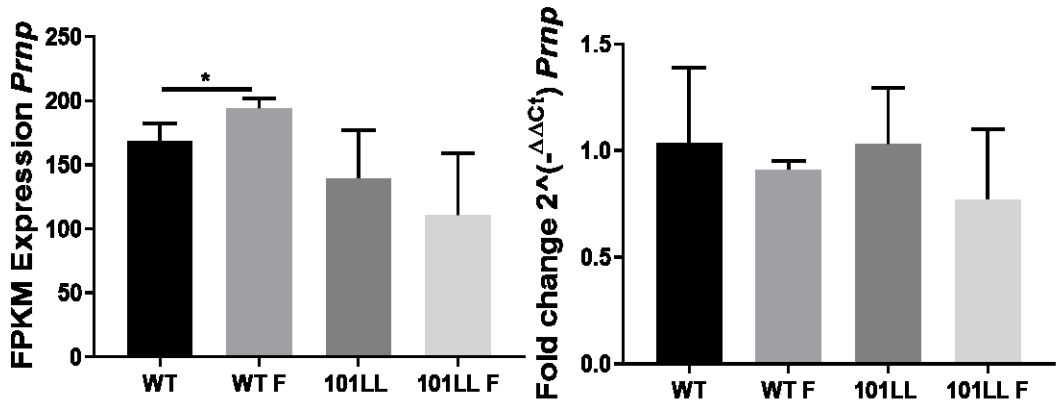

Figure 6.15: Prnp expression changes after fibril challenge were validated by RT-qPCR. Relative expression values and RT-qPCR results are shown from *in vitro* unchallenged and fibril-challenged cultures. Expression values obtained from RNA-seq generally matched with RT-qPCR results validating transcriptomic expression however, no significant differences were evident between groups (P-Value WT 0.50; 101LL 0.26). Reference gene *Ywhaz*, Graph mean plus standard deviation, n=4, n=individual samples, unpaired t test. Fold changes from RT-qPCR were calculated using 2-ΔΔCt method (Materials and Methods, 2.5.8) and Fragments Per Kilobase of transcript per Million (FPKM) values were obtained from RNA-seq data.

6.3.6 Fibril insult activated stronger DEG responses in WT cultures

As indicated in Section 6.3.4, initial investigations suggested both WT and 101LL cultures may respond differently to fibril insult. To investigate this in more detail and to gain further insights into specific genotype fibril response, DEG lists from RNA-seq data were generated based on unchallenged WT versus WT Plus Fibrils and unchallenged 101LL versus 101LL Plus Fibrils using standard filtering parameters (P-Value FDR of 0.05, FC 2). As shown in Table 6.4, a number of DEGs were identified in both unchallenged WT versus WT Plus Fibrils (1,080 DEGs) and unchallenged 101LL versus 101LL Plus Fibrils (545 DEGs). Based on gene numbers identified, fibril challenge elicited a greater DEG response in WT fibril-challenged cultures. Of the total 1,080 WT DEGs, 761 or 70% of DEGs were up-regulated and 319 or 30% DEGs were down-regulated in WT fibril-challenged cultures. In comparison, 101LL fibril-challenged cultures had 299 (55%) DEGs up-regulated and 246 (45%) DEGs down-regulated. These results confirmed differences were apparent between genotype fibril responses and the majority of DEGs identified in WT fibril-challenged cultures were associated with increased gene expression. To identify what responses were specifically associated to each genotype and to examine if any generic responses to fibril challenge were evident, DEG datasets were compared between unchallenged WT versus WT Plus Fibrils (1,080 DEGs) and unchallenged 101LL versus 101LL Plus Fibrils (545 DEGs). 737 DEGs were specific to WT genotype, 202 were specific to 101LL genotype and 343 DEGs were common to both genotypes (*Figure 6.16*). Overall, fibrils were activating stronger changes in gene expression in WT fibril-challenged cultures in comparison to 101LL fibril-challenged cultures. These gene sets were investigated further (Sections 6.3.7, 6.3.8, 6.3.9) using various platforms referred to in *Figure 6.1*, to identify molecular processes related to these specific genotype responses.

Contrast name	Up	Down
Unchallenged WT vs WT Plus Fibrils (1,080 DEGs)	761	319
Unchallenged 101LL vs 101LL Plus Fibrils (545 DEGs)	299	246

Table 6.4: Fibril insult caused DEG responses to double in WT cultures. DEG lists from RNA-seq data were generated based on unchallenged WT versus WT Plus Fibrils and unchallenged 101LL versus 101LL Plus Fibrils using standard filtering parameters (P-Value FDR of 0.05, FC 2). Fibril challenge generated a larger gene expression response in WT fibril-challenged cultures (1,080 DEGs) in comparison to 101LL fibril-challenged cultures (545 DEGs).

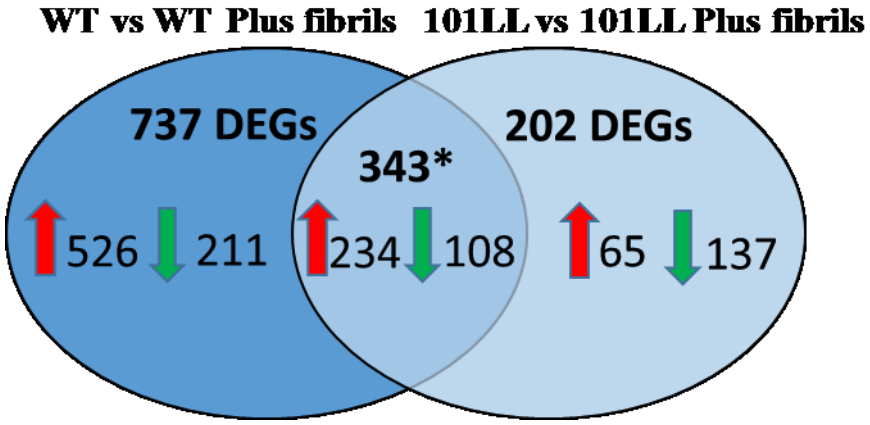

Figure 6.16: Specific genotype responses identified for WT and 101LL fibril-challenged cultures. DEG lists were compared between unchallenged WT versus WT Plus Fibrils and unchallenged 101LL versus 101LL Plus Fibrils to identify gene sets specific to each genotype response and to ascertain if any common genes were present between both WT and 101LL DEGs identified. Of the total 1,080 WT and 545 101LL DEGs identified, 737 were specific to WT genotype, 202 were specific to 101LL genotype and 343 were common to both genotypes. Of the 343* common genes identified 342 shared common up or down-regulation profiles in both genotypes. One gene however, namely purinergic receptor P2Y, G-protein coupled, 14 (*P2ry14*) showed an increase in gene expression in WT versus WT Plus Fibrils (LogFC 1.65, FC 3.14, FDR 0.04) and a decrease in gene expression in 101LL versus 101LL Plus Fibrils (LogFC -1.71, FC 0.30, FDR 0.01, reference Section 6.3.9).

6.3.7 WT cells are primed to curtail abnormal protein formation by increasing expression of genes associated with fibril degradation processes

To understand WT molecular responses to fibril challenge and possibly gain insights into how WT mice curtail abnormal PrP formation, data analysis of WT specific DEG lists (*Figure 6.16)* was carried out, using IPA and PANTHER. IPA searches through gene lists and determines genes that are involved in well documented canonical signal transduction pathways (Krämer et al. 2014). IPA generated information on top networks and diseases and disorders associated with specific gene lists identified in *Figure 6.16*. A summary of IPA reports is shown in Table 6.5. Both WT (737 DEGs) and 101LL (202 DEGs) specific DEG lists were associated with different top networks, WT were associated with cellular function and maintenance whilst 101LL response was associated with auditory disease. Cellular function and maintenance included engulfment by macrophages, and gene expressions associated with this process were predominantly increased (Table 6.6) in WT fibril-challenged cultures suggesting WT cells were positively responding to fibril insult by increasing macrophage degradation of misfolded fibrils. In comparison, the 202 DEG list specific to 101LL culture fibril response had seven genes (*Cd14, Dock2, Fas, Itgam, Itgb2, Si1 and Tlr9*) identified by IPA to be associated with engulfment by macrophages however, these were all down-regulated. Further enrichment of top genes lists generated in IPA was carried out using PANTHER, to gain more insight into biological process associations specific to genotype. Separating genes into up and down-regulated groups allowed applicable PANTHER GO enrichment analysis to be carried out. Genes shown in Table 6.6 were associated with top networks identified in IPA in WT fibril-challenged cultures (cellular function and maintenance, engulfment by macrophages). Up-regulated genes had associations with positive regulation of the adaptive immune system (*Cd44, Fcgr3* and *P2rx7*); defence response (*Hck, Capg, Fcgr3, Gsn, P2rx7* and *Cd44*); endocytosis (*Hck, Fcgr3, Gsn, Tgm2, Scarb1* and *P2rx7*) and finally response to stimulus (*Hck, Capg, Hgf, Pros1, Fcgr3, Nodal, Ch25h, Gsn, Tgm2, Scarb1, P2rx7* and *Cd44*).

Down-regulated genes *C3* and *Btk* were associated with positive regulation of hypersensitivity and acute inflammatory response. From this data, WT cultures seemed to be positively responding to stimulus (fibrils) by activating a defence and adaptive immune response whilst damping acute inflammatory responses. Additionally, up-regulation of endocytosis suggested WT cultures were escalating the engulfment of molecules such as fibrils into the cell for further processing. IPA identified inflammatory response to be top in diseases and disorders associations in WT fibril-challenged cultures (Table 6.5) and infectious disease was identified for 101LL fibril-challenged cultures. PANTHER enrichment of up-regulated genes from Table 6.7, identified innate immune response (*Cfh, Hck, Capg, Rap27a, Il12rb1, Gsn, Il34* and *SerpinG1*) and negative regulation of apoptotic processing and programmed cell death (*Hck, Vip, Agtr1, Prkcd, Cdknia, Cx3cr1, Cd44, Hgf, Vegfa, Itga5, Angptl4, Fn1, Spp1* and *Adoraa2a*) to be associated with the WT specific response. Conversely, gene associations with positive regulation of apoptotic processing and programmed cell death (*Agtr2, Tnfsf12, P2rx7, Cd40, Prkcd, Nupr1, Bmp2, Cd44, Nodal, Gsn, Tgm2, Casp8, Ripk3, Nfatc4* and *Adoraa2a*) were also identified suggesting these processes were both positively and negatively regulated in WT cultures. Down-regulated genes were associated with inflammatory response (*Gper1, Cxcl5, Chil3, C3* and *Hc*) and innate immune response (*Gper1, C3* and *Hc*). From this analysis we can conclude, WT fibril-challenged cultures were capable of both positively and negatively regulating innate immune response and apoptotic processes. Down-regulation of genes associated with major components of the innate immune response (*C3* and *Hc*) was an interesting finding. The activation of the Complement (C) system can occur through three pathways including classical, lectin and alternative, each triggered by different agents. Complement C3 which is part of both classical and alternative complement pathways, has been shown to exacerbate prion disease (Kane et al. 2017; Michel et al. 2013) suggesting down-regulation noted in WT fibril-challenged cultures (Table 6.6, LogFC -1.75, FC 0.29, FDR 0.02), may be inhibiting and curtailing misfolded protein replication and accumulation.

Complement factor H (*Cfh*) was up-regulated after challenge (LogFC 2.50, FC 5.66, FDR 0.001) and is a negative regulator of the alternative pathway of the complement system (suppresses conversion of C3b to C3a) therefore, this response may be promoting the downregulation of the complement cascade in WT fibril-challenged cultures (Table 6.7). In comparison, no significant changes in complement components were identified in 101LL fibril-challenged cultures however, complement C3d receptor 2 (*Cr2*) was up-regulated (LogFC 2.12, FC 4.36, FDR 0.007) after fibril challenge. Studies have shown *Cr2* is expressed in neuronal progenitor cells (NPCs) of the dentate gyrus and two of its ligands, C3d and interferon inhibit proliferation of NPCs (Moriyama et al. 2011). *Cr2* was up-regulated in 101LL fibril-challenged cultures suggesting fibril insult was possibly inhibiting the generation of neurons and glia after challenge. Inflammatory response was also identified in IPA for top network associations using 101LL specific DEG list (Table 6.5). For comparison, genes associated with this response (Table 6.8) of which were all down-regulated were enriched using PANTHER. Associations with innate immune response (*Lcn2, Cybb, Tgfb1, Tlr9, Cd14* and *Cc12*); positive regulation of immune response (*Fos, Icam1, NcKap1, Itgam, Itgb2, Tgfb1, Aif1, Tlr9, Cd14* and *Ccl2*); positive regulation of response to stimulus (*Icam1, Nckap1, Itgam, Tgfb1, Ctss, Aif1, Tlr9, Dock2, Cd14* and *Ccl2*); positive regulation of endocytosis (*Nckap1, Dock2, Cd14* and *Ccl2*); amyloid beta clearance (*Itgam* and *Itgb2*) and finally microglial and glial cell activation (*Itgam, Aif1* and *Tlr9*) were identified. As all genes were down-regulated it suggested immune response, response to stimulus, endocytosis, amyloid clearance and microglial and glial activation were all reduced in 101LL cultures. In conclusion, the data shown here based on both IPA and PANTHER analysis suggested WT cultures were positively responding to fibril challenge by activating defence and adaptive immune responses. Additionally, WT cultures appeared primed to respond to fibril insult as after challenge, endocytosis and macrophage degradation processes were up-regulated.

These molecular changes would actively reduce fibril burden in cultures whilst curtailing further abnormal formation. Interestingly, WT cultures appeared to be capable of both positively and negatively regulating responses such as innate immune response and apoptotic processes and this balancing influence may be advantageous in maintaining normal cellular homeostasis.

DEG Group	Top Networks	Diseases and Disorders
WT Fibril-challenged cultures (specific 737 DEGs)	Cellular function and maintenance, Cellular growth and proliferation, Cellular development, Cellular movement, Organismal injury and abnormalities, Cell-To-Cell signalling and interaction	Inflammatory response, Cancer, Organismal injury and abnormalities, Metabolic disease, Dermatological diseases and conditions
101LL Fibril-challenged cultures (202 specific DEGs)	Auditory disease, Organismal injury and abnormalities, Cell morphology; Inflammatory response	Infectious diseases, Endocrine system disorders, Gastrointestinal disease, Immunological disease

Table 6.5: Summary of IPA reports comparing genotype specific responses to fibril challenge. Top networks ranked by overall network score (data not shown) and diseases and disorders were ranked by P-Value (data not shown).

Gene Symbol	Gene Name	LogFC
Btk	Bruton tyrosine kinase	-1.65
C3	Complement C3	-1.76
Capg	Capping actin protein, gelsolin like	1.09
Cd44	CD44 molecule (Indian blood group)	1.53
Ch25h	Cholesterol 25-hydroxylase	1.97
Fcgr3	Fc fragment of IgG receptor IIa	1.01
Gsn	Gelsolin	1.29
Hck	HCK proto-oncogene, Src family tyrosine kinase	1.20
Hgf	Hepatocyte growth factor	1.40
Mirlet7c	MicroRNA let-7a-1	-1.66
Lum	Lumican	2.12
Nodal	Nodal growth differentiation factor	2.26
P2rx7	Purinergic receptor P2X 7	1.76
Pla2g5	Phospholipase A2 group V	-1.53
Pros1	Protein S	1.00
Scarb1	Scavenger receptor class B member 1	1.21
Tgm2	Transglutaminase 2	2.94

Table 6.6: WT specific fibril response included engulfment by macrophages response. IPA identified top networks for WT specific genes associated with fibril response. Gene lists shown here are associated with cellular function and maintenance and this specific gene list was associated with engulfment by macrophages and was predominantly associated with up-regulated genes suggesting WT cells were increasing processes associated with foreign material (fibril) degradation.

Gene Symbol	Gene Name	LogFC
Ache	Acetylcholinesterase (Cartwright blood group)	1.32
Adgre5	Adhesion G protein-coupled receptor E5	1.08
Adoraa	Adenosine A2a receptor	1.42
Agtr1a	Angiotensin II receptor type 1	2.31
Agtr2	Angiotensin II receptor type 2	2.50
Agtr1b	Angiotensin II receptor, type 1b	1.58
Angpt2	Angiopoietin 2	1.86
Angpt4	Angiopoietin like 4	3.15
Blnk	B-cell linker	-1.35
Bmp2	Bone morphogenetic protein 2	1.71
C3	Complement C3	-1.76
Hc	Complement C5	-2.31
C1qtn3	C1q and TNF related 3	-2.78
Calca	Calcitonin related polypeptide beta	2.47
Capg	Capping actin protein, gelsolin like	1.09
Casp8	Caspase 8	1.03
Cd40	CD40 molecule	2.07
Cd44	CD44 molecule (Indian blood group)	1.53
Cdkna	Cyclin dependent kinase inhibitor 1A	1.21
Cfh	Complement factor H	2.50
Chil3	Chitinase-like 3	-2.26
Creb33	CAMP responsive element binding protein 3 like 3	1.53
Crh	Corticotropin releasing hormone	1.44
Ctsg	Cathepsin G	-1.45
Cx3cr1	C-X3-C motif chemokine receptor 1	1.31
Cxcl1	C-X-C motif chemokine ligand 2	1.60
Cxcl2	C-X-C motif chemokine ligand 3	2.71
Cxcl5	C-X-C motif chemokine ligand 6	-2.63
Dpp4	Dipeptidyl peptidase 4	1.68
E2f2	E2F transcription factor 2	1.06
Edn3	Endothelin 3	1.94
Efs	Embryonal Fyn-associated substrate	1.18
Eng	Endoglin	1.15
Ets1	ETS proto-oncogene 1, transcription factor	1.79
Fcgr3	Fc fragment of IgG receptor IIa	1.01
Flt1	Fms related tyrosine kinase 1	1.09
Fn1	Fibronectin 1	1.09
Ggt5	Gamma-glutamyltransferase 5	2.07
Gli1	GLI family zinc finger 1	-2.67
Gper1	G protein-coupled estrogen receptor 1	-1.39
Gsn	Gelsolin	1.29
Hck	HCK proto-oncogene, Src family tyrosine kinase	1.20
Hgf	Hepatocyte growth factor	1.40
Gm899	Major histocompatibility complex, class I, A	2.88
Ier3	Immediate early response 3	2.36
Il34	Interleukin 34	1.02
Il12rb1	Interleukin 12 receptor subunit beta 1	1.60
Itga5	Integrin subunit alpha 5	1.26
Kdr	Kinase insert domain receptor	-1.75
Mirlet2	MicroRNA let-7a-1	-1.66

Loxl2	Lysyl oxidase like 2	1.75
Lum	Lumican	2.12
Mmp28	Matrix metallopeptidase 28	1.24
Nfatc4	Nuclear factor of activated T-cells 4	1.90
Nodal	Nodal growth differentiation factor	2.26
Nt5e	5'-nucleotidase ecto	1.59
Nupr1	Nuclear protein 1, transcriptional regulator	3.27
P2rx7	Purinergic receptor P2X 7	1.76
Pla2g5	Phospholipase A2 group V	-1.53
Prkcd	Protein kinase C delta	1.17
Pros1	Protein S	1.00
Ptgdr	Prostaglandin D2 receptor	3.79
Ptger2	Prostaglandin E receptor 2	2.47
Ptges	Prostaglandin E synthase	1.50
Ptgs1	Prostaglandin-endoperoxide synthase 1	2.31
Rab2a	RAB27A, member RAS oncogene family	1.45
Ripk3	Receptor interacting serine/threonine kinase 3	1.27
Scarb1	Scavenger receptor class B member 1	1.21
Serpia	Serpin family B member 1	-1.88
Serpi1	Serpin family F member 1	1.12
Serpi1	Serpin family G member 1	1.03
Slc1a5	Solute carrier family 1 member 5	1.96
Sod3	Superoxide dismutase 3	1.28
Spp1	Secreted phosphoprotein 1	1.57
Stat6	Signal transducer and activator of transcription 6	1.09
Tgm2	Transglutaminase 2	2.94
Thbd	Thrombomodulin	1.57
Thbs4	Thrombospondin 4	1.38
Tnfaip6	TNF alpha induced protein 6	1.49
Tnfsf12	TNF superfamily member 12	1.01
Trpm2	Transient receptor potential cation channel subfamily M member 2	1.12
Tuba8	Tubulin alpha 8	1.91
Vegfa	Vascular endothelial growth factor A	1.59
Vip	Vasoactive intestinal peptide	1.80

Table 6.7: IPA identified inflammatory response was top in diseases and disorders in genes specific to WT response. Genes were predominantly up-regulated in this dataset.

Gene Symbol	Gene Name	LogFC
Aif1	Allograft inflammatory factor 1	-1.07
Aoah	Acyloxyacyl hydrolase	-3.12
Ccl2	Chemokine (C-C motif) ligand 2	-2.63
Cd14	CD14 molecule	-1.58
Col18a1	Collagen type alpha 1 chain cathepsin S	-1.92
Ctss	Cytochrome b-245 beta chain	-2.04
Dock2	Dedicator of cytokinesis 2	-2.67
Dock5	Dedicator of cytokinesis 5	-1.96
Fas	Fas cell surface death receptor	-1.46
Fos	Fos proto-oncogene, AP-1 transcription factor	-1.11
Hpgds	Hematopoietic prostaglandin D synthase	-2.45
Icam1	Intercellular adhesion molecule 1	-2.63
Itgam	Integrin subunit alpha M	-2.95
Itgb2	Integrin subunit beta 2	-2.21
Lcn2	Lipocalin 2	-3.37
Lcp1	Lymphocyte cytosolic protein 1	-1.30
Myo1f	Myosin IF	-1.73
Ncka1l	NCK associated protein 1 like	-1.00
Plp1	Proteolipid protein 1	-1.22
Spi1	Spi-1 proto-oncogene	-3.75
Tgfb1	Transforming growth factor beta 1	-1.24
Tlr9	Toll like receptor 9	-2.48
Usp18	Ubiquitin specific peptidase 18	-2.24
Vsir	V-set immunoregulatory receptor	-1.49

Table 6.8: IPA inflammatory response associated genes specific to 101LL fibril response were all down-regulated.

6.3.8 101LL molecular response to fibrils provides insights into processes that imped efficient abnormal protein degradation

To gain insights into how the 101LL genotype supports abnormal PrP processing, data analysis of 101LL specific DEG lists (*Figure 6.16*) was carried out, using IPA and PANTHER. As previously shown in Table 6.5, IPA analysis of the 202 DEGs identified top network associations with auditory disease and organismal injury and abnormalities. As auditory disease was deemed unrelated to fibril response *in vitro*, further investigation into genes associated with organismal injury and abnormalities was carried out (organ degeneration, Table 6.9) using PANTHER. No GO enrichment was evident from the four up-regulated genes (*Esrrg, Mak, Ntf3* and *Pdzd7*). Down-regulated genes were associated with inflammatory response (*Cybb, Ngfr, Tgfb1* and *Ccl2*); defence response (*Cybb, Ngfr, Ddx58, Tgfb1* and *Ccl2*) and response to stresses (*Cybb, Ngfr, Msrb3, Ddx58, Slc2a4, Tgfb1* and *Ccl2*). As organ degeneration was not identified in IPA analysis of the WT specific DEG list no direct comparisons could be made. In conclusion, inflammatory responses were reduced in 101LL fibril-challenged cultures and defence response was impeded which was opposite to what was seen in WT fibril-challenged cultures. Additionally, genes associated with response to stress were identified suggesting fibril challenge was disturbing cellular homeostasis in 101LL cultures and as this GO term was associated with down-regulated genes it was concluded this stimulus may be restricting cellular response in 101LL cultures to fibrils. Infectious diseases (Table 6.5) was identified as top diseases and disorders. Briefly, no PANTHER GO terms were identified for up-regulated genes associated with this term and down-regulated gene associations identified included microglial and glial cell activation, amyloid beta clearance, regulation of endocytosis, defence response, inflammatory response, positive regulation of immune system and positive regulation of response to stimulus (data not shown). These processes were already shown to be down-regulated in 101LL fibril-challenged cultures (Section 6.3.7) indicating these were dominant responses in 101LL cultures after fibril challenge.

Previous results shown in Chapter 5 (*Figure 5.9*) have indicated a lack of fibril localisation with lysosomes in 101LL fibril-challenged cultures and therefore an impairment of the fibril degradation pathway. Although IPA did not identify any lysosomal related disorders, reduced expression of the gene Lysosomal protein transmembrane 5 (*Laptm5)* which is associated with lysosome organelles was found in the 101LL specific 202 DEG list (LogFC -2.03, FC 0.24, FDR 0.009). These molecular findings support immunocytochemical observations (*Figure 6.8*) and suggest endolysosomal processing was reduced in the 101LL genotype after fibril challenge. As this was an important finding, RT-qPCR was used to validate RNA-seq gene expression data and as shown in *Figure 6.17*, these observations were accurate. In conclusion, impedance of microglial and glial cell activation, endocytosis, defence response and lysosomal degradation pathways suggests fibrils would be maintained in 101LL fibril-challenged cultures and would not be actively degraded, possibly resulting in further abnormal protein generation over-time.

Gene Symbol	Gene Name	LogFC
Abca4	ATP binding cassette subfamily A member 4	-1.51
Ccl2	Chemokine (C-C motif) ligand 2	-2.63
Col181	Collagen type XVIII alpha 1 chain	-1.92
Cybb	Cytochrome b-245 beta chain	-2.08
Ddx58	DExD/H-box helicase 58	-1.05
Esrrg	Estrogen related receptor gamma	1.29
Folh1	Folate hydrolase 1	-1.23
Lrit3	Leucine rich repeat, Ig-like and transmembrane	-1.98
Mak	Male germ cell associated kinase	1.25
Msrb3	Methionine sulfoxide reductase B3	-1.75
Ngfr	Nerve growth factor receptor	-1.26
Ntf3	Neurotrophin 3	1.15
Pdzd7	PDZ domain containing 7	1.20
Slc2a4	Solute carrier family 2 member 4	-1.15
Tgfb1	Transforming growth factor beta 1	-1.24

Table 6.9: IPA identified organismal injury and abnormalities (organ degeneration) as one of the top networks associated in genes specific to 101LL fibril response. Genes were predominantly down-regulated suggesting this was possibly a protective response associated with 101LL cultures.

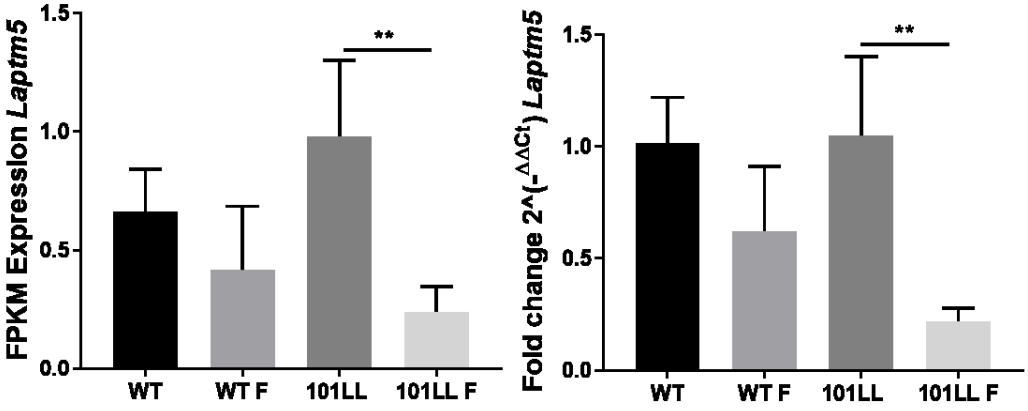

Figure 6.17: Lysosomal protein transmembrane 5 (*Laptm5*) expression changes after fibril challenge were validated by RT-qPCR. Relative expression values and RT-qPCR results are shown from *in vitro* unchallenged and fibril-challenged cultures. Expression values obtained from RNA-seq matched with RT-qPCR results validating transcriptomic expression showing *Laptm5* to be significantly down-regulated in 101LL fibril-challenged cultures (P-Value 0.004), and no change was reported in WT groups (P-Value 0.17). Reference gene *Ywhaz*, Graph mean plus standard deviation, n=4, n=individual samples, unpaired t test. Fold changes from RT-qPCR were calculated using 2-ΔΔCt method (Materials and Methods, 2.5.8) and Fragments Per Kilobase of transcript per Million (FPKM) values were obtained from RNA-seq data.

6.3.9 Generic gene responses to fibril insult provide therapeutic targets for impeding neurodegeneration

Generic fibril responses were evident between WT and 101LL cultures and were expected as baseline transcriptomic data indicated WT and 101LL genotypes were comparable (Table 6.1). Identifying specific genes associated with these generic responses would be advantageous for identify potential therapeutic targets for modulating neurodegenerative processes. Thus, 343 DEGs shown in *Figure 6.16*, were investigated and initial analysis showed 342 genes shared similar up and down-regulated profiles between genotypes although variations were noted in FC. Purinergic receptor P2Y, G-protein coupled, 14 (*P2ry14*) was the individual gene which was up-regulated in the WT fibril-challenged group (LogFC 1.65, FC 3.14, FDR 0.04) but down-regulated in the 101LL group (LogFC -1.71, FC 0.30, FDR 0.01) validated by RT-qPCR (*Figure 6.18*). *P2ry14* is expressed in immune, cardiovascular, digestive, endocrine and respiratory systems and is involved in immune system processes and response to stimulus and signalling. This gene may also play a role in neuroimmune function and may therefore, be stimulating a positive immune response in WT cultures whilst damping this response in 101LL cultures. Other genes of interest identified after fibril challenge and common to both genotypes included; Triggering receptor expressed on myeloid cells 2 (*Trem2*), SRY-box 7 and 10 (*Sox7*, *Sox10*), Solute carrier family 9 member b2 (*Slc9b2*) and Neurotrophic receptor tyrosine kinase 1 (*Ntrk1*) which were all up-regulated. Briefly *Trem2* (WT LogFC 2.56, FC 5.88, FDR 0.008 and 101LL LogFC 2.28, FC 4.86, FDR 0.02) is involved in phagocytic and anti-inflammatory pathways (Zhong et al. 2017), *Sox7* (WT LogFC 2.23, FC 4.69, FDR 0.001, 101LL LogFC 1.44, FC 2.71, FDR 0.01) is involved in promoting neuronal apoptosis (Wang et al. 2015), *Sox10* (WT LogFC 4.97, FC 31.44, FDR 1.46E-05 and 101LL LogFC 2.40, FC 5.30, FDR 0.03), is involved in development of glia (Kuhlbrodt et al. 1998) and as shown here was substantially up-regulated in WT cultures.

Slc9b2 (WT LogFC 2.68, FC 6.40, FDR 3.79E-05 and 101LL LogFC 2.07, FC 4.22, FDR 0.004), plays a role in clathrin-mediated endocytosis and *Ntrk1* (WT LogFC 3.59, FC 12.06, FDR 2.34E-05 and 101LL LogFC 2.32, FC 5.01, FDR 0.01) is essential for development and survival of neurons (Kaplan and Miller 2000) and was noticeably more up-regulated in WT cultures (both genes *Slc9b2* and *Ntrk1* validated RT-qPCR *Figure 6.19*). For down-regulated genes, Tumor necrosis factor (*Tnf*) (WT LogFC -3.21, FC 0.10, FDR 0.02 and 101LL LogFC -6.48, FC 0.01, FDR 0.009) which is involved in cell death apoptosis was substantially down-regulated in 101LL cultures (See Discussion 6.4, validated by RT-qPCR, *Figure 6.20*). Complement C3a receptor 1 (*C3aR*) (WT LogFC -1.14, FC 0.45, FDR 0.03 and 101LL LogFC -2.35, FC 0.19, FDR 0.001) is expressed in the central nervous system by neurons, reactive astrocytes and microglia (Rynkowski et al. 2008) and is involved in neuroprotection (van Beek et al. 2001). *C3a-C3aR* interactions are also a positive regulator of neurogenesis (Rahpeymai Bogestål et al. 2007). *C3aR* was down-regulated after fibril challenge in both 101LL and WT cultures suggesting neuroprotection response in both genotypes was reduced. Although generic DEGs were identified in both genotypes after fibril challenge, expression values did vary between genotypes for example, *Sox10* had a FC of 31.44 in WT fibril-challenged cultures as opposed to FC 5.30 in 101LL fibril-challenged cultures. Studies have shown *Sox10* involvement with the development of glial cells (Weider and Wegner 2017; Kuhlbrodt et al. 1998) and astrocyte differentiation (Kordes and Hagel 2006). Thus, WT fibril-challenged cultures were inflicting a greater glial response in comparison to 101LL cultures. Interestingly, immunolabelling studies shown in Chapter 5 (*Figure 5.4*), have also confirmed a dramatic change in astrocytic morphology in WT fibril-challenged cultures suggesting *Sox10* may also be playing a role in regulating astrocytic cellular response to fibrils. In conclusion, up-regulation of genes associated with endocytosis, phagocytosis, neuron development and survival was occurring in both genotypes respectively and therefore, may provide possible therapeutic targets for impeding neurodegeneration.

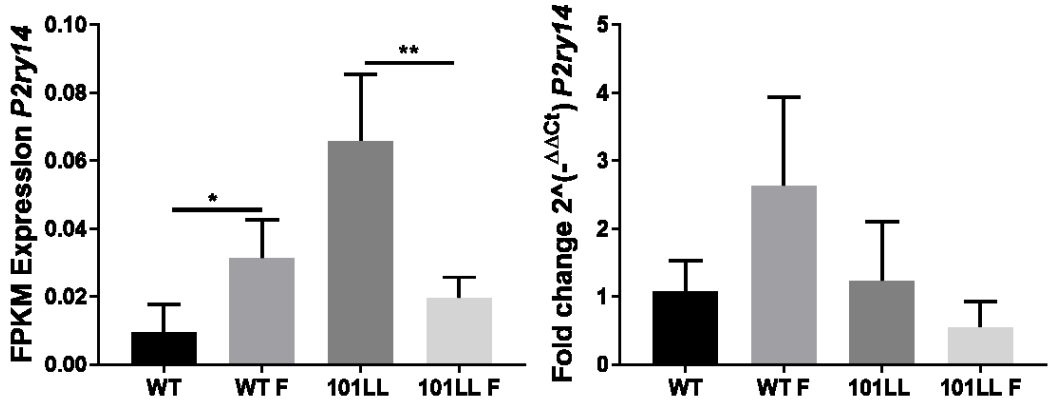

Figure 6.18: Purinergic receptor P2Y, G-protein coupled, 14 (*P2ry14*) expression changes after fibril challenge were validated by RT-qPCR. Relative expression values and RT-qPCR results are shown from *in vitro* unchallenged and fibril-challenged cultures. Expression values obtained from RNA-seq generally matched with RT-qPCR results validating transcriptomic expression however, significant differences were not evident between groups (P-Value 0.06; 0.20). Reference gene *Ywhaz*, Graph mean plus standard deviation, n=4, n=individual samples, unpaired t test. Fold changes from RT-qPCR were calculated using 2-ΔΔCt method (Materials and Methods, 2.5.8) and Fragments Per Kilobase of transcript per Million (FPKM) values were obtained from RNA-seq data.

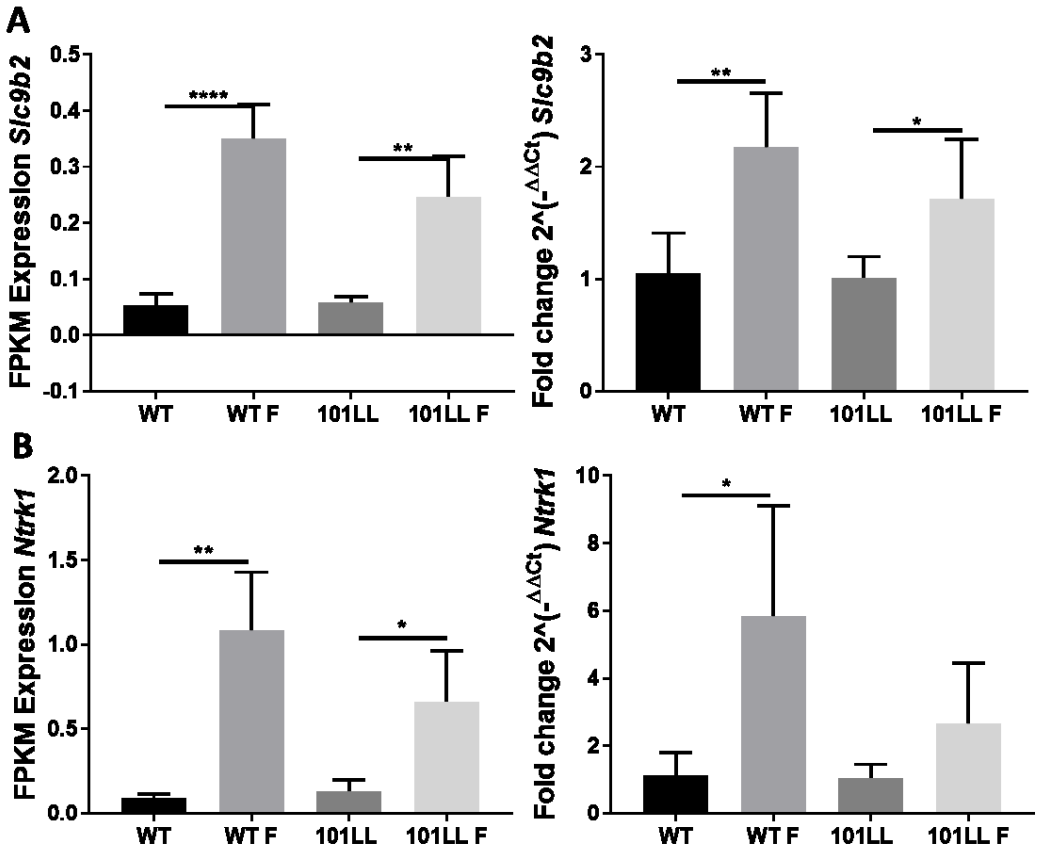

Figure 6.19: Validation of generic genotype responses by RT-qPCR. Relative expression values and RT-qPCR results are shown from *in vitro* unchallenged and fibril-challenged cultures. (A) Solute carrier family 9 member b2 (*Slc9b2*) and (B) Neurotrophic receptor tyrosine kinase 1 (*Ntrk1*). Expression values obtained from RNA-seq generally matched with RT-qPCR results validating transcriptomic results. (A) *Slc9b2* expression was confirmed to be significantly up-regulated in both genotypes (P-Values 0.009; 0.04). (B) *Ntrk1* expression was significantly up-regulated in WT fibril-challenged cultures (WT F) (P-Value 0.02) however, in 101LL fibril-challenged cultures it was up-regulated but not significantly (P-Value 0.13). Reference gene *Ywhaz*, Graph mean plus standard deviation, n=4, n=individual samples, unpaired t test. Fold changes from RT-qPCR were calculated using 2-ΔΔCt method (Materials and Methods, 2.5.8) and Fragments Per Kilobase of transcript per Million (FPKM) values were obtained from RNA-seq data.

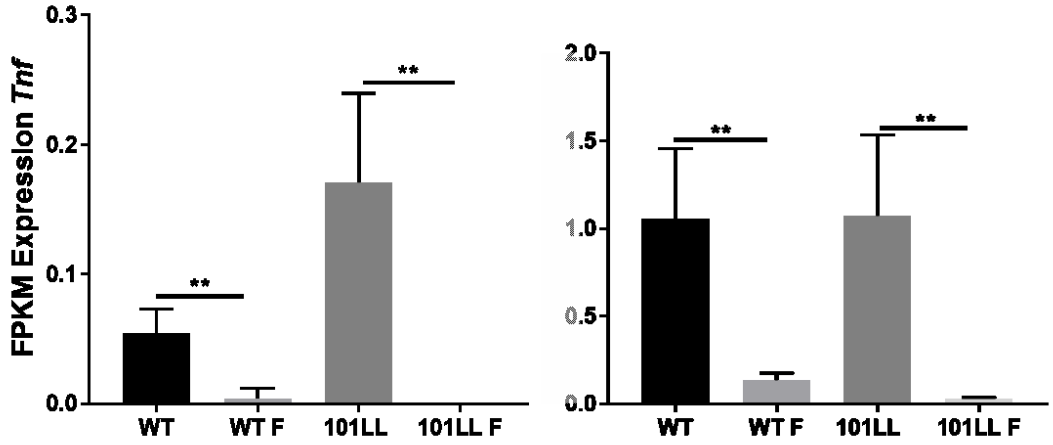

Figure 6.20: Tumor necrosis factor (*Tnf*) expression changes after fibril challenge were validated by RT-qPCR. Relative expression values and RT-qPCR results are shown from *in vitro* unchallenged and fibril-challenged cultures. Expression values obtained from RNA-seq matched with RT-qPCR results validating transcriptomic expression (P-Values 0.003; 0.004). Reference gene *Ywhaz*, Graph mean plus standard deviation, n=4, n=individual samples, unpaired t test. Fold changes from RT-qPCR were calculated using 2-ΔΔCt method (Materials and Methods, 2.5.8) and Fragments Per Kilobase of transcript per Million (FPKM) values were obtained from RNA-seq data.

6.3.10 Alternative platforms for investigating fibril response in WT and 101LL cultures

Miru software was used as an alternative platform to understand and visualise the different gene expression trends across all datasets in a non-bias manner and was used here as an alternative platform to gain insights into fibril response in WT and 101LL fibril-challenged cultures. As shown in *Figure 6.21,* genes up-regulated in WT fibril-challenged cultures only (53 genes, Cluster 0064) were enriched for GO terms using DAVID, as this platform works well with larger DEG lists. GO enrichment for biological processes confirmed associations with regulation of protein localisation to cell surface and ER-associated misfolded protein catabolic processes, which, are involved in breaking down misfolded proteins by targeting them to cytoplasmic proteasomes for degradation. These data provide insights into how WT mice may be more efficient at curtailing abnormal protein misfolding than 101LL. No clusters were identified in WT fibril-challenged cultures involving down-regulated genes. Genes predominantly up-regulated in 101LL fibril-challenged cultures (*Appendix Figure 6.d*), were associated with phosphorylation GO enrichment processes. Interestingly, studies have shown post-translational modifications such as phosphorylation are known to induce protein conformational changes (Giannopoulos et al. 2009) and therefore this response may be an indicator of more protein conformational changes occurring in 101LL fibril-challenged cultures. Genes down-regulated in 101LL fibril-challenged cultures were enriched for response to stimulus complementing previous reported data generated from PANTHER enrichment (Section 6.3.7). Miru identified Cluster 0001 (791 genes) and Cluster 0002 (262 genes) which were associated with up-regulated genes in both WT and 101LL fibril-challenged cultures (*Appendix Figure 6.e*). DAVID enrichment for Cluster 0001, confirmed associations with glycolytic processes, metabolic processes, synaptic transmission, apoptosis and response to stimulus. Cluster 0002 associations included response to mechanical stimulus, response to drug, apoptosis and nervous system development.

Genes associated with similar functions such as apoptosis and neuron and glia development were identified previously in Section 6.3.9, supporting observations here. Down-regulated clusters of genes identified in both WT and 101LL fibril-challenged cultures were associated with inflammatory response, immune response, endosomal transport and endocytosis (data not shown). It should be highlighted Miru software incorporates a complex pattern recognition algorithm which groups genes based only on expression profile and therefore does not take parameters such a P-Value into account however, similarities in results gained from Miru and DAVID analysis were evident when comparing to previously described results obtained from IPA and PANTHER platform analysis suggesting all observations reported here were genuine and provide additional non-bias insights in fibril responses in both genotypes. As a vast amount of data was generated from IPA, Miru, PANTHER and DAVID analysis a summary of results was constructed as shown in Figure *6.22*.

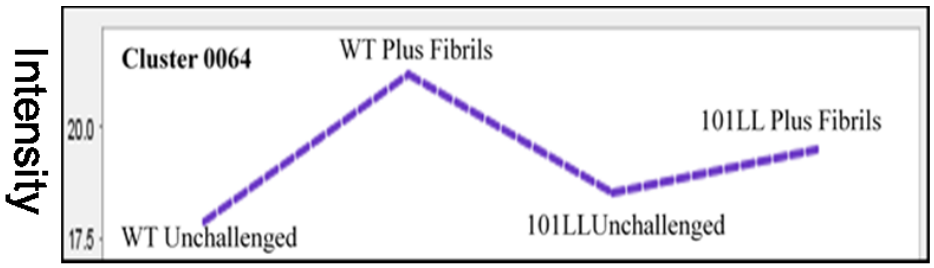

DAVID GO enrichment (Biological Process)	Gene count	P-Value
Regulation of protein localisation to cell surface	2	1.8E-2
ER-associated misfolded protein catabolic process	2	2.0E-2
Dopamine receptor signalling pathway	2	2.6E-2
Arachidonic acid secretion	2	3.5E-2
Antigen processing and presentation of peptide antigen via MHC class 1	2	5.6E-2
Positive regulation of cell-substrate adhesion	2	7.7E-2

Figure 6.21: Miru and DAVID analysis of RNA-seq data. Cluster 0064 was identified in Miru and genes associated with this cluster were up-regulated in WT fibril-challenged cultures only in comparison to other groups. Readings based on mean counts per million (normalised expressed intensity values). Class viewer scaling was raw, class plot was mean line. GO enrichment for Cluster 0064 (53 genes) using DAVID showed WT fibril-challenged cultures were associated with protein localisation and ER-associated misfolded protein catabolic processes. This biological process is associated with chemical reactions and pathways resulting in the breakdown of misfolded proteins, which are then transported from the endoplasmic reticulum and targeted to cytoplasmic proteasomes for degradation. Genes involved in this process were protein-O-mannosyltransferase 2 (*Pomt2*) and torsin family 1, member A (*Tor1a*).

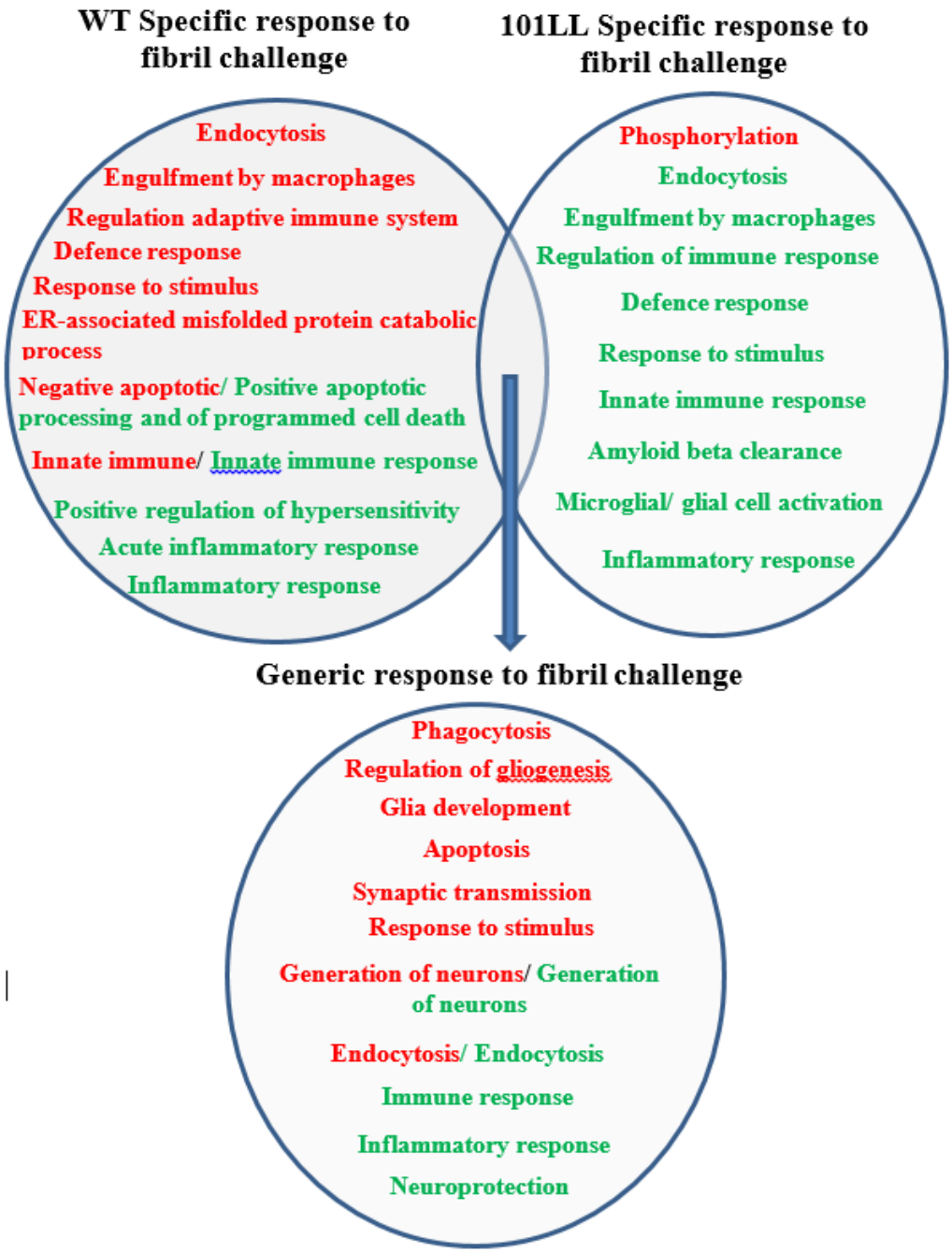

Figure 6.22: Summary of IPA, Miru, PANTHER and DAVID molecular analysis of DEGs lists associated with specific and generic genotype responses to fibril challenge. Gene associations and GO enrichment for up-regulated genes are shown in red text, down-regulated genes in green. Additionally, as shown in *Figure 6.14*, top 50 DEGs, astrocyte differentiation and proteolysis was associated with up-regulated genes in WT fibril-challenged cultures and nervous system development, neuron migration and axon guidance with up-regulated genes in 101LL fibril-challenged cultures.

6.4 Discussion

The overall aim of this study was to investigate gene expression responses to fibril challenge in both WT and 101LL genotypes to ascertain insights into how one model supports protein misfolding whilst the other curtails it. Initial transcriptome investigations pre-fibril challenge confirmed gene expression was comparable between genotypes in both *in vitro* and *in vivo* systems indicating the 101LL point mutation was not influencing gene expression levels. Comparison between both *in vitro* and *in vivo* systems suggested gene expression was broadly comparable between systems. Similar observations were shown by other groups (Dabrowski et al. 2003; Diaz et al. 2002) supporting the use of primary hippocampal cultures for studying protein misfolding interactions *in vitro*. In general, post-fibril challenge, WT cultures exhibited a stronger molecular response in comparison to 101LL. As summarised in *Figure 6.22*, analysis of gene expression data indicated biological processes such as endocytosis, macrophage engulfment, response to stimulus, defence response and ER-associated misfolded protein catabolic processes were enriched in WT cultures. Immunolabelling studies presented in Chapter 5 confirmed microglial engulfment of fibrils was occurring (*Appendix Figure 5.b*). As these processes appeared to support misfolded protein degradation and clearance it was concluded WT fibril-challenged cultures were responding positively and effectively to fibril challenge. These responses were not evident in 101LL fibril-challenged cultures. Reduced expression of genes associated with endocytosis, response to stimulus, amyloid clearance and microglial and glial activation were identified suggesting 101LL cultures were not responding proficiently to fibril challenge for efficient misfolded protein degradation and clearance. Again, immunological findings presented in Chapter 5 (*Figure 5.4*) supported some of these findings whereby no evidence of astrocytic activation in 101LL cultures was shown indicating, either a delayed response or an reduced astrocytic response as described here was occurring in 101LL fibril-challenged cultures.

The innate immune system has been mentioned throughout this chapter and is involved in the detection and clearance of invading microorganisms, senescent cells and aged proteins in the brain therefore, maintaining a healthy environment for both neuronal and glial cells. This immune response was predominantly associated with an increased expression of genes in WT fibril-challenged cultures suggesting this was a positively activated defence system in WT cultures, however a minority of genes associated with the innate immune response were also showing reduced gene expression, namely C3 and C5 (Table 6.6, 6.7). Complement factors are involved in neurogenesis, cell survival, cell death, synapse remodeling (Shinjyo et al. 2009; Ren et al. 2008; Stevens et al. 2007) and can be locally produced in the brain. Indeed, studies have shown that neuronal and glia cells can produce complement and express complement receptors (Veerhuis, Nielsen, and Tenner 2011). In Alzheimer's disease β-amyloid can induce complement activation by binding to C1q which promotes either neuroprotection or neurotoxicity (Guan et al. 1994). When C1q binds to and coats pathogens, a protease cascade involving complement protein C3 is activated. Unwanted material can then be eliminated by deposited C3 activating C3 receptors on microglia, triggering elimination by phagocytosis, or activated C3 can trigger terminal activation of the complement cascade, which involves formation of lytic membrane attack complex resulting in cell lysis (Stevens et al. 2007). Interestingly, the role of complement factors in prion neurodegeneration within the CNS remain unclear (Hasebe et al. 2012) however, studies have proposed complement proteins such as C3 can intensify neurodegeneration in prion disease by promoting trafficking of misfolded proteins to cells expressing normal PrP^{C} which act as substrates for prion replication (Kane et al. 2017; Michel et al. 2013). In this chapter, WT cultures were shown to be responding to fibril challenge by dampening the C3 complement cascade.

In comparison, no significant changes in these complement components were identified in 101LL fibril-challenged cultures however, activated microglia in both genotypes indicated that phagocytosis of fibrils was still possibly occurring (*Appendix Figure 5.b*), suggesting complement factors may not be influencing microglial phagocytosis (*Figure 6.22*). Collectively, these studies suggest complement processes were reduced in WT fibril-challenged cultures, possibly to limit trafficking of fibrils for prion replication and thus may be neuroprotective. These responses also identify specific targets for future therapeutic intervention studies.

Transcriptome analysis (validated by RT-qPCR, *Figure 6.17*) identified reduced expression of the gene *Laptm5* in 101LL fibril-challenged cultures. This gene is associated with lysosome organelles suggesting endolysosomal processing may be reduced in 101LL cultures. Additionally, studies have shown high *Laptm5* expression levels are associated with an increase in lysosomal activity of microglial cells (Williams et al. 1994). As gene expression was confirmed to be reduced in 101LL fibril-challenged cultures, it can be concluded a dampening of lysosomal processing and therefore fibril degradation was evident in 101LL cultures which was also supported by immunological findings presented in Chapter 5 (*Figure 5.9*). Miru analysis identified ER-associated misfolded protein catabolic processes to be associated with up-regulated genes in WT fibril-challenged cultures only (*Figure 6.22*). This was an important finding as this response was specific to WT fibril-challenged cultures and involves targeting misfolded proteins to cytoplasmic proteasomes for ER-associated degradation (Smith, Ploegh, and Weissman 2011). Conversely, phosphorylation processes were identified to be up-regulated in 101LL cultures (*Appendix Figure 6.d*) in response to fibril challenge and are known to induce protein conformational changes (Giannopoulos et al. 2009). Interestingly, recent studies have also shown synaptic activity is highly regulated by phosphorylation of PSD-95 (Pedersen et al. 2017) and as described in Chapter 5 (*Figure 5.5*) PSD-95 was significantly reduced in 101LL fibril-challenged cultures.

An increase in phosphorylation suggested 101LL neurons might be actively trying to maintain synaptic activity after fibril insult and PSD-95 maybe a vulnerable target for fibril proteins in 101LL neurons. From this data, it can be concluded fibrils elicited different responses in both genotypes; WT cultures appeared to be actively processing fibrils for degradation whereas the 101LL cultures seemed to be damping degradative processes possibly supporting fibril survival.

Genes common to both genotypes were identified after fibril challenge however, differences in FC values were noted for example, increased expression of *Ntrk1* was evident in both genotypes however, WT cultures had a FC of 12.06 in comparison to 101LL cultures that had a FC value of 5.01. RT-qPCR validated these observations (*Figure 6.19*) and indicated increases were only significant in WT fibril-challenged cultures. *Ntrk1* is essential for the regulation, growth, development, survival and repair of neurons mediated through binding to its primary ligand, nerve growth factor which regulates a number of signalling cascades such as GRB2-Ras-MAPK and Ras-PI3 kinase-AKT1 (Kaplan and Miller 2000). Post-mortem studies in brains from patients diagnosed with early stage Alzheimer's disease (AD) have also shown *Ntrk1* expression is reduced in basal forebrain cholinergic neurons, indicating downregulation of this gene contributes to the loss of neurons and early onset of AD (Counts and Mufson 2005). As *Ntrk1* expression was increased in both WT and 101LL fibril-challenged cultures (more so in WT) it can be concluded this generic response was supporting neuronal survival after fibril challenge. *Tnf* was down-regulated in both genotypes and more so in 101LL cultures (FC WT 0.10, 101LL 0.01), validated by RT-qPCR (*Figure 6.20*). *Tnf* gene encodes a multifunctional proinflammatory cytokine expressed predominantly by immune cells and is involved in immune response and inflammation, proliferation, differentiation and apoptosis (Malagoli 2016) however, the function of *Tnf* signalling in the hippocampus and cortex has not been fully elucidated (McCoy and Tansey 2008).

Some studies have shown *Tnf* regulates hippocampal neuronal development (Golan et al. 2004) and others have shown *Tnf* potentiates excitotoxicity directly through activation of glutamate-NMDA receptors (Zou and Crews 2005) and indirectly by inhibiting glial glutamate transporters on astrocytes (Choi 1988). *Tnf* signalling has also been shown to enhance AD-associated pathology and is detrimental to neuronal viability (Janelsins et al. 2008). Conversely, other studies have shown mice that overexpress *Tnf* were protected from glutamate toxicity (Marchetti et al. 2004). As *Tnf* expression was suppressed in both genotypes it may be possibly this generic response was to reduce inflammatory response and excitotoxicity in both cultures (more so in 101LL cultures) as a result of fibril insult. However, more studies will have to be carried out to address the overall effect of *Tnf* suppression on neurons and other brain-resident populations, including microglia and astrocytes and may provide a possible therapeutic target for the modulation of glial response in PMDs.

The data presented in this chapter confirm primary hippocampal neuronal cultures provide a genetically comparable representative model to hippocampal tissue for the investigation of protein misfolding interactions *in vitro*. Findings based on microarray and RNA–seq analysis complimented each other and further analysis using IPA and Miru confirmed specific gene associations with each genotype. PANTHER, GOrilla and DAVID platforms provided further insights into these DEG associations. From these analyses, it can be concluded both genotypes showed specific responses to fibril challenge and GO terms obtained suggested the WT cultures were processing fibrils for possible degradation and the 101LL cultures were damping this response. These data provide insights into how WT mice are more efficient at curtailing abnormal protein misfolding and seeding than 101LL genotypes that support it. Genes associated with processes or biological pathways identified in this chapter (*Figure 6.22*), provide possible test targets to investigate in future experiments for intervention in PMDs.

CHAPTER 7

Final discussion

7.1 Summary of findings

The generation and spread of misfolded protein aggregates is common to all PMDs however, the early mechanisms underpinning the apparent perturbations in protein handling and processing in such conditions remain poorly understood. The main aim of this thesis was to investigate the initial mechanisms associated with cellular processing and response to abnormal PrP fibrils using an *in vitro* model composed of neuronal and non-neuronal cell types derived from transgenic mouse lines that either support amyloid seeding and formation (101LL) or prevent its production (WT). Both histological and molecular techniques were used to monitor cellular responses to fibril challenge including visualisation of cellular interactions with fibrils, intracellular fibril trafficking and gene expression changes induced by fibril challenge. To address the hypothesis that WT and 101LL mice have different mechanisms of intracellular processing of abnormal protein that determine clearance versus the seeding of amyloid plaques, a range of objectives listed in Chapter 1 (Section 1.6.1), were carried out and completed.

7.1.1 Primary cultures are viable models to track early cellular processing of misfolded protein

Primary hippocampal neuronal cultures were developed and characterised at a morphological (*Figure 3.3, 3.6, 3.10*), biochemical (*Figure 3.15*), and immunocytochemical level (*Figure 3.4, 3.8, 3.14*). These analyses showed cultures contained readily accessible neurons (*Figure 3.4, 3.5*) that developed into highly branched mature networks connected by synapses as indicated by the presence of both pre and post-synaptic proteins (*Figure 3.12*). Cultures also supported the growth and development of non-neuronal cells such as astrocytes (*Figure 3.9*) and microglia (*Figure 3.11*) and were stable for up to twenty days *in vitro* (*Appendix Figure 3.b*). Characterisation of cultures provided baseline profiles of neuronal and glial cell population interactions pre-fibril challenge.

Understanding cellular composition and baseline characteristics of primary cultures was crucial to determine changes induced by fibril challenge. In order to study cellular responses to misfolded fibril protein, highly pure recombinant PrP fibrils were produced (*Figure 4.4*), characterised (*Figure 4.7*) then fluorescently labelled (*Figure 4.8*) which allowed direct visualisation of fibril protein trafficking and interactions in mixed cellular populations which was crucial to understanding the mechanisms involved in cellular responses to misfolded protein insult. In conclusion, primary cultures along with fluorescently labelled fibrils provided essential tools for investigating the intricacy of early misfolded PrP interactions with neuronal, astrocytic, microglial and synaptic populations in cultures from both WT and 101LL genotypes.

7.1.2 Cultures challenged with labelled fibrils mimicked neurodegenerative pathogenic events

Typical neurodegenerative features associated with abnormal protein misfolding in the brain include neuro-inflammation in the form of reactive astrocytes, activated microglial and synaptic alternations (B. Martin 1999). Exogenous fibrils added to culture interacted with neurons and PrP^C protein (*Figure 5.2*) in both 101LL and WT cultures without inducing neuronal loss (*Figure 5.1*) over a 24-hour exposure period indicating fibril concentrations used were not neurotoxic at this concentration and exposure time. Fibrils were internalised by cells and were processed via the endolysosomal pathway (*Figure 5.6, 5.7*). These processing mechanisms appeared to be functional in WT cultures (*Figure 5.8*) but were impaired in 101LL cultures (*Figure 5.9*). Microglial activation and possible phagocytosis of fibrils was evident in both genotypes (*Appendix Figure 5.b*). Hypertrophic astrocytes were evident only in WT fibril-challenged cultures (*Figure 5.4*) indicating differential glial responses were occurring between genotypes.

Fibrils localised to synapses in both genotypes however, a significant reduction in post-synaptic marker PSD-95 occurred only in 101LL cultures suggesting 101LL neurons were more susceptible to synaptic loss than WT. In agreement with these data, PSD-95 was reduced in the brains of AD patients (Yuki et al. 2014) and in mouse models of HD (Smith et al. 2014) suggesting PSD-95 may be a vulnerable target associated with many PMDs which will be discussed further in Section 7.2.3. Collectively, these results confirm that exogenously challenged fibrils interacted with all hippocampal derived cell populations resulting in genotype-specific differences in intracellular processing and cellular response to fibrils that may be related to susceptibility to disease pathology in PMDs.

7.1.3 Differential gene expression in response to fibril challenge

Comparison of baseline transcriptomic profiles obtained pre and post-fibril challenge showed an increase in expression of genes in WT cultures associated with endocytosis, macrophage engulfment, immune and defence response and ER-associated misfolded protein catabolic processes none of which were induced in 101LL fibril-challenged cultures (*Figure 6.22*). This suggests the dysfunction of multiple mechanisms may be associated with an inability to clear misfolded protein in the disease context and highlight targets to investigate further for intervention in PMDs. A decrease in expression of genes in 101LL cultures associated with endocytosis, amyloid clearance, an inability to respond to exogenous stimulus and activation of glial support cells suggested all these processes were reduced in 101LL fibril-challenged cultures (*Figure 6.22*). These data suggested 101LL cultures were not efficiently detecting and responding to fibril challenge for efficient misfolded protein degradation and clearance. Collectively these changes in gene expression in both genotypes support the hypothesis that differences in the initial processing of abnormal protein between WT and 101LL mice determine whether abnormal protein is cleared or is seeded as fibril amyloid.

7.2 Highlights of the research and future investigations

7.2.1 Primary hippocampal neuronal model and alternative systems

Primary neuronal cultures are one of the most important models used for performing advanced research in different PMDs (Schonfeld-Dado and Segal 2009), and complete characterisation of these models at baseline is essential to gain accurate information on neurodegenerative-associated processes. Unfortunately, numerous studies using these models to investigate neurodegeneration focus on the initial neuronal culture preparation procedures and fail to fully characterise the resulting cultures (Seibenhener and Wooten 2012; Beaudoin et al. 2012; Kaech and Banker 2006) or perform limited culture characterisation studies (Ray et al. 2009). In contrast, in this study, cultures were characterised at a morphological and histological level using antibodies to detect neurons (MAP2), astrocytes (GFAP), PrP^C (6H4, 7A12), microglia (Iba1, CD11b) and pre and post-synaptic markers (PSD-95, Synapsin 1) to profile factors crucial in analysing cellular response to challenge with misfolded protein including cellular composition, synaptic maturity and host PrP^C interactions. The primary hippocampal neurons developed here were highly branched neuronal networks connected via synapses and supported by both astrocytic and microglial populations. IMARIS reconstructions of these mixed cell cultures (*Figure 3.5, 3.6, 3.10, 3.11)* provided unique insights into the cellular morphologies of these cell types whilst providing baseline cellular profiles on proportions of neuronal, astrocytic, PrP^C and synaptic proteins (*Figure 3.12, 3.14*) present in WT and 101LL cultures pre-fibril challenge.

Advances in primary neuronal cultures include using agarose hydrogels (Bellamkonda et al. 1995) or most recently other matrices such as elastomeric scaffolds that are able to instruct 3D growth of primary neurons (Bosi et al. 2015) or starPEG-heparin-based hydrogels that promote proliferation of primary neuronal stem cells (Papadimitriou et al. 2018).

The recreation of 3D neuronal circuits *in vitro* is advantageous as it represents a more physiologically normal preparation of cultures including supporting glial cells that can be used for neurodegenerative related studies (Smith et al. 2015). As described in Chapter 3, IMARIS reconstructions of primary cultures (*Figure 3.5*) highlighted some 3D properties were maintained however; cultures were still primarily 2D or monolayer. GSS disease has already been modelled using adult murine stem cells infected with prion brain homogenate in 3D cultures and biochemical changes related to prion pathology were induced within 2-3 weeks in culture suggesting 3D cultures would provide a suitable physiological competent model of prion related neurodegeneration (Collins and Haigh 2017). However, these cultures were free-floating neurospheres (clusters of neural stem cells) and are associated with some major drawbacks, such as sensitivity to culturing methods used where variations in cell density can affect proliferation capacity (Tropepe et al. 1999). Media constituents or concentrations of factors in the media (Irvin et al. 2003; Arsenijevic et al. 2001), frequency and number of passages after isolation (Caldwell et al. 2001) also lead to differences in cellular composition and properties between individual neurospheres. Due to these sensitivities and variations, it can often be difficult to consolidate data from different groups (Parmar et al. 2002) or even interpret results within the same study (Eriksson, Bjorklund, and Wictorin 2003) to make comprehensive conclusions. The primary cell culture model presented in this thesis did not require any cell passage, is well established and contains distinct neuronal, astrocyte and microglial cellular populations and therefore provided a more robust model for studying neuronal and non-neuronal interactions *in vitro*.

3D cultures have previously been used to study mechanisms of AD pathogenesis due to the lack of relevant models that recapitulate all AD related features (Park et al. 2018). Researchers used a microfluidic device containing a 3D culture of human neurons (overexpressing APP with familial AD mutations) and glial cells was developed which displayed AD like pathology including beta-amyloid aggregation, phosphorylated tau accumulation and neuroinflammatory activity. This provided a model that can systematically recapitulate multistage intracellular interactions in human AD brains whilst providing insights into mechanistic neuronal-glial interactions related to AD pathogenesis. One limitation of this study was that it used immortalised neuronal precursor cells and microglial cells and therefore these cells did not accurately replicate the primary cells found *in vivo*. Overall, although 3D cultures appear more physiological relevant than 2D cultures, these models can be cumbersome, time-consuming and require specialised equipment unlike 2D models which are well established, require basic equipment and are easier to set-up.

Induced pluripotent stem cell (iPS) cell technology pioneered by Yamanaka's lab in 2006 is an another method for generating *in vitro* models of neurodegenerative diseases. This method involves the introduction of four specific genes encoding transcription factors that convert adult cells into pluripotent stem cells (Shi et al. 2017; Takahashi and Yamanaka 2006). Therefore, iPS cell technology can be used to generate *in vitro* models of disease-relevant cells reprogrammed directly from accessible tissues from living patients whereas neuronal stem cells have to be obtained post-mortem. This technology was applied to prion studies where iPS cells derived from somatic cells (dermal fibroblasts) from a human GSS case were differentiated into neuronal and non-neuronal cells (Matamoros-Angles et al. 2018). Although iPS cells were unable to spontaneously generate a human prion disease, cultures did show relevant prion disease associations such as astrogliosis, p-Tau and cell death, mostly recapitulating some of the neuropathological features reported in the donor patient.

These results show iPS cell technologies will be useful for future human associated neurodegenerative disease studies. Indeed, iPS cells have been generated from patients with AD (Muratore et al. 2014), PD (Schondorf et al. 2014), HD (Jeon et al. 2012) and ALS (Zhang et al. 2015). Although iPS cell technologies are widely used and can model human genetic diseases they are associated with low reprogramming rates and formation of genetic mutations and or tumours which are some of the disadvantages related to this cell reprogramming technology. Overall iPS cells are useful for investigating pathology associated with specific human disease gene alterations but not so useful for studying generic mechanisms common between diseases.

An alternative *in vitro* model that offers a three-dimensional system for studying cellular functions in a controlled environment is brain organotypic slice cultures (BOSCs). These models are easily accessible and retain tissue architecture along with functional synaptic circuitry and therefore are used to study many neurodegenerative diseases (Harwell and Coleman 2016; Novotny et al. 2016; Wolf et al. 2015; Falsig et al. 2012; Falsig et al. 2008; Duff et al. 2002; Bruce, Malfroy, and Baudry 1996). BOSCs were developed during this thesis (Supplementary Chapter 8) and characterisation results highlighted organotypic slices were susceptible to stretching and degradation (*Figure 8.2-8.4*), microglial activation (*Figure 8.5*) and astrocytic scarring (*Figure 8.9*) pre-fibril challenge and therefore were deemed unsuitable models for studying cellular interactions of abnormal fibril protein *in vitro*.

7.2.2 Analysis of transcriptional differences between *in vivo* tissue and *in vitro* cultures

A major finding in this thesis showed that primary hippocampal cultures and acutely dissected hippocampal tissues were broadly comparable based on gene expression profiles obtained from transcriptomic analysis (*Figure 6.7, 6.10*). These comparisons of both *in vitro* and *in vivo* systems were novel and confirmed primary cultures would provide a suitable *in vitro* model for studying abnormal protein interactions at a transcriptional level. Previous groups have attempted similar investigations however, direct comparisons between identical genotypes from both systems was not carried out and microarray data for system comparisons were obtained from separate studies, which were later combined. For example, one study focused on murine gene expression in developing hippocampus *in vivo* (Mody et al. 2001), and the second on expression profiling of primary hippocampal neurons undergoing differentiation *in vitro* (Dabrowski et al. 2003; Diaz et al. 2002). Both were then combined for comparisons to be carried out. Although results showed *in vitro* and *in vivo* expression profiles were similar complementing findings presented in this thesis, the study was comparing primary cultures obtained from CD1 outbred mice which have more genetic diversity (Dabrowski 2003) with hippocampal tissue from C57BL/6 inbred mice which are almost genetically identical (Mody 2001). Therefore, these studies did not represent an accurate comparison of *in vitro* and *in vivo* systems. A more recent study using a similar approach (combining two separate studies) described both similarities and differences of biological processes between neural cells grown *in vitro* and *in vivo* (LoVerso, Wachter, and Cui 2015). However, these results were based on rat neural cells obtained from commercial sources (*in vitro*) compared to mouse acutely purified neural cells (*in vivo*), so involved studying cross-species transcriptomic comparisons. Therefore, although *in vitro* and *in vivo* system comparisons have been carried out previously, the studies were limited.

In this thesis, novel direct comparisons between both genotypes and systems were carried out and although some DEGs were identified between both system comparisons (*Figure 6.7, 6.10*) biologically, no major differences were identified suggesting both systems were broadly comparable. These data highlighted primary hippocampal cultures would provide a realistic neuronal cell model for studying misfolded protein interactions *in vitro* at a transcriptional level.

7.2.3 Specific targeting of synapses in 10LL derived neuronal cultures

A major obstruction in studying prion neurotoxicity has been the lack of amenable model systems in which changes associated with degeneration can be studied in cell culture and the mechanisms by which prions cause toxicity are still poorly understood. Increasing evidence points to synapses as the site where AD, PD and HD pathology begins. In these studies, primary hippocampal cultures presented relatively early pathogenic events (24 hours, *Figure 5.5*) in response to fibril challenge. PSD-95 was significantly reduced in 101LL fibril-challenged cultures however, this decrease did not induce neurotoxicity at this time point. These data support previous findings in *in vivo* models showing the hippocampus is a target area associated with early synaptic loss in prion diseases which also precedes neuronal decline (Hilton et al. 2013). It is interesting to note that fibrils were interacting with neurons in both WT and 101LL cultures (*Figure 5.2*), but only causing a decline in post-synaptic proteins in those derived from the 101LL genotype suggesting the 101LL mutation induced specific vulnerability to the post-synapse after fibril challenge. Indeed, although the precise function of PrP^{C} is unknown one of the proposed roles is maintenance of synapses (Brown 2003), and it may be possible the 101LL mutation reduces this function resulting in increased vulnerability to misfolded protein pathological effects. Future studies using additional synaptic markers could examine if synapses were actually degenerating or were just losing PSD-95 proteins.

Additionally, during synaptic pruning microglia actively engulf synaptic material (Paolicelli et al. 2011), however, this was shown in developmental brain studies and it is currently unknown if synaptic material found within microglia is due to active pruning or due to debris clearance from degenerated synapses, and these interactions could also be a focus for future investigations. Fibril-induced loss of PSD-95 may be associated with the binding of fibrils to PrP^C on target neurons, as cell-surface PrP^C was expressed along dendrites and can act as a receptor for abnormal PrP (*Figure 5.2*), which then may elicit a toxic signal or result in dendritic damage. Transcriptomic analysis of WT and 101LL fibril-challenged cultures identified an increase in gene expression associated with phosphorylation in 101LL fibril-challenged cultures (*Figure 6.22*). Phosphorylation processes are known to be involved in protein conformational changes (Giannopoulos et al. 2009) and therefore this response in 101LL fibril-challenged cultures may be an indicator that more protein conformational changes were occurring in 101LL cultures possibly resulting in a toxic decline in PSD-95. Interestingly, it has also been shown that synaptic activity is highly regulated by phosphorylation of PSD-95 (Pedersen et al. 2017). Therefore promoting phosphorylation processes in 101LL fibril-challenged cultures could be a cellular response to loss of PSD-95 by actively trying to maintain synaptic activity after fibril insult. Alternatively, phosphorylation could be inducing PSD-95 loss. Further studies are required to definitively determine the association between increased phosphorylation and synaptic loss in 101LL fibril-challenged cells. Similar PSD-95 vulnerabilities and loss have also been reported in neurodegenerative diseases such as AD (Yuki et al. 2014) and HD (Smith et al. 2014), suggesting this protein is a vulnerable target associated with many PMDs and current studies have highlighted that activity and distribution of post-synaptic components may provide promising targets for the detection of subtle but measurable changes related to synaptopathy (Ghiglieri, Calabrese, and Calabresi 2018).

Remarkably, Aβ oligomer-induced loss of PSD-95 in hippocampal brain slices can be recovered using compounds such Ferruginol, Jatrophone, and Junicedric Acid isolated from medicinal plants (Zolezzi et al. 2018), again confirming a role of PSD-95 in neurodegeneration whilst highlighting potential therapeutic avenues for future research to recover or reduce synaptic decline. One limitation of this study was that synaptic images obtained using the confocal microscope were of relatively low resolution in comparison to high resolution microscopy and therefore, interactions between fibrils and pre and post-synaptic markers could not be reconstructed using specialised software for further analysis. For future studies, super-resolution microscopy as described in Chapter 5 (*Figure 5.2*), could be used to obtain higher resolution images that could then be reconstructed providing more accurate information on interactions between neurons, PrP^{C}, fibrils and synapses in primary fibril-challenged cultures. Further investigations into the mechanisms that determine why synapses are specifically targeted in 101LL neurons or why WT neurons are not vulnerable are essential for the development of new strategies for therapeutic intervention. The primary culture model used in this thesis provides an ideal system for these investigations to be carried out in a controlled, readily accessible model system.

7.2.4 Differential responses of glia in WT and 101LL fibril-challenged cultures

Glial cells are essential for maintenance of neuronal networks and protection of neurons from toxicity (Boehler, Wheeler, and Brewer 2007; Ye and Sontheimer 1998) and studies characterising cellular composition of cultures confirmed both microglia and astrocytes were present and in surveillance mode in primary cultures pre-fibril challenge (*Figure 3.10, 3.11*). Although fibrils did not induce neurotoxicity after 24-hour challenge (*Figure 5.1*), a rapid and activated microglial response was evident in both genotypes based on phenotypical changes observed (Arcuri et al. 2017; Ling and Wong 1993).

Microglia morphology converted from extended processes indicative of surveillance mode (*Figure 3.11*) to a more rounded, ramified cell body (*Appendix Figure 5.b*) indicating a switch to activation mode which was evident in cultures from both genotypes after fibril challenge. These data are in agreement with studies showing microglia activation was detected at early stages of murine prion disease *in vivo* (Perry and Teeling 2013; Sofroniew and Vinters 2010). The localisation of fibrils with activated microglia (*Appendix Figure 5.b*), alongside a reduction in fibril size after addition to both WT and 101LL cultures (*Figure 5.3*) suggested this was a generic response to fibril insult, possibly to limit neuronal damage and promote fibril degradation through phagocytosis. Transcriptome analyses also identified an increase in expression of genes associated with phagocytosis in both genotypes (*Figure 6.22*) supporting immunocytochemical observations. These results were not surprising as microglia are capable of both engulfment and phagocytosis of Aβ fibril material (Lee and Landreth 2010). Research in our lab has previously shown activated microglia were present at the periphery of amyloid plaques in 101LL mice challenged with recombinant PrP fibrils (Barron et al. 2016), indicating microglial response to fibril insult may play a role in maintaining neuronal homeostasis as challenged animals did not reproduce a pathological phenotype of prion disease. As highlighted by Ginhoux, there is lack of relevant microglial cell model systems available for studying the mechanistic responses by which microglial activation states reduce neurodegeneration (Ginhoux 2016). The model system presented in this thesis helps bridge this gap and provides insights into how non-neuronal cell types may also play a role in maintaining neuronal homeostasis after fibril insult. Modulating these responses could provide possible therapeutic treatments to encourage the removal of abnormal proteins in all PMDs. Fibril challenge also induced differential responses in astrocyte populations. WT fibril-challenged cultures were associated with astrocyte morphology conversion from a multiple process phenotype indicative of surveillance mode (*Figure 3.10*) to a shorter and thicker cell phenotype (*Figure 5.4*) indicating a switch from surveillance to astrocytic activation was occurring in WT fibril-challenged cultures.

101LL fibril-challenged cultures displayed no astrocyte activation possibly due to a delayed or an inactivated response due to the 101LL mutation (*Figure 5.4*). In accordance with previous data, a delayed response may be more realistic as reactive astrocytes were previously shown to be present at the periphery of amyloid plaques in 101LL mice challenged with fibril recombinant PrP (Barron et al. 2016). However, these observations were only made approximately 500 days post-inoculation with fibrils, a time point where terminal disease would be reached in other prion models. This suggests astrocytes would eventually react to fibril challenge but response may be delayed in 101LL cells. Activation of reactive astrocytes is reported to reduce CNS degeneration (Sofroniew 2009, 2005; Schenk et al. 1999) suggesting reactive astrocytic cell responses in WT fibril-challenged cultures may also be neuroprotective. Other studies have indicated reactive astrocytes may contribute to neurodegeneration via a loss of normal astrocyte function resulting in reduced maintenance of neurons (Sofroniew and Vinters 2010). Studies have also shown activation of astrocytes is important in removing fibrillar amyloid from neurons and reducing plaque degradation (Wegiel et al. 2000). As astrocytes were only activated in WT fibril-challenged cultures and no reduced PSD-95 was observed in these cultures (*Figure 5.5*), there may be an association between protective responses of astrocytes to fibril challenge and reduced synaptic loss. However, further investigation would be required to determine any such role. In agreement with these findings transcriptomic analysis of fibril-challenged cultures showed increased expression of genes associated with astrocyte differentiation in WT fibril-challenged cultures (*Figure 6.14*) and an increased expression of the *Sox10* gene (Section 6.3.9). *Sox10* is reported to play a role in the development of glial cells (Weider and Wegner 2017; Kuhlbrodt et al. 1998) and astrocyte differentiation (Kordes and Hagel 2006). Increased *Sox10* expression may be an indicator of the rapid astrocytic response in WT fibril-challenged cultures. Fibrils were found to be associated with lysosomal domains in WT hypertrophic astrocytic cells (*Appendix Figure 5.d*), suggesting they were been processed for degradation.

In support of this, similar lysosomal associations were evident in studies investigating prion uptake in cultures derived from adult hamster brains (Hollister et al. 2015; Magalhaes et al. 2005). Astrocytic internalisation and trafficking of fibrils to lysosome organelles in WT fibril-challenged cultures preceded any neuropathological changes associated with fibril insult (*Figure 5.1, 5.5, Appendix Figure 5.a*). This suggested astrocytic associated activation may be an important contributor to degradation of fibrils during early stages of PMDs. Broadening our understandings of astroglial responses to abnormal protein may therefore be useful to determine future therapeutic strategies for internalisation.

7.2.5 A failure of endolysosomal control systems in 101LL fibril-challenged cultures

The lysosomal quality control pathway acts as a terminal degradative compartment of cells and is one one of the primary targets for abnormal forms of PrP to manipulate to promote abnormal protein propagation (Majumder and Chakrabarti 2017). The endolysosomal and autophagic pathways are the two main routes involved in delivering misfolded protein to lysosomes (Saftig and Klumperman 2009). Preliminary results indicated fibrils were localising with autophagic vacuoles in WT fibril-challenged cultures and no evidence of fibril localisation was noted in 101LL fibril-challenged cultures (*Appendix Figure 5.g*), indicating fibril degradation via autophagic pathways was only occurring in WT fibril-challenged cultures. However, due to time constraints, further investigations of this pathway could not be completed therefore, processing in the endolysosomal control system will be the focus of this discussion. Endolysosomal pathways have been associated with processing abnormal PrP in prion-infected human and mammalian brain tissue (Yao et al. 2013; Jeffrey et al. 2010) and aberrations in this system have also been detected in neurons from human sporadic CJD brains (Kovacs et al. 2007).

Intracellular labelling showed localisation of fibrils with both endosomes and lysosomes in WT cells (*Figure 5.6, 5.7, 5.8*) indicating a normal functional endolysosomal pathway was operative. However, localisation in 101LL cells was primarily endosomal and no localisation with lysosomes was evident (*Figure 5.9*). These data suggest malfunctions in the endolysosomal quality control system in 101LL cultures. Complementary to these results, no intra-lysosomal abnormal PrP accumulations were found in the brains of 101LL mice inoculated with recombinant fibrils as observed by electron microscopy suggesting *in vitro* observations presented here were an accurate representation of abnormal PrP processing in 101LL mice *in vivo* (Barron et al. 2016). Transcriptomic analysis further supported these results by identifying reduced expression of genes *Laptm5*, which is directly associated with lysosomal activity (Williams et al. 1994), and the gene *Ctsz*, which belongs to lysosomal cysteine proteases family involved in intercellular protein degradation (Santamaria et al. 1998), in 101LL fibril-challenged cultures (*Figure 6.17, 6.15*). These findings indicate endolysosomal processing was reduced in the 101LL genotype after fibril challenge. Previous attempts to follow abnormal PrP processing and trafficking have been carried out using primary cortical cultures from adult hamster brains (Hollister et al. 2015; Magalhaes et al. 2005), and abnormal PrP obtained from prion infected animals or recombinant PrP fibrils. These studies also showed abnormal PrP was processed via endolysosomal pathways complementing results presented in this thesis. However, these studies showed limited baseline characterisation of primary cultures and in the case of Magalhaes et al., results were primarily based on murine SN56 cell lines which are immortalised neuronal cells and therefore lack biological relevance.

Analysis of early localisation of fibrils after challenge in WT and 101LL primary cultures indicates the 101LL genotype confers a failure of lysosomal processing of abnormal protein that may be associated with reduced degradation and a propensity to accumulate misfolded protein. This impairment in the endolysosomal pathway in 101LL cultures should induce cytotoxicity over-time however, due to limited time further analysis of this pathway could not be carried out. Nevertheless, these data do indicate the endolysosomal control system was impaired in 101LL fibril-challenged cultures, and this could be a focus for future studies. Such investigations could involve examining longer fibril challenge incubation times and a more detailed analysis of endolysosomal mechanisms. For example, blocked vesicular fusion (Majumder and Chakrabarti 2015), improper loading of abnormal protein into vesicles and lysosomal associated enzymes such as cathepsins (Kovacs et al. 2007), are all of major concern in PMDs and would be useful to investigate in the 101LL model. Additionally, proteins such as Rab7 which have been identified as main regulators of membrane trafficking at late endosomes and membrane fusion of late endosomes to lysosomes could also be investigated (Modica and Lefrancois 2017). Thus, the primary fibril-challenged culture model presented in this thesis could provide a means for carrying out these investigations to gain further insights into abnormal protein degradation via regulation of endolysosomal fusion to acidic organelles.

Treatment with various compounds can be used to manipulate endolysosomal or autophagy pathways. For example, tamoxifen has been shown to modulate prion disease in infected neuronal cells, where it was reported to divert and traffic abnormal PrP to lysosomes for degradation (Marzo et al. 2013). Recently, pharmacological activation of autophagy has also been shown to favour clearance of intracellular aggregates of abnormal prion protein in an immortalised murine neuronal cell line (Thellung et al. 2018).

These pharmaceutical intervention methods could be applied to primary fibril-challenged cultures in future studies to provide insights into the effectiveness of these therapeutic treatments in a more biologically relevant model, where any beneficial findings may be applicable to other neurodegenerative conditions. Interestingly, a recent review has highlighted the endolysosomal quality control system may be one of the primary targets for disease-causing iso-forms of PrP, and may also be involved in many other neurodegenerative diseases such as AD, PD, HD and ALS and therefore these disorders are collectively referred to as “lysosomal diseases” (Majumder and Chakrabarti 2017). The data presented in this thesis support these observations that endolysosomal pathways may be important modulators of neurodegeneration whilst proving tools that can be used for future investigations into fibril trafficking pathways and lysosomal processing essential for degradation of abnormal proteins in models that support protein misfolding (101LL) or that curtail it (WT).

One aspect that could not be investigated using primary cultures which might be involved in fibril clearance *in vivo* was the glymphatic system. This system involves the flow of interstitial fluid (ISF) in the brain along basement membranes of capillaries and arteries which finally drains into the leptomeningeal arteries and cervical lymph nodes (Weller et al. 2008). This flow of ISF is essential for clearance of solutes from extracellular spaces (Abbott 2004), and studies have indicated partial ISF blockage appeared to be a possible contributer to pathology in amyloid prion disease (Rangel et al. 2013). The possibility that this blockage of fibril material or inefficient drainage of fibrils may also be occurring in 101LL mouse brains could not be addressed using primary cultures. However, for future work a number of studies could be carried out to investigate these mechanisms *in vivo* using inoculated fluorescently-labelled fibrils to provide further insights into lymphatic drainage systems associated with abnormal protein in a living brain.

7.2.6 Transcriptome insights into molecular responses of primary cultures to fibril insult

Transcriptomic comparisons between *in vivo* tissue and *in vitro* cultures has been already discussed (Section 6.2.2) and supported the use of primary cultures for studying abnormal fibril interactions *in vitro* (*Figure 6.7*). Transcriptomic analysis was also advantageous to confirm levels of astrocyte and microglial related genes were expressed at similar levels to verify cellular composition of cultures at baseline (*Figure 3.9, 3.11*). These analyses suggested a similar frequency of these cells were present in cultures from both genotypes in agreement with immunocytochemical observations (*Figure 3.14*). After fibril challenge, as discussed in Section 6.1.3, WT cultures appeared primed to respond efficiently to fibril insult, whilst 101LL cultures appeared to have an impaired or delayed response (*Figure 6.22*) supporting the hypotheses that WT and 101LL mice have different mechanisms of intracellular processing of abnormal protein that determine clearance versus the seeding of amyloid plaques. Gene expression profile changes relating to glial and endolysosomal control system responses were also discussed in Section 6.2.4 and 6.2.5 and differences between genotypes were evident and supported immunocytochemical results. Collectively, these results along with immunocytochemical analyses provided a complete multi-cellular response profile to fibril insult, which was lacking in similar investigations carried out by other groups using only neuronal cultures (Hollister et al. 2015; Magalhaes et al. 2005). These data support the original hypothesis and provide key information on pathways and cellular mechanisms involved in either clearance of misfolded protein or initiation of amyloid formation. Identifying these pathways provides a number of possible test targets with the potential of impacting diagnosis and/or intervention in PMD's such as AD, PD and prions.

Due to limited time, transcriptomic datasets obtained in these studies were not compared to previously obtained datasets obtained from genomic studies investigating differential gene expression in prion disease. For example, studies using murine models of scrapie, a prion disease in sheep (Chapter 1, Section 1.2.1, 1.2.3, 1.2.4) compared gene expression between scrapie-infected mice and mock-infected mice at both pre-symptomatic and symptomatic time points (Skinner et al. 2006). This study identified disease-associated alterations in gene expression related to endosome/lysosome functions, immunity and synapse function. Another, more comprehensive, study described by Hwang et al. (Hwang et al. 2009) compared a number of mouse and scrapie stains at different time points of TSE disease and identified changes in gene expression associated with microglial activation, reactive astrocytic gliosis and synapse loss lending support to the data gathered in *in vitro* cultures in this study. Although no direct comparisons of these scrapie datasets and fibril-challenged datasets were carried out, similar pathways identified between these studies indicated processes identified are important in neurodegeneration. Gene expression changes in a human prion-infected brain have also been determined (Tian et al. 2013) and although limited samples were included in this study, it could provide additional datasets for comparisons which would identify if gene alterations were species specific or non-specific. Cross-referencing with other transcriptome profiling studies investigating AD, PD and HD (Matarin et al. 2015; Courtney et al. 2010; Reddy et al. 2004) could additionally provide information if gene expression changes identified in prion challenged cultures were common to multiple PMDs. All studies cited were carried out using microarray analysis and therefore were subject to limiting factors such as reference information available during production and/or high signal-to-noise ratios, all of which are eliminated in the RNA-seq analysis carried out in this thesis.

7.3 Further research questions identified from this thesis

Analysis of data within this thesis provided a number of differences in cellular processing of fibrils that could explain why WT mice can clear misfolded protein whereas 101LL mice instead accumulate plaques. However, a number of research questions that warrant further investigation have also been identified during analysis of this data that due to time constraints were unable to be carried out. Some of these questions will be briefly discussed here including potential experimental methods that could be useful for future investigations.

7.3.1 Biochemical analysis of fibril-challenged cultures

It was determined that fibrils did not localise with lysosomes in 101LL fibril-challenged cultures suggesting aberrant activation of endolysosomal processing of fibrils. It may be possible that 101LL cultures were capable of biochemically modifying fibrils resulting in a lack of co-localisation in lysosomes, whilst fibrils remained intact in WT lysosomes. The investigation of the biochemical characterisation of fibrils after challenge using fluorescence gel scanning would be useful to determine if cultures were modifying fibril forms within the 24-hour challenge period. Furthermore, biochemical analysis of lysosomal crude fractions obtained from fibril-challenged cultures could be used to validate immunocytochemistry results that showed fibril localisation in WT lysosomes and no associations in 101LL lysosome organelles. Biochemical studies could also be used to investigate if abnormal PrP replication was occurring in fibril-challenged cultures. Conformational changes are thought to occur through a seeded-nucleation model where abnormal PrP acts as the template for the conversion of normal PrP^{C} to an abnormal form (Kocisko et al. 1994). Biochemical analysis could confirm if these conformational changes were occurring in fibril-challenged cultures and thus, provide further insights into seeded-nucleation and prion related neurodegeneration.

7.3.2 Optimisation of microscopy platforms

Immunocytochemical analysis of cells and protein trafficking in cultures was mainly carried out using standard 96-well plates. Although 96 well platforms were ideal to carry out multiple experiments using minimal volumes of cells and fibrils, imaging of these platforms was limited by resolution. Therefore, many images shown in Chapter 5 were obtained using unconventional methods. For example, as an oil lens could not be used with plastic plates, it was substituted with an air lens, which did produce informative images however, resolution was not optimal. Optically enhanced confocal 96 well plates were introduced at a later stage but were still not completely compatible with high magnification microscope lenses. As shown in *Figure 5.2*, when glass coverslips were used in combination with the confocal AiryScan 880, high resolution images were obtained however, these methods required higher volumes and concentrations of both cells and fibrils which were only available in limited quantities. Furthermore, the AiryScan 880 high resolution microscope was not available for the majority of these studies. For future studies, the consistent use of glass coverslips for challenge experiments along with the confocal 710 or 880 would improve image quality and resolution dramatically, allowing for more detailed analysis and co-localising experiments to be carried out regarding future fibril trafficking experiments. Live cell confocal microscopy would also be beneficial for monitoring exactly when fibrils were internalised in both WT and 101LL models in real-time.

7.3.3 Cross-seeding investigations

Studies have proposed that AD and other neurodegenerative diseases may spread through a cross-seeding mechanism which proposes seeds composed of one protein can accelerate a second misfolding process in an unrelated protein (Morales et al. 2010). Future investigations could involve challenging primary cultures with a different source of abnormal protein such as Aβ to examine these mechanisms and clarify if cellular PrP^C does act as a high-affinity neuronal receptor for Aβ (Rushworth et al. 2013). As discussed in Chapter 1 (Section 1.2.3), *Prnp*$^{-/-}$ mice are more resistant to the neurotoxic effect of Aβ oligomers than WT mice in both *in vivo* and *in vitro* models (Kudo et al. 2012), implying Aβ/PrP^C binding mediates neurotoxicity. Alternative reports showed PrP^C was capable of binding and detoxifying Aβ oligomers (Biasini et al. 2011). The primary culture model described in this thesis could be used as a tool to investigate precise mechanisms associated with PrP^C in Aβ oligomer-induced neurotoxicity.

7.4 Conclusion

Selective synaptic alternations and neuro-inflammation in the form of reactive astrocytes and activated microglia are typical features of neurodegeneration associated with abnormal protein misfolding, aggregation and accumulation in the brain (B. Martin 1999). Similar traits were evident in fibril-challenged primary cultures presented in this thesis supporting the use of these models for studying neurodegeneration and for investigating the impact of abnormal proteins which are hypothesised to be implicated in a range of neurodegenerative related disorders (Soto and Estrada 2008). During fibril challenge experiments, there was no evidence of neuronal loss suggesting that homeostatic alterations identified were all related to initial or early events that would later possibly trigger neurodegeneration.

In conclusion, the data presented in this thesis support the hypothesis that WT and 101LL mice have different mechanisms of intracellular processing of abnormal protein that determine clearance versus the seeding of amyloid plaques, whilst providing key information on cellular mechanisms and molecular pathways involved in either clearance of misfolded protein (WT) or initiation of amyloid formation (101LL). Identifying these pathways and understanding their neurodegenerative-related mechanisms provides a number of possible test targets and candidate genes with the potential of impacting diagnosis and/or intervention in PMD's such as AD, PD and prions for future investigations.

CHAPTER 8 (Supplementary)

Organotypic slice culture development and characterisation

8.1 Abstract

In vitro cell cultures provide an essential tool for gaining insights into cellular processes associated with the brain. Brain organotypic slice cultures (BOSCs) are an example of such an *in vitro* model that offers a three-dimensional system for studying cellular functions in a controlled environment. As BOSCs maintain brain cell composition and architecture these models are commonly used to study neurodegeneration *in vitro*. To investigate if this system would provide a suitable model for studying misfolded PrP protein interactions *in vitro*, brain organotypic slice cultures were established from WT, 101LL and $PrP^{-/-}$ Day 6 postnatal mouse brains. Characterisation of cell representation in these models confirmed the presence of neurons and other glial cells such as astrocytes and microglia. Astroglial cells were however shown to form atypical scarring, which enclosed the entire brain slice tissue in culture and microglial cells appeared hypertrophic indicating these glial populations were in an activated state, normally associated with neurodegeneration. Long-term culturing of BOSCs (DIV56) showed organotypic brain slices were prone to structural defects caused from tissue stretching and neuronal loss. This resulted in loss of tissue architecture therefore it was concluded BOSCs may not provide an effective and useful system for the investigation of misfolded protein processing *in vitro.*

8.2 Introduction

BOSCs provide easily accessible brain tissue models which retain functional synaptic circuitry along with tissue architecture and are therefore used to study neurodegenerative diseases and pathological processes (Harwell and Coleman 2016; Novotny et al. 2016; Wolf et al. 2015; Falsig et al. 2012; Falsig et al. 2008; Duff et al. 2002; Bruce, Malfroy, and Baudry 1996). In this chapter a BOSC model was established and characterised to ascertain its suitability in providing an *in vitro* system for studying and advancing our understanding of misfolded protein interactions in the brain. Over-time the original organotypic method using the roller-tube technique has evolved to a more sophisticated interface system (Gähwiler 1981; Hogue 1947), involving culturing tissue slices on a permeable membrane between an interface of air and culture medium referred to as the membrane interface method (Bahr 1995; Stoppini, Buchs, and Muller 1991). This method was used to establish BOSCs in this study. A majority of BOSC studies have focused on culturing isolated areas of the brain such as the hippocampus and the cerebellum (Harwell and Coleman 2016; Novotny et al. 2016; Wolf et al. 2015; Falsig et al. 2012) and limited studies exist which culture whole brain slices (Staal et al. 2011). Both whole brain and hippocampal slices were cultured in this study from WT, 101LL and $PrP^{-/-}$ mice. Brain slices were obtained from postnatal Day 6 pups as at this time point tissues showed a high degree of plasticity and were not as susceptible to mechanical damage during the sectioning stage (Cho, Wood, and Bowlby 2007). Cultures were characterised using immunohistochemistry in conjunction with IMARIS software analysis. The main focus of this study was to develop a working organotypic culturing system, explore cellular populations present and finally challenge organotypic slices with misfolded PrP fibrils. Unfortunately, initial characterisation results showed tissue architecture degradation, astrocytic scarring, and neuronal loss were evident in BOSC models from early time points in culture therefore, this culturing system was deemed not suitable for future fibril challenge experiments.

8.3 Results

8.3.1 Brain sectioning using the Mcilwain tissue chopper

Day 6 postnatal pup brains were processed as described in Materials and Methods (2.6). After incubation in oxygenated artificial cerebrospinal fluid (aCSF), a buffer solution used for maintaining oxygen supply to the exposed brain region, the brain sample was placed on the Mcilwain tissue chopper as shown in *Figure 8.1* and whole brain coronal sections were cut at 400µm thickness. The freshly prepared slices were then separated into either whole brain or hippocampal slices. Slices were placed on sterile 0.4µm pore membrane inserts containing culture medium, and were incubated for a selected number of weeks.

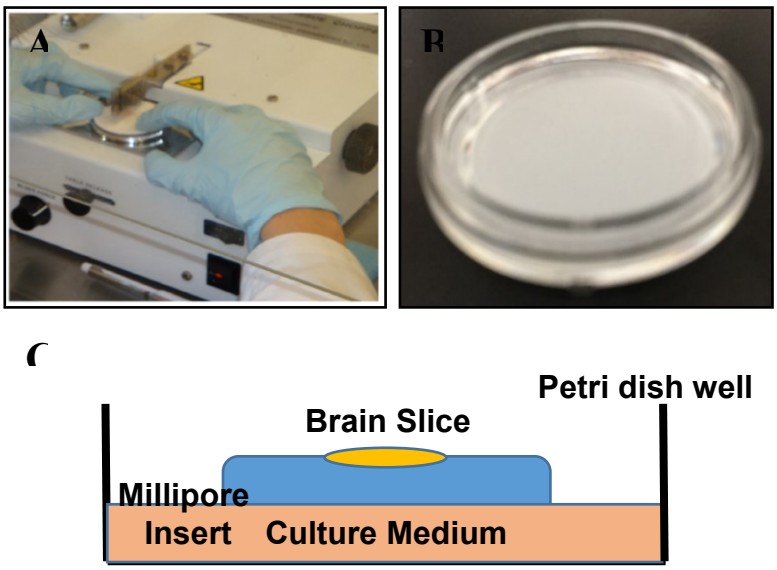

Figure 8.1: Illustration of the organotypic modelling set-up for culturing brain slices *in vitro* using the membrane interface method. (A) Mcilwain tissue chopper set-up for slicing brains. (B) Millipore insert that tissue was placed on and (C) Schematic representation of the membrane interface system.

8.3.2 Immunolabelling and imaging of whole organotypic brain slices

Whole brain organotypic slices established from Day 6 WT, 101LL and $PrP^{-/-}$ pup brains were maintained in culture for approximately three to eight weeks. Tissues were then fixed and immunolabelled with specific markers for neurons, astrocytes and PrP^{C} protein (Materials and Methods, 2.6). In all immunolabelled experiments, the entire tissue slice was imaged by combining multiple images together using the Zeiss LSM710 confocal microscope. As shown in *Figure 8.2*, tiled imaging allowed for entire slices to be displayed which was advantageous for morphological characterisation. Additionally, neuronal and astrocytic cell populations were confirmed by immunolabelling and PrP^{C} protein was detectable however, tissue stretching was evident in whole brain slices. A clear reduction in neuronal and astrocytic immunolabelling coincided with these atypically stretched areas. These results suggested cellular degradation alongside architectural displacement of the brain slice was occurring over-time in these cultures. Tissue stretching was evident in all BOSC genotypes (*Figure 8.3*) suggesting these abnormalities were not specific to one genotype. Comparison of replicate tissue sections also demonstrated that all regions were sensitive to stretching in all genotypes examined. Further investigation using long-term culture studies (DIV56) showed brain slices were susceptible to neuronal and therefore architectural loss (data not included). As neuronal loss was evident at DIV56 in culture, earlier time points were investigated to determine if these defects developed in slices cultured over shorter periods of time. Additionally although tiled imaging was advantageous for producing images of the entire brain slice sections, the resolution was poor making tissue morphological characterisation analysis difficult. To counteract this images were taken at higher magnification and higher resolution. High resolution imaging allowed improved analysis of cellular immunolabelling (*Figure 8.4*).

This highlighted that even as early as DIV23 in culture, brain slices were susceptible to neuronal tissue stretching. High resolution images also displayed high signal intensities for GFAP (astrocytic) immunolabelling at the edges of tissue slices which was common to both genotypes and present in both short and long-term tissue slice cultures (data not shown, see *Figure 8.9*) for similar hippocampal related scarring). These observations suggested tissue scarring was occurring in response to the initial slicing of the brain tissue. High magnification imaging also allowed the detection of microglial populations previously difficult to locate using low power tiled imaging. Iba1 and CD11b immunolabelling confirmed microglia were present and distributed throughout organotypic tissue slices (data not shown). These cells types appeared hypertrophic suggesting they were in an activated state. This activation may be in response to damage introduced during the chopping of brain tissue during initial preparation steps. IMARIS software was used to examine immunolabelled images using similar protocols described for primary hippocampal neuronal analysis (Materials and Methods, 2.2.9). Due to the thickness of slices and uneven tissue mounting, accurate analysis proved difficult however, Z stack confocal imaging helped overcome this obstacle. IMARIS Z stack analysis showed no significant differences were apparent in neuronal or microglial immunolabelling between similarly aged slices from WT and 101LL genotypes (*Figure 8.5*). These similarities confirmed earlier observations that slices from both genotypes were responding similarly to culturing conditions. In conclusion, whole brain slice cultures supported neuronal, astrocyte and microglial populations of cells along with expressing detectable amounts of PrP^{C}. However, sections were prone to tissue stretching resulting in degradation of random areas of brain slice which occurred in all genotypes and became more pronounced over-time in culture. For the aims of this study whole brain organotypic slice culturing will not provide a suitable *in vitro* model for fibril challenge experiments.

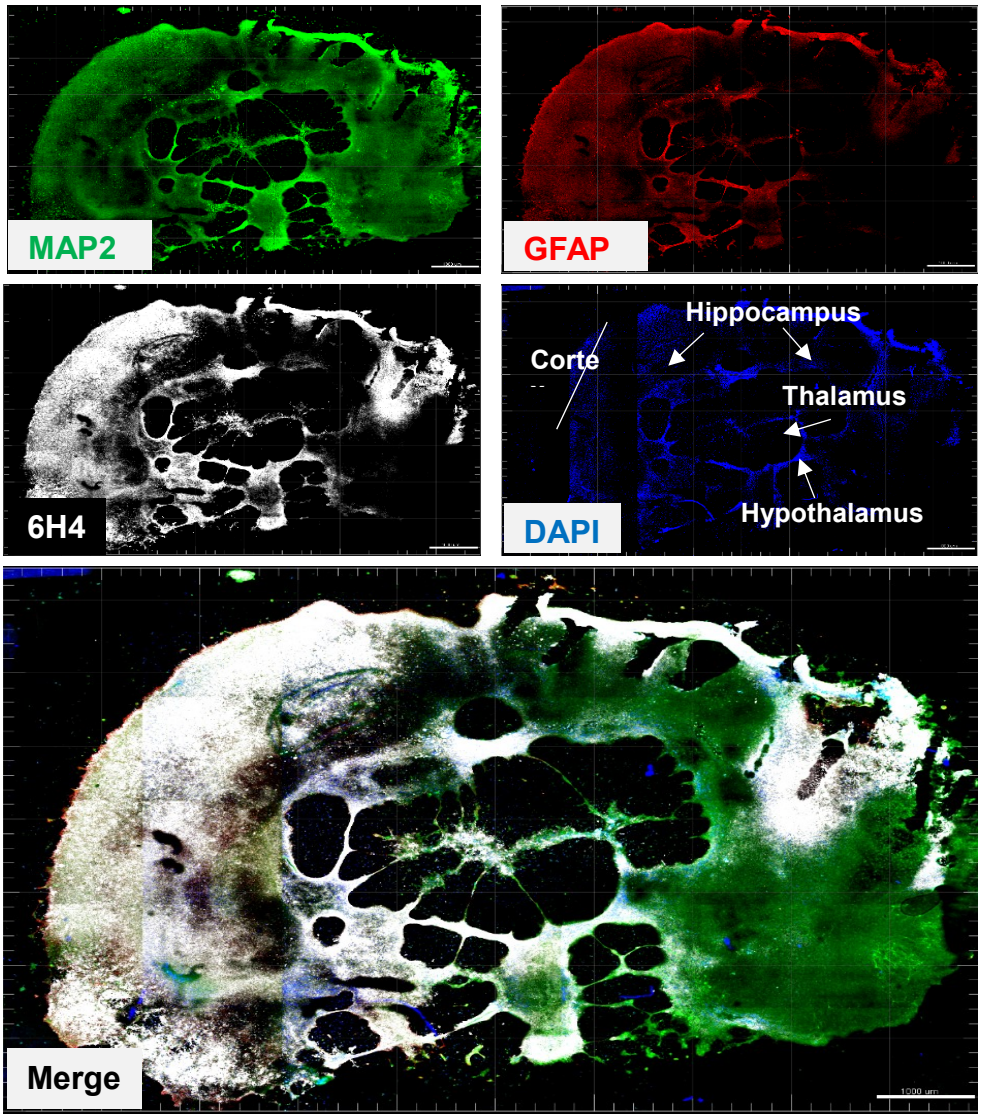

Figure 8.2: Multiple image tiling allowed for entire tissues to be imaged. Immunolabelling and image tiling were used to investigate what cells were present in organotypic slices and also to examine entire brain slice architecture in culture. Immunolabelling for neurons (MAP2/Green); astrocytes (GFAP/Red); PrP^{C} (6H4/White) and nuclear (DAPI/Blue) confirmed the presence of these cells and proteins within slices. Tiled images show tissue stretching and degradation was evident in many areas including the hippocampus, thalamus and hypothalamus. Both neuronal and astrocytic populations were absent in these areas suggesting a loss of these cell types within stretched areas. DIV37 WT brain slice coronal section (400µm), Scale Bar 1000µm.

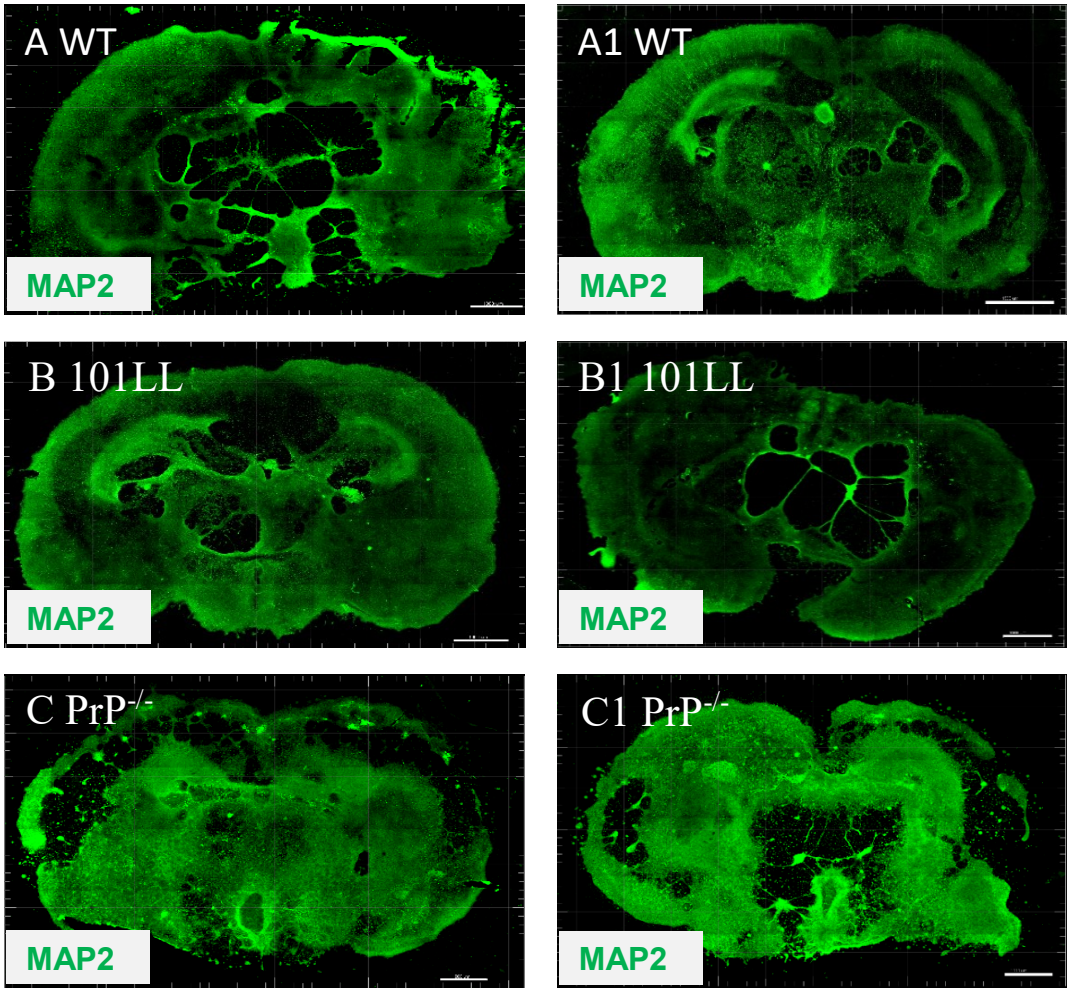

Figure 8.3: Tissue stretching was evident in all BOSC genotypes. Neuronal marker MAP2 was used to monitor tissue changes in organotypic slices to identify if tissue stretching was area and or genotype specific. Tiled images of replicate brain slices, (A-A1) WT DIV37, (B-B1) 101LL DIV41 and (C-C1) $PrP^{-/-}$ DIV42 immunolabelled with neuronal marker MAP2 (Green). All genotypes showed brain slice stretching was present and comparisons of neuronal architecture between duplicate brain slices showed tissue stretching was not specific to brain area for example in panel (A-A1) WT DIV37, slice defects were present in the hippocampus and thalamus areas in image on left however, section on right displayed limited stretching in these areas. 101LL DIV41 and $PrP^{-/-}$ DIV42 slices displayed similar contrasting results. Although timeframes were not identical, tissue stretching was occurring in all genotypes. Scale Bar 1000µm.

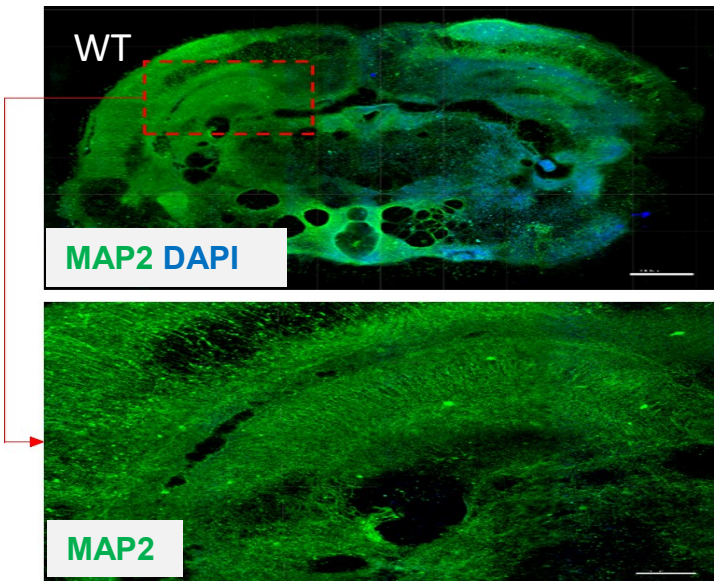

Figure 8.4: High resolution imaging was advantageous for investigating tissue degradation. Tissue architecture was studied using neuronal immunolabelling (MAP2/Green) to monitor neuronal degradation. Top image: Immunolabelling with neuronal marker MAP2 (Green), and bottom enlarged image. Tiled high resolution imaging of organotypic whole brain coronal sections was useful for investigating neuronal degradation which was evident in this brain slice, and tissue morphology changes. Images processed using IMARIS software, DIV23 WT, Scale Bar 1000µm and 200µm.

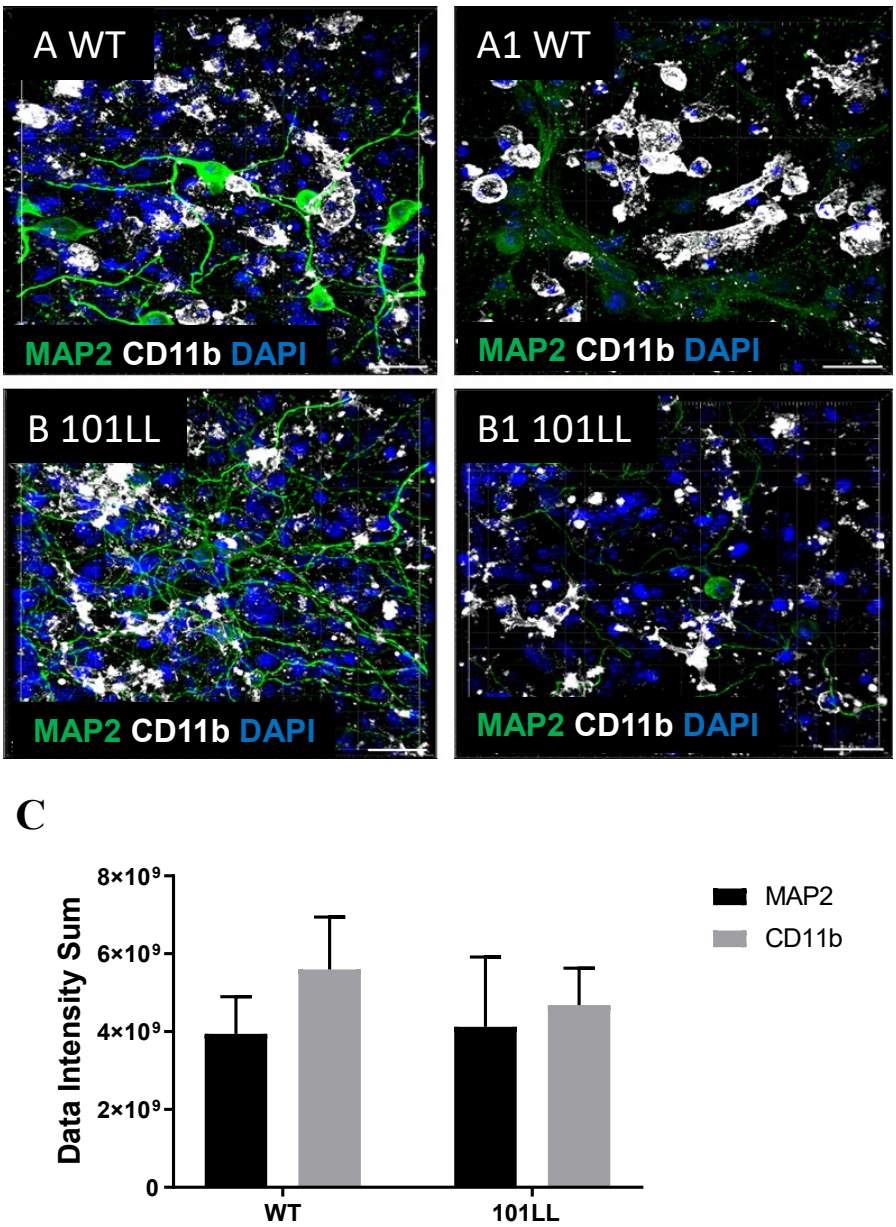

Figure 8.5: Z stack images allowed for accurate immunolabelling analysis to be carried out in IMARIS. To allow for detailed analysis of organotypic brain slices and cellular populations present, Z stacks were created using the confocal LSM710 microscope which were then analysed using IMARIS. (A-A1) WT DIV37 and (B-B1) 101LL DIV41 slices immunolabelled with neuronal marker MAP2 (Green), microglial marker CD11b (White) and nuclear marker DAPI (Blue). (C) IMARIS analysis (Materials and Methods, 2.2.9) quantified cellular populations present in all images. Neuronal populations were present and microglia appeared to be in an activated state based on their hypertrophic morphology, in both WT and 101LL cultures. IMARIS analysis showed no significant differences in signal intensities were evident between WT and 101LL immunolabelled neurons (P-Value 0.91) and microglia (P-Value 0.13), N=2, unpaired t test. Scale Bar 30µm.

8.3.3 Immunolabelling and imaging of hippocampal organotypic brain slices

The experiments described so far have shown tissue stretching and defects were evident in whole organotypic brain slices. To investigate if isolated areas of the brain were more structurally stable *in vitro*, organotypic hippocampal sections from WT and 101LL brains were cultured (Materials and Methods, 2.6). Hippocampal sections were more intact and showed limited stretching in comparison to whole brain cultures (*Figure 8.6*). However, these observations were carried out over shorter timeframes in culture (DIV6-DIV28) and by DIV13 some neuronal loss was also evident in hippocampal slices. Higher magnification imaging confirmed substantial neuronal loss was evident by DIV28 suggesting that isolated brain structures were also susceptible to neuronal degradation and stretching over-time (*Figure 8.7*). As shown in *Figure 8.8*, hippocampal sections cultured for longer periods of time displayed a similar neuronal degradation pattern to whole brain organotypic slices and therefore long-term culturing of hippocampal slices was not further explored in this study (WT showed similar results, data not shown). One prominent feature evident in both full brain and hippocampal slice cultures was the presence of glial scarring which was investigated in detail in short-term cultured hippocampal slices using IMARIS filament tracer module (Materials and Methods, 2.2.9). GFAP immunolabelling confirmed glial scarring and IMARIS filament analysis showed astrocyte cells formed a protective barrier around the entire hippocampal tissue slice (*Figure 8.9*). In conclusion, tissue stretching was reduced in hippocampal slice cultures in comparison to whole brain slices however, substantial neuronal degradation was still evident over-time. Additionally, glial scarring formed an astrocytic envelope surrounding the entire hippocampal tissue slice which would be problematic for future fibril challenge experiments regarding fibril penetration into the brain slice.

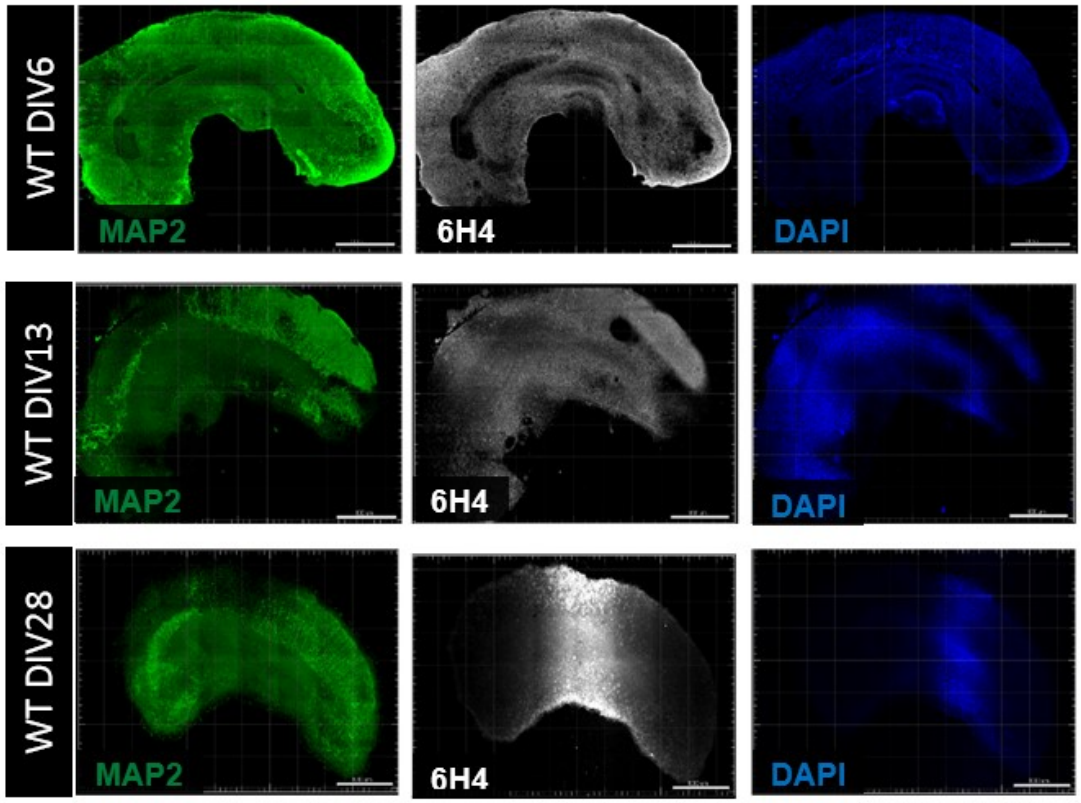

Figure 8.6: Isolated hippocampal tissues were less prone to tissue stretching. Tissue morphology changes were monitored in hippocampal slices to access neuronal degradation over-time in these isolated sections. Tiled images of organotypic hippocampal slices were obtained from WT mice maintained in culture for 6, 13 and 28 days, immunolabelled with neuronal marker MAP2 (Green), PrP marker 6H4 (White) and nuclear stain DAPI (Blue). Tissue structure was grossly maintained within the above timeframes and PrP^{C} protein expression was detectable in all sections. Neuronal loss did appear evident over DIV13 and DIV28 timeframes. Additionally, some DAPI stained areas were out of the focus field of the confocal microscope, and this was a limiting factor associated with mounting organotypic membranes for imaging. WT hippocampi, Scale Bar 1000µm.

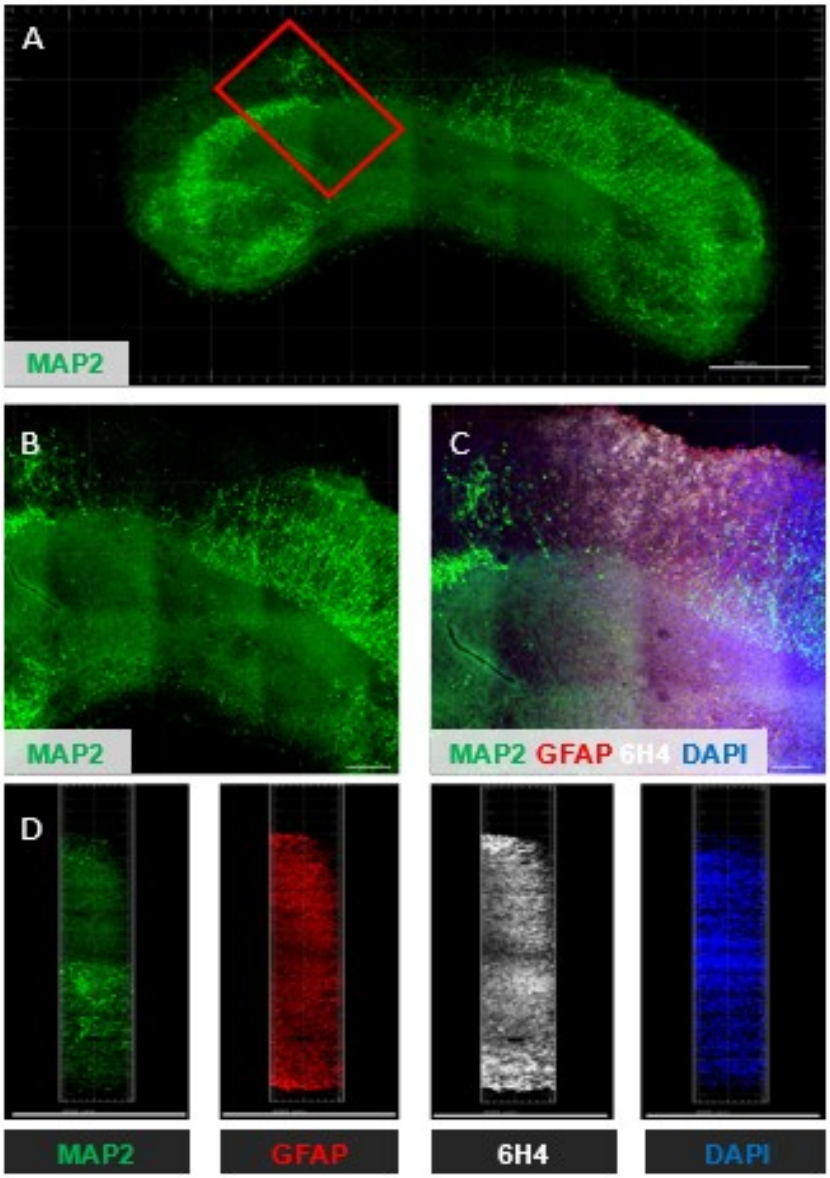

Figure 8.7: Neuronal loss was evident in isolated hippocampal slices. Tiled high magnification image of DIV28 WT organotypic hippocampal slice allowed for detailed analysis of tissue structure to be carried out. (A) Full image of tissue section immunolabelled with neuronal marker MAP2 (Green). Red box indicates area of magnification. (B) Magnified area showed substantial neuronal loss was evident in the hippocampal slice. (C) Merged image of additional markers (Astrocytes/GFAP/Red, PrP^{C}/6H4/White, Nuclear/DAPI/Blue) confirmed neuronal loss observations were accurate and not due to mounting detection limitations. (D) Cross-sections of hippocampal slice (Red box) showing absence of MAP2 immunolabelling in top tissue section in comparison to detectable GFAP, 6H4 and DAPI signals, which were visible on this plane. These analysis suggested neuronal loss was occurring in hippocampal brain slices. Scale Bar (A) 700µm, (B)-(C) 200µm and (D) 500µm.

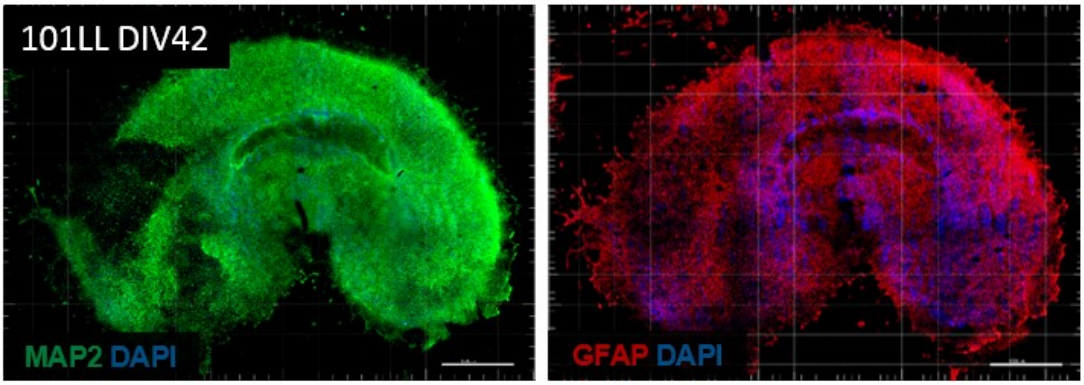

Figure 8.8: Long-term cultures are susceptible to neuronal degradation. Hippocampal slice cultures were maintained in culture for extended timeframes (DIV42), to investigate if isolated tissues would be susceptible to degradation over-time. 101LL hippocampal tissue immunolabelled with neuronal marker (MAP2/Green), astrocytic marker (GFAP/Red) and nuclear stain (DAPI/Blue). Tissues displayed neuronal loss was evident in large sections of the hippocampus, suggesting hippocampal cultures could not be maintained over longer time periods. Scale Bar 1000µm.

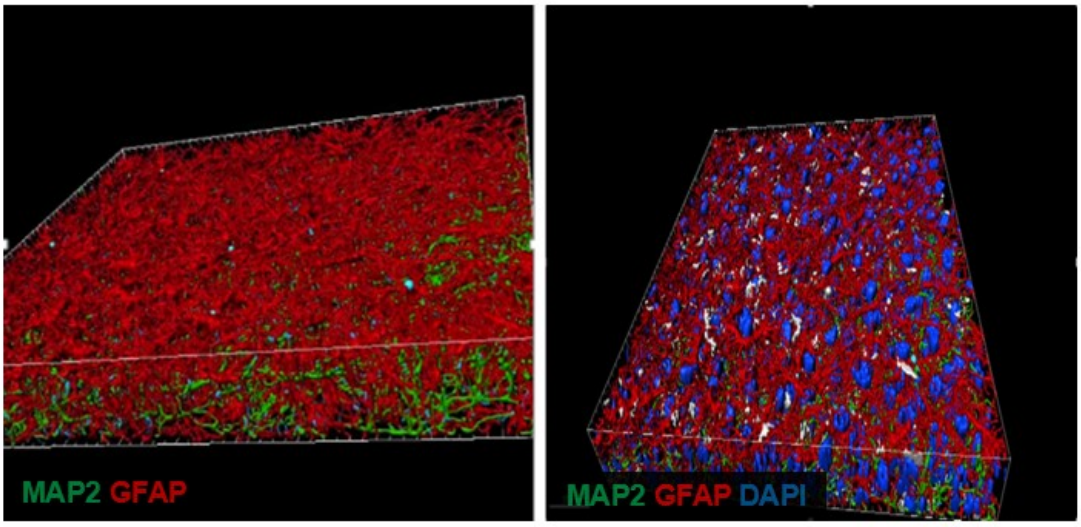

Figure 8.9: Glial scarring was evident in hippocampal slices. To investigate if astrocytic scarring was evident from initial tissue processing, Z stacked images were created of WT DIV6 tissue sections immunolabelled with neuronal marker MAP2 (Green) and astrocytic marker GFAP (Red). IMARIS analysis was carried out using filament tracer and 3D constructs created displayed an envelope of astrocytes surrounding and enclosing neurons were present along the entire organotypic slice confirming glial scarring was occurring in hippocampal organotypic slices.

8.4 Discussion

The overall aim of this study was to develop a representative model of the brain using organotypic brain slices to study neuron-glia interactions after challenge with misfolded PrP fibrils. BOSC cultures were therefore established and characterised from WT, 101LL and $PrP^{-/-}$ genotypes using immunohistochemistry in conjunction with IMARIS software analysis. Previous studies by other groups have focused on isolating and culturing specific regions of the brain (Harwell and Coleman 2016; Novotny et al. 2016; Wolf et al. 2015; Falsig et al. 2012) however, in this study both full brain and hippocampal organotypic slices were established and compared to determine suitability for future fibril challenge experiments.

A number of brain slice isolation methods were investigated during the development of the organotypic culturing system to maximise the efficiency of the technique. Originally up to four pups were culled at one time and extracted brains were immersed in aCSF for approximately 20 minutes. This method resulted in obtaining approximately two tissue slices from each pup brain. The revised protocol (Materials and Methods, 2.6) focused on preparing one pup at a time, reduced tissue incubation time in aCSF from 20 to 3 minutes and used a dissection microscope for efficient separation of slices. These improvements resulted in obtaining approximately five tissue slices per brain, more than double the amount of the original protocol. Other preparative techniques may also be used to prepare tissue slices such as tissue embedding in low melting agarose which is then sliced on a vibratome (Elias and Kriegstein 2007). This method was not investigate here but could have the potential to reduce tissue stretching in brain slices cultures.

To avoid introducing any bias regarding tissue slice analysis multiple images of each tissue were taken using the Zeiss LSM710 confocal microscope which were then stitched together forming one entire image of the organotypic slice. This allowed for the entire organotypic tissue to be viewed and analysed after immunolabelling. Immunohistochemical analysis of whole organotypic brain sections established from WT, 101LL and $PrP^{-/-}$ genotypes confirmed cultures supported neuronal, astrocyte and microglial populations of cells, and also confirmed PrP^{C} was present. Additionally, IMARIS analysis showed no significant differences were apparent between immunolabelled neuronal and microglial cell populations in both WT and 101LL cultures, which was similar to findings observed in Chapter 3 (*Figure 3.11, 3.14*) investigating genotype similarities between WT and 101LL primary hippocampal culture models.

Hippocampal organotypic slice cultures displayed similar characteristics to whole brain slices for the presence of neurons, astrocytes and PrP^{C} in both WT and 101LL cultures. However, morphological tissue abnormalities were noted between both whole slice and hippocampal slices. Whole organotypic brain slices were more prone to tissue stretching resulting in random areas of degradation in the tissue which was applicable to all genotypes investigated and became more pronounced over-time in culture. This may explain why the majority of published studies focus on culturing isolated areas of the brain rather than whole brain slices. Hippocampal sections did appear more structurally stable in culture and less susceptible to tissue stretching however, substantial neuronal loss and degradation was also noted in these isolated slices. Although neurons appeared viable in brain slices immunolabelled with MAP2 (*Figure 8.6*), only limited viability studies (LDH assay, data not shown) were carried out during characterisation to confirm these observations. Other studies have used the exclusion non-fluorescent dye propidium iodide (PI) to evaluate cell viability (Cater et al. 2007). PI can enter through damaged plasma membranes and on binding to nuclear DNA becomes intensely fluorescent. PI viability examinations were not carried out in this study.

IMARIS characterisation of organotypic slices was difficult due to the thickness of the organotypic tissues. Thicker slices were difficult to image on the confocal and low resolution tiled images obtained could not be analysed accurately in IMARIS. Additionally, mounting tissues on glass slides resulted in producing irregular plains of view which could not be imaged by confocal microscopy. Careful mounting and replacing standard slides with concave mounting slides reduced these complications to an extent. Capturing Z stack confocal images of organotypic slices also improved IMARIS analysis of cultures however, this was a timely and costly process. An alternative method of tissue processing using a microtome (Au - Brachmann and Au - Tucker 2011) produces thinner slices which could be easily imaged after immunolabelling by confocal microscopy, therefore improving the quality of images obtained for IMARIS analysis, and this method could be used in future studies. IMARIS analysis of Z stacked hippocampal slice images showed slices were surrounded by an envelope of astrocytic cells. These glial scars inflicted by tissue processing as a result of astrocyte activation and proliferation were unavoidable and presented a physical astrocytic barrier which would be difficult to penetrate for future challenge experiments involving the addition of recombinant PrP fibrils to the brain slices. Additionally, microglial cells appeared hypertrophic (*Figure 8.5*) indicating these glial cells were also responding to cellular damage induced by tissue processing. Astrocytes and microglia are known to respond to CNS damage in the form of increased proliferation at the site of injury (Hill et al. 2014). This response was a limiting factor of the slice culture method and for this particular study it would be difficult to distinguish between glial response associated with tissue processing and that associated with fibril challenge.

The development of organotypic brain slice cultures has revolutionized many experimental studies and has provided many suitable models for studying neuronal injury (Yu and Barclay Morrison 2010), neuronal protection (Noraberg et al. 2005; McKinney et al. 1997), oligodendrocyte differentiation (Hill et al. 2014) and stroke (McManus et al. 2004; Kristensen, Noraberg, and Zimmer 2001). In the majority of these studies however, brain slices used were maintained in culture for short periods of time, for example, oligodendrocyte studies used slices cultured for 5-7 days (Hill et al. 2014); neuronal protection studies used 14 day old cultures (McKinney et al. 1997) and neuronal injury studies used 22 day old slices (Yu and Barclay Morrison 2010). These data suggest maintaining BOSCs over a shorter timeframe may be advantageous for carrying out some experimental studies and this observation was already concluded based on results shown in *Figure 8.6*.

In conclusion, organotypic brain slice culturing of hippocampal slices may be advantageous for culturing tissue slices over very short periods of time however, not for prolonged incubation periods. A combination of experimental findings described in this chapter including, neuronal degradation, tissue stretching, astrocytic scarring, microglial activation, technicalities of mounting and cost of Z stack imaging emphasised that BOSCs did not provide a suitable *in vitro* model system for studying abnormal protein interactions. The method described in this chapter could be developed and optimised further however, due to time constraints this was not a feasible option. Additionally, primary hippocampal neuronal cultures described in Chapter 3 provided a suitable alternative *in vitro* model for studying cellular interactions after fibril challenge, therefore, for the overall aims of this thesis primary hippocampal neuronal cultures were be the only *in vitro* system used for fibril challenge experiments.

Bibliography

Abbott, N. J. 2004. 'Evidence for bulk flow of brain interstitial fluid: significance for physiology and pathology', *Neurochem Int*, 45: 545-52.

Agarwal, Amit, and Dwight E Bergles. 2014. 'Astrocyte Morphology Is Controlled by Neuron-Derived FGF', *Neuron*, 83: 255-57.

Aguib, Y., A. Heiseke, S. Gilch, C. Riemer, M. Baier, H. M. Schatzl, and A. Ertmer. 2009. 'Autophagy induction by trehalose counteracts cellular prion infection', *Autophagy*, 5: 361-9.

Aguzzi, A., and J. Falsig. 2012. 'Prion propagation, toxicity and degradation', *Nat Neurosci*, 15: 936-9.

Aguzzi, Adriano, and Caihong Zhu. 2017. 'Microglia in prion diseases', *The Journal of Clinical Investigation*, 127: 3230-39.

Alais, S., S. Simoes, D. Baas, S. Lehmann, G. Raposo, J. L. Darlix, and P. Leblanc. 2008. 'Mouse neuroblastoma cells release prion infectivity associated with exosomal vesicles', *Biol Cell*, 100: 603-15.

Anderson, V. L., and W. W. Webb. 2011. 'Transmission electron microscopy characterization of fluorescently labelled amyloid beta 1-40 and alpha-synuclein aggregates', *BMC Biotechnol*, 11: 125.

Anelli, T., and R. Sitia. 2008. 'Protein quality control in the early secretory pathway', *Embo J*, 27: 315-27.

Araki, K., and K. Nagata. 2011. 'Protein folding and quality control in the ER', *Cold Spring Harb Perspect Biol*, 3: a007526.

Aranda-Orgillés, Beatriz, Johanna Aigner, Melanie Kunath, Rudi Lurz, Rainer Schneider, and Susann Schweiger. 2008. 'Active transport of the ubiquitin ligase MID1 along the microtubules is regulated by protein phosphatase 2A', *PLoS ONE*, 3: e3507.

Arcuri, Cataldo, Carmen Mecca, Roberta Bianchi, Ileana Giambanco, and Rosario Donato. 2017. 'The Pathophysiological Role of Microglia in Dynamic Surveillance, Phagocytosis and Structural Remodeling of the Developing CNS', *Frontiers in Molecular Neuroscience*, 10: 191.

Arsenijevic, Y., S. Weiss, B. Schneider, and P. Aebischer. 2001. 'Insulin-like growth factor-I is necessary for neural stem cell proliferation and demonstrates distinct actions of epidermal growth factor and fibroblast growth factor-2', *J Neurosci*, 21: 7194-202.

Arvan, P., X. Zhao, J. Ramos-Castaneda, and A. Chang. 2002. 'Secretory pathway quality control operating in Golgi, plasmalemmal, and endosomal systems', *Traffic*, 3: 771-80.

Ashok, A., and R. S. Hegde. 2008. 'Retrotranslocation of prion proteins from the endoplasmic reticulum by preventing GPI signal transamidation', *Mol Biol Cell*, 19: 3463-76.

Au - Brachmann, Isabel, and Kerry L. Au - Tucker. 2011. 'Organotypic Slice Culture of GFP-expressing Mouse Embryos for Real-time Imaging of Peripheral Nerve Outgrowth', *JoVE*: e2309.

Ayers, J. I., J. Diamond, A. Sari, S. Fromholt, A. Galaleldeen, L. W. Ostrow, J. D. Glass, P. J. Hart, and D. R. Borchelt. 2016. 'Distinct conformers of transmissible misfolded SOD1 distinguish human SOD1-FALS from

other forms of familial and sporadic ALS', *Acta Neuropathol*, 132: 827-40.
B. Martin, Joseph. 1999. *Molecular Basis of the Neurodegenerative Disorders*.
Bahr, B. A. 1995. 'Long-term hippocampal slices: a model system for investigating synaptic mechanisms and pathologic processes', *J Neurosci Res*, 42: 294-305.
Baker, C. A. , D. Martin, and L. Manuelidis. 2002. 'Microglia from Creutzfeldt-Jakob disease-infected brains are infectious and show specific mRNA activation profiles.', *Journal Of Virology*, 76: 10905-13.
Baker, H. F., L. W. Duchen, J. M. Jacobs, and R. M. Ridley. 1990. 'Spongiform encephalopathy transmitted experimentally from Creutzfeldt-Jakob and familial Gerstmann-Straussler-Scheinker diseases', *Brain*, 113 (Pt 6): 1891-909.
Banker, G. A., and W. M. Cowan. 1977. 'Rat hippocampal neurons in dispersed cell culture', *Brain Res*, 126: 397-42.
Banks, P. R., and D. M. Paquette. 1995. 'Comparison of three common amine reactive fluorescent probes used for conjugation to biomolecules by capillary zone electrophoresis', *Bioconjug Chem*, 6: 447-58.
Barbanti, P., G. Fabbrini, M. Salvatore, R. Petraroli, F. Cardone, B. Maras, M. Equestre, G. Macchi, G. L. Lenzi, and M. Pocchiari. 1996. 'Polymorphism At Codon-129 or Codon-219 Of Prnp and Clinical Heterogeneity In a Previously Unreported Family With Gerstmann-Straussler-Scheinker Disease (Prp-P102l Mutation)', *Neurology*, 47: 734-41.
Barbanti, P., G. Fabbrini, M. Salvatore, R. Petraroli, M. Pocchiari, G. Macchi, and G. L. Lenzi. 1994. 'No Correlation between Clinical Heterogeneity and Codon-129 Polymorphism of the Prion Protein Gene (Prnp) in Gerstmann-Straussler-Scheinker-Syndrome (Gss) with Prnp Codon-102 Mutation', *Neurobiology of Aging*, 15: S156-S56.
Barron, R. M., S. L. Campbell, D. King, A. Bellon, K. E. Chapman, R. A. Williamson, and J. C. Manson. 2007. 'High titers of transmissible spongiform encephalopathy infectivity associated with extremely low levels of PrPSc in vivo', *J Biol Chem*, 282: 35878-86.
Barron, R. M., V. Thomson, D. King, J. Shaw, D. W. Melton, and J. C. Manson. 2003. 'Transmission of murine scrapie to P101L transgenic mice', *Journal Of General Virology*, 84: 3165-72.
Barron, Rona M., Declan King, Martin Jeffrey, Gillian McGovern, Sonya Agarwal, Andrew C. Gill, and Pedro Piccardo. 2016. 'PrP aggregation can be seeded by pre-formed recombinant PrP amyloid fibrils without the replication of infectious prions', *Acta Neuropathologica*, 132: 611-24.
Bartolome, F., M. de la Cueva, C. Pascual, D. Antequera, T. Fernandez, C. Gil, A. Martinez, and E. Carro. 2018. 'Amyloid beta-induced impairments on mitochondrial dynamics, hippocampal neurogenesis, and memory are restored by phosphodiesterase 7 inhibition', *Alzheimers Res Ther*, 10: 24.
Bate, C., S. Reid, and A. Williams. 2001. 'Killing of prion-damaged neurones by microglia', *Neuroreport*, 12: 2589-94.

Beaudoin, Gerard M. J., Seung-Hye Lee, Dipika Singh, Yang Yuan, Yu-Gie Ng, Louis F. Reichardt, and Jyothi Arikkath. 2012. 'Culturing pyramidal neurons from the early postnatal mouse hippocampus and cortex', *Nat. Protocols*, 7: 1741-54.

Bellamkonda, R., J. P. Ranieri, N. Bouche, and P. Aebischer. 1995. 'Hydrogel-based three-dimensional matrix for neural cells', *J Biomed Mater Res*, 29: 663-71.

Bendheim, P. E., H. R. Brown, R. D. Rudelli, L. J. Scala, N. L. Goller, G. Y. Wen, R. J. Kascsak, N. R. Cashman, and D. C. Bolton. 1992. 'Nearly ubiquitous tissue distribution of the scrapie agent precursor protein', *Neurology*, 42: 149-56.

Benjamini, Y, and Y Hochberg. 1995. 'Controlling the False Discovery Rate: A Practical and Powerful Approach to Multiple Testing', *J R Stat Soc Ser B Methodol*, 57: 289 - 300.

Benoit, M. E., M. X. Hernandez, M. L. Dinh, F. Benavente, O. Vasquez, and A. J. Tenner. 2013. 'C1q-induced LRP1B and GPR6 proteins expressed early in Alzheimer disease mouse models, are essential for the C1q-mediated protection against amyloid-beta neurotoxicity', *J Biol Chem*, 288: 654-65.

Beranger, F., A. Mange, B. Goud, and S. Lehmann. 2002. 'Stimulation of PrP(C) retrograde transport toward the endoplasmic reticulum increases accumulation of PrP(Sc) in prion-infected cells', *J Biol Chem*, 277: 38972-7.

Bhat, K. P., S. Yan, C. E. Wang, S. Li, and X. J. Li. 2014. 'Differential ubiquitination and degradation of huntingtin fragments modulated by ubiquitin-protein ligase E3A', *Proc Natl Acad Sci U S A*, 111: 5706-11.

Bianca, M., S. Bianca, I. Vecchio, R. Raffaele, C. Ingegnosi, and F. Nicoletti. 2003. 'Gerstmann-Straussler-Scheinker disease with P102L-V129 mutation: a case with psychiatric manifestations at onset', *Ann Genet*, 46: 467-9.

Biasini, Emiliano, Jessie A. Turnbaugh, Ursula Unterberger, and David A. Harris. 2011. 'Prion protein at the crossroads of physiology and disease', *Trends in Neurosciences*, 35: 92-103.

Bishop, M.T., Pennington, C., Heath, C.A. et al. 2009, '*PRNP* variation in UK sporadic and variant Creutzfeldt Jakob disease highlights genetic risk factors and a novel non-synonymous polymorphism' BMC Med Genet 10: 146.

Bjorkoy, G., T. Lamark, A. Brech, H. Outzen, M. Perander, A. Overvatn, H. Stenmark, and T. Johansen. 2005. 'p62/SQSTM1 forms protein aggregates degraded by autophagy and has a protective effect on huntingtin-induced cell death', *J Cell Biol*, 171: 603-14.

Block, M. L., L. Zecca, and J. S. Hong. 2007. 'Microglia-mediated neurotoxicity: uncovering the molecular mechanisms', *Nat Rev Neurosci*, 8: 57-69.

Boche, D., C. Cunningham, F. Docagne, H. Scott, and V. H. Perry. 2006. 'TGFbeta1 regulates the inflammatory response during chronic neurodegeneration', *Neurobiol Dis*, 22: 638-50.

Boehler, Michael D., Bruce C. Wheeler, and Gregory J. Brewer. 2007. 'Added astroglia promote greater synapse density and higher activity in neuronal networks', *Neuron glia biology*, 3: 127-40.
Boellaard, J. W., M. Kao, W. Schlote, and H. Diringer. 1991. 'Neuronal autophagy in experimental scrapie', *Acta Neuropathol*, 82: 225-8.
Boissonneault, V., M. Filali, M. Lessard, J. Relton, G. Wong, and S. Rivest. 2009. 'Powerful beneficial effects of macrophage colony-stimulating factor on beta-amyloid deposition and cognitive impairment in Alzheimer's disease', *Brain*, 132: 1078-92.
Borchelt, D. R., A. Taraboulos, and S. B. Prusiner. 1992. 'Evidence for synthesis of scrapie prion proteins in the endocytic pathway', *J Biol Chem*, 267: 16188-99.
Bosi, S., R. Rauti, J. Laishram, A. Turco, D. Lonardoni, T. Nieus, M. Prato, D. Scaini, and L. Ballerini. 2015. 'From 2D to 3D: novel nanostructured scaffolds to investigate signalling in reconstructed neuronal networks', *Sci Rep*, 5: 9562.
Bosque, P. J., and S. B. Prusiner. 2000. 'Cultured cell sublines highly susceptible to prion infection', *J Virol*, 74: 4377-86.
Bourke, Justin L., Harold A. Coleman, Vi Pham, John S. Forsythe, and Helena C. Parkington. 2014. 'Neuronal Electrophysiological Function and Control of Neurite Outgrowth on Electrospun Polymer Nanofibers Are Cell Type Dependent', *Tissue Eng Part A*, 20: 1089-95.
Braak, H., E. Braak, and J. Bohl. 1993. 'Staging of Alzheimer-related cortical destruction', *Eur Neurol*, 33.
Braak, H., K. Del Tredici, U. Rub, R. A. de Vos, E. N. Jansen Steur, and E. Braak. 2003. 'Staging of brain pathology related to sporadic Parkinson's disease', *Neurobiol Aging*, 24: 197-211.
Bradford, Barry M., and Neil A. Mabbott. 2012. 'Prion Disease and the Innate Immune System', *Viruses*, 4: 3389-419.
Brettschneider, Johannes, Kelly Del Tredici, Virginia M. Y. Lee, and John Q. Trojanowski. 2015. 'Spreading of pathology in neurodegenerative diseases: a focus on human studies', *Nature reviews. Neuroscience*, 16: 109-20.
Brewer, G. J., and P. J. Price. 1996. 'Viable cultured neurons in ambient carbon dioxide and hibernation storage for a month', *Neuroreport*, 7: 1509-12.
Brewer, G. J., J. R. Torricelli, E. K. Evege, and P. J. Price. 1993. 'Optimized survival of hippocampal neurons in B27-supplemented neurobasal™, a new serum-free medium combination', *Journal of Neuroscience Research*, 35: 567-76.
Breydo, L., N. Makarava, and I. V. Baskakov. 2008. 'Methods for conversion of prion protein into amyloid fibrils', *Methods Mol Biol*, 459: 105-15.
Brohawn, David G., Laura C. O'Brien, and James P. Bennett. 2016. 'RNAseq Analyses Identify Tumor Necrosis Factor-Mediated Inflammation as a Major Abnormality in ALS Spinal Cord', *PLoS ONE*, 11: e0160520.
Browman, D., and C. Zurzolo. 2013. 'Not on the menu: autophagy-independent clearance of prions', *Prion*, 7: 286-90.

Brown, D. R. 2003. 'Prion protein expression modulates neuronal copper content', *J Neurochem*, 87: 377-85.

Brown, P., L. Cervenakova, L. G. Goldfarb, W. R. Mccombie, R. Rubenstein, R. G. Will, M. Pocchiari, J. F. Martinezlage, C. Scalici, C. Masullo, G. Graupera, J. Ligan, and D. C. Gajdusek. 1994. 'Iatrogenic Creutzfeldt-Jakob-Disease - an Example of the Interplay between Ancient Genes and Modern Medicine', *Neurology*, 44: 291-93.

Bruce, A. J., B. Malfroy, and M. Baudry. 1996. 'beta-Amyloid toxicity in organotypic hippocampal cultures: protection by EUK-8, a synthetic catalytic free radical scavenger', *Proceedings Of the National Academy Of Sciences Of the United States Of America*, 93: 2312-16.

Bucciantini, M., E. Giannoni, F. Chiti, F. Baroni, L. Formigli, J. Zurdo, N. Taddei, G. Ramponi, C. M. Dobson, and M. Stefani. 2002. 'Inherent toxicity of aggregates implies a common mechanism for protein misfolding diseases', *Nature*, 416: 507-11.

Bueler, H., A. Aguzzi, A. Sailer, R. A. Greiner, P. Autenried, M. Aguet, and C. Weissmann. 1993. 'Mice devoid of PrP are resistant to scrapie', *Cell*, 73: 1339-47.

Butovsky, Oleg, Mark P. Jedrychowski, Craig S. Moore, Ron Cialic, Amanda J. Lanser, Galina Gabriely, Thomas Koeglsperger, Ben Dake, Pauline M. Wu, Camille E. Doykan, Zain Fanek, LiPing Liu, Zhuoxun Chen, Jeffrey D. Rothstein, Richard M. Ransohoff, Steven P. Gygi, Jack P. Antel, and Howard L. Weiner. 2014. 'Identification of a unique TGF-[beta]-dependent molecular and functional signature in microglia', *Nat Neurosci*, 17: 131-43.

Cahoy, John D., Ben Emery, Amit Kaushal, Lynette C. Foo, Jennifer L. Zamanian, Karen S. Christopherson, Yi Xing, Jane L. Lubischer, Paul A. Krieg, Sergey A. Krupenko, Wesley J. Thompson, and Ben A. Barres. 2008. 'A Transcriptome Database for Astrocytes, Neurons, and Oligodendrocytes: A New Resource for Understanding Brain Development and Function', *The Journal of Neuroscience*, 28: 264-78.

Cai, Y., J. Arikkath, L. Yang, M. L. Guo, P. Periyasamy, and S. Buch. 2016. 'Interplay of endoplasmic reticulum stress and autophagy in neurodegenerative disorders', *Autophagy*, 12: 225-44.

Calabresi, P., A. Castrioto, M. Di Filippo, and B. Picconi. 2013. 'New experimental and clinical links between the hippocampus and the dopaminergic system in Parkinson's disease', *Lancet Neurol*, 12: 811-21.

Caldwell, M. A., X. He, N. Wilkie, S. Pollack, G. Marshall, K. A. Wafford, and C. N. Svendsen. 2001. 'Growth factors regulate the survival and fate of cells derived from human neurospheres', *Nat Biotechnol*, 19: 475-9.

Cam, J. A., and G. Bu. 2006. 'Modulation of beta-amyloid precursor protein trafficking and processing by the low density lipoprotein receptor family', *Mol Neurodegener*, 1: 8.

Cammarata, S., and M. Tabaton. 1992. 'Ubiquitin-reactive axons have a widespread distribution and are unrelated to prion protein plaques in Creutzfeldt-Jakob disease', *J Neurol Sci*, 110: 32-6.

Campana, V., D. Sarnataro, and C. Zurzolo. 2005. 'The highways and byways of prion protein trafficking', *Trends Cell Biol*, 15: 102-11.

Cater, H. L., D. Gitterman, S. M. Davis, C. D. Benham, B. Morrison, 3rd, and L. E. Sundstrom. 2007. 'Stretch-induced injury in organotypic hippocampal slice cultures reproduces in vivo post-traumatic neurodegeneration: role of glutamate receptors and voltage-dependent calcium channels', *J Neurochem*, 101: 434-47.

Caughey, B., and P. T. Lansbury. 2003. 'Protofibrils, pores, fibrils, and neurodegeneration: Separating the responsible protein aggregates from the innocent bystanders', *Annual Review of Neuroscience*, 26: 267-98.

Caughey, B., G. J. Raymond, D. Ernst, and R. E. Race. 1991. 'N-terminal truncation of the scrapie-associated form of PrP by lysosomal protease(s): implications regarding the site of conversion of PrP to the protease-resistant state', *J Virol*, 65: 6597-603.

Caughey, Byron, Gerald S. Baron, Bruce Chesebro, and Martin Jeffrey. 2009. 'Getting a grip on prions: oligomers, amyloids and pathological membrane interactions', *Annual Review Of Biochemistry*, 78: 177-204.

Chen, W. S., C. Y. Yueh, Y. A. Huang, and E. Hwang. 2011. 'An inverted method for culturing dissociated mouse hippocampal neurons', *Neurosci Res*, 70: 118-23.

Cheng, X. T., Y. X. Xie, B. Zhou, N. Huang, T. Farfel-Becker, and Z. H. Sheng. 2018. 'Characterization of LAMP1-labeled nondegradative lysosomal and endocytic compartments in neurons', *J Cell Biol*.

Chevallet, Mireille, Sylvie Luche, and Thierry Rabilloud. 2006. 'Silver staining of proteins in polyacrylamide gels', *Nature Protocols*, 1: 1852-58.

Chiarini, L. B., A. R. Freitas, S. M. Zanata, R. R. Brentani, V. R. Martins, and R. Linden. 2002. 'Cellular prion protein transduces neuroprotective signals', *Embo J*, 21: 3317-26.

Chiti, F., and C. M. Dobson. 2006. 'Protein misfolding, functional amyloid, and human disease', *Annual Review Of Biochemistry*, 75: 333-66.

Cho, Eun-Gyung, Jeffrey D. Zaremba, Scott R. McKercher, Maria Talantova, Shichun Tu, Eliezer Masliah, Shing Fai Chan, Nobuki Nakanishi, Alexey Terskikh, and Stuart A. Lipton. 2011. 'MEF2C enhances dopaminergic neuron differentiation of human embryonic stem cells in a parkinsonian rat model', *PLoS ONE*, 6: e24027.

Cho, Seongeun, Andrew Wood, and Mark R. Bowlby. 2007. 'Brain Slices as Models for Neurodegenerative Disease and Screening Platforms to Identify Novel Therapeutics', *Current Neuropharmacology*, 5: 19-33.

Choi, D. W. 1988. 'Glutamate neurotoxicity and diseases of the nervous system', *Neuron*, 1: 623-34.

Ciechanover, Aaron, and Yong Tae Kwon. 2015. 'Degradation of misfolded proteins in neurodegenerative diseases: therapeutic targets and strategies', *Exp Mol Med*, 47: e147.

Clemens, M. J. 2004. 'Targets and mechanisms for the regulation of translation in malignant transformation', *Oncogene*, 23: 3180-8.

Colby, D. W., R. Wain, I. V. Baskakov, G. Legname, C. G. Palmer, H. O. Nguyen, A. Lemus, F. E. Cohen, S. J. DeArmond, and S. B. Prusiner. 2010. 'Protease-sensitive synthetic prions', *PLoS Pathog*, 6: e1000736.

Collinge, J., M. S. Palmer, and A. J. Dryden. 1991. 'Genetic Predisposition to Iatrogenic Creutzfeldt-Jakob Disease', *Lancet*, 337: 1441-42.

Collinge, J., K. C. Sidle, J. Meads, J. Ironside, and A. F. Hill. 1996. 'Molecular analysis of prion strain variation and the aetiology of 'new variant' CJD', *Nature*, 383: 685-90.

Collins, S. J., and C. L. Haigh. 2017. 'Simplified Murine 3D Neuronal Cultures for Investigating Neuronal Activity and Neurodegeneration', *Cell Biochem Biophys*, 75: 3-13.

Cortes, C. J., K. Qin, J. Cook, A. Solanki, and J. A. Mastrianni. 2012. 'Rapamycin delays disease onset and prevents PrP plaque deposition in a mouse model of Gerstmann-Straussler-Scheinker disease', *J Neurosci*, 32: 12396-405.

Counts, Scott E., and Elliott J. Mufson. 2005. 'The Role of Nerve Growth Factor Receptors in Cholinergic Basal Forebrain Degeneration in Prodromal Alzheimer Disease', *Journal of Neuropathology & Experimental Neurology*, 64: 263-72.

Courtney, Eliza, Shan Kornfeld, Karolina Janitz, and Michal Janitz. 2010. 'Transcriptome profiling in neurodegenerative disease', *Journal of Neuroscience Methods*, 193: 189-202.

Cuervo, A. M., E. Bergamini, U. T. Brunk, W. Droge, M. Ffrench, and A. Terman. 2005. 'Autophagy and aging: the importance of maintaining "clean" cells', *Autophagy*, 1: 131-40.

Cunningham, C., R. Deacon, H. Wells, D. Boche, S. Waters, C. P. Diniz, H. Scott, J. N. Rawlins, and V. H. Perry. 2003. 'Synaptic changes characterize early behavioural signs in the ME7 model of murine prion disease', *Eur J Neurosci*, 17: 2147-55.

Dabrowski, Michal, Stein Aerts, Paul Van Hummelen, Katleen Craessaerts, Bart De Moor, Wim Annaert, Yves Moreau, and Bart De Strooper. 2003. 'Gene profiling of hippocampal neuronal culture', *Journal of Neurochemistry*, 85: 1279-88.

DaRocha-Souto, B., T. C. Scotton, M. Coma, A. Serrano-Pozo, T. Hashimoto, L. Sereno, M. Rodriguez, B. Sanchez, B. T. Hyman, and T. Gomez-Isla. 2011. 'Brain oligomeric beta-amyloid but not total amyloid plaque burden correlates with neuronal loss and astrocyte inflammatory response in amyloid precursor protein/tau transgenic mice', *J Neuropathol Exp Neurol*, 70: 360-76.

Davies, C. A., D. M. Mann, P. Q. Sumpter, and P. O. Yates. 1987. 'A quantitative morphometric analysis of the neuronal and synaptic content of the frontal and temporal cortex in patients with Alzheimer's disease', *J Neurol Sci*, 78: 151-64.

Dearmond, S. J., and K. Bajsarowicz. 2010. 'PrPSc accumulation in neuronal plasma membranes links Notch-1 activation to dendritic degeneration in prion diseases', *Mol Neurodegener*, 5: 6.

Deng, J., H. P. Harding, B. Raught, A. C. Gingras, J. J. Berlanga, D. Scheuner, R. J. Kaufman, D. Ron, and N. Sonenberg. 2002. 'Activation of GCN2 in UV-irradiated cells inhibits translation', *Curr Biol*, 12: 1279-86.

Deriziotis, P., R. Andre, D. M. Smith, R. Goold, K. J. Kinghorn, M. Kristiansen, J. A. Nathan, R. Rosenzweig, D. Krutauz, M. H. Glickman, J. Collinge, A. L. Goldberg, and S. J. Tabrizi. 2011. 'Misfolded PrP impairs the UPS by interaction with the 20S proteasome and inhibition of substrate entry', *Embo J*, 30: 3065-77.

Diaz, E., Y. Ge, Y. H. Yang, K. C. Loh, T. A. Serafini, Y. Okazaki, Y. Hayashizaki, T. P. Speed, J. Ngai, and P. Scheiffele. 2002. 'Molecular analysis of gene expression in the developing pontocerebellar projection system', *Neuron*, 36: 417-34.

Diedrich, J. F., P. E. Bendheim, Y. S. Kim, R. I. Carp, and A. T. Haase. 1991. 'Scrapie-associated prion protein accumulates in astrocytes during scrapie infection', *Proceedings Of the National Academy Of Sciences Of the United States Of America*, 88: 375-79.

Doh-ura, K., J. Tateishi, H. Sasaki, T. Kitamoto, and Y. Sakaki. 1989. 'Pro---- leu change at position 102 of prion protein is the most common but not the sole mutation related to Gerstmann-Straussler syndrome', *Biochem Biophys Res Commun*, 163: 974-9.

Duff, K., W. Noble, K. Gaynor, and Y. Matsuoka. 2002. 'Organotypic slice cultures from transgenic mice as disease model systems', *J Mol Neurosci*, 19: 317-20.

Eden, Eran, Roy Navon, Israel Steinfeld, Doron Lipson, and Zohar Yakhini. 2009. 'GOrilla: a tool for discovery and visualization of enriched GO terms in ranked gene lists', *BMC Bioinformatics*, 10: 48.

Elias, Laura, and Arnold Kriegstein. 2007. 'Organotypic Slice Culture of E18 Rat Brains', *J Vis Exp*: 235.

Eriksson, C., A. Bjorklund, and K. Wictorin. 2003. 'Neuronal differentiation following transplantation of expanded mouse neurosphere cultures derived from different embryonic forebrain regions', *Exp Neurol*, 184: 615-35.

Ertmer, A., S. Gilch, S. W. Yun, E. Flechsig, B. Klebl, M. Stein-Gerlach, M. A. Klein, and H. M. Schatzl. 2004. 'The tyrosine kinase inhibitor STI571 induces cellular clearance of PrPSc in prion-infected cells', *J Biol Chem*, 279: 41918-27.

Eskelinen, Eeva-Liisa. 2006. 'Roles of LAMP-1 and LAMP-2 in lysosome biogenesis and autophagy', *Molecular Aspects of Medicine*, 27: 495-502.

Falsig, J., C. Julius, I. Margalith, P. Schwarz, F. L. Heppner, and A. Aguzzi. 2008. 'A versatile prion replication assay in organotypic brain slices', *Nat Neurosci*, 11: 109-17.

Falsig, Jeppe, Tiziana Sonati, Uli S. Herrmann, Dino Saban, Bei Li, Karina Arroyo, Boris Ballmer, Pawel P. Liberski, and Adriano Aguzzi. 2012. 'Prion Pathogenesis Is Faithfully Reproduced in Cerebellar Organotypic Slice Cultures', *PLOS Pathogens*, 8: e1002985.

Fang, Cheng, Thibaut Imberdis, Maria Carmen Garza, Holger Wille, and David A. Harris. 2016. 'A Neuronal Culture System to Detect Prion Synaptotoxicity', *PLoS Pathog*, 12: e1005623.
Farquhar, C. F., R. A. Somerville, and L. A. Ritchie. 1989. 'Post-mortem immunodiagnosis of scrapie and bovine spongiform encephalopathy', *J Virol Methods*, 24: 215-21.
Fath, T., Y. D. Ke, P. Gunning, J. Gotz, and L. M. Ittner. 2009. 'Primary support cultures of hippocampal and substantia nigra neurons', *Nature Protocols*, 4: 78-85.
Ferrer, Isidro, Margarita Carmona, Rosa Blanco, MariaJesusRey Recio, and R. M. San Segundo. 2011. 'Gerstmann-Straüssler-Scheinker PRNP P102L-129V mutation', *Translational Neuroscience*, 2: 23-32.
Fogarty, Matthew Joseph, Luke A Hammond, Refik Kanjhan, Mark Christian Bellingham, and Peter Gerrard Noakes. 2013. 'A method for the three-dimensional reconstruction of Neurobiotin™-filled neurons and the location of their synaptic inputs', *Frontiers in Neural Circuits*, 7.
Forloni, G., L. Terreni, I. Bertani, S. Fogliarino, R. Invernizzi, A. Assini, G. Ribizzi, A. Negro, E. Calabrese, M. A. Volonte, C. Mariani, M. Franceschi, M. Tabaton, and A. Bertoli. 2002. 'Protein misfolding in Alzheimer's and Parkinson's disease: genetics and molecular mechanisms', *Neurobiol Aging*, 23: 957-76.
Fuller, H. R., L. C. Graham, M. Llavero Hurtado, and T. M. Wishart. 2016. 'Understanding the molecular consequences of inherited muscular dystrophies: advancements through proteomic experimentation', *Expert Rev Proteomics*, 13: 659-71.
Gabizon, Ruth, Hana Rosenman, Zeev Meiner, Irit Kahana, Esther Kahana, Yin Shugart, Jurg Ott, and Stanley B. Prusiner. 1994. 'Mutation in Codon 200 and Polymorphism in Codon 129 of the Prion Protein Gene in Libyan Jews with Creutzfeldt-Jakob Disease', *Philosophical Transactions: Biological Sciences*, 343: 385-90.
Gage, F. H., J. Ray, and L. J. Fisher. 1995. 'Isolation, characterization, and use of stem cells from the CNS', *Annu Rev Neurosci*, 18: 159-92.
Gähwiler, B. H. 1981. 'Organotypic monolayer cultures of nervous tissue', *Journal of Neuroscience Methods*, 4: 329-42.
Gardner, Asa, Peter Jukkola, and Chen Gu. 2012. 'Myelination of rodent hippocampal neurons in culture', *Nat. Protocols*, 7: 1774-82.
Gauczynski, S., J. M. Peyrin, S. Haik, C. Leucht, C. Hundt, R. Rieger, S. Krasemann, J. P. Deslys, D. Dormont, C. I. Lasmezas, and S. Weiss. 2001. 'The 37-kDa/67-kDa laminin receptor acts as the cell-surface receptor for the cellular prion protein', *Embo J*, 20: 5863-75.
Gelpi, E., Colom-Cadena, M. and Budka, H. (2015). Molecular Genetics of Creutzfeldt–Jakob Disease and Gerstmann– Sträussler– Scheinker Disease. In eLS, John Wiley & Sons, Ltd (Ed.).
Ghiglieri, V., V. Calabrese, and P. Calabresi. 2018. 'Alpha-Synuclein: From Early Synaptic Dysfunction to Neurodegeneration', *Front Neurol*, 9: 295.
Giannopoulos, Paresa N., Catherine Robertson, Julie Jodoin, Hemant Paudel, Stephanie A. Booth, and Andrea C. LeBlanc. 2009. 'Phosphorylation of prion protein at serine 43 induces prion protein conformational change',

The Journal of neuroscience : the official journal of the Society for Neuroscience, 29: 8743-51.

Gill, A. C., M. A. Ritchie, L. G. Hunt, S. E. Steane, K. G. Davies, S. P. Bocking, A. G. Rhie, A. D. Bennett, and J. Hope. 2000. 'Post-translational hydroxylation at the N-terminus of the prion protein reveals presence of PPII structure in vivo', *Embo J*, 19: 5324-31.

Ginhoux, Florent. 2016. 'Modeling microglial differentiation and function in vitro using induced pluripotent stem cells', *Frontiers in Cellular Neuroscience*.

Golan, H., T. Levav, A. Mendelsohn, and M. Huleihel. 2004. 'Involvement of tumor necrosis factor alpha in hippocampal development and function', *Cereb Cortex*, 14: 97-105.

Gómez-Nicola, Diego, Nina L. Fransen, Stefano Suzzi, and V. Hugh Perry. 2013. 'Regulation of Microglial Proliferation during Chronic Neurodegeneration', *The Journal of Neuroscience*, 33: 2481-93.

Gong, Yuesong, Lei Chang, Kirsten L. Viola, Pascale N. Lacor, Mary P Lambert, Caleb E. Finch, Grant A. Krafft, and William L. Klein. 2003. 'Alzheimer's disease-affected brain: Presence of oligomeric Aβ ligands (ADDLs) suggests a molecular basis for reversible memory loss', *Proceedings of the National Academy of Sciences*, 100: 10417-22.

Goold, R., C. McKinnon, S. Rabbanian, J. Collinge, G. Schiavo, and S. J. Tabrizi. 2013. 'Alternative fates of newly formed PrPSc upon prion conversion on the plasma membrane', *J Cell Sci*, 126: 3552-62.

Goold, R., S. Rabbanian, L. Sutton, R. Andre, P. Arora, J. Moonga, A. R. Clarke, G. Schiavo, P. Jat, J. Collinge, and S. J. Tabrizi. 2011. 'Rapid cell-surface prion protein conversion revealed using a novel cell system', *Nat Commun*, 2: 281.

Graham, J. F., S. Agarwal, D. Kurian, L. Kirby, T. J. Pinheiro, and A. C. Gill. 2010. 'Low density subcellular fractions enhance disease-specific prion protein misfolding', *J Biol Chem*, 285: 9868-80.

Graner, E., A. F. Mercadante, S. M. Zanata, O. V. Forlenza, A. L. Cabral, S. S. Veiga, M. A. Juliano, R. Roesler, R. Walz, A. Minetti, I. Izquierdo, V. R. Martins, and R. R. Brentani. 2000a. 'Cellular prion protein binds laminin and mediates neuritogenesis', *Brain Res Mol Brain Res*, 76: 85-92.

Graner, E., A. F. Mercadante, S. M. Zanata, V. R. Martins, D. G. Jay, and R. R. Brentani. 2000. 'Laminin-induced PC-12 cell differentiation is inhibited following laser inactivation of cellular prion protein', *FEBS Letters*, 482: 257-60.

Graner, Edgard, Adriana F. Mercadante, Silvio M. Zanata, Orestes V. Forlenza, Ana L. B. Cabral, Silvio S. Veiga, Maria A. Juliano, Rafael Roesler, Roger Walz, Alejandra Minetti, Ivan Izquierdo, Vilma R. Martins, and Ricardo R. Brentani. 2000b. 'Cellular prion protein binds laminin and mediates neuritogenesis', *Molecular Brain Research*, 76: 85-92.

Grathwohl, S. A., R. E. Kalin, T. Bolmont, S. Prokop, G. Winkelmann, S. A. Kaeser, J. Odenthal, R. Radde, T. Eldh, S. Gandy, A. Aguzzi, M. Staufenbiel, P. M. Mathews, H. Wolburg, F. L. Heppner, and M. Jucker.

2009. 'Formation and maintenance of Alzheimer's disease beta-amyloid plaques in the absence of microglia', *Nat Neurosci*, 12: 1361-3.
Gregersen, N., and P. Bross. 2010. 'Protein misfolding and cellular stress: an overview', *Methods Mol Biol*, 648: 3-23.
Guan, E, S L Robinson, E B Goodman, and A J Tenner. 1994. 'Cell-surface protein identified on phagocytic cells modulates the C1q-mediated enhancement of phagocytosis', *The Journal of Immunology*, 152: 4005-16.
Haass, Christian, and Dennis J. Selkoe. 2007. 'Soluble protein oligomers in neurodegeneration: lessons from the Alzheimer's amyloid [beta]-peptide', *Nat Rev Mol Cell Biol*, 8: 101-12.
Hainfellner, J. A., S. Brantnerinthaler, L. Cervenakova, P. Brown, T. Kitamoto, J. Tateishi, H. Diringer, P. P. Liberski, H. Regele, R. Feucht, N. Mayr, P. Wessely, K. Summer, F. Seitelberger, and H. Budka. 1995. 'The original Gerstmann-Straussler-Scheinker family of Austria - Divergent clinicopathological phenotypes but constant PrP genotype', *Brain Pathology*, 5: 201-11.
Hao, R., P. Nanduri, Y. Rao, R. S. Panichelli, A. Ito, M. Yoshida, and T. P. Yao. 2013. 'Proteasomes activate aggresome disassembly and clearance by producing unanchored ubiquitin chains', *Mol Cell*, 51: 819-28.
Hara, T., K. Nakamura, M. Matsui, A. Yamamoto, Y. Nakahara, R. Suzuki-Migishima, M. Yokoyama, K. Mishima, I. Saito, H. Okano, and N. Mizushima. 2006. 'Suppression of basal autophagy in neural cells causes neurodegenerative disease in mice', *Nature*, 441: 885-9.
Haraguchi, T., S. Fisher, S. Olofsson, T. Endo, D. Groth, A. Tarentino, D. R. Borchelt, D. Teplow, L. Hood, A. Burlingame, E. Lycke, A. Kobata, and S. B. Prusiner. 1989. 'Asparagine-Linked Glycosylation of the Scrapie and Cellular Prion Proteins', *Archives of Biochemistry and Biophysics*, 274: 1-13.
Harding, H. P., Y. Zhang, and D. Ron. 1999. 'Protein translation and folding are coupled by an endoplasmic-reticulum-resident kinase', *Nature*, 397: 271-4.
Harris, D. A. 1999. 'Cellular biology of prion diseases', *Clinical Microbiology Reviews*, 12: 429 (18 pages).
———. 2003. 'Trafficking, turnover and membrane topology of PrP', *Br Med Bull*, 66: 71-85.
Hartmann, Alexander, Christiane Muth, Oliver Dabrowski, Susanne Krasemann, and Markus Glatzel. 2017. 'Exosomes and the Prion Protein: More than One Truth', *Frontiers in Neuroscience*, 11: 194.
Harwell, Claire S., and Michael P. Coleman. 2016. 'Synaptophysin depletion and intraneuronal Aβ in organotypic hippocampal slice cultures from huAPP transgenic mice', *Molecular Neurodegeneration*, 11: 44.
Hasebe, Rie, Gregory J. Raymond, Motohiro Horiuchi, and Byron Caughey. 2012. 'Reaction of complement factors varies with prion strains in vitro and in vivo', *Virology*, 423: 205-13.
Heiseke, A., Y. Aguib, C. Riemer, M. Baier, and H. M. Schatzl. 2009. 'Lithium induces clearance of protease resistant prion protein in prion-infected cells by induction of autophagy', *J Neurochem*, 109: 25-34.

Heiseke, A., Y. Aguib, and H. M. Schatzl. 2010. 'Autophagy, prion infection and their mutual interactions', *Curr Issues Mol Biol*, 12: 87-97.

Hettich, Moritz M., Frank Matthes, Devon P. Ryan, Nadine Griesche, Susanne Schröder, Stephanie Dorn, Sybille Krauß, and Dan Ehninger. 2014. 'The Anti-Diabetic Drug Metformin Reduces BACE1 Protein Level by Interfering with the MID1 Complex', *PLoS ONE*, 9: e102420.

Hetz, C., and B. Mollereau. 2014. 'Disturbance of endoplasmic reticulum proteostasis in neurodegenerative diseases', *Nat Rev Neurosci*, 15: 233-49.

Hill, A. F., M. Desbruslais, S. Joiner, K. C. Sidle, I. Gowland, J. Collinge, L. J. Doey, and P. Lantos. 1997. 'The same prion strain causes vCJD and BSE', *Nature*, 389: 448-50, 526.

Hill, Robert A., Jelena Medved, Kiran D. Patel, and Akiko Nishiyama. 2014. 'Organotypic Slice Cultures to Study Oligodendrocyte Dynamics and Myelination', *J Vis Exp*: 51835.

Hilmert, H., and H. Diringer. 1984. 'A rapid and efficient method to enrich SAF-protein from scrapie brains of hamsters', *Biosci Rep*, 4: 165-70.

Hilton, Kathryn J., Colm Cunningham, Richard A. Reynolds, and V. Hugh Perry. 2013. 'Early Hippocampal Synaptic Loss Precedes Neuronal Loss and Associates with Early Behavioural Deficits in Three Distinct Strains of Prion Disease', *PLoS ONE*, 8: e68062.

Hogue, M. J. 1947. 'Human fetal brain cells in tissue cultures; their identification and motility', *J Exp Zool*, 106: 85-107.

Hollister, Jason R., Kil Sun Lee, David W. Dorward, and Gerald S. Baron. 2015. 'Efficient Uptake and Dissemination of Scrapie Prion Protein by Astrocytes and Fibroblasts from Adult Hamster Brain', *PLoS ONE*, 10: e0115351.

Holmes, Brandon B., and Marc I. Diamond. 2012. 'Cellular mechanisms of protein aggregate propagation', *Curr Opin Neurol*, 25: 721-26.

Homma, T., D. Ishibashi, T. Nakagaki, K. Satoh, K. Sano, R. Atarashi, and N. Nishida. 2014. 'Increased expression of p62/SQSTM1 in prion diseases and its association with pathogenic prion protein', *Sci Rep*, 4: 4504.

Hornemann, S., C. Korth, B. Oesch, R. Riek, G. Wider, K. Wuthrich, and R. Glockshuber. 1997. 'Recombinant full-length murine prion protein, mPrP(23-231): purification and spectroscopic characterization', *FEBS Lett*, 413: 277-81.

Hsiao, K., H. F. Baker, T. J. Crow, M. Poulter, F. Owen, J. D. Terwilliger, D. Westaway, J. Ott, and S. B. Prusiner. 1989. 'Linkage of a prion protein missense variant to Gerstmann-Straussler Syndrome', *Nature*, 338: 342-45.

Hsiao, K. K., D. Groth, M. Scott, S. L. Yang, H. Serban, D. Raff, D. Foster, M. Torchia, S. J. Dearmond, and S. B. Prusiner. 1994. 'Serial transmission in rodents of neurodegeneration from transgenic mice expressing mutant prion protein', *Proceedings Of the National Academy Of Sciences Of the United States Of America*, 91: 9126-30.

Hsiao, K. K., M. Scott, D. Foster, D. F. Groth, S. J. DeArmond, and S. B. Prusiner. 1990. 'Spontaneous neurodegeneration in transgenic mice with mutant prion protein.', *Science*, 250: 1587-90.

Hsiao, K., M. Scott, D. Foster, S. J. DeArmond, D. Groth, H. Serban, and S. B. Prusiner. 1991. 'Spontaneous neurodegeneration in transgenic mice with prion protein codon 101 proline----leucine substitution', *Annals of the New York Academy of Sciences*, 640: 166-70.

Huang, Da Wei, Brad T. Sherman, and Richard A. Lempicki. 2008. 'Systematic and integrative analysis of large gene lists using DAVID bioinformatics resources', *Nat. Protocols*, 4: 44-57.

Huff, Joseph. 2015. 'The Airyscan detector from ZEISS: confocal imaging with improved signal-to-noise ratio and super-resolution', *Nat Meth*, 12.

Hwang, Daehee, Inyoul Y. Lee, Hyuntae Yoo, Nils Gehlenborg, Ji-Hoon Cho, Brianne Petritis, David Baxter, Rose Pitstick, Rebecca Young, Doug Spicer, Nathan D. Price, John G. Hohmann, Stephen J. DeArmond, George A. Carlson, and Leroy E. Hood. 2009. 'A systems approach to prion disease', *Molecular Systems Biology*, 5: 252-52.

Imran, M., and S. Mahmood. 2011. 'An overview of human prion diseases', *Virol J*, 8.

Invernizzi, G., E. Papaleo, R. Sabate, and S. Ventura. 2012. 'Protein aggregation: mechanisms and functional consequences', *Int J Biochem Cell Biol*, 44: 1541-54.

Irvin, D. K., A. Dhaka, C. Hicks, G. Weinmaster, and H. I. Kornblum. 2003. 'Extrinsic and intrinsic factors governing cell fate in cortical progenitor cultures', *Dev Neurosci*, 25: 162-72.

Irwin, D. J., J. Y. Abrams, L. B. Schonberger, E. W. Leschek, J. L. Mills, V. M. Lee, and J. Q. Trojanowski. 2013. 'Evaluation of potential infectivity of Alzheimer and Parkinson disease proteins in recipients of cadaver-derived human growth hormone', *JAMA Neurol*, 70: 462-8.

Jackson, G. S., A. F. Hill, C. Joseph, L. Hosszu, A. Power, J. P. Waltho, A. R. Clarke, and J. Collinge. 1999. 'Multiple folding pathways for heterologously expressed human prion protein', *Biochim Biophys Acta*, 1431: 1-13.

Janelsins, Michelle C., Michael A. Mastrangelo, Keigan M. Park, Kelly L. Sudol, Wade C. Narrow, Salvatore Oddo, Frank M. LaFerla, Linda M. Callahan, Howard J. Federoff, and William J. Bowers. 2008. 'Chronic neuron-specific tumor necrosis factor-alpha expression enhances the local inflammatory environment ultimately leading to neuronal death in 3xTg-AD mice', *The American journal of pathology*, 173: 1768-82.

Jarrett, J. T., and P. T. Lansbury, Jr. 1993. 'Seeding "one-dimensional crystallization" of amyloid: a pathogenic mechanism in Alzheimer's disease and scrapie?', *Cell*, 73: 1055-58.

Jeffrey, Martin, Gillian McGovern, Emily V. Chambers, Declan King, Lorenzo González, Jean C. Manson, Bernardino Ghetti, Pedro Piccardo, and Rona M. Barron. 2012. 'Mechanism of PrP-amyloid formation in mice without transmissible spongiform encephalopathy', *Brain pathology (Zurich, Switzerland)*, 22: 58-66.

Jeffrey, Martin, Gillian McGovern, Stuart Martin, Silvia Siso, and Lorenzo Gonzalez. 2010. *Neuropathology of Animal Prion Diseases Toxic Effects of PrPd, Relationships with Strain and Clinical Disease*.

Jeon, I., N. Lee, J. Y. Li, I. H. Park, K. S. Park, J. Moon, S. H. Shim, C. Choi, D. J. Chang, J. Kwon, S. H. Oh, D. A. Shin, H. S. Kim, J. T. Do, D. R. Lee, M. Kim, K. S. Kang, G. Q. Daley, P. Brundin, and J. Song. 2012. 'Neuronal properties, in vivo effects, and pathology of a Huntington's disease patient-derived induced pluripotent stem cells', *Stem Cells*, 30: 2054-62.

Jones, Raasay S., Aedín M. Minogue, Thomas J. Connor, and Marina A. Lynch. 2013. 'Amyloid-β-Induced Astrocytic Phagocytosis is Mediated by CD36, CD47 and RAGE', *Journal of Neuroimmune Pharmacology*, 8: 301-11.

Kaech, Stefanie, and Gary Banker. 2006. 'Culturing hippocampal neurons', *Nat. Protocols*, 1: 2406-15.

Kane, Sarah J., Taylor K. Farley, Elizabeth O. Gordon, Joshua Estep, Heather R. Bender, Julie A. Moreno, Jason Bartz, Glenn C. Telling, Matthew C. Pickering, and Mark D. Zabel. 2017. 'Complement Regulatory Protein Factor H Is a Soluble Prion Receptor That Potentiates Peripheral Prion Pathogenesis', *The Journal of Immunology*, 199: 3821-27.

Kaneko, K., H.L. Ball, H. Wille, H. Zhang, D. Groth, M. Torchia, P. Tremblay, J. Safar, S. Prusiner, S.J. DeArmond, M.A. Baldwin, and F. Cohen. 2000. 'A synthetic peptide initiates Gerstmann-Straussler-Scheinker (GSS) disease in transgenic mice.', *J. Mol. Biol.*, 295: 997-1007.

Kaneko, K., M. Vey, M. Scott, S. Pilkuhn, F. E. Cohen, and S. B. Prusiner. 1997. 'COOH-terminal sequence of the cellular prion protein directs subcellular trafficking and controls conversion into the scrapie isoform', *Proc Natl Acad Sci U S A*, 94: 2333-8.

Kang, S. C., D. R. Brown, M. Whiteman, R. Li, T. Pan, G. Perry, T. Wisniewski, M. S. Sy, and B. S. Wong. 2004. 'Prion protein is ubiquitinated after developing protease resistance in the brains of scrapie-infected mice', *J Pathol*, 203: 603-8.

Kaplan, D. R., and F. D. Miller. 2000. 'Neurotrophin signal transduction in the nervous system', *Curr Opin Neurobiol*, 10: 381-91.

Kascsak, R. J., R. Rubenstein, P. A. Merz, R. I. Carp, H. M. Wisniewski, and H. Diringer. 1985. 'Biochemical Differences among Scrapie-Associated Fibrils Support the Biological Diversity of Scrapie Agents', *Journal Of General Virology*, 66: 1715-22.

Kaur, G., and A. Lakkaraju. 2018. 'Early Endosome Morphology in Health and Disease', *Adv Exp Med Biol*, 1074: 335-43.

Kayed, R., E. Head, J. L. Thompson, T. M. McIntire, S. C. Milton, C. W. Cotman, and C. G. Glabe. 2003. 'Common structure of soluble amyloid oligomers implies common mechanism of pathogenesis', *Science*, 300: 486-89.

Kim, Y. E., M. S. Hipp, A. Bracher, M. Hayer-Hartl, and F. U. Hartl. 2013. 'Molecular chaperone functions in protein folding and proteostasis', *Annu Rev Biochem*, 82: 323-55.

Kirby, Louise, Christopher R. Birkett, Helene Rudyk, Ian H. Gilbert, and James Hope. 2003. 'In vitro cell-free conversion of bacterial recombinant PrP to PrPres as a model for conversion', *Journal Of General Virology*, 84: 1013-20.

Kirkin, V., T. Lamark, Y. S. Sou, G. Bjorkoy, J. L. Nunn, J. A. Bruun, E. Shvets, D. G. McEwan, T. H. Clausen, P. Wild, I. Bilusic, J. P. Theurillat, A. Overvatn, T. Ishii, Z. Elazar, M. Komatsu, I. Dikic, and T. Johansen. 2009. 'A role for NBR1 in autophagosomal degradation of ubiquitinated substrates', *Mol Cell*, 33: 505-16.

Kitada, T., S. Asakawa, N. Hattori, H. Matsumine, Y. Yamamura, S. Minoshima, M. Yokochi, Y. Mizuno, and N. Shimizu. 1998. 'Mutations in the parkin gene cause autosomal recessive juvenile parkinsonism', *Nature*, 392: 605-8.

Kiyota, T., J. Machhi, Y. Lu, B. Dyavarshetty, M. Nemati, G. Zhang, R. Lee Mosley, H. A. Gelbard, and H. E. Gendelman. 2018. 'URMC-099 facilitates amyloid-beta clearance in a murine model of Alzheimer's disease', *J Neuroinflammation*, 15: 137.

Knowles, T. P., M. Vendruscolo, and C. M. Dobson. 2014. 'The amyloid state and its association with protein misfolding diseases', *Nat Rev Mol Cell Biol*, 15: 384-96.

Kochergin, I. A., and M. N. Zakharova. 2016. 'The role of autophagy in neurodegenerative diseases', *Neurochemical Journal*, 10: 7-18.

Kocisko, D. A., J. H. Come, S. A. Priola, B. Chesebro, G. J. Raymond, P. T. Lansbury, and B. Caughey. 1994. 'Cell-free formation of protease-resistant prion protein', *Nature*, 370: 471-74.

Kordes, U., and C. Hagel. 2006. 'Expression of SOX9 and SOX10 in Central Neuroepithelial Tumor', *J Neurooncol*, 80: 151-55.

Korolchuk, V. I., F. M. Menzies, and D. C. Rubinsztein. 2010. 'Mechanisms of cross-talk between the ubiquitin-proteasome and autophagy-lysosome systems', *FEBS Lett*, 584: 1393-8.

Kovacs, G. G., E. Gelpi, T. Strobel, G. Ricken, J. R. Nyengaard, H. Bernheimer, and H. Budka. 2007. 'Involvement of the endosomal-lysosomal system correlates with regional pathology in Creutzfeldt-Jakob disease', *J Neuropathol Exp Neurol*, 66: 628-36.

Kovacs, G. G., M. Preusser, M. Strohschneider, and H. Budka. 2005. 'Subcellular localization of disease-associated prion protein in the human brain', *Am J Pathol*, 166: 287-94.

Krämer, Andreas, Jeff Green, Jr Jack Pollard, and Stuart Tugendreich. 2014. 'Causal analysis approaches in Ingenuity Pathway Analysis', *Bioinformatics*, 30: 523-30.

Kretzschmar, H. A., P. Kufer, G. Riethmuller, S. DeArmond, S. B. Prusiner, and D. Schiffer. 1992. 'Prion protein mutation at codon 102 in an Italian family with Gerstmann-Straussler-Scheinker syndrome', *Neurology*, 42: 809-10.

Kretzschmar, H. A., S. B. Prusiner, L. E. Stowring, and S. J. DeArmond. 1986. 'Scrapie prion proteins are synthesized in neurons', *Am J Pathol*, 122: 1-5.

Kristensen, Bjarne W., Jens Noraberg, and Jens Zimmer. 2001. 'Comparison of excitotoxic profiles of ATPA, AMPA, KA and NMDA in organotypic hippocampal slice cultures', *Brain Research*, 917: 21-44.

Kristiansen, M., P. Deriziotis, D. E. Dimcheff, G. S. Jackson, H. Ovaa, H. Naumann, A. R. Clarke, F. W. van Leeuwen, V. Menendez-Benito, N.

P. Dantuma, J. L. Portis, J. Collinge, and S. J. Tabrizi. 2007. 'Disease-associated prion protein oligomers inhibit the 26S proteasome', *Mol Cell*, 26: 175-88.

Kristiansen, M., M. J. Messenger, P. C. Klohn, S. Brandner, J. D. Wadsworth, J. Collinge, and S. J. Tabrizi. 2005. 'Disease-related prion protein forms aggresomes in neuronal cells leading to caspase activation and apoptosis', *J Biol Chem*, 280: 38851-61.

Kudo, W., H. P. Lee, W. Q. Zou, X. L. Wang, G. Perry, X. W. Zhu, M. A. Smith, R. B. Petersen, and H. G. Lee. 2012. 'Cellular prion protein is essential for oligomeric amyloid-beta-induced neuronal cell death', *Human Molecular Genetics*, 21: 1138-44.

Kuhlbrodt, K., B. Herbarth, E. Sock, I. Hermans-Borgmeyer, and M. Wegner. 1998. 'Sox10, a novel transcriptional modulator in glial cells', *J Neurosci*, 18: 237-50.

Kuhn, Thomas S. 1996. *The structure of scientific revolutions* (London : University of Chicago Press: Chicago).

Kunkel, T. A., J. D. Roberts, and R. A. Zakour. 1987. 'Rapid and Efficient Site-Specific Mutagenesis without Phenotypic Selection', *Methods in Enzymology*, 154: 367-82.

Kuo, Y. M., M. R. Emmerling, C. Vigo-Pelfrey, T. C. Kasunic, J. B. Kirkpatrick, G. H. Murdoch, M. J. Ball, and A. E. Roher. 1996. 'Water-soluble Abeta (N-40, N-42) oligomers in normal and Alzheimer disease brains', *J Biol Chem*, 271: 4077-81.

Kurji, Khaliq H., Jing Z. Cui, Tony Lin, David Harriman, Shiv S. Prasad, Ljuba Kojic, and Joanne A. Matsubara. 2010. 'Microarray Analysis Identifies Changes in Inflammatory Gene Expression in Response to Amyloid-β Stimulation of Cultured Human Retinal Pigment Epithelial Cells', *Investigative Ophthalmology & Visual Science*, 51: 1151-63.

Kuwahara, C., A. M. Takeuchi, T. Nishimura, K. Haraguchi, A. Kubosaki, Y. Matsumoto, K. Saeki, Y. Matsumoto, T. Yokoyama, S. Itohara, and T. Onodera. 1999. 'Prions prevent neuronal cell-line death', *Nature*, 400: 225-6.

Lacasse, R. A., J. F. Striebel, C. Favara, L. Kercher, and B. Chesebro. 2008. 'Role of Erk1/2 activation in prion disease pathogenesis: Absence of CCR1 leads to increased Erk1/2 activation and accelerated disease progression', *J Neuroimmunol*, 5: 5.

Lamb, C. A., T. Yoshimori, and S. A. Tooze. 2013. 'The autophagosome: origins unknown, biogenesis complex', *Nat Rev Mol Cell Biol*, 14: 759-74.

Laplanche, J. L. 1994. 'Molecular-Basis of Familial and Sporadic Human Prion Diseases', *Transfusion Clinique Et Biologique*, 1: 345-53.

Laszlo, Lajos, James Lowe, Tim Self, Nigel Kenward, Michael Landon, Trisha McBride, Christine Farquhar, Irene McConnell, John Brown, James Hope, and R. John Mayer. 1992. 'Lysosomes as key organelles in the pathogenesis of prion encephalopathies', *The Journal of Pathology*, 166: 333-41.

Lazarov, O., M. Lee, D. A. Peterson, and S. S. Sisodia. 2002. 'Evidence that synaptically released beta-amyloid accumulates as extracellular

deposits in the hippocampus of transgenic mice', *Journal of Neuroscience*, 22: 9785-93.
Lee, C. Y. Daniel, and GaryE Landreth. 2010. 'The role of microglia in amyloid clearance from the AD brain', *Journal of Neural Transmission*, 117: 949-60.
Legname, G., I. V. Baskakov, H. O. Nguyen, D. Riesner, F. E. Cohen, S. J. DeArmond, and S. B. Prusiner. 2004. 'Synthetic mammalian prions', *Science*, 305: 673-6.
Li, A., S. Sakaguchi, K. Shigematsu, R. Atarashi, B. C. Roy, R. Nakaoke, K. Arima, N. Okimura, J. Kopacek, and S. Katamine. 2000. 'Physiological expression of the gene for PrP-like protein, PrPLP/Dpl, by brain endothelial cells and its ectopic expression in neurons of PrP-deficient mice ataxic due to Purkinje cell degeneration', *The American journal of pathology*, 157: 1447-52.
Liberski, P. P. 2012. 'Gerstmann-Straussler-Scheinker disease', *Adv Exp Med Biol*, 724: 128-37.
Liberski, P. P., and H. Budka. 2004. 'Gerstmann-Straussler-Scheinker disease. I. Human diseases', *Folia Neuropathol*, 42 Suppl B: 120-40.
Liberski, P. P., B. Sikorska, J. J. Hauw, N. Kopp, N. Streichenberger, P. Giraud, J. Boellaard, H. Budka, G. G. Kovacs, J. Ironside, and P. Brown. 2010. 'Ultrastructural characteristics (or evaluation) of Creutzfeldt-Jakob disease and other human transmissible spongiform encephalopathies or prion diseases', *Ultrastruct Pathol*, 34: 351-61.
Lim, J. P., and P. A. Gleeson. 2011. 'Macropinocytosis: an endocytic pathway for internalising large gulps', *Immunol Cell Biol*, 89: 836-43.
Ling, E. A., and W. C. Wong. 1993. 'The origin and nature of ramified and amoeboid microglia: a historical review and current concepts', *Glia*, 7: 9-18.
Livak, K. J., and T. D. Schmittgen. 2001. 'Analysis of relative gene expression data using real-time quantitative PCR and the 2(-Delta Delta C(T)) Method', *Methods*, 25: 402-8.
Locht, C., B. Chesebro, R. Race, and J. M. Keith. 1986. 'Molecular cloning and complete sequence of prion protein cDNA from mouse brain infected with the scrapie agent', *Proceedings Of the National Academy Of Sciences Of the United States Of America*, 83: 6372-76.
Loov, C., L. Hillered, T. Ebendal, and A. Erlandsson. 2012. 'Engulfing astrocytes protect neurons from contact-induced apoptosis following injury', *PLoS ONE*, 7: e33090.
LoVerso, P. R., C. M. Wachter, and F. Cui. 2015. 'Cross-species Transcriptomic Comparison of In Vitro and In Vivo Mammalian Neural Cells', *Bioinform Biol Insights*, 9: 153-64.
Lue, L. -. F., Y. -. M. Kuo, A. E. Roher, L. Brachova, Y. Shen, and L. Sue. 1999. 'Soluble amyloid β peptide concentration as a predictor of synaptic change in Alzheimer's disease', *Am J Pathol*, 155.
MacGregor, I. 2001. 'Prion protein and developments in its detection', *Transfus Med*, 11: 3-14.
Magalhaes, A. C., G. S. Baron, K. S. Lee, O. Steele-Mortimer, D. Dorward, M. A. Prado, and B. Caughey. 2005. 'Uptake and neuritic transport of

scrapie prion protein coincident with infection of neuronal cells', *J Neurosci*, 25: 5207-16.
Magalhaes, A. C., J. A. Silva, K. S. Lee, V. R. Martins, V. F. Prado, S. S. Ferguson, M. V. Gomez, R. R. Brentani, and M. A. Prado. 2002. 'Endocytic intermediates involved with the intracellular trafficking of a fluorescent cellular prion protein', *J Biol Chem*, 277: 33311-8.
Majumdar, A., D. Cruz, N. Asamoah, A. Buxbaum, I. Sohar, P. Lobel, and F. R. Maxfield. 2007. 'Activation of microglia acidifies lysosomes and leads to degradation of Alzheimer amyloid fibrils', *Mol Biol Cell*, 18: 1490-6.
Majumder, P., and O. Chakrabarti. 2015. 'Mahogunin regulates fusion between amphisomes/MVBs and lysosomes via ubiquitination of TSG101', *Cell Death Dis*, 6: e1970.
———. 2017. 'Lysosomal Quality Control in Prion Diseases', *Mol Neurobiol*.
Makarava, N., and I. V. Baskakov. 2008. 'Expression and purification of full-length recombinant PrP of high purity', *Methods Mol Biol*, 459: 131-43.
———. 2012. 'Purification and fibrillation of full-length recombinant PrP', *Methods Mol Biol*, 849: 33-52.
Makarava, N., G. G. Kovacs, O. Bocharova, R. Savtchenko, I. Alexeeva, H. Budka, R. G. Rohwer, and I. V. Baskakov. 2010. 'Recombinant prion protein induces a new transmissible prion disease in wild-type animals', *Acta Neuropathol*, 119: 177-87.
Makarava, N., G. G. Kovacs, R. Savtchenko, I. Alexeeva, H. Budka, R. G. Rohwer, and I. V. Baskakov. 2011. 'Genesis of mammalian prions: from non-infectious amyloid fibrils to a transmissible prion disease', *PLoS Pathog*, 7: e1002419.
———. 2012. 'Stabilization of a prion strain of synthetic origin requires multiple serial passages', *J Biol Chem*, 287: 30205-14.
Makarava, N., G. G. Kovacs, R. Savtchenko, I. Alexeeva, V. G. Ostapchenko, H. Budka, R. G. Rohwer, and I. V. Baskakov. 2012. 'A new mechanism for transmissible prion diseases', *J Neurosci*, 32: 7345-55.
Malagoli, Davide. 2016. 'The evolution of the immune system : conservation and diversification'.
Malchiodi-Albedi, Fiorella, Valentina Contrusciere, Carla Raggi, Katia Fecchi, Gabriella Rainaldi, Silvia Paradisi, Andrea Matteucci, Maria Teresa Santini, Massimo Sargiacomo, Claudio Frank, Maria Cristina Gaudiano, and Marco Diociaiuti. 2010. 'Lipid raft disruption protects mature neurons against amyloid oligomer toxicity', *Biochimica et Biophysica Acta (BBA) - Molecular Basis of Disease*, 1802: 406-15.
Mallucci, G., A. Dickinson, J. Linehan, P. C. Klohn, S. Brandner, and J. Collinge. 2003. 'Depleting neuronal PrP in prion infection prevents disease and reverses spongiosis', *Science*, 302: 871-4.
Mallucci, G. R., M. D. White, M. Farmer, A. Dickinson, H. Khatun, A. D. Powell, S. Brandner, J. G. Jefferys, and J. Collinge. 2007. 'Targeting cellular prion protein reverses early cognitive deficits and neurophysiological dysfunction in prion-infected mice', *Neuron*, 53: 325-35.
Manson, J. C. , E. Jamieson, H. Baybutt, N. L. Tuzi, R. Barron, I. McConnell, R. Somerville, J. Ironside, R. Will, M. S. Sy, D. W. Melton, J. Hope, and C. Bostock. 1999. 'A single amino acid alteration (101L) introduced

into murine PrP dramatically alters incubation time of transmissible spongiform encephalopathy.', *EMBO Journal*, 18: 6855-64.

Manson, J. C., A. R. Clarke, M. L. Hooper, L. Aitchison, I. McConnell, and J. Hope. 1994. '129/Ola mice carrying a null mutation in PrP that abolishes messenger-RNA production are developmentally normal', *Mol. Neurobiol.*, 8: 121-27.

Manson, J. C., A. R. Clarke, P. A. McBride, I. McConnell, and J. Hope. 1994. 'PrP gene dosage determines the timing but not the final intensity or distribution of lesions in scrapie pathology', *Neurodegeneration*, 3: 331-40.

Manson, J., J. D. West, V. Thomson, P. McBride, M. H. Kaufman, and J. Hope. 1992. 'The prion protein gene: a role in mouse embryogenesis?', *Development*, 115: 117-22.

Manson, J.; Bradford, B.; Baybutt, H.; Marshall, A.; Brown, D.; Kisielewski, D.; Alibhai, J.; Barron, R.; Piccardo, P.; Whitehouse, I.; et al. 2011. 'Pathways to Neurodegeneration Associated with Protein Misfolding', *Prion 5:13-14*.

Marchetti, L., M. Klein, K. Schlett, K. Pfizenmaier, and U. L. Eisel. 2004. 'Tumor necrosis factor (TNF)-mediated neuroprotection against glutamate-induced excitotoxicity is enhanced by N-methyl-D-aspartate receptor activation. Essential role of a TNF receptor 2-mediated phosphatidylinositol 3-kinase-dependent NF-kappa B pathway', *J Biol Chem*, 279: 32869-81.

Marijanovic, Z., A. Caputo, V. Campana, and C. Zurzolo. 2009. 'Identification of an intracellular site of prion conversion', *PLoS Pathog*, 5: e1000426.

Marzo, L., Z. Marijanovic, D. Browman, Z. Chamoun, A. Caputo, and C. Zurzolo. 2013. '4-hydroxytamoxifen leads to PrPSc clearance by conveying both PrPC and PrPSc to lysosomes independently of autophagy', *J Cell Sci*, 126: 1345-54.

Masliah, E., M. Mallory, M. Alford, R. DeTeresa, L.A. Hansen, D.W. McKeel, and J.C. Morris. 2001. 'Altered expression of synaptic proteins occurs early during progression of Alzheimer's disease', *Neurology*, 56: 127-29.

Mason, C. A. 1986. 'Axon development in mouse cerebellum: embryonic axon forms and expression of synapsin I', *Neuroscience*, 19: 1319-33.

Matamoros-Angles, A., L. M. Gayosso, Y. Richaud-Patin, A. di Domenico, C. Vergara, A. Hervera, A. Sousa, N. Fernandez-Borges, A. Consiglio, R. Gavin, R. Lopez de Maturana, I. Ferrer, A. Lopez de Munain, A. Raya, J. Castilla, R. Sanchez-Pernaute, and J. A. Del Rio. 2018. 'iPS Cell Cultures from a Gerstmann-Straussler-Scheinker Patient with the Y218N PRNP Mutation Recapitulate tau Pathology', *Mol Neurobiol*, 55: 3033-48.

Matarin, Mar, Dervis A Salih, Marina Yasvoina, Damian M Cummings, Sebastian Guelfi, Wenfei Liu, Muzammil A Nahaboo Solim, Thomas G Moens, Rocio Moreno Paublete, Shabinah S Ali, Marina Perona, Roshni Desai, Kenneth J Smith, Judy Latcham, Michael Fulleylove, Jill C Richardson, John Hardy, and Frances A Edwards. 2015. 'A Genome-wide Gene-Expression Analysis and Database in Transgenic

Mice during Development of Amyloid or Tau Pathology', *Cell Rep*, 10: 633-44.
Mattei, V., M. G. Barenco, V. Tasciotti, T. Garofalo, A. Longo, K. Boller, J. Lower, R. Misasi, F. Montrasio, and M. Sorice. 2009. 'Paracrine diffusion of PrP(C) and propagation of prion infectivity by plasma membrane-derived microvesicles', *PLoS ONE*, 4: e5057.
Mattson, P. 2000. *Genetic Aberrancies and Neurodegenerative Disorders* (Elsevier Science).
McBride, P. A., M. E. Bruce, and H. Fraser. 1988. 'Immunostaining of scrapie cerebral amyloid plaques with antisera raised to scrapie-associated fibrils (SAF)', *Neuropathol Appl Neurobiol*, 14: 325-36.
McCoy, Melissa K., and Malú G. Tansey. 2008. 'TNF signaling inhibition in the CNS: implications for normal brain function and neurodegenerative disease', *Journal of Neuroinflammation*, 5: 45.
McKinley, M. P., D. C. Bolton, and S. B. Prusiner. 1983. 'A protease-resistant protein is a structural component of the scrapie prion', *Cell*, 35: 57-62.
McKinney, R. A., D. Debanne, B. H. Gahwiler, and S. M. Thompson. 1997. 'Lesion-induced axonal sprouting and hyperexcitability in the hippocampus in vitro: implications for the genesis of posttraumatic epilepsy', *Nat Med*, 3: 990-6.
McLean, C. A., R. A. Cherny, F. W. Fraser, S. J. Fuller, M. J. Smith, K. Beyreuther, A. I. Bush, and C. L. Masters. 1999. 'Soluble pool of Abeta amyloid as a determinant of severity of neurodegeneration in Alzheimer's disease', *Ann Neurol*, 46: 860-6.
McManus, Terence, Matthew Sadgrove, Ashley K. Pringle, John E. Chad, and Lars E. Sundstrom. 2004. 'Intraischaemic hypothermia reduces free radical production and protects against ischaemic insults in cultured hippocampal slices', *Journal of Neurochemistry*, 91: 327-36.
Meijering, E., M. Jacob, J. C. Sarria, P. Steiner, H. Hirling, and M. Unser. 2004. 'Design and validation of a tool for neurite tracing and analysis in fluorescence microscopy images', *Cytometry A*, 58: 167-76.
Merz, P. A., R. A. Somerville, H. M. Wisniewski, and K. Iqbal. 1981. 'Abnormal fibrils from scrapie-infected brain', *Acta Neuropathol*, 54: 63-74.
Meyer-Luehmann, Melanie, Janaky Coomaraswamy, Tristan Bolmont, Stephan Kaeser, Claudia Schaefer, Ellen Kilger, Anton Neuenschwander, Dorothee Abramowski, Peter Frey, Anneliese L. Jaton, Jean-Marie Vigouret, Paolo Paganetti, Dominic M. Walsh, Paul M. Mathews, Jorge Ghiso, Matthias Staufenbiel, Lary C. Walker, and Mathias Jucker. 2006. 'Exogenous Induction of Cerebral {beta}-Amyloidogenesis Is Governed by Agent and Host', *Science*, 313: 1781-84.
Mi, H., A. Muruganujan, J. T. Casagrande, and P. D. Thomas. 2013. 'Large-scale gene function analysis with the PANTHER classification system', *Nature Protocols*, 8: 1551-66.
Michel, B., A. Ferguson, T. Johnson, H. Bender, C. Meyerett-Reid, A. C. Wyckoff, B. Pulford, G. C. Telling, and M. D. Zabel. 2013. 'Complement protein C3 exacerbates prion disease in a mouse model of chronic wasting disease', *Int Immunol*, 25: 697-702.

Mirabile, Ilaria, Parmjit S. Jat, Sebastian Brandner, and John Collinge. 2015. 'Identification of clinical target areas in the brainstem of prion-infected mice', *Neuropathology and Applied Neurobiology*, 41: 613-30.

Modica, G., and S. Lefrancois. 2017. 'Post-translational modifications: How to modulate Rab7 functions', *Small GTPases*: 1-7.

Mody, Monica, Yanxiang Cao, Zhenzhong Cui, Khoon-Yen Tay, Andy Shyong, Eiji Shimizu, Kelvin Pham, Peter Schultz, Douglas Welsh, and Joe Z. Tsien. 2001. 'Genome-wide gene expression profiles of the developing mouse hippocampus', *Proceedings Of the National Academy Of Sciences Of the United States Of America*, 98: 8862-67.

Monif, Mastura, Geoffrey Burnstock, and David A. Williams. 2010. 'Microglia: Proliferation and activation driven by the P2X7 receptor', *The International Journal of Biochemistry & Cell Biology*, 42: 1753-56.

Monji, Akira, Ken-ichiro Tashiro, Ichiro Yoshida, Yoshihito Hayashi, and Nobutada Tashiro. 1998. 'Laminin inhibits Aβ42 fibril formation in vitro', *Brain Research*, 788: 187-90.

Moore, R. C., I. Y. Lee, G. L. Silverman, P. M. Harrison, R. Strome, C. Heinrich, A. Karunaratne, S. H. Pasternak, M. A. Chishti, Y. Liang, P. Mastrangelo, K. Wang, A. F. A. Smit, S. Katamine, G. A. Carlson, F. E. Cohen, S. B. Prusiner, D. W. Melton, P. Tremblay, L. E. Hood, and D. Westaway. 1999. 'Ataxia in prion protein (PrP)-deficient mice is associated with upregulation of the novel PrP-like protein Doppel', *Journal of Molecular Biology*, 292: 797-817.

Moore, R. C., N. J. Redhead, J. Selfridge, J. Hope, J. C. Manson, and D. W. Melton. 1995. 'Double replacement gene targeting for the production of a series of mouse strains with different prion protein gene alterations', *Bio/Technology*, 13: 999-1004.

Morales, Rodrigo, Lisbell D. Estrada, Rodrigo Diaz-Espinoza, Diego Morales-Scheihing, Maria C. Jara, Joaquin Castilla, and Claudio Soto. 2010. 'Molecular Cross Talk between Misfolded Proteins in Animal Models of Alzheimer's and Prion Diseases', *The Journal of Neuroscience*, 30: 4528-35.

Moreno-Gonzalez, Ines, and Claudio Soto. 2011. 'Misfolded Protein Aggregates: Mechanisms, Structures and Potential for Disease Transmission', *Seminars in Cell & Developmental Biology*, 22: 482-87.

Moreno, J. A., M. Halliday, C. Molloy, H. Radford, N. Verity, J. M. Axten, C. A. Ortori, A. E. Willis, P. M. Fischer, D. A. Barrett, and G. R. Mallucci. 2013. 'Oral treatment targeting the unfolded protein response prevents neurodegeneration and clinical disease in prion-infected mice', *Sci Transl Med*, 5: 206ra138.

Moreno, Julie A., Helois Radford, Diego Peretti, Joern R. Steinert, Nicholas Verity, Maria Guerra Martin, Mark Halliday, Jason Morgan, David Dinsdale, Catherine A. Ortori, David A. Barrett, Pavel Tsaytler, Anne Bertolotti, Anne E. Willis, Martin Bushell, and Giovanna R. Mallucci. 2012. 'Sustained translational repression by eIF2[agr]-P mediates prion neurodegeneration', *Nature*, 485: 507-11.

Moriyama, Maiko, Takeshi Fukuhara, Markus Britschgi, Yingbo He, Ramya Narasimhan, Saul Villeda, Hector Molina, Brigitte T. Huber, Mike

Holers, and Tony Wyss-Coray. 2011. 'Complement Receptor 2 Is Expressed in Neural Progenitor Cells and Regulates Adult Hippocampal Neurogenesis', *The Journal of Neuroscience*, 31: 3981-89.

Moser, Markus, Raymond J. Colello, Uwe Pott, and Bruno Oesch. 1995. 'Developmental expression of the prion protein gene in glial cells', *Neuron*, 14: 509-17.

Mu, Yangling, and Fred H. Gage. 2011. 'Adult hippocampal neurogenesis and its role in Alzheimer's disease', *Molecular Neurodegeneration*, 6: 1-9.

Mucke, L., E. Masliah, G. -. Q. Yu, M. Mallory, E. M. Rockenstein, and G. Tatsuno. 2000. 'High-level neuronal expression of Aβ1–42 in wild-type human amyloid protein precursor transgenic mice: synaptotoxicity without plaque formation', *J Neurosci*, 20.

Muratore, C. R., H. C. Rice, P. Srikanth, D. G. Callahan, T. Shin, L. N. Benjamin, D. M. Walsh, D. J. Selkoe, and T. L. Young-Pearse. 2014. 'The familial Alzheimer's disease APPV717I mutation alters APP processing and Tau expression in iPSC-derived neurons', *Hum Mol Genet*, 23: 3523-36.

Nazor, K.E., F. Kuhn, T. Seward, M. Green, D. Zwald, M. Pürro, J. Schmid, K. Biffiger, A.M. Power, B. Oesch, A. Raeber, and G. Telling. 2005. 'Immunodetection of disease-associated mutant PrP, which accelerates disease in GSS transgenic mice ', *EMBO Journal*, 24: 2472-80.

Nedelsky, N. B., P. K. Todd, and J. P. Taylor. 2008. 'Autophagy and the ubiquitin-proteasome system: collaborators in neuroprotection', *Biochim Biophys Acta*, 1782: 691-9.

Nichols, B. J., A. K. Kenworthy, R. S. Polishchuk, R. Lodge, T. H. Roberts, K. Hirschberg, R. D. Phair, and J. Lippincott-Schwartz. 2001. 'Rapid cycling of lipid raft markers between the cell surface and Golgi complex', *J Cell Biol*, 153: 529-41.

Nilsson, M. R. 2004. 'Techniques to study amyloid fibril formation in vitro', *Methods*, 34: 151-60.

Nixon, R. A. 2013. 'The role of autophagy in neurodegenerative disease', *Nat Med*, 19: 983-97.

Noraberg, J., F. R. Poulsen, M. Blaabjerg, B. W. Kristensen, C. Bonde, M. Montero, M. Meyer, J. B. Gramsbergen, and J. Zimmer. 2005. 'Organotypic Hippocampal Slice Cultures for Studies of Brain Damage, Neuroprotection and Neurorepair', *Current Drug Targets - CNS & Neurological Disorders*, 4: 435-52.

Novitskaya, V., O. V. Bocharova, I. Bronstein, and I. V. Baskakov. 2006. 'Amyloid fibrils of mammalian prion protein are highly toxic to cultured cells and primary neurons', *J Biol Chem*, 281: 13828-36.

Novotny, R., F. Langer, J. Mahler, A. Skodras, A. Vlachos, B. M. Wegenast-Braun, S. A. Kaeser, J. J. Neher, Y. S. Eisele, M. J. Pietrowski, K. P. Nilsson, T. Deller, M. Staufenbiel, B. Heimrich, and M. Jucker. 2016. 'Conversion of Synthetic Abeta to In Vivo Active Seeds and Amyloid Plaque Formation in a Hippocampal Slice Culture Model', *J Neurosci*, 36: 5084-93.

Oesch, B., D. Westaway, M. Walchli, M. P. McKinley, S. B. Kent, R. Aebersold, R. A. Barry, P. Tempst, D. B. Teplow, L. E. Hood, and et al. 1985. 'A cellular gene encodes scrapie PrP 27-30 protein', *Cell*, 40: 735-46.

Orth, Matthias, and Stefano Bellosta. 2012. 'Cholesterol: Its Regulation and Role in Central Nervous System Disorders', *Cholesterol*, 2012: 19.

Oueslati, Abid, Methodios Ximerakis, and Kostas Vekrellis. 2014. 'Protein Transmission, Seeding and Degradation: Key Steps for α-Synuclein Prion-Like Propagation', *Exp Neurobiol*, 23: 324-36.

Ozcelik, S., G. Fraser, P. Castets, V. Schaeffer, Z. Skachokova, K. Breu, F. Clavaguera, M. Sinnreich, L. Kappos, M. Goedert, M. Tolnay, and D. T. Winkler. 2013. 'Rapamycin attenuates the progression of tau pathology in P301S tau transgenic mice', *PLoS ONE*, 8: e62459.

Palmer, M. S., A. J. Dryden, J. T. Hughes, and J. Collinge. 1991. 'Homozygous prion protein genotype predisposes to sporadic Creutzfeldt-Jakob disease', *Nature*, 352: 340-42.

Pan, K. M., M. Baldwin, J. Nguyen, M. Gasset, A. Serban, D. Groth, I. Mehlhorn, Z. Huang, R. J. Fletterick, F. E. Cohen, and et al. 1993. 'Conversion of alpha-helices into beta-sheets features in the formation of the scrapie prion proteins', *Proc Natl Acad Sci U S A*, 90: 10962-6.

Pandeya, D. R, Acharya, N.K, Hong, S-T. 2010. 'Review: The Prion and its Potentiality', International Journal of Medical Sciences, 21:2

Pankiv, S., T. H. Clausen, T. Lamark, A. Brech, J. A. Bruun, H. Outzen, A. Overvatn, G. Bjorkoy, and T. Johansen. 2007. 'p62/SQSTM1 binds directly to Atg8/LC3 to facilitate degradation of ubiquitinated protein aggregates by autophagy', *J Biol Chem*, 282: 24131-45.

Paolicelli, R. C., G. Bolasco, F. Pagani, L. Maggi, M. Scianni, P. Panzanelli, M. Giustetto, T. A. Ferreira, E. Guiducci, L. Dumas, D. Ragozzino, and C. T. Gross. 2011. 'Synaptic pruning by microglia is necessary for normal brain development', *Science*, 333: 1456-8.

Papadimitriou, C., H. Celikkaya, M. I. Cosacak, V. Mashkaryan, L. Bray, P. Bhattarai, K. Brandt, H. Hollak, X. Chen, S. He, C. L. Antos, W. Lin, A. K. Thomas, A. Dahl, T. Kurth, J. Friedrichs, Y. Zhang, U. Freudenberg, C. Werner, and C. Kizil. 2018. '3D Culture Method for Alzheimer's Disease Modeling Reveals Interleukin-4 Rescues Abeta42-Induced Loss of Human Neural Stem Cell Plasticity', *Dev Cell*, 46: 85-101.e8.

Parchi, P., W. Zou, W. Wang, P. Brown, S. Capellari, B. Ghetti, N. Kopp, W. J. Schulz-Schaeffer, H. A. Kretzschmar, M. W. Head, J. W. Ironside, P. Gambetti, and S. G. Chen. 2000. 'Genetic influence on the structural variations of the abnormal prion protein', *Proceedings Of the National Academy Of Sciences Of the United States Of America*, 97: 10168-72.

Park, J., I. Wetzel, I. Marriott, D. Dreau, C. D'Avanzo, D. Y. Kim, R. E. Tanzi, and H. Cho. 2018. 'A 3D human triculture system modeling neurodegeneration and neuroinflammation in Alzheimer's disease', *Nat Neurosci*, 21: 941-51.

Parmar, M., C. Skogh, A. Bjorklund, and K. Campbell. 2002. 'Regional specification of neurosphere cultures derived from subregions of the embryonic telencephalon', *Mol Cell Neurosci*, 21: 645-56.

Pearce, M. M., E. J. Spartz, W. Hong, L. Luo, and R. R. Kopito. 2015. 'Prion-like transmission of neuronal huntingtin aggregates to phagocytic glia in the Drosophila brain', *Nat Commun*, 6: 6768.

Pedersen, Søren W., Louise Albertsen, Griffin E. Moran, Brié Levesque, Stine B. Pedersen, Lina Bartels, Hannah Wapenaar, Fei Ye, Mingjie Zhang, Mark E. Bowen, and Kristian Strømgaard. 2017. 'Site-Specific Phosphorylation of PSD-95 PDZ Domains Reveals Fine-Tuned Regulation of Protein–Protein Interactions', *ACS Chemical Biology*, 12: 2313-23.

Perry, V. H., C. Cunningham, and D. Boche. 2002. 'Atypical inflammation in the central nervous system in prion disease', *Curr Opin Neurol*, 15: 349-54.

Perry, V. Hugh, and Jessica Teeling. 2013. 'Microglia and macrophages of the central nervous system: the contribution of microglia priming and systemic inflammation to chronic neurodegeneration', *Seminars in Immunopathology*, 35: 601-12.

Peters, O. M., M. Ghasemi, and R. H. Brown, Jr. 2015. 'Emerging mechanisms of molecular pathology in ALS', *J Clin Invest*, 125: 1767-79.

Peters, Peter J., Alexander Mironov, David Peretz, Elly van Donselaar, Estelle Leclerc, Susanne Erpel, Stephen J. DeArmond, Dennis R. Burton, R. Anthony Williamson, Martin Vey, and Stanley B. Prusiner. 2003. 'Trafficking of prion proteins through a caveolae-mediated endosomal pathway', *The Journal of Cell Biology*, 162: 703-17.

Piccardo, P., J. C. Manson, D. King, B. Ghetti, and R. M. Barron. 2007. 'Accumulation of prion protein in the brain that is not associated with transmissible disease', *Proc Natl Acad Sci U S A*, 104: 4712-7.

Pollard, Thomas D. 2017. 'Chapter 22 - Endocytosis and the Endosomal Membrane System A2 - Pollard, Thomas D.' in William C. Earnshaw, Jennifer Lippincott-Schwartz and Graham T. Johnson (eds.), *Cell Biology (Third Edition)* (Elsevier).

Prusiner, S. B. 1982. 'Novel proteinaceous infectious particles cause scrapie', *Science*, 216: 136-44.

———. 1993. 'Genetic and infectious prion diseases', *Arch Neurol*, 50: 1129-53.

———. 1996. 'Molecular biology and pathogenesis of prion diseases', *Trends in Biochemical Sciences*, 21: 482-87.

Prusiner, SB. 1998. 'Prions', *Proc Natl Acad Sci USA*, 95: 13363 - 83.

Prusiner, Stanley B., Michael P. McKinley, Karen A. Bowman, David C. Bolton, Paul E. Bendheim, Darlene F. Groth, and George G. Glenner. 1983. 'Scrapie prions aggregate to form amyloid-like birefringent rods', *Cell*, 35: 349-58.

Qin, Song, Xiang-You Hu, Hao Xu, and Jiang-Ning Zhou. 2004. 'Regional alteration of synapsin I in the hippocampal formation of Alzheimer's disease patients', *Acta Neuropathologica*, 107: 209-15.

Quist, Arjan, Ivo Doudevski, Hai Lin, Rushana Azimova, Douglas Ng, Blas Frangione, Bruce Kagan, Jorge Ghiso, and Ratnesh Lal. 2005. 'Amyloid ion channels: A common structural link for protein-misfolding disease', *PNAS*, 102: 10427-32.

Race, R. E., S. A. Priola, R. A. Bessen, D. Ernst, J. Dockter, G. F. Rall, L. Mucke, B. Chesebro, and M. B. Oldstone. 1995. 'Neuron-specific expression of a hamster prion protein minigene in transgenic mice induces susceptibility to hamster scrapie agent', *Neuron*, 15: 1183-91.

Raeber, A. J., R. E. Race, S. Brandner, S. A. Priola, A. Sailer, R. A. Bessen, L. Mucke, J. Manson, A. Aguzzi, M. B. Oldstone, C. Weissmann, and B. Chesebro. 1997. 'Astrocyte-specific expression of hamster prion protein (PrP) renders PrP knockout mice susceptible to hamster scrapie', *Embo J*, 16: 6057-65.

Rahpeymai Bogestål, Yalda, Scott Barnum, Peter Smith, Victor Mattisson, Milos Pekny, and Marcela Pekna. 2007. *Signaling through C5aR is not involved in basal neurogenesis*.

Rangel, A., B. Race, J. Striebel, and B. Chesebro. 2013. 'Non-amyloid and amyloid prion protein deposits in prion-infected mice differ in blockage of interstitial brain fluid', *Neuropathol Appl Neurobiol*, 39: 217-30.

Ravikumar, B., C. Vacher, Z. Berger, J. E. Davies, S. Luo, L. G. Oroz, F. Scaravilli, D. F. Easton, R. Duden, C. J. O'Kane, and D. C. Rubinsztein. 2004. 'Inhibition of mTOR induces autophagy and reduces toxicity of polyglutamine expansions in fly and mouse models of Huntington disease', *Nat Genet*, 36: 585-95.

Ray, Balmiki, Jason A. Bailey, Sumit Sarkar, and Debomoy K. Lahiri. 2009. 'Molecular and immunocytochemical characterization of primary neuronal cultures from adult rat brain: differential expression of neuronal and glial protein markers', *Journal of Neuroscience Methods*, 184: 294-302.

Raymond, G. J., B. Race, J. R. Hollister, D. K. Offerdahl, R. A. Moore, R. Kodali, L. D. Raymond, A. G. Hughson, R. Rosenke, D. Long, D. W. Dorward, and G. S. Baron. 2012. 'Isolation of novel synthetic prion strains by amplification in transgenic mice co-expressing wild-type and anchorless prion proteins', *J Virol*.

Reddy, P. Hemachandra, Shannon McWeeney, Byung S. Park, Maria Manczak, Ramana V. Gutala, Dara Partovi, Youngsin Jung, Vincent Yau, Robert Searles, Motomi Mori, and Joseph Quinn. 2004. 'Gene expression profiles of transcripts in amyloid precursor protein transgenic mice: up-regulation of mitochondrial metabolism and apoptotic genes is an early cellular change in Alzheimer's disease', *Human Molecular Genetics*, 13: 1225-40.

Ren, Guohui, Carl Huynh, Krikor Bijian, and Andrey V. Cybulsky. 2008. 'Role of apoptosis signal-regulating kinase 1 in complement-mediated glomerular epithelial cell injury', *Molecular Immunology*, 45: 2236-46.

Rezaei, H., D. Marc, Y. Choiset, M. Takahashi, G. Hui Bon Hoa, T. Haertle, J. Grosclaude, and P. Debey. 2000. 'High yield purification and physico-chemical properties of full-length recombinant allelic variants of sheep prion protein linked to scrapie susceptibility', *Eur J Biochem*, 267: 2833-9.

Rieger, R., F. Edenhofer, C. I. Lasmezas, and S. Weiss. 1997. 'The human 37-kDa laminin receptor precursor interacts with the prion protein in eukaryotic cells', *Nat Med*, 3: 1383-8.

Riek, R., S. Hornemann, G. Wider, R Glockschuber, and K. Wuthrich. 1997. 'NMR characterization of the full-length recombinant murine prion protein, mPrP(23-231).', *FEBS Lett*, 413: 282-88.
Riesner, D. 2003. 'Biochemistry and structure of PrP(C) and PrP(Sc)', *Br Med Bull*, 66: 21-33.
Rink, J., E. Ghigo, Y. Kalaidzidis, and M. Zerial. 2005. 'Rab conversion as a mechanism of progression from early to late endosomes', *Cell*, 122: 735-49.
Roher, A. E., M. O. Chaney, Y. M. Kuo, S. D. Webster, W. B. Stine, L. J. Haverkamp, A. S. Woods, R. J. Cotter, J. M. Tuohy, G. A. Krafft, B. S. Bonnell, and M. R. Emmerling. 1996. 'Morphology and toxicity of A beta-(1-42) dimer derived from neuritic and vascular amyloid deposits of Alzheimer's disease', *Journal Of Biological Chemistry*, 271: 20631-35.
Ross, C. A., and M. A. Poirier. 2004. 'Protein aggregation and neurodegenerative disease', *Nat Med*, 10 Suppl: S10-7.
Roucou, X., M. Gains, and A. C. LeBlanc. 2004. 'Neuroprotective functions of prion protein', *J Neurosci Res*, 75: 153-61.
Rouvinski, A., S. Karniely, M. Kounin, S. Moussa, M. D. Goldberg, G. Warburg, R. Lyakhovetsky, D. Papy-Garcia, J. Kutzsche, C. Korth, G. A. Carlson, S. F. Godsave, P. J. Peters, K. Luhr, K. Kristensson, and A. Taraboulos. 2014. 'Live imaging of prions reveals nascent PrPSc in cell-surface, raft-associated amyloid strings and webs', *J Cell Biol*, 204: 423-41.
Rushworth, Jo V., Heledd H. Griffiths, Nicole T. Watt, and Nigel M. Hooper. 2013. 'Prion Protein-mediated Toxicity of Amyloid-β Oligomers Requires Lipid Rafts and the Transmembrane LRP1', *Journal Of Biological Chemistry*, 288: 8935-51.
Rynkowski, Michal, Grace H Kim, Matthew C Garrett, Brad Zacharia, Marc L Otten, Sergei A Sosunov, Ricardo J Komotar, Benjamin G Hassid, Andrew Ducruet, John Lambris, and E. Connolly. 2008. *C3a receptor antagonist attenuates brain injury after intracerebral hemorrhage*.
Saftig, P., and J. Klumperman. 2009. 'Lysosome biogenesis and lysosomal membrane proteins: trafficking meets function', *Nat Rev Mol Cell Biol*, 10: 623-35.
Salvatore, M., M. Genuardi, R. Petraroli, C. Masullo, M. Dalessandro, and M. Pocchiari. 1994. 'Polymorphisms of the Prion Protein Gene in Italian Patients with Creutzfeldt-Jakob-Disease', *Hum Genet*, 94: 375-79.
Santamaria, I., G. Velasco, A. M. Pendas, A. Fueyo, and C. Lopez-Otin. 1998. 'Cathepsin Z, a novel human cysteine proteinase with a short propeptide domain and a unique chromosomal location', *J Biol Chem*, 273: 16816-23.
Santuccione, A., V. Sytnyk, I. Leshchyns'ka, and M. Schachner. 2005. 'Prion protein recruits its neuronal receptor NCAM to lipid rafts to activate p59fyn and to enhance neurite outgrowth', *J Cell Biol*, 169: 341-54.
Scheff, Stephen W., Douglas A. Price, Frederick A. Schmitt, and Elliott J. Mufson. 2006. 'Hippocampal synaptic loss in early Alzheimer's disease and mild cognitive impairment', *Neurobiology of Aging*, 27: 1372-84.
Schenk, D., R. Barbour, W. Dunn, G. Gordon, H. Grajeda, T. Guido, K. Hu, J. Huang, K. Johnson-Wood, K. Khan, D. Kholodenko, M. Lee, Z. Liao, I.

Lieberburg, R. Motter, L. Mutter, F. Soriano, G. Shopp, N. Vasquez, C. Vandevert, S. Walker, M. Wogulis, T. Yednock, D. Games, and P. Seubert. 1999. 'Immunization with amyloid-beta attenuates Alzheimer-disease-like pathology in the PDAPP mouse', *Nature*, 400: 173-7.

Schlachetzki, Johannes C.M., Soraya Wilke Saliba, and Antonio Carlos Pinheiro de Oliveira. 2013. 'Studying neurodegenerative diseases in culture models', *Revista Brasileira de Psiquiatria*, 35: S92-S100.

Schondorf, D. C., M. Aureli, F. E. McAllister, C. J. Hindley, F. Mayer, B. Schmid, S. P. Sardi, M. Valsecchi, S. Hoffmann, L. K. Schwarz, U. Hedrich, D. Berg, L. S. Shihabuddin, J. Hu, J. Pruszak, S. P. Gygi, S. Sonnino, T. Gasser, and M. Deleidi. 2014. 'iPSC-derived neurons from GBA1-associated Parkinson's disease patients show autophagic defects and impaired calcium homeostasis', *Nat Commun*, 5: 4028.

Schonfeld-Dado, E., and M. Segal. 2009. 'Activity-dependent survival of neurons in culture: a model of slow neurodegeneration', *J Neural Transm (Vienna)*, 116: 1363-9.

Scotter, E. L., C. Vance, A. L. Nishimura, Y. B. Lee, H. J. Chen, H. Urwin, V. Sardone, J. C. Mitchell, B. Rogelj, D. C. Rubinsztein, and C. E. Shaw. 2014. 'Differential roles of the ubiquitin proteasome system and autophagy in the clearance of soluble and aggregated TDP-43 species', *J Cell Sci*, 127: 1263-78.

Seibenhener, Michael L., and Marie W. Wooten. 2012. 'Isolation and Culture of Hippocampal Neurons from Prenatal Mice', *J Vis Exp*: 3634.

Sheng, M., and E. Kim. 2011. 'The postsynaptic organization of synapses', *Cold Spring Harb Perspect Biol*, 3.

Shi, Y., H. Inoue, J. C. Wu, and S. Yamanaka. 2017. 'Induced pluripotent stem cell technology: a decade of progress', *Nat Rev Drug Discov*, 16: 115-30.

Shinjyo, Noriko, Anders Ståhlberg, Mike Dragunow, Milos Pekny, and Marcela Pekna. 2009. 'Complement-Derived Anaphylatoxin C3a Regulates In Vitro Differentiation and Migration of Neural Progenitor Cells', *Stem Cells*, 27: 2824-32.

Shmerling, Doron, Ivan Hegyi, Marek Fischer, Thomas Blättler, Sebastian Brandner, Jürgen Götz, Thomas Rülicke, Eckhard Flechsig, Antonio Cozzio, Christian von Mering, Christoph Hangartner, Adriano Aguzzi, and Charles Weissmann. 1998. 'Expression of Amino-Terminally Truncated PrP in the Mouse Leading to Ataxia and Specific Cerebellar Lesions', *Cell*, 93: 203-14.

Sikorska, B. 2004. 'Mechanisms of neuronal death in transmissible spongiform encephalopathies', *Folia Neuropathol*, 42 Suppl B: 89-95.

Sikorska, B., P. P. Liberski, P. Giraud, N. Kopp, and P. Brown. 2004. 'Autophagy is a part of ultrastructural synaptic pathology in Creutzfeldt-Jakob disease: a brain biopsy study', *Int J Biochem Cell Biol*, 36: 2563-73.

Silverman, J. M., S. M. Fernando, L. I. Grad, A. F. Hill, B. J. Turner, J. J. Yerbury, and N. R. Cashman. 2016. 'Disease Mechanisms in ALS: Misfolded SOD1 Transferred Through Exosome-Dependent and Exosome-Independent Pathways', *Cell Mol Neurobiol*, 36: 377-81.

Simoneau, S., H. Rezaei, N. Sales, G. Kaiser-Schulz, M. Lefebvre-Roque, C. Vidal, J. G. Fournier, J. Comte, F. Wopfner, J. Grosclaude, H. Schatzl, and C. I. Lasmezas. 2007. 'In vitro and in vivo neurotoxicity of prion protein oligomers', *PLoS Pathog*, 3: e125.

Skinner, Pamela J., Hayet Abbassi, Bruce Chesebro, Richard E. Race, Cavan Reilly, and Ashley T. Haase. 2006. 'Gene expression alterations in brains of mice infected with three strains of scrapie', *BMC Genomics*, 7: 114.

Smith, G. A., E. M. Rocha, J. R. McLean, M. A. Hayes, S. C. Izen, O. Isacson, and P. J. Hallett. 2014. 'Progressive axonal transport and synaptic protein changes correlate with behavioral and neuropathological abnormalities in the heterozygous Q175 KI mouse model of Huntington's disease', *Hum Mol Genet*, 23: 4510-27.

Smith, I., M. Haag, C. Ugbode, D. Tams, M. Rattray, S. Przyborski, A. Bithell, and B. J. Whalley. 2015. 'Neuronal-glial populations form functional networks in a biocompatible 3D scaffold', *Neurosci Lett*, 609: 198-202.

Smith, M. H., H. L. Ploegh, and J. S. Weissman. 2011. 'Road to ruin: targeting proteins for degradation in the endoplasmic reticulum', *Science*, 334: 1086-90.

Smith, Shilo M., Michael B. Wunder, David A. Norris, and Yiqun G. Shellman. 2011. 'A Simple Protocol for Using a LDH-Based Cytotoxicity Assay to Assess the Effects of Death and Growth Inhibition at the Same Time', *PLoS ONE*, 6: e26908.

Sofroniew, M. V. 2005. 'Reactive astrocytes in neural repair and protection', *Neuroscientist*, 11: 400-7.

———. 2009. 'Molecular dissection of reactive astrogliosis and glial scar formation', *Trends Neurosci*, 32: 638-47.

Sofroniew, Michael V., and Harry V. Vinters. 2010. 'Astrocytes: biology and pathology', *Acta Neuropathologica*, 119: 7-35.

Söllvander, Sofia, Elisabeth Nikitidou, Robin Brolin, Linda Söderberg, Dag Sehlin, Lars Lannfelt, and Anna Erlandsson. 2016. 'Accumulation of amyloid-β by astrocytes result in enlarged endosomes and microvesicle-induced apoptosis of neurons', *Molecular Neurodegeneration*, 11: 38.

Soto, C., and L. D. Estrada. 2008. 'Protein misfolding and neurodegeneration', *Arch Neurol*, 65: 184-9.

Soto, Claudio. 2003. 'Unfolding the role of protein misfolding in neurodegenerative diseases', *Nat Rev Neurosci*, 4: 49-60.

Staal, Jerome A., Samuel R. Alexander, Yao Liu, Tracey D. Dickson, and James C. Vickers. 2011. 'Characterization of Cortical Neuronal and Glial Alterations during Culture of Organotypic Whole Brain Slices from Neonatal and Mature Mice', *PLoS ONE*, 6: e22040.

Stahl, N., M. A. Baldwin, D. B. Teplow, L. Hood, B. W. Gibson, A. L. Burlingame, and S. B. Prusiner. 1993. 'Structural studies of the scrapie prion protein using mass spectrometry and amino acid sequencing', *Biochemistry*, 32: 1991-2002.

Stahl, N., D. R. Borchelt, K. Hsiao, and S. B. Prusiner. 1987. 'Scrapie Prion Protein Contains a Phosphatidylinositol Glycolipid', *Cell*, 51: 229-40.

Stevens, Beth, Nicola J. Allen, Luis E. Vazquez, Gareth R. Howell, Karen S. Christopherson, Navid Nouri, Kristina D. Micheva, Adrienne K. Mehalow, Andrew D. Huberman, Benjamin Stafford, Alexander Sher, Alan M Litke, John D. Lambris, Stephen J. Smith, Simon W. M. John, and Ben A. Barres. 2007. 'The Classical Complement Cascade Mediates CNS Synapse Elimination', *Cell*, 131: 1164-78.

Stoppini, L., P. A. Buchs, and D. Muller. 1991. 'A simple method for organotypic cultures of nervous tissue', *J Neurosci Methods*, 37: 173-82.

Sun, Wei, Adam Cornwell, Jiashu Li, Sisi Peng, M. Joana Osorio, Nadia Aalling Su Wanga, Abdellatif Benraiss, Nanhong Lou, Steven A. Goldman, and Maiken Nedergaard. 2017. 'SOX9 is an astrocyte-specific nuclear marker in the adult brain outside the neurogenic regions', *The Journal of Neuroscience*.

Swanson, J. A., and C. Watts. 1995. 'Macropinocytosis', *Trends Cell Biol*, 5: 424-8.

Takahashi, K., and S. Yamanaka. 2006. 'Induction of pluripotent stem cells from mouse embryonic and adult fibroblast cultures by defined factors', *Cell*, 126: 663-76.

Tamguney, Gultekin, Kurt Giles, David V. Glidden, Pierre Lessard, Holger Wille, Patrick Tremblay, Darlene F. Groth, Fruma Yehiely, Carsten Korth, Richard C. Moore, Jorg Tatzelt, Eric Rubinstein, Claude Boucheix, Xiaoping Yang, Pamela Stanley, Michael P. Lisanti, Raymond A. Dwek, Pauline M. Rudd, Jackob Moskovitz, Charles J. Epstein, Tracey Dawson Cruz, William A. Kuziel, Nobuyo Maeda, Jan Sap, Karen Hsiao Ashe, George A. Carlson, Ina Tesseur, Tony Wyss-Coray, Lennart Mucke, Karl H. Weisgraber, Robert W. Mahley, Fred E. Cohen, and Stanley B. Prusiner. 2008. 'Genes contributing to prion pathogenesis', *Journal Of General Virology*, 89: 1777-88.

Taraboulos, A., A. J. Raeber, D. R. Borchelt, D. Serban, and S. B. Prusiner. 1992. 'Synthesis and trafficking of prion proteins in cultured cells', *Mol Biol Cell*, 3: 851-63.

Taraboulos, A., M. Scott, A. Semenov, D. Avrahami, L. Laszlo, and S. B. Prusiner. 1995. 'Cholesterol depletion and modification of COOH-terminal targeting sequence of the prion protein inhibit formation of the scrapie isoform', *J Cell Biol*, 129: 121-32.

Tateishi, J., T. Kitamoto, H. Hashiguchi, and H. Shii. 1988. 'Gerstmann-Straussler-Scheinker disease: immunohistological and experimental studies', *Ann Neurol*, 24: 35-40.

Taylor, D. R., and N. M. Hooper. 2006. 'The prion protein and lipid rafts', *Mol Membr Biol*, 23: 89-99.

Telling, G. C., T. Haga, M. Torchia, P. Tremblay, S. J. Dearmond, and S. B. Prusiner. 1996. 'Interactions between wild-type and mutant prion proteins modulate neurodegeneration in transgenic mice', *Genes and Development*, 10: 1736-50.

Thackray, Alana M., Andrew N. McKenzie, Michael A. Klein, Angus Lauder, and Raymond Bujdoso. 2004. 'Accelerated Prion Disease in the Absence of Interleukin-10', *Journal Of Virology*, 78: 13697-707.

Thellung, Stefano, Elena Gatta, Francesca Pellistri, Valentina Villa, Alessandro Corsaro, Mario Nizzari, Mauro Robello, and Tullio Florio. 2017. 'Different Molecular Mechanisms Mediate Direct or Glia-Dependent Prion Protein Fragment 90–231 Neurotoxic Effects in Cerebellar Granule Neurons', *Neurotox Res*, 32: 381-97.

Thellung, Stefano, Beatrice Scoti, Alessandro Corsaro, Valentina Villa, Mario Nizzari, Maria Gagliani, Carola Porcile, Claudio Russo, Aldo Pagano, Carlo Tacchetti, Katia Cortese, and Tullio Florio. 2018. *Pharmacological activation of autophagy favors the clearing of intracellular aggregates of misfolded prion protein peptide to prevent neuronal death*.

Theocharidis, Athanasios, Stjin van Dongen, Anton J. Enright, and Tom C. Freeman. 2009. 'Network visualization and analysis of gene expression data using BioLayout Express3D', *Nat. Protocols*, 4: 1535-50.

Thompson, S., A. R. Clarke, A. M. Pow, M. L. Hooper, and D. W. Melton. 1989. 'Germ Line Transmission and Expression of a Corrected Hprt Gene Produced by Gene Targeting in Embryonic Stem-Cells', *Cell*, 56: 313-21.

Tian, C., D. Liu, C. Chen, Y. Xu, H. S. Gong, C. Chen, Q. Shi, B. Y. Zhang, J. Han, and X. P. Dong. 2013. 'Global transcriptional profiling of the postmortem brain of a patient with G114V genetic Creutzfeldt-Jakob disease', *Int J Mol Med*, 31: 676-88.

Towbin, H., T. Staehelin, and J. Gordon. 1979. 'Electrophoretic Transfer of Proteins from Polyacrylamide Gels to Nitrocellulose Sheets - Procedure and Some Applications', *Proceedings Of the National Academy Of Sciences Of the United States Of America*, 76: 4350-54.

Tracey, T. J., F. J. Steyn, E. J. Wolvetang, and S. T. Ngo. 2018. 'Neuronal Lipid Metabolism: Multiple Pathways Driving Functional Outcomes in Health and Disease', *Front Mol Neurosci*, 11: 10.

Tremblay, P., H. L. Ball, K. Kaneko, D. Groth, R. S. Hegde, F. E. Cohen, S. J. DeArmond, S. B. Prusiner, and J. G. Safar. 2004. 'Mutant PrPSc conformers induced by a synthetic peptide and several prion strains', *Journal Of Virology*, 78: 2088-99.

Treusch, S., D. M. Cyr, and S. Lindquist. 2009. 'Amyloid deposits: protection against toxic protein species?', *Cell Cycle*, 8: 1668-74.

Tropepe, V., M. Sibilia, B. G. Ciruna, J. Rossant, E. F. Wagner, and D. van der Kooy. 1999. 'Distinct neural stem cells proliferate in response to EGF and FGF in the developing mouse telencephalon', *Dev Biol*, 208: 166-88.

Turk, E., D. B. Teplow, L. E. Hood, and S. B. Prusiner. 1988. 'Purification and Properties of the Cellular and Scrapie Hamster Prion Proteins', *European Journal of Biochemistry*, 176: 21-30.

Urwin, H., A. Authier, J. E. Nielsen, D. Metcalf, C. Powell, K. Froud, D. S. Malcolm, I. Holm, P. Johannsen, J. Brown, E. M. Fisher, J. van der Zee, M. Bruyland, C. Van Broeckhoven, J. Collinge, S. Brandner, C. Futter, and A. M. Isaacs. 2010. 'Disruption of endocytic trafficking in frontotemporal dementia with CHMP2B mutations', *Hum Mol Genet*, 19: 2228-38.

Valastyan, Julie S., and Susan Lindquist. 2014. 'Mechanisms of protein-folding diseases at a glance', *Disease Models & Mechanisms*, 7: 9-14.

van Beek, Johan, Olivier Nicole, Cheraghalikhani Ali, Alexander Ischenko, Eric Mackenzie, Alain Buisson, and Marc Fontaine. 2001. *Complement anaphylatoxin C3a is selectively protective against NMDA-induced neuronal cell death*.

van Keulen, L. J., B. E. Schreuder, R. H. Meloen, M. Poelen-van den Berg, G. Mooij-Harkes, M. E. Vromans, and J. P. Langeveld. 1995. 'Immunohistochemical detection and localization of prion protein in brain tissue of sheep with natural scrapie', *Vet Pathol*, 32: 299-308.

van Leeuwen, F. W., P. van Tijn, M. A. Sonnemans, B. Hobo, D. M. Mann, C. Van Broeckhoven, S. Kumar-Singh, P. Cras, G. Leuba, A. Savioz, M. L. Maat-Schieman, H. Yamaguchi, J. M. Kros, W. Kamphorst, E. M. Hol, R. A. de Vos, and D. F. Fischer. 2006. 'Frameshift proteins in autosomal dominant forms of Alzheimer disease and other tauopathies', *Neurology*, 66: S86-92.

Veerhuis, Robert, Henrietta M. Nielsen, and Andrea J. Tenner. 2011. 'Complement in the brain', *Molecular Immunology*, 48: 1592-603.

Vella, L. J., R. A. Sharples, V. A. Lawson, C. L. Masters, R. Cappai, and A. F. Hill. 2007. 'Packaging of prions into exosomes is associated with a novel pathway of PrP processing', *The Journal of Pathology*, 211: 582-90.

Vey, M., S. Pilkuhn, H. Wille, R. Nixon, S. J. DeArmond, E. J. Smart, R. G. Anderson, A. Taraboulos, and S. B. Prusiner. 1996. 'Subcellular colocalization of the cellular and scrapie prion proteins in caveolae-like membranous domains', *Proc Natl Acad Sci U S A*, 93: 14945-9.

Victoria, G. S., A. Arkhipenko, S. Zhu, S. Syan, and C. Zurzolo. 2016. 'Astrocyte-to-neuron intercellular prion transfer is mediated by cell-cell contact', *Sci Rep*, 6: 20762.

Walsh, D. M., B. P. Tseng, R. E. Rydel, M. B. Podlisny, and D. J. Selkoe. 2000. 'The oligomerization of amyloid beta-protein begins intracellularly in cells derived from human brain', *Biochemistry*, 39: 10831-39.

Walter, Peter, and David Ron. 2011. 'The Unfolded Protein Response: From Stress Pathway to Homeostatic Regulation', *Science*, 334: 1081-86.

Walz, R., O. B. Amaral, I. C. Rockenbach, R. Roesler, I. Izquierdo, E. A. Cavalheiro, V. R. Martins, and R. R. Brentani. 1999. 'Increased sensitivity to seizures in mice lacking cellular prion protein', *Epilepsia*, 40: 1679-82.

Wang, C., L. Qin, Z. Min, Y. Zhao, L. Zhu, J. Zhu, and S. Yu. 2015. 'SOX7 interferes with beta-catenin activity to promote neuronal apoptosis', *Eur J Neurosci*, 41: 1430-7.

Wang, Xin, Francesca Cattaneo, Lisa Ryno, John Hulleman, Natàlia Reixach, and Joel N. Buxbaum. 2014. 'The Systemic Amyloid Precursor Transthyretin (TTR) Behaves as a Neuronal Stress Protein Regulated by HSF1 in SH-SY5Y Human Neuroblastoma Cells and APP23 Alzheimer's Disease Model Mice', *The Journal of Neuroscience*, 34: 7253-65.

Webb, J. L., B. Ravikumar, J. Atkins, J. N. Skepper, and D. C. Rubinsztein. 2003. 'Alpha-Synuclein is degraded by both autophagy and the proteasome', *J Biol Chem*, 278: 25009-13.

Wechselberger, C., S. Wurm, W. Pfarr, and O. Hoglinger. 2002. 'The physiological functions of prion protein', *Exp Cell Res*, 281: 1-8.

Wegiel, Jerzy, K. C Wang, M. and Tarnawski, and Boleslaw Lach. 2000. *Microglia cells are the driving force in fibrillar plaque formation, whereas astrocytes are a leading factor in plague degradation*.

Weider, Matthias, and Michael Wegner. 2017. 'SoxE factors: Transcriptional regulators of neural differentiation and nervous system development', *Seminars in Cell & Developmental Biology*, 63: 35-42.

Weller, Roy O., Effie Djuanda, Hong-Yeen Yow, and Roxana O. Carare. 2008. 'Lymphatic drainage of the brain and the pathophysiology of neurological disease', *Acta Neuropathologica*, 117: 1.

Westaway, D. 1987. 'Distinct prion proteins in short and long scrapie incubation period mice', *Cell*, 51: 651-62.

Westergard, L., H. M. Christensen, and D. A. Harris. 2007. 'The cellular prion protein (PrP(C)): its physiological function and role in disease', *Biochim Biophys Acta*, 1772: 629-44.

Westermark, P., M. D. Benson, J. N. Buxbaum, A. S. Cohen, B. Frangione, S. Ikeda, C. L. Masters, G. Merlini, M. J. Saraiva, and J. D. Sipe. 2005. 'Amyloid: toward terminology clarification. Report from the Nomenclature Committee of the International Society of Amyloidosis', *Amyloid*, 12: 1-4.

Will, R. G., J. W. Ironside, M. Zeidler, S. N. Cousens, K. Estibeiro, A. Alperovitch, S. Poser, M. Pocchiari, A. Hofman, and P. G. Smith. 1996. 'A new variant of Creutzfeldt-Jakob disease in the UK', *Lancet*, 347: 921-25.

Williams, A. E., L. J. Lawson, V. H. Perry, and H. Fraser. 1994. 'Characterization of the microglial response in murine scrapie', *Neuropathology and Applied Neurobiology*, 20: 47-55.

Winner, B., Z. Kohl, and F. H. Gage. 2011. 'Neurodegenerative disease and adult neurogenesis', *Eur J Neurosci*, 33.

Wolf, H., A. Hossinger, A. Fehlinger, S. Buttner, V. Sim, D. McKenzie, and I. M. Vorberg. 2015. 'Deposition pattern and subcellular distribution of disease-associated prion protein in cerebellar organotypic slice cultures infected with scrapie', *Front Neurosci*, 9: 410.

Wolfe, Katie J., and Douglas M. Cyr. 2011. 'Amyloid in neurodegenerative diseases: Friend or foe?', *Seminars in Cell & Developmental Biology*, 22: 476-81.

Wu, Chunlei, Camilo Orozco, Jason Boyer, Marc Leglise, James Goodale, Serge Batalov, Christopher L. Hodge, James Haase, Jeff Janes, Jon W. Huss, and Andrew I. Su. 2009. 'BioGPS: an extensible and customizable portal for querying and organizing gene annotation resources', *Genome Biology*, 10: R130-R30.

Wüthrich, Kurt, and Roland Riek. 2001. 'Three-dimensional structures of prion proteins.' in Caughey Byron (ed.), *Advances in Protein Chemistry* (Academic Press).

Xanthopoulos, Konstantinos, Magdalini Polymenidou, Sue J. Bellworthy, Sylvie L. Benestad, and Theodoros Sklaviadis. 2009. 'Species and Strain Glycosylation Patterns of PrPSc', *PLoS ONE*, 4: e5633.

Yamasaki, T., G. S. Baron, A. Suzuki, R. Hasebe, and M. Horiuchi. 2014. 'Characterization of intracellular dynamics of inoculated PrP-res and newly generated PrP(Sc) during early stage prion infection in Neuro2a cells', *Virology*, 450-451: 324-35.

Yang, Y., S. Vidensky, L. Jin, C. Jie, I. Lorenzini, M. Frankl, and J. D. Rothstein. 2011. 'Molecular comparison of GLT1+ and ALDH1L1+ astrocytes in vivo in astroglial reporter mice', *Glia*, 59: 200-7.

Yao, H., D. Zhao, S. H. Khan, and L. Yang. 2013. 'Role of autophagy in prion protein-induced neurodegenerative diseases', *Acta Biochim Biophys Sin (Shanghai)*, 45: 494-502.

Ye, Z. C., and H. Sontheimer. 1998. 'Astrocytes protect neurons from neurotoxic injury by serum glutamate', *Glia*, 22: 237-48.

Yim, Y. I., B. C. Park, R. Yadavalli, X. Zhao, E. Eisenberg, and L. E. Greene. 2015. 'The multivesicular body is the major internal site of prion conversion', *J Cell Sci*, 128: 1434-43.

Yu, Zhe, and III Barclay Morrison. 2010. 'Experimental Mild Traumatic Brain Injury Induces Functional Alteration of the Developing Hippocampus', *Journal of Neurophysiology*, 103: 499-510.

Yuan, Jue, Xiangzhu Xiao, John McGeehan, Zhiqian Dong, Ignazio Cali, Hisashi Fujioka, Qingzhong Kong, Geoff Kneale, Pierluigi Gambetti, and Wen-Quan Zou. 2006. 'Insoluble Aggregates and Protease-resistant Conformers of Prion Protein in Uninfected Human Brains', *Journal Of Biological Chemistry*, 281: 34848-58.

Yuki, D., Y. Sugiura, N. Zaima, H. Akatsu, S. Takei, and I. Yao. 2014. 'DHA-PC and PSD-95 decrease after loss of synaptophysin and before neuronal loss in patients with Alzheimer's disease', *Sci Rep*, 4.

Zahn, R., C. von Schroetter, and K. Wuthrich. 1997. 'Human prion proteins expressed in Escherichia coli and purified by high-affinity column refolding', *FEBS Lett*, 417: 400-4.

Zahn, Ralph, Christine von Schroetter, and Kurt Wüthrich. 1997. 'Human prion proteins expressed in Escherichia coli and purified by high-affinity column refolding', *FEBS Letters*, 417: 400-04.

Zanata, S. M., M. H. Lopes, A. F. Mercadante, G. N. Hajj, L. B. Chiarini, R. Nomizo, A. R. Freitas, A. L. Cabral, K. S. Lee, M. A. Juliano, E. de Oliveira, S. G. Jachieri, A. Burlingame, L. Huang, R. Linden, R. R. Brentani, and V. R. Martins. 2002. 'Stress-inducible protein 1 is a cell surface ligand for cellular prion that triggers neuroprotection', *Embo J*, 21: 3307-16.

Zhang, K., C. J. Donnelly, A. R. Haeusler, J. C. Grima, J. B. Machamer, P. Steinwald, E. L. Daley, S. J. Miller, K. M. Cunningham, S. Vidensky, S. Gupta, M. A. Thomas, I. Hong, S. L. Chiu, R. L. Huganir, L. W. Ostrow, M. J. Matunis, J. Wang, R. Sattler, T. E. Lloyd, and J. D. Rothstein. 2015. 'The C9orf72 repeat expansion disrupts nucleocytoplasmic transport', *Nature*, 525: 56-61.

Zhang, Ye, Gengyun Wen, Genze Shao, Cuidong Wang, Chyuansheng Lin, Hongbo Fang, Adayabalam S. Balajee, Govind Bhagat, Tom K. Hei, and Yongliang Zhao. 2009. 'TGFBI deficiency predisposes mice to spontaneous tumor development', *Cancer Res*, 69: 37-44.

Zhong, Li, Zhen-Lian Zhang, Xinxiu Li, Chunyan Liao, Pengfei Mou, Tingting Wang, Zongqi Wang, Zhe Wang, Min Wei, Huaxi Xu, Guojun Bu, and Xiao-Fen Chen. 2017. 'TREM2/DAP12 Complex Regulates Inflammatory Responses in Microglia via the JNK Signaling Pathway', *Frontiers in Aging Neuroscience*, 9: 204.

Zolezzi, J. M., C. B. Lindsay, F. G. Serrano, R. C. Ureta, C. Theoduloz, G. Schmeda-Hirschmann, and N. C. Inestrosa. 2018. 'Neuroprotective Effects of Ferruginol, Jatrophone, and Junicedric Acid Against Amyloid-beta Injury in Hippocampal Neurons', *J Alzheimers Dis*, 63: 705-23.

Zomosa-Signoret, V., J. D. Arnaud, P. Fontes, M. T. Alvarez-Martinez, and J. P. Liautard. 2007. 'Physiological role of the cellular prion protein', *Vet Res*, 39: 9.

Zou, J. Y., and F. T. Crews. 2005. 'TNF alpha potentiates glutamate neurotoxicity by inhibiting glutamate uptake in organotypic brain slice cultures: neuroprotection by NF kappa B inhibition', *Brain Res*, 1034: 11-24.

Appendices

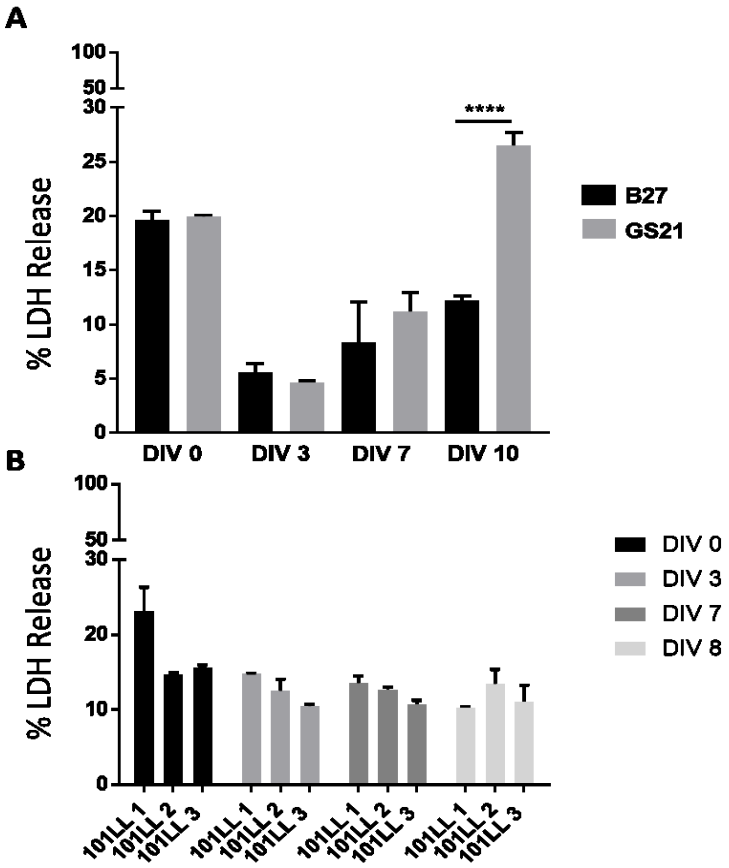

Figure 3.a: B27 supplemented media supported neuronal viability, and minimal levels of LDH were found in 101LL cultures. Comparisons were carried out of two commercial media supplements, B27 and GS21 to ascertain which one would support better neuronal growth and viability. Additionally, LDH release was measured in 101LL cultures to monitor cellular viability over-time. (A) LDH was measured in the supernatant of primary cultures prepared from WT mice at 0, 3, 7 and 10 days *in vitro* (DIV) and was used to monitor cellular viability over-time using both supplements. (B) LDH was measured in the supernatant of primary cultures prepared from 101LL mice at 0, 3, 7 and 8 days *in vitro* (DIV). As shown in (A), at DIV10 GS21 supplement did not support long-term cellular viability in comparison to B27 based on LDH release readings therefore, B27 was used in future culture experiments. Cell viability was maintained in 101LL cultures up to DIV8 as shown in (B) however, cytotoxicity readings were elevated at DIV0. Individual sample readings also confirmed viability was reproducible in cultures. Fluorescent values were normalized to Triton X-100 treated lysis cells that represent the maximum amount of LDH available for release. WT and 101LL cells plated at 400,000 cells per well on PLL 6 well plate, Graph mean plus standard deviation, n=3 triplicate technical replicates, unpaired t test, P-Value <0.0001.

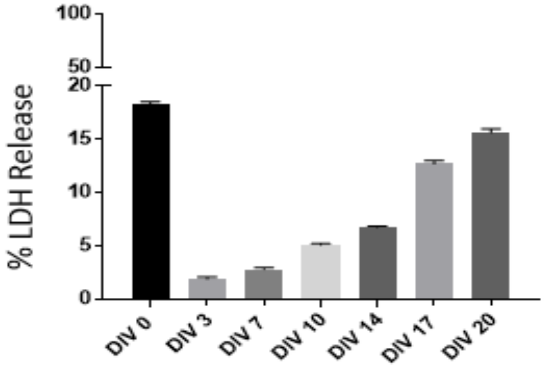

Figure 3.b: Primary cultures were viable up to 20 days *in vitro*. LDH analysis was used to explore stress levels associated with neuronal growth over an extended timeframe in culture. Cytotoxicity readings were elevated at DIV0 but then reduced and stabilised. A gradual increase in cytotoxicity from DIV10 up to DIV20 was occurring however approximately 84% of cells were still viable at this time point. Fluorescent values were normalized to Triton X-100 treated lysis cells that represent the maximum amount of LDH available for release. 101LL cells plated at 150,000 cells per well on PDL/Fibronectin glass coverslips, Graph mean plus standard deviation, n=3 triplicate technical replicates, unpaired t test.

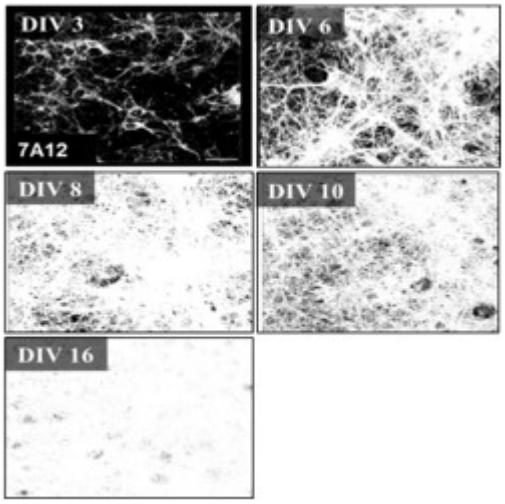

Figure 3.c: PrP^C abundance increased over-time in culture. To investigate if PrP^C levels were increasing with neuronal development over-time, immunolabelling of cultures using a PrP^C antibody was carried out at DIV3, 6, 8, 10 and 16. Images show PrP^C (7A12/White) immunolabelling amplified over-time suggesting PrP^C was increasing with neuronal developed. 101LL cultures 1500,000 cells, plated on PDL/Fibronectin glass coverslips, Scale Bar 30µm.

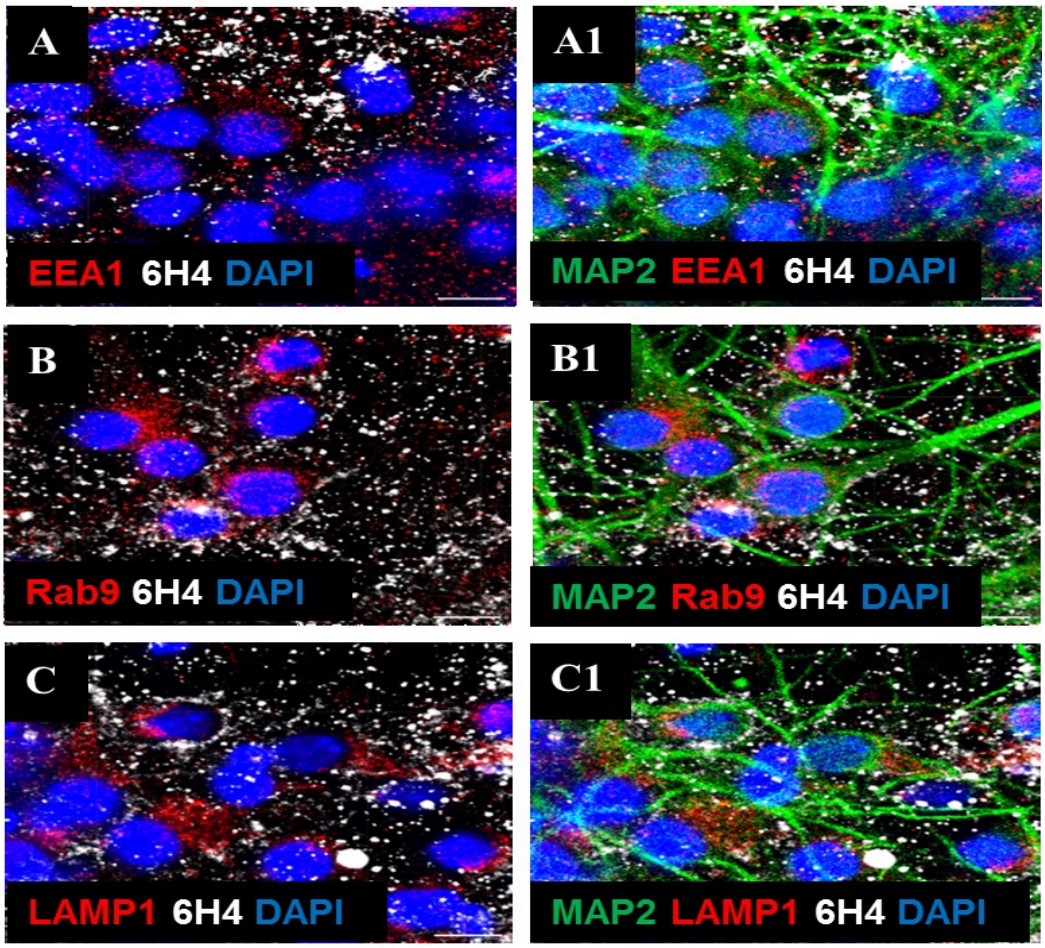

Figure 3.d: Organelle associations were dominant with neuronal cell populations. To investigate if organelles essential for endolysosomal protein processing were detectable in cultures and to ascertain where these domains were located, dual-immunolabelling investigations were carried out. (A) Early endosomes (EEA1/Red), (B) Late endosomes (Rab9/Red) and (C) Lysosomes (LAMP1/Red) co-labelled with antibody for PrP^{C} (6H4/White). (A1, B1, C1) Organelles plus neuronal marker (MAP2/Green). Immunolabelling of neuronal populations confirmed majority of organelles were associated with these cell types. WT cultures, Scale bar 10µm, Zeiss LSM 710.

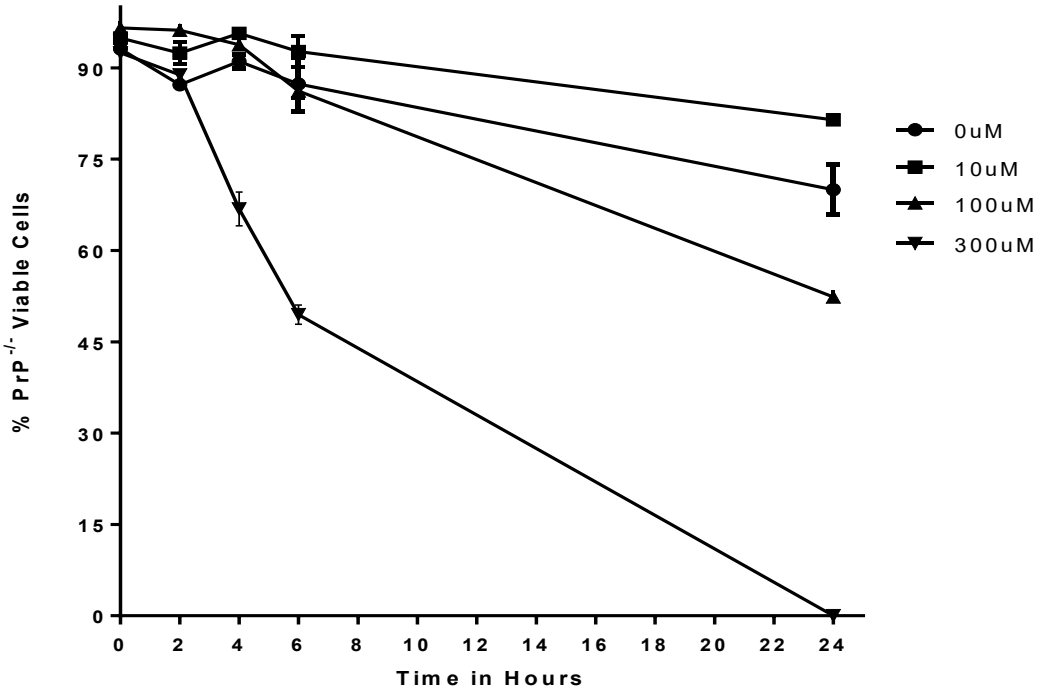

Figure 3.e: Monitoring stress levels in cultures lacking PrP^C expression. LDH cytotoxicity assay was used to measure cellular stress levels of $PrP^{-/-}$ primary hippocampal cultures after challenge with increasing concentrations of H_2O_2 (0, 10, 100, 300µM) to examine if PrP^C was needed for neuroprotection. Culture supernatants were sampled at 0, 2, 4, 6 and 24hrs for LDH activity. Over 50% of cells were viable at 100µM H_2O_2 in $PrP^{-/-}$ primary hippocampal cultures indicating that PrP^C may not be actively involved in neuroprotection as WT and 101LL cultures displayed a significant reduction in cell viability at these parameters (*Figure 3.17*). Fluorescent values were normalized to Triton X-100 treated lysis cells that represent the maximum amount of LDH available for release then the % of viable cells were calculated by % LDH release value minus 100. $PrP^{-/-}$ cells plated at 150,000 cells per well on PDL/Fibronectin glass coverslips, Graph mean plus standard deviation, n= 2 duplicate technical replicates.

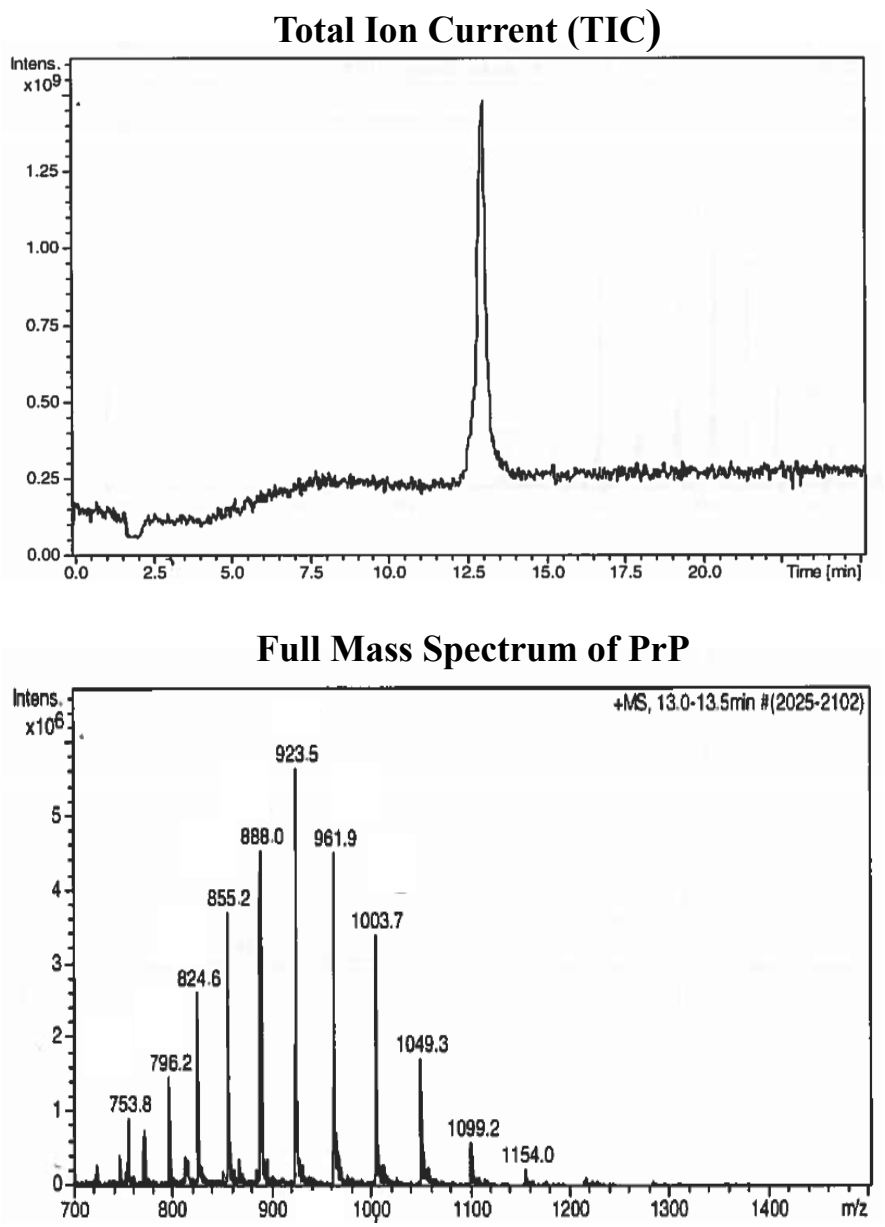

Figure 4.a: Mass spectrometry confirmed recombinant PrP purity. Total Ion Current (TIC) histograms were plotted as intensity versus time (minutes) and full mass spectrum plot below as intensity versus m/z (mass-to-charge ratio). Data in TIC plot confirmed protein fraction was relatively pure and mass spectrum confirmed predicted PrP protein ion to mass profile was present.

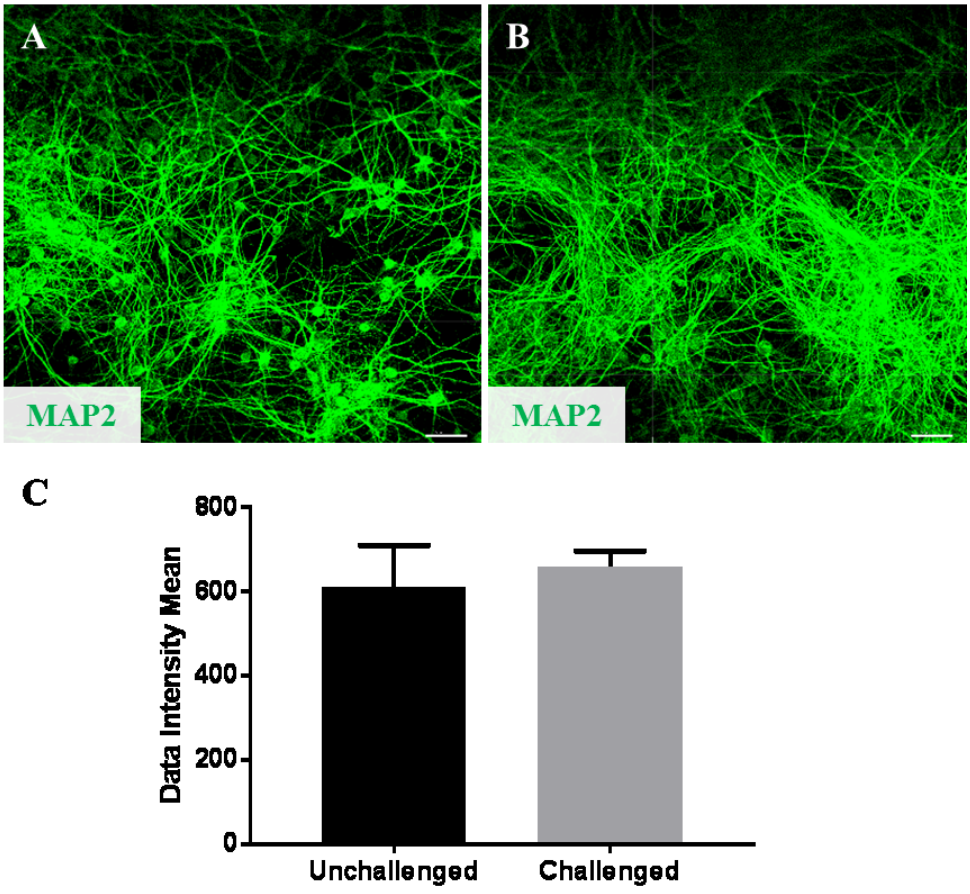

Figure 5.a: Fibrils did not induce cellular cytotoxicity after initial challenge. Immunolabelling using neuronal marker MAP2 was used to investigate if fibrils were inducing neurotoxicity in cultures. (A) Control unchallenged WT cultures stained with neuronal marker (MAP2/ Green) and (B) Challenged WT cultures after 6 hours. (C) IMARIS statistics based on intensity mean of MAP2 signal. No obvious neuronal changes were evident between unchallenged and challenged cultures and this observation was confirmed by IMARIS analysis which showed no significant differences (P-Value 0.48) were evident between both groups. WT cultures 30,000 cells, challenged with 7.5µg/ml WT fibrils for 6 hours, Scale Bar 50µm. Graph mean plus standard deviation, n=3, n= data intensity sum of individual wells, unpaired t test.

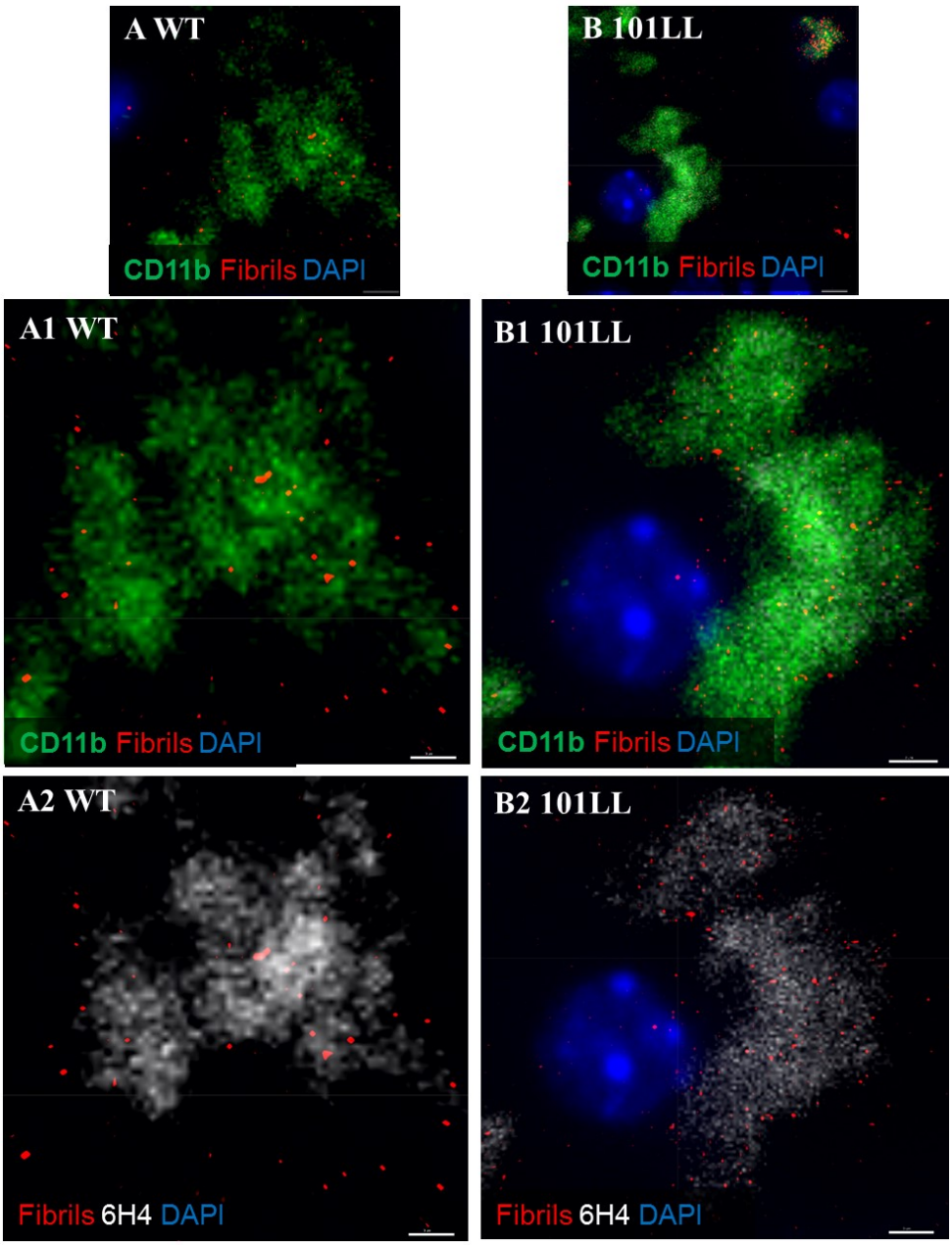

Figure 5.b: Microglia response to fibril challenge. Immunolabelling was used to investigate if microglial cell morphology was changing in response to fibril insult. (A-B) Images showing complete microglial cell (CD11b/Green) and fibril (Red) interactions and (A1-A2; B1-B2) show enlarged images of WT and 101LL microglia including PrP^{C} (6H4/White) labelling. Microglia appeared to be in an activated state, based on immunolabelling results showing cell bodies were large and processes were short and thick, a phenotype correlated with microglial activation in response to neuronal injury. Enlarged images indicated microglial were associated with smaller sized fibrils suggesting phagocytosis may be occurring and this was evident in both genotypes. Cultures 75,000 cells, challenged with 7.5µg/ml WT fibrils, Scale bar (A-B) 5µm, (A1-A2; B1-B2) 3µm, Confocal LSM710.

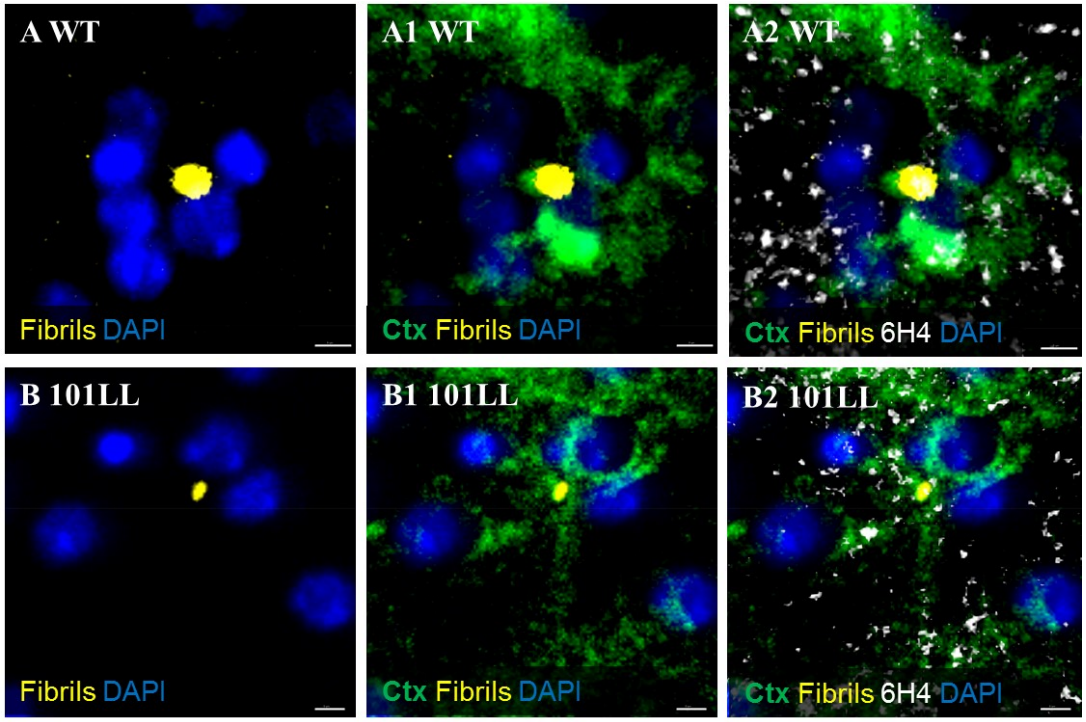

Figure 5.c: Limited fibrils were targeted to lipid-raft domains. To address possible routes of fibril internalisation into cells a marker for labelling lipid-rafts was used to investigate localisation of fibrils within these microdomains which would provide a viable route for fibril internalisation. (A, A1,A2) WT and (B, B1,B2) 101LL fibril-challenged cultures (WT Fibrils/Yellow) labelled with lipid-raft marker Cholera toxin Subunit B (Ctx/Green) and 6H4 (PrP^C/White). Limited fibril localisation within these domains was evident in both genotypes suggesting this was not a main route of entry into cells. Cultures 75,000 cells, challenged with 7.5µg/ml WT fibrils, Scale bar 5µm, Confocal LSM710.

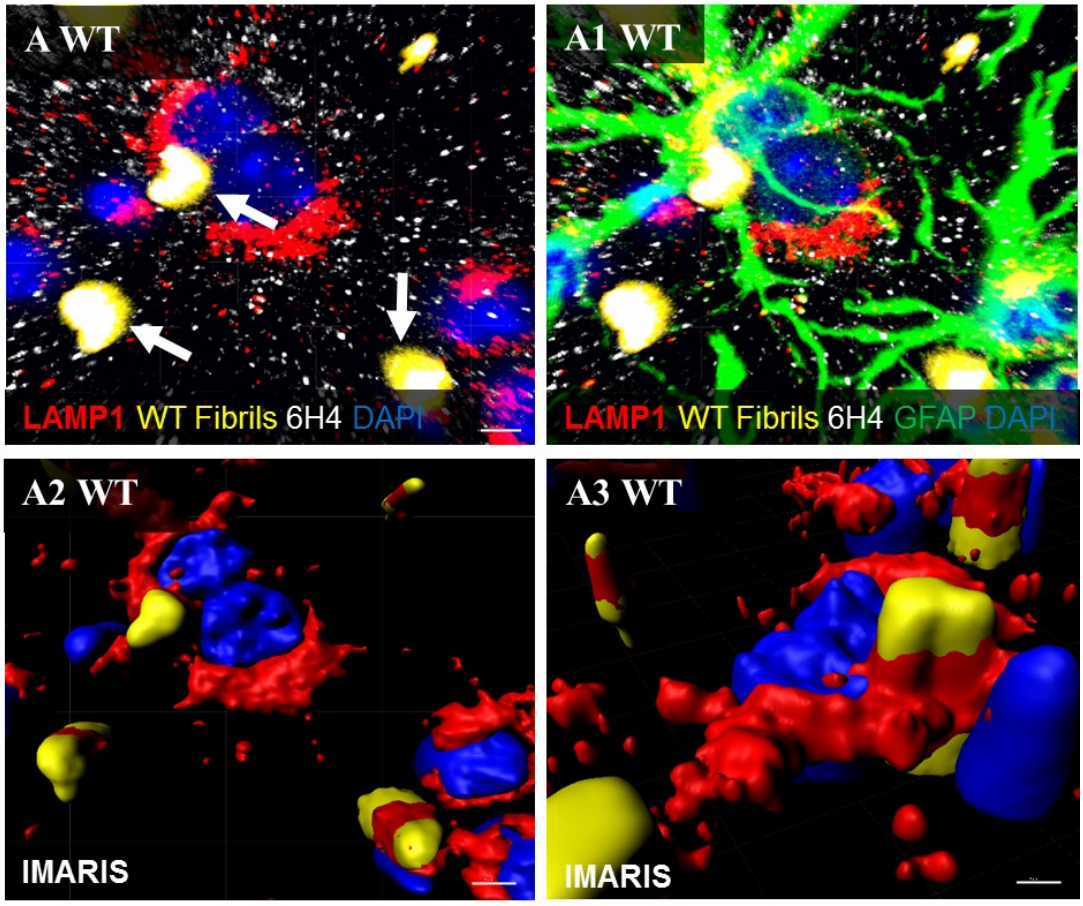

Figure 5.d: Fibrils were targeted to lysosomal organelles in astrocytes. To examine if fibrils were been targeted to lysosomal domains in glial cells for degradation, dual-labelling of astrocytic populations and lysosomal markers was carried out in WT challenged cultures. (A-A1) WT cultures challenged with WT fibrils (Yellow/Arrows), lysosomal marker LAMP1 (Red), astrocytes (GFAP/Green), PrP^{C} (6H4/White) and DAPI (Nuclear/Blue). (A2-A3) IMARIS reconstructions of fibrils and organelle interactions. Fibril lysosomal interactions were evident in glial cells and IMARIS reconstruction confirmed fibrils were embedded in these acidic structures in WT cultures. Astrocytes appeared hypertrophic and therefore, were in an activated state. Assuming the neighbouring cell shown here is a neuron, astrocytes were internalising fibrils beside neuronal cell bodies suggesting a glial neuroprotective response was evident in WT cultures. WT Cultures 30,000 cells, challenged with 30µg/ml WT fibrils for 24-hours, Scale bar 5µm, Confocal LSM710.

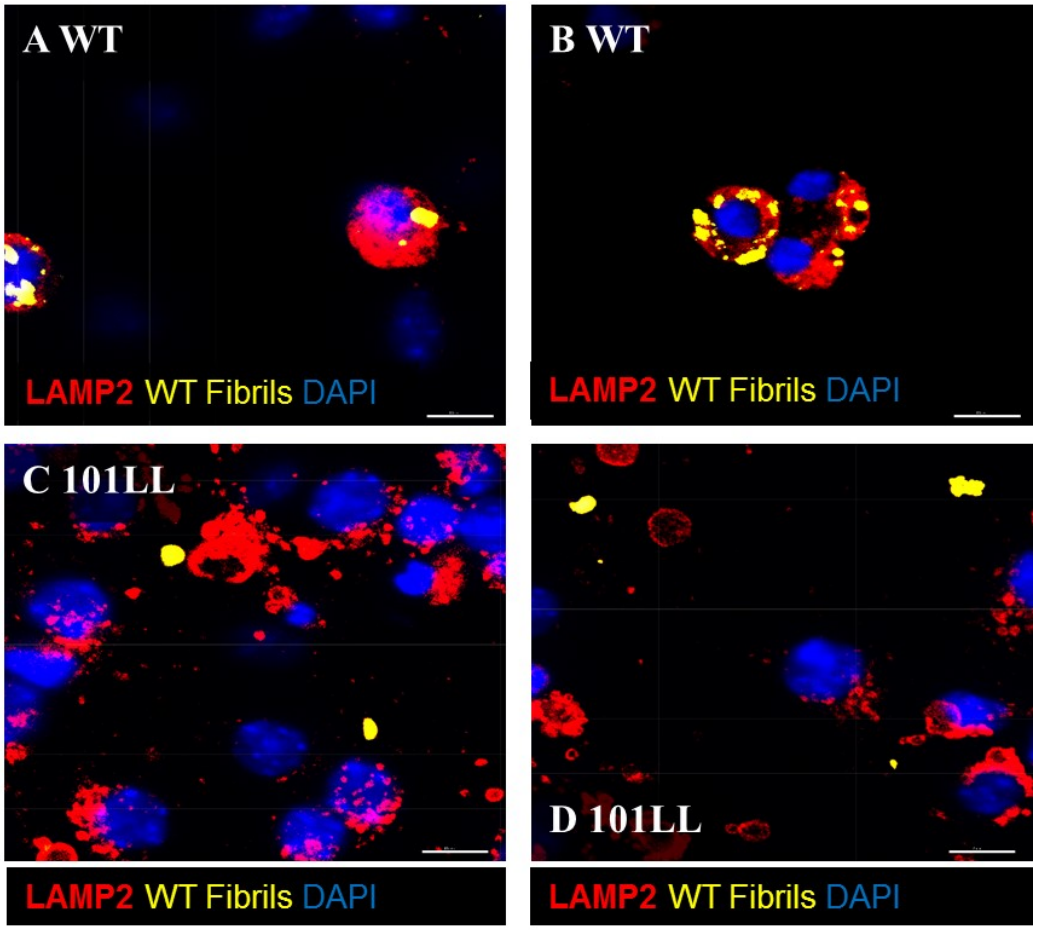

Figure 5.e: Fibrils were targeted to lysosomes in WT cultures. To examine if fibrils were been trafficked to lysosomal domains, WT and 101LL cultures were labelled with a lysosomal marker to examine if lysosomal degradation pathways were operative in these genotypes. (A-B) WT and (C-D) 101LL cultures challenged with WT fibrils (Yellow), labelled with Lysosomal marker LAMP2 (Red), and DAPI (Nuclear/Blue). Lysosomal labelling in WT cultures showed WT fibrils were present in lysosomal acidic organelle domains, and this was not evident in 101LL cultures. WT and 101LL cultures 30,000 cells, challenged with 30µg/ml WT fibrils for 24-hours, Scale bar 10µm, Confocal LSM710.

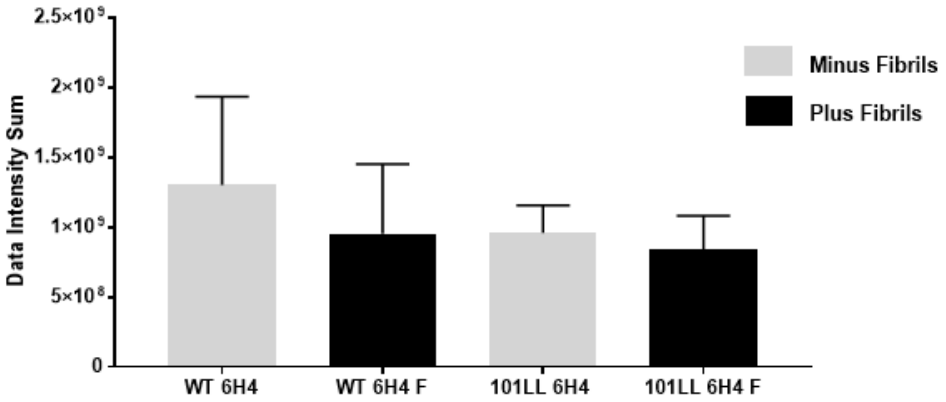

Figure 5.f: Fibril challenge did not change detectable PrP^C levels. Levels of normal PrP^C in WT and 101LL cultures were compared using IMARIS software before and after fibril-challenged to investigate if conformational changes of the normal PrP^C to the abnormal form was occurring. No significant differences in PrP^C levels (based on 6H4 immunolabelling) were noted in either WT or 101LL cultures suggesting no conformational changes were taking place within the 24-hour timeframe. WT and 101LL cultures 30,000 cells, challenged with 30µg/ml WT fibrils for 24-hours. Graph mean plus standard deviation, WT minus fibrils n=9, WT plus fibrils n=21, 101LL minus fibrils n=6 and 101LL plus fibrils n=14, n= data intensity sum of individual wells, unpaired t test.

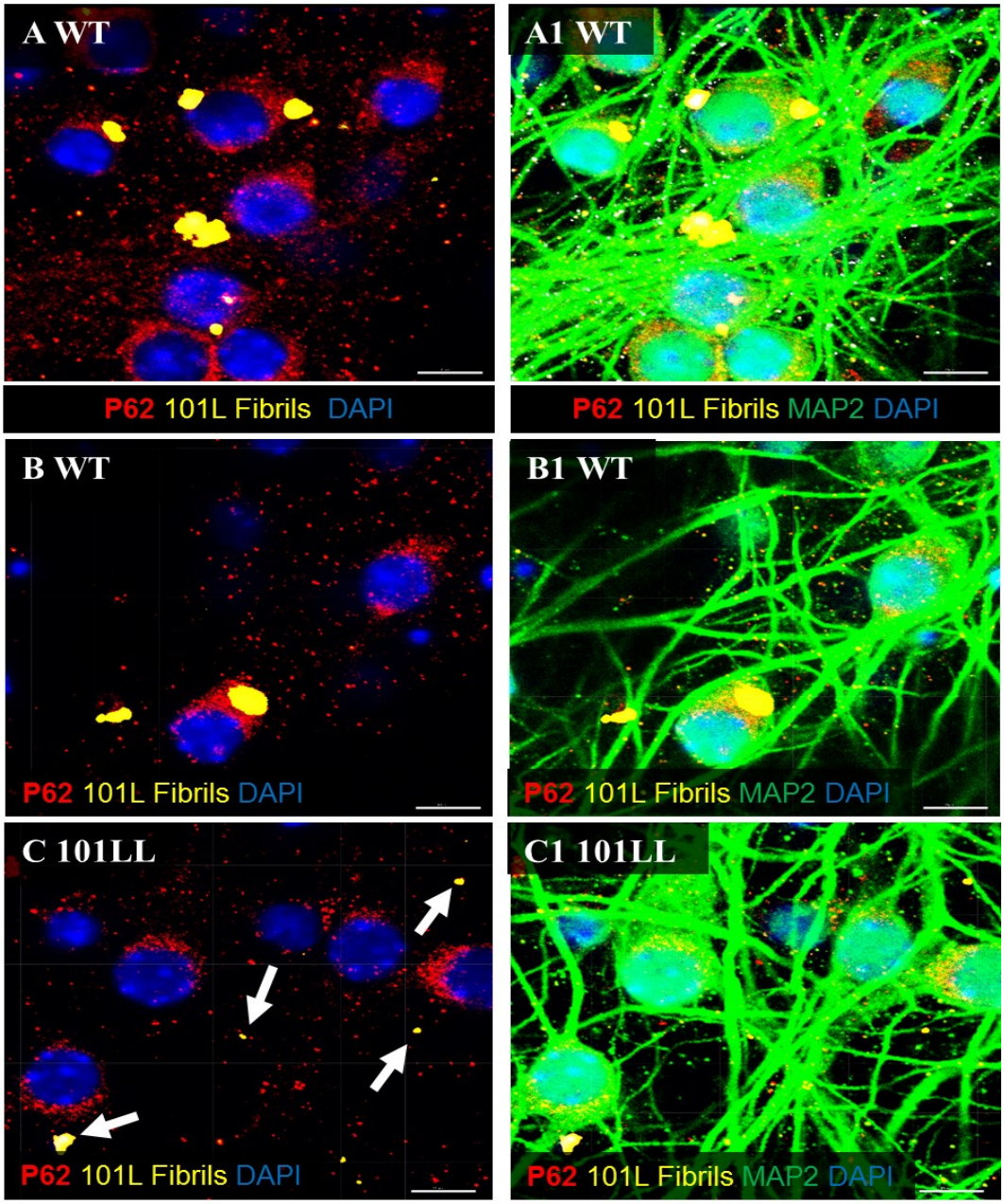

Figure 5.g: Fibril processing by autophagy was evident in WT challenged cultures. To ascertain if autophagy processing of fibrils was occurring in WT and 101LL cultures, the autophagosome marker p62 was used to label challenged cultures. (A-A1; B-B1) WT cultures challenged with 101L fibrils (Yellow), autophagosome marker p62 (Red) and DAPI (Blue). (C-C1) 101LL cultures challenged with 101L fibrils (Yellow/Arrows). Autophagosome labelling showed WT fibrils were present in these spherical structures however, no fibril associations were noted in 101LL cultures indicating an autophagy pathway was only activated in WT cultures. WT and 101LL cultures 30,000 cells, challenged with 30µg/ml 101L fibrils for 24 hours, Scale bar 10µm, Confocal LSM710.

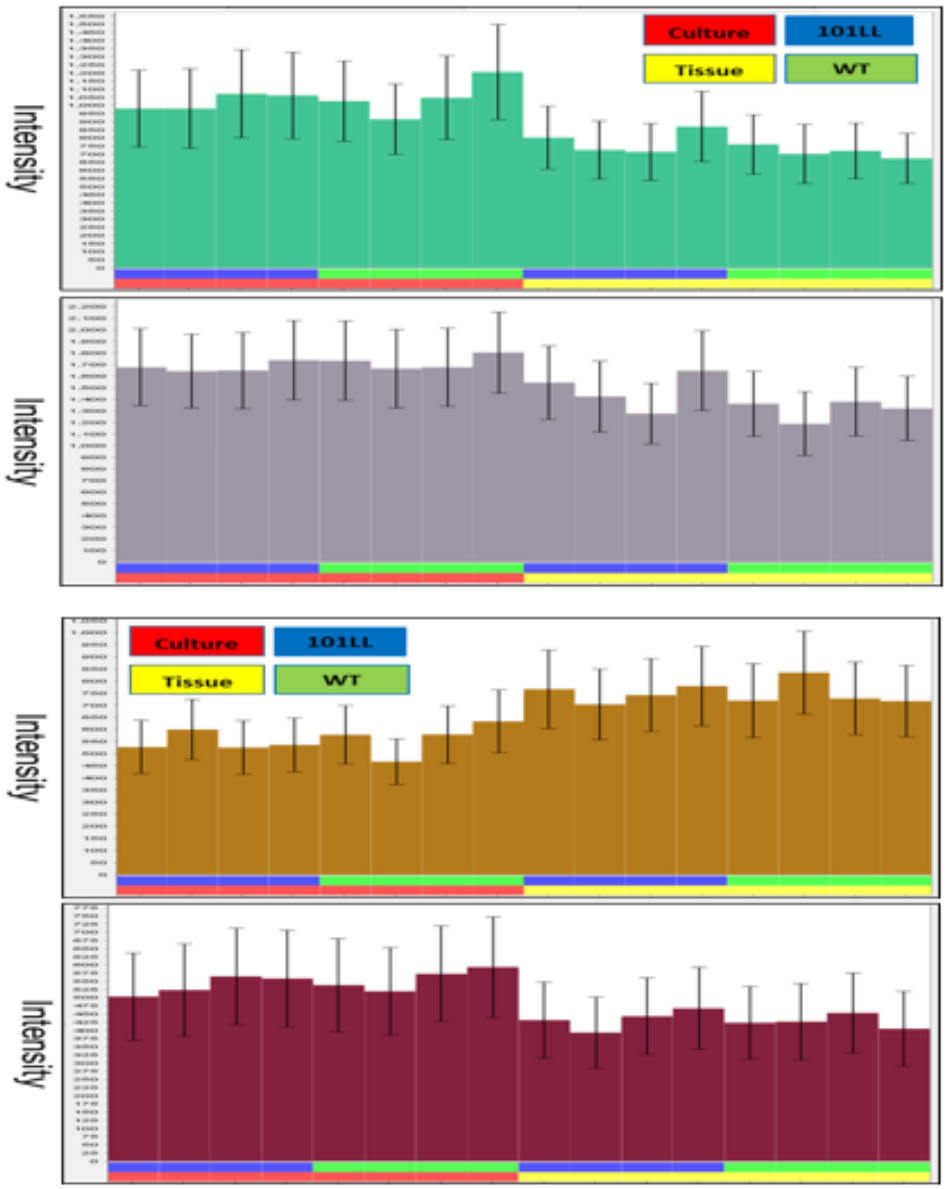

Figure 6.a: Miru identified similar clusters of genes between *in vivo* and *in vitro* system comparisons, Cluster 025 (Green) 11 genes, Cluster 038 (Grey) 9 genes, Cluster 041 (Brown) 9 genes and Cluster 067 (Maroon) 8 genes showed similar normalised expression intensity values across both systems and genotypes. GO enrichment (DAVID) for Cluster 025 identified protein transport, proteolysis, response to metal ion and lipid metabolic processes, Cluster 038 enrichment was associated with protein targeting to mitochondria, intracellular protein transport, tumor necrosis factor-mediated signalling pathway, Cluster 041 was enriched for proteolysis, G-protein coupled receptor signalling pathway, myeloid cell differentiation and Cluster 067 was enriched for cell surface receptor signalling pathway, actin cytoskeleton organisation, regulation of canonical Wnt signalling pathway. Normalised expression intensity values are shown on the y axis.

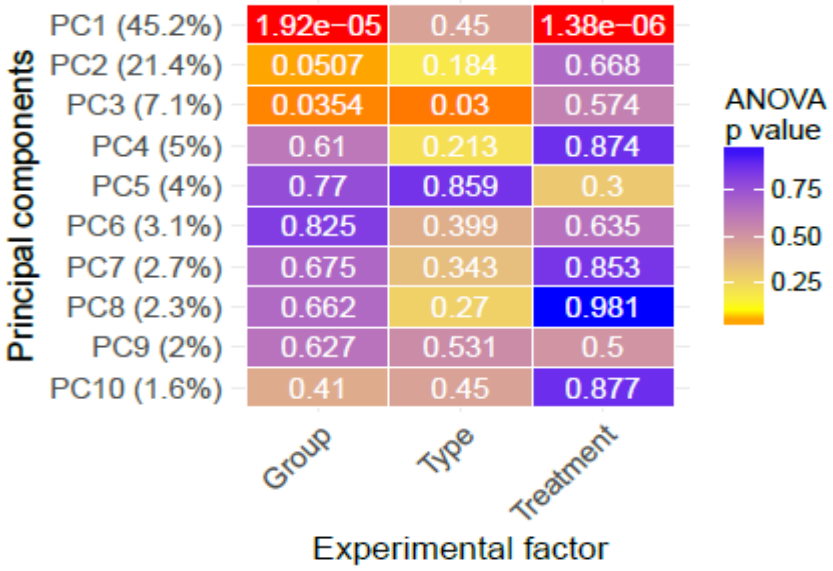

Figure 6.b: Heatmap showing ANOVA P-Values for the association between principal components and categorical experimental variables. Where different values of categorical variables (e.g. different treatment conditions) are associated with large changes in the data, these P-Values are expected to be significant for early components responsible for large proportions of variance.

Contrast	Gene	LogFC	P-Value	FDR
Unchallenged 101LL vs WT	*Tnfaip2* *Tgfbi*	2.30 3.91	3.51E-06 4.15E-06	0.02 0.02
WT Plus Fibrils vs WT	*Tnfaip2* *Tgfbi*	0.81 2.65	0.11 0.0001	0.11 0.002
101LL Plus Fibrils vs 101LL	*Tnfaip2* *Tgfbi*	-1.06 -1.01	0.0007 0.08	0.02 0.24

Table 6.a: RNA-seq analysis identified two DEGs in unchallenged 101LL vs WT comparison namely *Tnfaip2* and *Tgfbi*, which showed an increase in expression in 101LL cultures. After challenge, *Tnfaip2* expression was significantly reduced in 101LL cultures and *Tgfbi* expression was significantly increased in WT cultures. *Tgfbi* and *Tnfaip2* expression was reduced in 101LL and WT challenged cultures however, this observation was not significant.

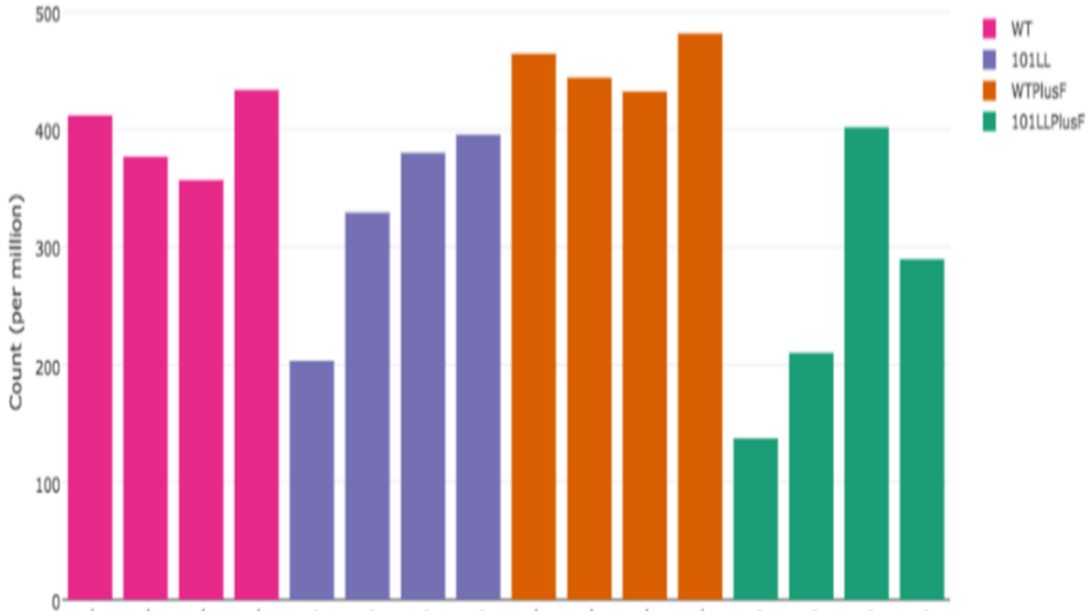

Figure 6.c: Prnp expression profile showed this gene was highly variable in unchallenged and challenged 101LL cultures (purple and green) and was highly consistent in unchallenged and challenged WT cultures (pink and orange). Expression increased subtly but significantly in challenged WT cultures (LogFC 0.20, P-Value 0.004, FDR 0.02) after fibril challenge and no significant changes in were noted in 101LL challenged cultures (LogFC -0.33, P-Value 0.36, FDR 0.59).

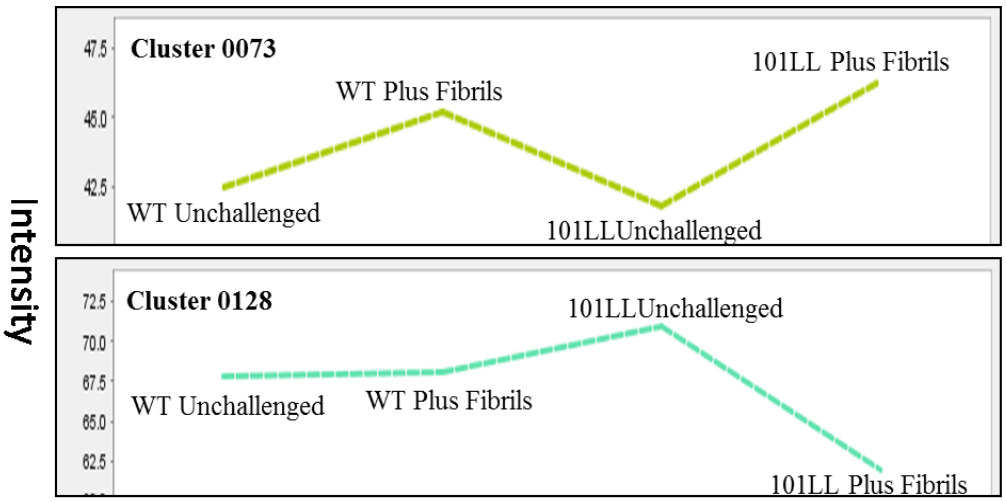

DAVID GO enrichment (Biological Process Cluster 0073)	Gene Count	P-Value	Benjamini
Phosphorylation	6	2.6E-3	4.7E-1
Protein phosphorylation	5	1.3E-2	7.9E-1
Negative regulation of axon extension	2	3.2E-2	9.2E-1
Protein autophosphorylation	3	3.5E-2	8.8E-1
Antigen processing and presentation	2	8.3E-2	9.8E-1

DAVID GO enrichment (Biological Process)	Gene Count	P-Value	Benjamini
Ion transmembrane transport	2	4.3E-2	9.9E-1
Response to stimulus	2	5.8E-2	9.7E-1

Figure 6.d: Miru identified genes clusters specific to 101LL response to fibril challenge. Cluster 0073 was identified and genes associated with this cluster were predominantly up-regulated in 101LL fibril challenge cultures in comparison to other groups. Cluster 0128 showed the opposite result and were only down-regulated in 101LL fibril challenge cultures. Readings based on mean counts per million (normalised expressed intensity values). Class viewer scaling was raw, class plot was mean line. GO enrichment for Cluster 0073 (48 genes) using DAVID showed challenged cultures were associated with only five biological processes, and top two were related to phosphorylation. Genes associated with phosphorylation were *Flt3, Ak8, Camk1g, Cdk5, Cdkl3* and *Mapk15*. GO enrichment for Cluster 0128 (33 DEGs) using DAVID showed response to stimulus (*Asic3* and *Stat1*) which was previously shown to be associated with down-regulated genes in 101LL challenged cultures.

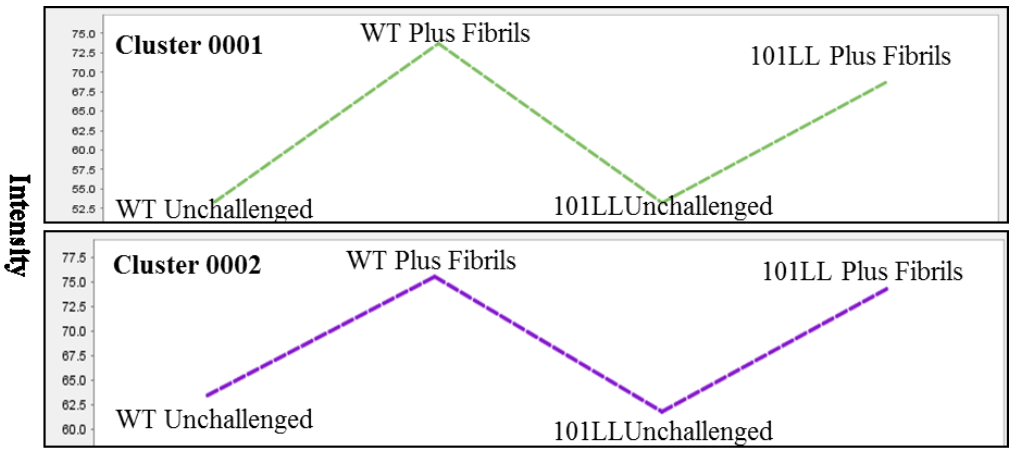

DAVID GO enrichment (Biological Process Cluster 0001)	Gene count	P-Value	Benjamini
Glycolytic process - chemical reactions resulting in the breakdown of a carbohydrate into pyruvate	13	1.3E-9	2.8E-6
Gluconeogenesis - formation of glucose from noncarbohydrate precursors, such as pyruvate, amino acids and glycerol	9	1.6E-6	1.7E-3
Metabolic process	37	3.7E-6	2.8E-3
Chemical synaptic transmission	19	2.4E-5	1.3E-2
Apoptotic process	38	1.4E-4	5.9E-2
Carbohydrate metabolic process	19	2.5E-4	8.8E-2

DAVID GO enrichment (Biological Process 0002)	Gene count	P-Value	Benjamini
Response to mechanical stimulus	6	5.6E-4	4.3E-1
Cellular amino acid biosynthetic process	4	2.3E-3	6.9E-1
Response to drug	11	3.6E-3	7.0E-1
Apoptotic process	5	5.7E-3	7.6E-1
tRNA aminoacylation from protein translation	4	6.6E-3	7.4E-1
Nervous system development	10	2.0E-2	9.7E-1

Figure 6.e: Miru identified generic gene clusters in response to fibril challenge. Cluster0001 and 0002 were identified in Miru and genes associated with these clusters were up-regulated in both WT and 101LL fibril-challenged cultures in comparison to untreated cells. Readings based on mean counts per million (normalised expressed intensity values). Class viewer scaling was raw, class plot was mean line. GO enrichment for Cluster 0001 (791 genes) using DAVID showed glycolytic process to be a top hit. GO enrichment for Cluster 0002 (263 genes) showed challenged cultures were associated with response to stimulus.